



University of HUDDERSFIELD

University of Huddersfield Repository

Alba, Katerina

Isolation, characterization and Functional Properties of Okra Pectin

Original Citation

Alba, Katerina (2015) Isolation, characterization and Functional Properties of Okra Pectin. Doctoral thesis, University of Huddersfield.

This version is available at <http://eprints.hud.ac.uk/26440/>

The University Repository is a digital collection of the research output of the University, available on Open Access. Copyright and Moral Rights for the items on this site are retained by the individual author and/or other copyright owners. Users may access full items free of charge; copies of full text items generally can be reproduced, displayed or performed and given to third parties in any format or medium for personal research or study, educational or not-for-profit purposes without prior permission or charge, provided:

- The authors, title and full bibliographic details is credited in any copy;
- A hyperlink and/or URL is included for the original metadata page; and
- The content is not changed in any way.

For more information, including our policy and submission procedure, please contact the Repository Team at: E.mailbox@hud.ac.uk.

<http://eprints.hud.ac.uk/>

**ISOLATION, CHARACTERIZATION AND
FUNCTIONAL PROPERTIES OF OKRA
PECTIN**

KATERINA ALBA

A thesis submitted to the University of Huddersfield in partial fulfilment
of the requirements for the degree of Doctor of Philosophy

SCHOOL OF APPLIED SCIENCES
DEPARTMENT OF BIOLOGICAL SCIENCES

2015

ACKNOWLEDGEMENTS

I must express my gratitude to my supervisor Dr. Vassilis Kontogiorgos for his guidance, advice and encouragement during my research. I am grateful that he cared so much about my work and responded to my questions and queries so promptly.

I would also like to thank my second supervisors Dr. Gordon Morris and Prof. Andy Laws for their valuable comments on analysis of pectin macromolecular characteristics and $^1\text{H-NMR}$, and $^{13}\text{C-NMR}$ spectra. Prof. Stefan Kasapis is acknowledged for his advice, guidance and troubleshooting approach in analysis of pectin high solid systems. I would like to thank Prof. Christos Ritzoulis who guided me in the field of colloidal dispersions and analytical techniques that are used to characterize those systems.

I am grateful to the School of Applied Sciences, University of Huddersfield for the valuable fee-waiver scholarship. GEN Foundation and SCI for funding part of research activities and conference attendance.

I am thankful to all staff of School of Applied Sciences and particularly Ibrahim George, Hayley Markham and Dr. Neil McLay for their laboratory support and technical advice.

Finally, I would like to express my deepest thanks to my family especially my mother Larissa Davõdova and grandmother Nadia Davõdova for all of the support.

ABSTRACT

Pectin was isolated by aqueous extraction at pH 6.0 or 2.0 from okra (*Abelmoschus esculentus L.*) pods. An isolation protocol was designed to extract pectin and study the influence of the extraction pH on its chemical composition, macromolecular and functional properties. The extraction protocols resulted in the isolation of pectin of high purity as evidenced by their high total carbohydrate (70.0 – 82%) and low protein (4.3 – 6.3%) contents. Samples contained between 47-57% galacturonic acid, had broad molecular weight distributions, a low degree of methylation (40 and 25 %) and high degree of acetylation (52 and 38 %). Neutral sugar analysis showed that pectin extracted at pH 6.0 contained more neutral sugars, particularly, galactose, rhamnose and arabinose than that extracted at pH 2.0 indicating variations in fine structure. In addition, molecular parameters of the isolated pectins, such as intrinsic viscosity (2.8 – 4.4 dL g⁻¹), critical concentration (0.15 – 0.45 dL g⁻¹) and coil overlap parameter (0.66 – 1.51), showed that extraction conditions resulted in pectin with different chain macromolecular characteristics.

Following extraction, the functional properties of okra pectin were investigated in high and low moisture systems and also in colloidal dispersions. It has been shown that okra polysaccharides are non-gelling pectins and their inability to form ordered structures was attributed to the high degree of acetylation and branching of the side-chains. The pH sensitivity of okra pectins has been further demonstrated in high solid systems, where the mechanical relaxation of LM-pectin in the presence of co-solute has been altered by pH. It has been shown that high pH values result in extended chain conformation and early vitrification events. In contrast, viscoelastic functions of polyelectrolyte decreased and resulted in delayed vitrification events at low pH.

The next step of present work was focused on potential utilization of okra polysaccharides in fabrication of oil-in-water emulsions for food and pharmaceutical applications. The emulsifying properties of crude okra extracts and okra isolates (rich in pectin) have been investigated under different conditions (e.g., oil volume fraction, biopolymer concentration, pH values, energy input methods) in order to produce fine emulsions with long-term stability. It has been shown that pH of extraction has a pronounced effect on the interfacial activity of both crude extract and pectin isolates. Extracts or isolates obtained at high pH demonstrated higher emulsifying capacity than those extracted at low pH. In general, okra pectin isolates were more efficient in emulsion stabilisation than crude extracts by producing emulsions of smaller droplet sizes. Moreover, emulsifying capacity of okra pectin was affected by the pH and stable emulsions were produced only at low pH values (pH 2.0 or 3.0). It has been shown that okra pectin-stabilized emulsions evolve under the effects of Ostwald ripening and coalescence during the long-term storage.

The present work shows the potential of okra pectins as emulsifiers under acidic conditions and serves as the basis for the development of such systems in encapsulation technology of bioactive components.

TABLE OF CONTENTS

ACKNOWLEDGEMENTS	1
ABSTRACT	2
LIST OF FIGURES	7
LIST OF TABLES	13
CHAPTER 1: INTRODUCTION	15
1.1 Context of work	16
1.2 Biopolymers	19
1.3 Chemical structure of pectin	20
1.3.1 Homogalacturonan (HG)	22
1.3.2 Rhamnogalacturonan II (RG-II)	23
1.3.3 Rhamnogalacturonan I (RG-I)	24
1.3.4 Macromolecular organization of HG, RG-I and RG-II in the primary wall	27
1.4 Isolation of pectin	28
1.5 Pectin conformation	30
1.6 Physical properties of pectin	34
1.6.1 Pectin solubility	34
1.6.2 Molecular weight distributions and averages	37
1.6.3 Viscosity and flow properties of pectin solutions	39
1.7 Okra plant	45
1.8 Pectin as a functional food ingredient	47
1.8.1 High moisture regime - Gelation	47
1.8.2 Low moisture regime – High solid biopolymer systems	50
1.8.3 Colloidal systems	55
1.8.3.1 Thermodynamics of mixing	56
1.8.3.2 Interaction forces between emulsion droplets	57
1.8.3.3 Mechanisms of emulsification	62
1.8.3.4 Emulsion kinetic stability	63
1.9 Hypothesis, aims and objectives	69
1.9.1 Hypothesis	69
1.9.2 Aims	69
1.9.3 Objectives	69
CHAPTER 2: ISOLATION AND CHARACTERIZATION OF OKRA PECTIN	70
2.1 Introduction	71
2.2 Materials and methods	72
2.2.1 Materials	72
2.2.2 Isolation of okra pectins	73
2.2.3 Chemical characterization	73
2.2.4 FT-IR spectroscopy	76
2.2.5 ¹ H-NMR and ¹³ C-NMR spectroscopy	76
2.2.6 Molecular weight determination	77
2.2.7 Dilute solution rheology	77
2.3 Results and discussion	78
2.3.1 Isolation and compositional analysis	78
2.3.2 FT-IR spectroscopy	86
2.3.3 ¹ H and ¹³ C-NMR spectra	88
2.3.4 Macromolecular characteristics of pectin	90

2.3.5 Dilute solution viscometry	93
2.4 Conclusions	98
CHAPTER 3: APPLICATIONS OF OKRA PECTIN IN HIGH AND LOW MOISTURE CONTENT SYSTEMS	99
3.1 Introduction	100
3.2 Materials and Methods	103
3.2.1 Pectin extraction	103
3.2.2 Glucose syrup	103
3.2.3 Sample preparation	103
3.2.4 Rheological measurements	103
3.2.5 Differential scanning calorimetry	104
3.2.6 ζ -potential titration	104
3.2.5 Numerical computation	105
3.3. Results and discussion	105
3.3.1 Viscoelasticity of pectin–co-solute mixtures	105
3.3.2 Calculation of relaxation spectra	117
3.4 Conclusions	120
CHAPTER 4: EMULSIFYING PROPERTIES OF OKRA PECTIN	121
4.1 Crude Okra extracts as emulsifiers for acidic emulsions	122
4.1.1 Introduction	122
4.1.2 Materials and Methods	123
4.1.2.1 Isolation and partial characterization of okra extracts	123
4.1.2.4 Preparation of okra extract solutions and emulsions	123
4.1.2.5 Determination of particle droplet distribution	124
4.1.2.6 Rheological measurements of okra extracts and emulsions	124
4.1.2.7 Determination of interfacial protein concentration	125
4.1.2.8 Determination of ζ -potential	125
4.1.2.9 Emulsion morphology	126
4.1.3 Results and discussion	126
4.1.3.1 Emulsification capacity – emulsion stability	126
4.1.3.2 Surface coverage	130
4.1.3.3 ζ -Potential measurements	132
4.1.3.4 Rheology of emulsions	133
4.1.4 Conclusions	137
4.2 Effect of isolation conditions on interfacial activity of okra biopolymers.	138
4.2.1 Introduction	138
4.2.2 Materials and methods	138
4.2.2.1 Isolation of okra pectin	138
4.2.2.3 Preparation of emulsions	138
4.2.2.4 Determination of particle droplet size distribution	139
4.2.2.5 Determination of ζ -potential	139
4.2.2.6 Rheological measurements of okra extracts and emulsions	139
4.2.3 Results and discussion	139
4.2.3.1 Emulsification capacity of OP6	139
4.2.3.2 Flow behaviour of okra pectin solutions and emulsions	142
4.2.4 Conclusions	144
4.3 Surface engineering of o/w interfaces with okra pectin	145
4.3.1 Introduction	145
4.3.2 Materials and Methods	147

4.3.2.1 Materials	147
4.3.2.2 Preparation of okra emulsions	147
4.3.2.3 Determination of particle droplet distribution	148
4.3.2.4 Interfacial composition analysis	148
4.3.2.5 Rheological characterization of okra pectin solutions and emulsions	149
4.3.2.6 Determination and titration of ζ -potential.....	150
4.3.2.7 Pectin immunolocalization at the o/w interface.....	150
4.3.3. Results and discussion	151
4.3.3.1 Emulsifying capacity of okra pectin and ageing of emulsions	151
4.3.3.2 Examination of destabilisation mechanisms.....	156
4.3.3.3 Interfacial composition	166
4.3.3.4 Electric properties of alkane-in-water interface.....	173
4.3.3.5 Flow behavior of emulsions and pectin solutions.....	176
4.3.3.6 Pectin immunolocalization at the alkane-water interface.	178
4.3.4 Conclusions.....	182
CHAPTER 5: GENERAL CONCLUSIONS AND FUTURE WORK.....	184
CHAPTER 6: REFERENCES	188

LIST OF FIGURES

Figure 1.1. The primary structure of homogalacturonan.....	23
Figure 1.2. The structure of rhamnogalacturonan II.....	24
Figure 1.3. The structure of rhamnogalacturonan I (a) and general structure of pectin (highly simplified) (b).....	26
Figure 1.4. Model of torsion angles (φ , ψ and ω) in a polygalacturonate chain.....	32
Figure 1.5. Pectin chain conformations a) extended ($\text{pH} > \text{p}K_a$), b) compact ($\text{pH} < \text{p}K_a$).....	35
Figure 1.6. Huggins-Kraemer plot from okra pectin (OP6) in phosphate buffer and 0.1 M NaCl at 25°C.....	42
Figure 1.7. Schematic representation of the effect of shear rates on polymer chain rotation. Hydrodynamic work is converted into heat, resulting in an increased solution viscosity. 1 - Ubbelohde type viscometer, 2 – relative velocity of solvent in capillary, 3 – rotational motion of polymer molecule.	44
Figure 1.8. Acid-induced gelation of citrus LM-pectin ($\omega=6.283$ rad/s, 1% strain, $T=20^\circ\text{C}$).....	49
Figure 1.9. The gelation mechanism of LM-pectins is based on the egg-box (adapted from.....	51
Figure 1.10. Variation of G' , G'' and $\tan \delta$ as a function of temperature, frequency, molecular weight and concentration for amorphous polymers.....	54
Figure 1.11. Schematic representation of the distribution of ions on the surface of a droplet.....	60
Figure 1.12. Schematic representation of the interaction potential between two emulsion droplets.....	61
Figure 1.13. Interfacial orientation of polymeric emulsifiers.....	62

Figure 1.14. Schematic representation of Ostwald ripening-driven droplet growth.....	68
Figure 2.1. Isolation protocol for pectins isolated from okra pods.....	74
Figure 2.2. UV absorption spectra for 0.167 % w/v OP2, OP6 solutions and 0.01 % w/v of ferulic acid solution (pH 4.0).....	82
Figure 2.3. GC-chromatograms of a) OP6 and b) OP2.....	84
Figure 2.4. Fourier transform–infrared spectra (FT-IR) of commercial pectin standards with different DM and OP2, OP6.....	87
Figure 2.5. ¹ H-NMR spectra of OP2 (a) and OP6 (b) samples in D ₂ O at 70 °C. Acetone reference at 2.22 ppm.....	89
Figure 2.6. ¹³ C-NMR spectra of OP2 (a) and OP6 (b) samples in D ₂ O at 70 °C. Acetone reference at 31.25 ppm.....	90
Figure 2.7. Refractive index (RI) and MALLS traces (LS) of size exclusion chromatograms of OP2 and OP6.....	91
Figure 2.8. Viscosity (η) as a function of shear rate for OP6 at different concentrations (0.01 – 5% w/v) and two buffer pH values a) pH 3.0 and b) pH 7.0.....	96
Figure 2.9. Double logarithmic plots of zero shear specific viscosity (η_{sp}) ₀ vs. reduced concentration $c[\eta]$ of OP2 and OP6 at pH 3 and pH 7.....	97
Figure 3.1. DSC thermograms of 80% glucose syrup and 1% LM-pectin plus 79% glucose syrup at pH 3.0 and 7.0. Top left inset shows ζ -potential titration of the pectin solution. Bottom right inset shows a typical first derivative curve of heat flow of the samples and calculations used to derive the onset of the glass transition.....	109

Figure 3.2. Temperature dependence of the storage and loss modulus for systems containing 1% LM-pectin and 79% glucose syrup at pH 3.0 and 7.0 (scan rate: 2 °C/min; frequency: 1 rad/s; strain: 0.01%).....110

Figure 3.3. Double logarithmic plots of (a) storage and (b) loss modulus against frequency of oscillation for a sample containing 1% LM-pectin and 79% glucose syrup at pH 7.0 (temperature interval: 4.4 °C; strain: 0.01%).....113

Figure 3.4. Master curves of viscoelasticity as a function of reduced frequency of oscillation (ωa_T) for systems containing 1% LM-pectin and 79% glucose syrup at pH 3.0 and 7.0 at the reference temperature of -19 °C.....115

Figure 3.5. Logarithmic shift factor, a_T , for systems containing 1% LM-pectin and 79% glucose syrup at pH 3.0 and 7.0 plotted against temperature from the data of the master curves presented in Figure 3.4 (WLF fits are also shown for both samples).....116

Figure 3.6. Semi logarithmic plots of relaxation spectrum of 1% LM-pectin and 79% glucose syrup at pH 7.0 obtained using data from master curves in Figure 3.4; Solid or dashed lines were obtained after discretization of the loss or storage modulus, respectively; Top right inset shows a typical shape of L-curves that were used to calculate the optimum regularization parameter, and bottom right inset shows the relaxation spectrum of 1% LM-pectin and 79% glucose syrup at pH 3.....119

Figure 4.1.1. Particle size distributions of emulsions prepared using a) 1.5% OE4 and b) 1.5% OE6. The time development of the distributions is also shown. c) Variations in the cube of $d_{0,1}$ with time for emulsions stabilized by extract OE4 (square) or OE6 (circle).....127

Figure 4.1.2. Fluorescent micrographs of emulsions containing 1.5% w/v (a) OE4 and (b) OE6 after 6 hours of preparation ($\phi = 0.2$, 25 °C, citric buffer pH 3.0). The bottom

micrographs (c) and (d) depict the same emulsions after dilution in buffer (1:1000). Scale bars represent 100 μm	131
Figure 4.1.3. Rheological behavior of 1.5% w/v emulsions containing OE4, OE6 and rheological behavior of fresh 1.875% w/v okra extract solutions pH 4.0 or 6.0 (25 $^{\circ}\text{C}$).....	134
Figure 4.1.4. (a): Influence of ageing (0-30 days) on the rheological behavior of 1.5% w/v emulsion containing OE4 and rheological behavior of fresh 1.875% w/v okra extract solution pH 4.0 (25 $^{\circ}\text{C}$), (b): Influence of ageing (0-30 days) on the rheological behavior of 1.5% w/v emulsion containing OE6 and rheological behavior of fresh 1.875% w/v okra extract solution pH 6.0 (25 $^{\circ}\text{C}$).....	136
Figure 4.2.1: Particle size distributions of 0.5% w/v emulsions stabilized with OP6. The time development of the distributions is also shown.....	142
Figure 4.2.2. Influence of aging (0–30 days) on the rheological behaviour of 0.5% w/v emulsion containing OP6 and rheological behaviour of fresh 0.625% w/v OP6 solution (25 $^{\circ}\text{C}$).....	144
Figure 4.3.1. Particle size distributions of a) <i>n</i> -hexadecane-in-water emulsion with OP6 and b) <i>n</i> -dodecane-in-water emulsion with OP6 at 25 $^{\circ}\text{C}$	154
Figure 4.3.2. Particle size distributions of a) <i>n</i> -hexadecane-in-water emulsion with OP2 and b) <i>n</i> -dodecane-in-water emulsion with OP2. Inset shows $d_{3,2}$ profiles of <i>n</i> - hexadecane emulsions with OP2 as a function of biopolymer concentration 25 $^{\circ}\text{C}$	155
Figure 4.3.3. Macroscopic examination of <i>n</i> -hexadecane-in-water emulsions stored at 25 $^{\circ}\text{C}$	158
Figure 4.3.4. Time evolution of <i>n</i> -hexadecane-in-water emulsions stabilized with a) OP6 and b) OP2 at 25 $^{\circ}\text{C}$ for 1 h (0-60 min) with 5 min increments.....	159

Figure 4.3.5. Dependence $((d_{0,1})^3$ versus time) of Ostwald ripening rates on *n*-hydrocarbon type in 1.5% w/v OP2 and OP6 stabilized emulsions at pH 2.0 (25 °C).....163

Figure 4.3.6. Dependence $((d_{3,2})^3$ versus time) of Ostwald ripening rates on *n*-hydrocarbon type in 1.5% w/v OP2 and OP6 stabilized emulsions at pH 2.0 (25 °C).....163

Figure 4.3.7. Surface tension of OP2 and OP6 solutions (pH 2.0) as a function of polymer concentration at 25°C.....169

Figure 4.3.8. ζ -potential titration of 1.67% w/v pectin solutions and 1.5% w/v pectin stabilized emulsions at 1/1000 dilution. Inset shows the emulsifying capacity of okra biopolymers as affected by the pH and hydrocarbon chain length (25 °C)

Inset - ○ both biopolymers do not form emulsion, ● both biopolymers form emulsion, ◐ OP6 forms emulsion, ◑ OP2 forms emulsion.....174

Figure 4.3.9. Flow behavior of 1.5% w/v emulsions stabilized with OP2 and OP6 and flow behavior of fresh 1.67% w/v okra pectin sonicated and non-sonicated solutions at pH 2.0 (25 °C). Okra biopolymer solutions were sonicated under the same conditions as emulsions.....177

Figure 4.3.10. a) Influence of aging (0–30days) on the flow behavior of 1.5% w/v emulsion stabilized with OP6 and flow behavior of 1.67% w/v OP6 sonicated solution (25 °C), b) influence of aging (0–30 days) on the flow behavior of 1.5% w/v emulsion stabilized with OP2 and flow behavior of 1.67% w/v OP2 sonicated solution (25 °C).....178

Figure 4.3.11. Fluorescent images a1-4) 1.67% fixed OP2 solutions at pH 7.4, b1-4) 1.5% w/v emulsions stabilized with OP2 at pH 7.4, c1-4) 1.5% w/v *n*-dodecane-in-

water emulsions stabilized with OP2 at pH 7.4 (images are in hydrated state).....180

Figure 4.3.12. Fluorescent images (1, 2) of 1.5% w/v *n*-dodecane-in-water OP2-stabilized emulsions at pH 7.4, a- bottom, b- middle, c- top planes and d- z-projected image.....181

LIST OF TABLES

Table 2.1. Chemical composition of okra pectins extracted at pH 2.0 or 6.0.....	80
Table 2.2. Retention times of methanolysis products of standard sugars. Inositol was used as an internal standard.....	84
Table 2.3. Sugar molar (%) ratios for OP2 and OP6.....	85
Table 2.4. Molecular characteristics of OP2 and OP6. Slopes, intrinsic viscosity ($[\eta]$), critical concentration (c^*) and coil overlap parameter ($c^*[\eta]$) of OP2 or OP6 at two different buffer pH values.....	92
Table 3.1. Experimental conditions used to form gelled network in okra pectin solutions.....	102
Table 3.2. Values of WLF Parameters for 1% LM-pectin and 79% glucose syrup at pH 3.0 and 7.0.....	116
Table 4.1.1. Influence of okra extract type and storage time (days) on the average droplet diameters ($d_{3,2}$ and $d_{4,3}$) and ζ -potential in emulsions formed with 1.5% (w/v) OE4 and OE6 ^a	129
Table 4.1.2. Interfacial protein concentration Γ (mg m^{-2}), percentage of protein adsorbed at the oil-water interface of fresh emulsions and protein content of okra extracts.....	131
Table 4.2.1. Influence of ageing on the surface weighted average droplet size (d_{32}), (d_{43}) and ζ -potential in emulsions formed with 0.5% OP6.....	140
Table 4.3.1. Influence of okra pectin type and storage time on the average droplet diameters ($d_{3,2}$ and $d_{4,3}$) and span in <i>n</i> -dodecane and <i>n</i> -hexadecane emulsions formed with 1.5% (w/v) OP2 and OP6.....	153

Table 4.3.2. Physical properties required for calculations of theoretical Ostwald ripening rates in <i>n</i> -dodecane and <i>n</i> -hexadecane-in-water emulsions (25°).....	162
Table 4.3.3. Theoretical (ω_{th}) and experimental (ω_{exp}) rates of Ostwald ripening for various oil-in-water emulsions.....	164
Table 4.3.4. Weight percentage and amount of adsorbed protein, pectin and acetyl at the oil-water interface of fresh 1.5% w/v <i>n</i> -hexadecane emulsions stabilized with OP2 and OP6 at $\varphi = 0.1$, pH 2.0.....	167

CHAPTER 1

INTRODUCTION

1.1 CONTEXT OF WORK

Food science in the modern era focuses on several critical aspects to improve human health and wellbeing. Modern marketplaces induce competition between food manufacturers and force them to produce food products according to consumer-tailored specifications (e.g., products for vegetarians). Recently, the challenges for the food industry arise from the increasing public interest in the availability of “natural” or “healthy” food ingredients where only naturally available materials such as carbohydrates or proteins are used. For instance, replacement of gelatin (animal origin) that has been utilized for structuring of confectionery products over decades or the elimination of synthetic surfactants (e.g., Tweens) from formulations of food emulsions are some examples of these demands. Therefore, the investigation of novel biopolymer structures and sources that can replace existing ingredients is ongoing.

Pectin is widely utilized across food and pharmaceutical industries as a gelling agent (e.g., jams, jellies, gums), stabilizer (e.g., acidified dairy products) or delivery agent (e.g., flavors, vitamins). The structural diversity of pectin results in a multitude of functional properties and pectin is considered as a potential multifunctional food or as a pharmaceutical ingredient. Pectin applicability is widely governed by the type and availability of fruit from which commercial grade pectin can be manufactured. This indicates that only sustainable plant sources could be considered for development and manufacturing of novel pectin. Moreover, extraction should be inexpensive and yield reasonable quantities of pectin. Okra plant could be considered as a potential source of pectin. Okra (*Abelmoschus esculentus L.*) is an economically important and sustainable vegetable crop grown in tropical and sub-tropical parts of the world. The worldwide production of okra is estimated to be around 8.7 million tonnes grossing more than \$4 billion (FAOSTAT, 2013). Okra water-extracts have a

slimy texture due to its polysaccharide content and were suggested as a promising source of texture modifiers for complex food matrices.

Since chemical composition of pectin is something that restrains its functional properties and therefore its application in various formulations, the first experimental chapter of this thesis attempts to evaluate the effect of extraction conditions on chemical and macromolecular characteristics of okra pectin. An experimental design was developed to study the influence of different parameters (e.g., pH, temperature, time, number of extraction, ethanol volume) on extraction yield of pectic substances from fresh okra pods. Structurally different polysaccharides could be extracted according to the conditions of pH, time and temperature. Therefore, the extractions of pectic substances from okra were performed with two acidic media (pH 2.0 and 6.0) in order to facilitate the conversion of insoluble pectic substances (protopectin) into soluble pectins and yield polysaccharides with individual characteristics in terms of galacturonic acid and neutral sugars content, degree of methylation and acetylation and molecular weight distributions. Extracted pectins were analysed in terms of total sugars, galacturonic acid, protein and ferulic acid contents with the following measurements of degree of esterification and acetylation. Physicochemical properties of extracted pectins were assessed using FT-IR spectroscopy, NMR spectroscopy, size exclusion chromatography (SEC) and dilute solution rheology. The given extraction methodology resulted in isolation of a high molecular weight LM-pectin with high degree of acetylation and branching of the side chains.

Following the isolation and characterization step the evaluation of okra pectin structure-function relationships was investigated. The degrees of methyl esterification and acetylation have a profound impact on the functional properties of pectin such as gelling or colloidal stabilizing capacity and therefore determine the potential

applications in food formulations. The first system to be examined was okra pectin/calcium matrix at pH 3.0, the gelation conditions that are typically applied for LM-pectins. The results indicated that okra pectin is a non-gelling pectin and its inability for structuring was mainly attributed to the presence of a high amount of acetyl groups that restrict the formation of hydrogen bonds between the carboxyl groups of galacturonic acid and calcium ions. It has been previously reported that non-gelling acetylated pectin from sugar beet exhibits interfacial activity and could be utilized as emulsifying agent in colloidal dispersions.

Following these observations emulsifying properties of isolated okra pectins have been investigated in model oil-in-water systems. Resulting okra pectin-stabilized emulsions were analysed by means of static light scattering to evaluate the droplet size distribution (PSD), ζ -potential measurements, rheometry and confocal laser scanning microscopy. Interfacial composition analysis was also performed by determining protein, pectin and acetyl contents at the of oil-water interface. It has been shown that both okra pectins exhibit interfacial activity by producing stable emulsions for a period of 30 days. However, okra pectins extracted at high pH have greater emulsion stabilizing capacity than those extracted at low pH as revealed by particle size distribution and long-term stability measurements. Moreover, the emulsifying capacity of okra pectin was affected by pH as evidenced by the formation of stable emulsions only at pH below its pK_a . The pH sensitivity of okra pectin could be successfully utilized for formulation of emulsion-based targeted delivery system of bioactive compounds. An advantage of such system would be the resistance to acidic pH of stomach with consequent release of bioactive compound in the small intestine where pH is slightly alkaline.

1.2 BIOPOLYMERS

Colloids are categorized into two groups: hydrophobic and hydrophilic. Hydrophilic colloids are easily miscible with the solvent and thermodynamically stable whereas hydrophobic colloids are not easily miscible and are thermodynamically unstable. Over a decade, macromolecules have been erroneously classified as associated colloids or lyophilic (e.g., micelle) colloidal systems (Sun, 2004). Colloids are dispersions of small molecules formed as a result of the interplay between attractive vs. repulsive forces and are highly dependent on the physical environment (e.g., solvent). Modifications of solvent properties may result in irreversible changes of colloidal dispersions. In contrast, macromolecules are composed of repeating units that are connected by covalent bonds. Changes in solvent nature have an impact on properties of macromolecules, but they do not cause structure degradation unless its covalent bonds are broken. Macromolecules are divided into two groups: synthetic and biological polymers. Biopolymers are polymers produced by living organisms and composed of a diverse range of monomers (e.g., carbohydrates, amino acids etc.). In contrast to synthetic polymers (e.g., polyethylene, polyvinyl chloride, or polystyrene) that have small number of identical repeating units, biopolymers are complex molecular assemblies that adopt precise and defined three-dimensional shapes and structures (Sun, 2004). Biopolymers can be classified in three groups, depending on the nature of the repeating unit they composed of and the structure of biopolymer formed: (i) polynucleotides, which are long polymers composed of >13 nucleotide monomers covalently bonded in a chain, (ii) polypeptides which are polymers of amino acids bound by peptide bond, and (iii) polysaccharides that are complex carbohydrates in which simple sugars are linked through glycosidic bonds (McMurry, 2008).

Polysaccharides and proteins that are currently widely utilized in food and pharmaceutical industries to accomplish a number of functions, such as thickening and gelling of aqueous solutions, stabilizing of dispersions, inhibiting of ice and sugar crystal formation, delivering and release of bioactive ingredients, are referred to as “food hydrocolloids” (Williams & Phillips, 2000). Protein or polysaccharide-based formulations are suitable for many industrial applications due to their biodegradability, biocompatibility and high potential to be modified to achieve the desired chemical and physical properties. Sources of commercially available hydrocolloids include botanical (e.g., cellulose, gum arabic, starch, pectin, guar gum), algal (e.g., carrageenan, alginate), microbial (e.g., xanthan gum, gellan gum) and animal (e.g., gelatin, caseinate, whey protein, chitosan) origin (Williams & Phillips, 2000). Polysaccharides composed of only one type of monomer are defined as homopolysaccharides (e.g., starch, cellulose), but those composed of different types of monomers are referred as heteropolysaccharides (e.g., xanthan, gum arabic and pectin). The functional properties and application field of each biopolymer are dictated by a range of physicochemical characteristics, such as molecular weight, electrical charge, conformation, flexibility, hydrophobicity and molecular interactions (BeMiller, Whistler & Barbalowm, 1993). Conformational diversity, presence of functional groups, formation of high viscosity solutions and the high temperature stability of polysaccharides makes them versatile components to stabilize a wide variety of food and pharmaceutical systems.

1.3 CHEMICAL STRUCTURE OF PECTIN

Pectins belong to family of covalently linked galacturonic acid-rich plant cell wall polysaccharides. They are detected in primary walls of dicots and non-graminaceous monocots with ~35%, in grass and other commelinoid primary walls

(~2-10%) and in walls of woody tissues (~5%) (Ridley, O'Neill & Mohnen, 2001). Pectin is abundant in walls that surround growing and dividing cells, walls of cells in the soft parts of the plant, and in the middle lamella and the cell corners (Mohnen, 2008). In plants, pectins accomplish vital biological functions, such as growth, morphogenesis, wall structure, cell expansion, cell-cell adhesion, signaling, binding of ions, growth regulators and enzyme modulation, pollen tube growth, leaf abscission and fruit development (Mohnen, 2008). The contribution of pectin to the firmness and structure of plant tissues is similar to that of collagen in tissues of animal origin. Some pectin molecules are covalently bonded or tightly associated with other types of wall polysaccharides, such as hemicelluloses and cellulose (McCann & Roberts, 1991; Mohnen, 2008). Hemicelluloses are a group of complex polysaccharides with a backbone composed of β -(1 \rightarrow 4)-linked pyranosyl residues with an equatorial configuration at C1 and C4 (Caffall & Mohnen, 2009). Hemicelluloses comprise of xyloglucans, xylans and mannans. It has been shown that a cellulose-hemicellulose network is embedded in a matrix of pectic polysaccharides, which form a hydrated and cross-linked three-dimensional network (Zandleven, et al., 2007).

Early work on carbohydrate chemistry of plant cells used the umbrella term “pectic substances”, which included pectin and other gel- and slime-forming polysaccharides, such as xyloglucans (Sinnott, 2007). Modern usage confines the word “pectin” to a series of polysaccharides based on poly- α -(1 \rightarrow 4)-galacturonan. Therefore, pectin is a group of heteropolysaccharides with backbone mainly composed of D-galacturonic acid units (D-GalA, ~70%) bonded with α -(1 \rightarrow 4) glycosidic linkages. Similarly to other plant polysaccharides, pectin shows a wide variety of structures and has a polydisperse nature (Sriamornsak, 2003). The diversity

of pectin chemical structures and molecular weight depends on the source, plant ripening state and extraction conditions applied. The structural classes of pectic polysaccharides involve homogalacturonan (HG), rhamnogalacturonan I (RG-I), rhamnogalacturonan II (RG-II), xylogalacturonan (XGA), and apiogalacturonan (AGA). The apiogalacturonan was found in the walls of aquatic plants such duckweeds (*Lemnaceae*) and marine seagrasses (*Zosteraceae*) with D-apiose residues 2,3-linked to homogalacturonan (Caffall & Mohnen, 2009). The xylogalacturonan has a HG backbone (α -(1 \rightarrow 4)-linked D-galacturonic acid) substituted by β -D-xylose at the O-3 position and has been detected in cell walls of marine seagrasses, cotton seeds, watermelons, peas, apples, and soybeans (Zandleven, Sørensen, Harholt, Beldman, Schols, Scheller & Voragen, 2007). Complexes of RG-I, AG-I, and arabinan are often referred to as the “hairy” regions whereas HG is defined as “smooth”.

1.3.1 Homogalacturonan (HG)

Homogalacturonan (HG) is the most abundant polymer in pectins and it comprises about ~65% of pectin in plant cell walls (Mohnen, 2008). HG is composed of long chains of linear 1,4-linked α -D-GalpA residues and some of the carboxyl groups are partially methyl-esterified at C-6 position and/or acetyl-esterified at O-2 and/or O-3 positions of GalpA depending on plant species (Figure 1.1) (Sinnott, 2007). Those HGs with >50% methyl-esterification of GalpA residues are described as high methyl-esterified HGs and those with <50% are defined as low methyl-esterified HGs. The methyl esterification of linear HG units determines the industrial applicability (gelling agent) of pectin, which depends not only on the amount of methyl-esterification, but also on distribution of methyl groups on the HG backbone.

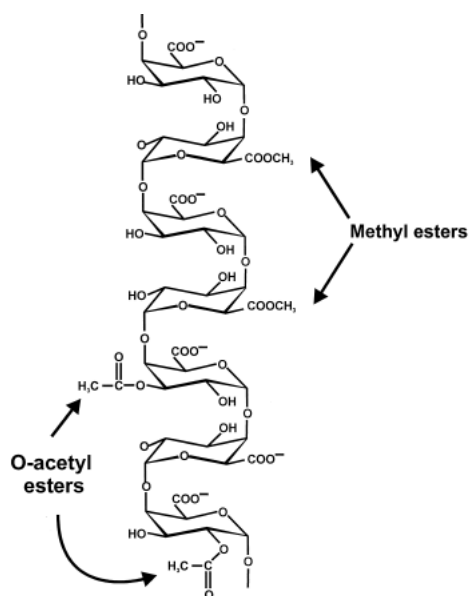


Figure 1.1. The primary structure of homogalacturonan (Caffall & Mohnen, 2009).

1.3.2 Rhamnogalacturonan II (RG-II)

Rhamnogalacturonan II (RG-II) is a minor pectic component of plant cell walls and represents about 0.5 to 8% in dicots, non-graminaceous, monocots, and gymnosperms, and less than 0.1% in primary walls of commelinoid monocots (Matsunaga, Ishii, Matsunamoto, Higuchi, Darvill, Albersheim & O'Neill, 2004). RGs-II have been detected in the cell walls of many tissues of edible plants including apple, kiwi, carrot, tomato and radish (Cui, 2005). RG-II is not structurally related to RG-I since it does not have rhamnogalacturonan backbone as RG-I. However, Rha residues are represented in RG-II structure to a lower extent and mainly in the side-chains of RG-II rather than in backbone. RG-II is described as a stretch of HG backbone, approximately seven to nine 1,4-linked α -D-GalpA residues with four long side-chains attached (labeled A-D, Figure 1.2) (Caffall & Mohnen, 2009). The structure of RG-II is highly complex with 12 different types of sugars and over 20 different linkages.

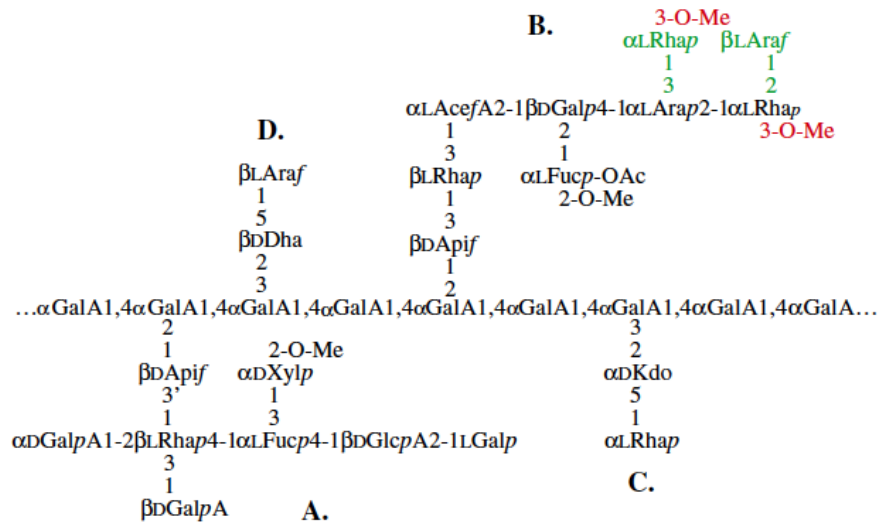


Figure 1.2. The structure of rhamnogalacturonan II (O'Neill, Ishii, Albersheim & Darvill, 2004).

A number of uncommon sugars occur in RG-II structure including 2-keto-3-deoxy-D-manno octulosonic acid (Kdo), 2-keto-3-deoxy-D-*lyxo*-heptulosaric acid (Dha), apiose, 2-O-methyl xylose, 2-O-methyl fucose and aceric acid (Caffall & Mohnen, 2009; Stevenson, Darvill & Albersheim, 1988). Despite its complexity, the RG-II structure is largely conserved across plant species. RG-II molecules are known to self-associate, forming RG-II dimers *via* a boron diester bond that was first demonstrated in sugar beet pectin (Caffall & Mohnen, 2009).

1.3.3 Rhamnogalacturonan I (RG-I)

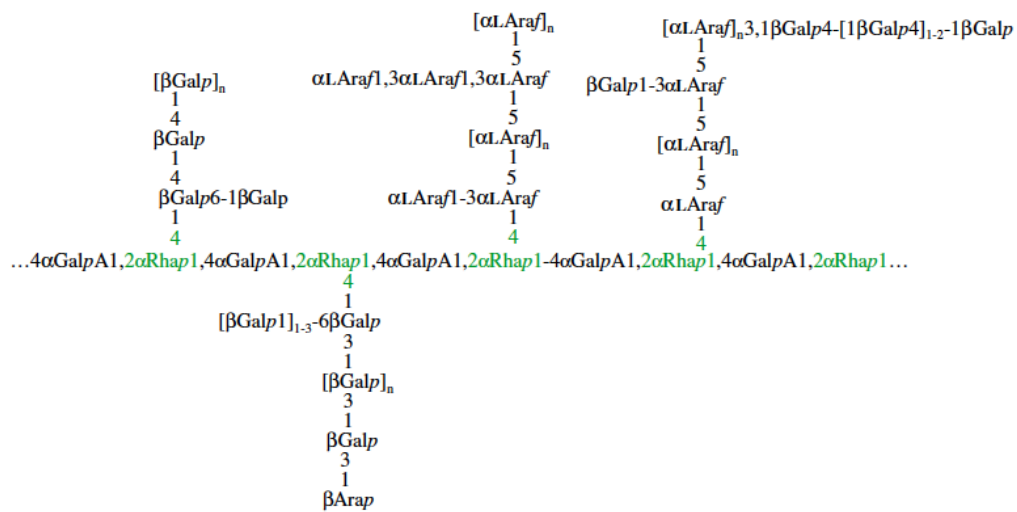
Another constituent polysaccharide of pectin is rhamnogalacturonan I (RG-I) that represents around 20-35% of pectin in plant cell wall (Obro, Harholt, Scheller & Orfila, 2004). Its backbone is composed of the repeating disaccharide galacturonic acid and rhamnose [α -(1,2)-D-GalpA- α -(1,4)-L-Rhap] $_n$ where n can be larger than 100 (Figure 1.3a). The RG-I backbone is partially substituted at O-4 and/or O-3 positions of α -L-Rhap residues with polymeric side-chains predominantly composed of α -(1,5)-L arabinans and β -(1,4)-D galactans, arabinogalactans I (AG-I), arabinogalactans II

(AG-II) and galacto-arabinans (Mohnen, 2008). The side-chains can be a single unit as [β -D-Galp-(1 \rightarrow 4)], but also polymeric, such as arabinan and arabinogalactan I (AG-I). The arabinans consist of a 1,5-linked α -L-Araf backbone, which can be substituted with α -L-Araf-(1 \rightarrow 2)-, α -L-Araf-(1 \rightarrow 3)- and/or α -L-Araf-(1 \rightarrow 3)- α -L-Araf-(1 \rightarrow 3)- side chains depending on the pectin source (e.g., sugar beet, soybean) (Ridley, O'Neill & Mohnen, 2001). It has been also shown that the galactan and arabinan side-chains of RG-I are the most mobile parts of the pectin molecule with the higher degree of mobility exhibited by arabinan (Sinnott, 2007). AG-I is composed of a 1,4 linked β -D-Galp backbone and α -L-Araf are attached to the O-3 position of galactosyl residues (Ridley, O'Neill & Mohnen, 2001). The galactan chain of AG-I can have branches of one or more Araf residues or single terminal Arap residues. Arabinogalactans II (AG-II) are predominantly associated with proteins (arabinogalactan proteins or AGPs), and its participation in a pectin complex is still debatable. Pectin and AG-II often seem to co-extract and are subsequently difficult to separate from each other, suggesting that they can be covalently linked (Vincken, 2003). AG-II is composed of 1,3-linked β -D-Galp backbone, containing short side chains of α -L-Araf-(1 \rightarrow 6)-[β -D-Galp-(1 \rightarrow 6)]_n, where galactosyl residues of the side-chains can be substituted with α -L-Araf-(1 \rightarrow 3) residues (Vincken, 2003).

The proportion and distribution of branched Rhap residues typically varies in the range of 20-80% depending on the source of polysaccharide (Visser & Voragen, 1996). This also results in a heterogeneous structure of RG-I arabinan and galactan side-chains from source to source, something that has been observed for pectic polysaccharides from the walls of apple, sugar beet, soybean, persimmon, and potato (Duan, Wang, Dong, Fang & Li, 2003; Huisman, Brüll, Thomas-Oates, Haverkamp, Schols & Voragen, 2001; Obro, Harholt, Scheller & Orfila, 2004; Sakamoto & Sakai,

1995; Schols & Voragen, 1996). However, unbranched RG-I molecules have been also reported in seed mucilages (Western, Young, Dean, Tan, Samuels & Haughn, 2004). The RG-I backbone can be acetylated at *O*-2 and/or *O*-3 positions of GalpA or at *O*-3 position of Rhap residues depending on the plant species (Sengkhampan, Bakx, Verhoef, Schols, Sajjaanantakul & Voragen, 2009; Vincken, 2003).

a)



b)

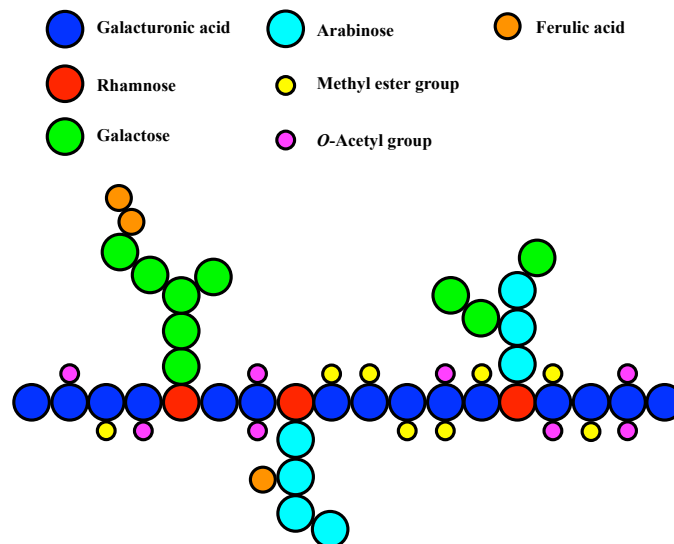


Figure 1.3. The structure of rhamnogalacturonan I (a) (Caffall & Mohnen, 2009) and general structure of pectin (highly simplified) (b).

Typically, carboxyl groups of α -D-GalpA residue are not methyl-esterified in RG-I, however RG-I fraction isolated from flax has been reported to contain methyl esters (Rihouey, Morvan, Borissova, Jauneau, Demarty & Jarvis, 1995). Many plant cell walls contain phenolic acids that are ester-linked to pectic polysaccharides. The presence of feruloylated pectins has been reported in spinach, sugar beet, glasswort, quinoa and butternut (Fissore, Rojas, Gerschenson & Williams, 2013; Fry, 1982; Renard, Champenois & Thibault, 1993; Renard, Wende & Booth, 1999; Rombouts & Thibault, 1986). In beet and spinach cell walls, ferulic acids are linked to L-Araf residues of the main core of α -(1–5)-linked arabinan chains at the O-2 position and to D-Galp residues of the main core of β -(1–4)-linked galactan chains at O-6 position.

1.3.4 Macromolecular organization of HG, RG-I and RG-II in the primary wall

The fine structure of pectin has been widely investigated, however how these structural elements are incorporated in the macromolecular structure is still a matter of debate. The endo-polygalacturonase (EPG) treatment of pectic polysaccharides (O'Neill, Warrenfeltz, Kates, Pellerin, Doco, Darvill & Albersheim, 1996) demonstrated that HG, RG-I, and RG-II backbones are covalently cross-linked. It has been suggested that the RG-I and RG-II backbones are continuous with the HG backbone indicating the presence of a macromolecular structure with specific domains, however, the arrangement of these domains *in vivo* has still not been reported (Caffall & Mohnen, 2009). The pectic network is based on multiple levels of cross-linking that include, but are not limited, to backbone glycosidic linkages, calcium crosslinking, borate ester crosslinking, and covalent linkages to phenolic and possibly other compounds (Caffall & Mohnen, 2009). The HG segments of pectin self-associate depending on the degree of methyl-esterification through the calcium cross-linking and RG-I side-chains could be cross-linked to other wall components

such as xylans, xyloglucans, proteins, and lignins. RG-II domains form crosslinks to other RG-II molecules through borate diester linkages. Alternative models of macromolecular structure of pectin have been also proposed, where HG was depicted as a side chain of RG-I (Vincken, 2003).

HG, RG-I, and RG-II are typically isolated from cell by treating the walls with aqueous buffers or calcium chelators. Extracted polysaccharides have high molecular weight ($> 200 \text{ g mol}^{-1}$) and therefore, cannot be separated from each other by size-exclusion chromatography (Ridley, O'Neill & Mohnen, 2001). Therefore, most of pectic polysaccharides isolated using conventional extraction methods are polydisperse and represent complex mixtures of HG, RG-I and RG-II rather than one uniform polysaccharide species (Figure 1.3b). Typical molecular weight distribution of polydisperse mixture of pectin will be shown in Chapter 2. Isolation of HG, RG-I or RG-II enriched fractions can be performed using enzymatic treatment (e.g., polygalacturonases, lyases) of high molecular weight material. Generally, the abundance of “smooth” and “hairy” pectic polysaccharides, and distribution and length of side-chains varies considerably from species to species and is controlled by the extraction conditions. It has been reported that pectic polysaccharides isolated from apple, citrus and sugar beet are primarily composed of HG, whereas those isolated from soybean, linseed mucilages, green tea leaves and okra (Chapter 2) mainly contained RG-I (Ele-Ekouna, Pau-Roblot, Courtois & Courtois, 2011; Leroux, Langendorff, Schick, Vaishnav & Mazoyer, 2003; Muralikrishna, Salimath & Tharanathan, 1987; Nakamura, Furuta, Maeda, Nagamatsu & Yoshimoto, 2001).

1.4 ISOLATION OF PECTIN

Over the past decade, various novel extraction methods of pectic polysaccharides have been introduced and investigated to satisfy the demand for more

efficient and/or environmentally friendly pectin production. The techniques include the isolation of pectins with enzymes (e.g., polymethylgalacturonases, polygalacturonases, polygalacturonate lyases), electromagnetic induction heating, and microwave- and ultrasound- assisted isolation (Bagherian, Zokaee Ashtiani, Fouladitajar & Mohtashamy, 2011; Kashyap, Vohra, Chopra & Tewari, 2001a; Kashyap, Vohra, Chopra & Tewari, 2001b; Wang, Chen, Wu, Wang, Liao & Hu, 2007). The more conventional methods of pectin cell wall extraction are cold and/or hot aqueous, buffers, use of chelating agents (e.g., potassium-oxalate), diluted acids (e.g., HCl) or diluted sodium hydroxide solutions. Although the various alternative extraction methods have been recently proposed, the isolation of pectin until now is mainly performed using hot acid (nitric acid, sulfuric acid and hydrochloric acid) treatment in combination with high temperatures between 70 - 90°C. The pH varies between 1.5 and 2.5 and the time of extraction depends on raw material (e.g., efficiency of protopectin release), desired chemical composition of pectin and manufacturer's individual needs. Moreover, the chemical composition of isolated pectin also varies with respect to the extractant used. It has been shown (Visser & Voragen, 1996) that pectins isolated from various plant sources (e.g., leek, pineapple, sugar beet, cucumber, lemon, fennel) appear to be rich in HG when isolated with mild agents (e.g., water or K-oxalate) and become considerably richer in RG-I when extracted by stronger agents (e.g., HCl, NaOH). Following the hot extraction step, the precipitation of pectin from extraction liquor is performed with organic solvent (e.g., methanol, ethanol or isopropanol). Therefore, the pectin extract obtained by commercial acid extraction is composed of those polymer molecules that are soluble at a certain pH and time-temperature regime. However, those harsh acidic conditions of pectin extraction particularly during longer times could contribute to the

depolymerisation of pectin. The isolation of pectic substances from cell walls is pH sensitive and could be also performed in the presence of basic extraction medium. The modification of pH of extraction results in pectins with a different degree of methyl-esterification (DM) and therefore, functional properties. Extractions performed at high pH typically result in isolation of pectin with low DM due to the saponification of the ester groups. In contrast, acidic extractions yield pectins of high DM. Previous work on isolation of pectin reported the remarkable effect of extraction time, temperature, pH, type of acid, number of extraction cycles, the ratio of water to raw material and volumes of organic solvent on the yield and chemical composition of pectin from various plant sources, such as apple and peach pomace, mango peel, okra pods and passionfruit (Kliemann, de Simas, Amante, Prudêncio, Teófilo, Ferreira & Amboni, 2009; Kumar & Chauhan, 2010; Pagan, Ibarz, Llorca & Coll, 1999; Samavati, 2013; Sudhakar & Maini, 2000).

1.5 PECTIN CONFORMATION

The molecular architecture of polysaccharides has a profound effect on the functional properties and therefore, evaluation of shapes and conformational diversity is a critical step in polysaccharide analysis. Polysaccharide chains consist of many structural units and depending on the nature of monomer could be classified as homo- or hetero-polysaccharides as described in section 1.2. Biopolymers are commonly used in the form of solutions where under the effect of Brownian motion their physical properties change and this results in modification of molecule dimensions and shapes (Cui, 2005). Solvent molecules collide with individual monomer units and therefore cause a continuous change in conformation of the biopolymer. Biopolymers may exist in many different conformations (compact, extended, random, rod and sphere) and their occurrence is restricted by the chemical bonds in the molecule. A

molecule may possess a variety of structures, however, only certain conformations are possible due to the interference and restrictions imposed by rotational angles under certain conditions. In polysaccharides, the global conformation primarily depends on rotations about the glycosidic linkages due to the limited flexibility of pyranose ring and insufficient influence of attached groups on the conformational space of molecule (Perez, Mazeau & Herve du Penhoat, 2000). Therefore, the main source of polymer flexibility originates from the variation of torsion angles of the glycosidic linkages. The monosaccharide units in polysaccharides rotate about the glycosidic linkage with two torsion angles (φ , ψ). Angle φ is located between the anomeric carbon and the oxygen of the glycosidic linkage of the first monomer, and ψ between the oxygen of the glycosidic linkage and the non-anomeric carbon of the second monomer (Figure 1.4). The formation of 1→6 glycosidic linkage between two monosaccharides introduces an extra torsion angle (ω) about C-5 and C-6 bond (Kontogiorgos, 2014). Those angles increase the freedom of a molecule to adopt the most stable conformation, which is typically the one with the lowest energy and referred as secondary structure (e.g., ribbon or helix). In case of branched RG-I polysaccharide, three degrees of rotational freedom (φ , ψ , ω) are observed for arabinan side-chains making them the most mobile parts of pectin molecule (Figure 1.4) (Sinnott, 2007). However, the influence of α -L-rhamnosyl residues, methoxyl and acetyl groups on the overall conformation of pectic backbone has not been shown (Perez, Mazeau & Herve du Penhoat, 2000).

Polysaccharides can adopt either ordered or disordered conformations. Ordered conformations are characterized by the fixed values of torsion angles due to the complex interactions between sugar residues (Cui, 2005). Overall, the shape of a polysaccharide chain will be dictated by the geometrical relationship within each

monosaccharide unit (e.g., β -(1 \rightarrow 4) is ribbon-like, β -(1 \rightarrow 3) and α -(1 \rightarrow 4) is a hollow helix, β -(1 \rightarrow 2) is a crumpled ribbon). Therefore, homopolysaccharide chains could adopt ribbon-like (e.g., cellulose, xylan, mannan), hollow helix (e.g., amylose, curdlan) and crumpled (e.g., pectin RG-I sequences) types of conformations. Some anionic (1 \rightarrow 4)-linked polysaccharides, such as poly- α -D-galacturonic acid sequences in pectin can adopt buckled ribbon conformation. This type of chain arrangement may leave interstices when they pack together that are usually stabilized by accommodating metal cations (e.g., Ca^{2+}) (Cui, 2005). This type of ribbon-ribbon association is described as the so called egg-box model and some polysaccharides, such as low-methoxylated pectins and alginates form ordered structures (e.g., gels) *via* this model (Jarvis & Apperley, 1995).

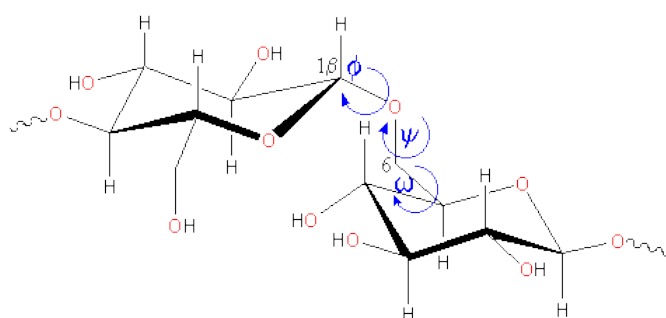


Figure 1.4. Model of torsion angles (ϕ , ψ and ω) in a polygalacturonate chain.

A number of polysaccharides do not show sequence regularities and are composed of alternating units of different monosaccharides. It has been shown that most polysaccharides (e.g., alginates, κ -carrageenan) even with a certain degree of regularity, will adapt a random coil conformation in dilute solutions (Cui, 2005). However, the biopolymer chains with certain structural regularities could form ordered conformations under specific conditions (e.g., high concentration, T , pH,

binding agents). In contrast, irregularly sequenced polysaccharides can adapt only random coil conformation. Pectins in a solid state mainly exist in the form of right-handed helices that are stabilized by intra-molecular and inter-molecular hydrogen bonding (Morris, Rees, Thom & Welsh, 1977). In solutions, pectin adopts a random coil conformation with a certain degree of rigidity. The term “random coil” is often used to describe the unperturbed shape of ideal polymer chain in dilute solutions (Sperling, 2006). The simplest mathematical model of an ideal polymer chain in a space is the freely jointed chain (Rubinstein & Colby, 2003). It has n segments, each of length L , joined in a linear sequence, where all orientations have equal probability (Walstra, 2003). Every possible conformation of an ideal chain can be mapped onto a random walk model. If the length of each step is constant and the direction of each step is independent of all previous steps, the trajectory of this random walk is one conformation of an ideal chain (Sperling, 2006). The dimensions of linear chains are typically characterized by mean-square end-to-end distance (Flory radius) (r_m , Eq. 1). However, branched or ring biopolymers cannot be treated in the same way and the radius of gyration (r_g , Eq. 2) is used to characterize biopolymers of any architecture in the absence of any physical interference (idealized conditions).

$$r_m = Ln^{0.5} \quad (1)$$

$$r_g = 0.41Ln^{0.5} \quad (2)$$

The qualitative models used for the characterization of ideal chain conformation are oversimplified and based on the model of polymer chain that has no volume and short (steric hindrances) or long-range interactions between polysaccharide segments. The real chains have volume and cannot cross themselves in the space and therefore, cannot “walk” randomly. As a result, the statistical model of self-avoiding random walk that includes the excluded volume parameter (V_e) (same

chain segments do not occupy the same space) is used to adjust the random coil concept for the characterization of real chains. Interactions and preferred configuration of polysaccharide chains at the molecular level depend most commonly on the quality of the solvent and temperature of the system. In a good solvent, solvent-segment interactions are greater than chain segment-segment interactions and polysaccharide molecule follows self-avoiding random walk resulting in higher solubility and more extended conformation (Cui, 2005). In contrast, polymer-polymer attraction is dominant in poor solvents resulting in aggregation and phase separation. The θ -temperature differentiates the poor ($T < T_\theta$) and good ($T > T_\theta$) solvents, and defines θ solvent. In θ solvent, the net excluded volume is zero, because of the cancelation between the short-range and long-range interactions (Rubinstein & Colby, 2003). Therefore, the chains of polymer in a θ solvent have nearly ideal conformations at all concentrations. Polydispersity, stiffness, polyelectrolyte nature and branching of many natural polysaccharides are additional parameters that also control the dimensions of random coil conformation. A real polysaccharide chain has fixed bond angles indicating lower freedom of orientation and therefore, natural polysaccharide chains are stiffer than the ideal chains. Polysaccharides can adopt a wide variety of orientations that leads to a great diversity of chain conformations. For instance, pectins, xanthan, κ -carrageenan adopt elongated conformations, gellans form short rods whereas arabic gum has a globular structure.

1.6 PHYSICAL PROPERTIES OF PECTIN

1.6.1 Pectin solubility

Molecular architecture and molecular weight are two important parameters that determine polysaccharide solubility. Neutral polysaccharides are less soluble than polyelectrolytes and solubility typically increases with reduced regularity of

molecular structure. For instance, linear polysaccharides with high degree of regularity, such as cellulose are insoluble in hot or cold water and therefore, chemical modification is required in order to produce derivatives (e.g., hydroxymethyl, carboxymethyl cellulose) with improved chain solvation and swelling properties (Belitz, Grosch & Schieberle, 2009). Monovalent cation pectic salts (e.g., sodium and potassium pectates) and pectic acids are typically soluble in water whereas di- and trivalent cation pectic salts are almost insoluble in water. Higher solubility of pectic polysaccharides is attributed to the heterogeneous structure (HG, RG-I, RG-II), the presence of hydrophilic carboxyl (degree of methyl esterification) and hydroxyl groups that interact with water mainly through hydrogen bonding. Other factors affecting pectin solubility kinetics include pH of solution, DM, branching of side-chains, solution concentration, presence of counterions and molecular weight.

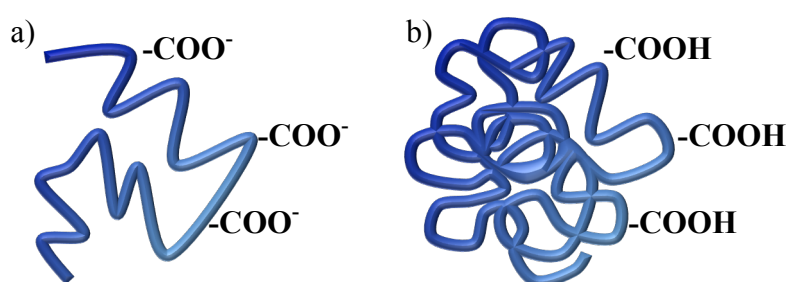


Figure 1.5. Pectin chain conformations a) extended ($\text{pH} > \text{p}K_a$), b) compact ($\text{pH} < \text{p}K_a$).

At high pH values ($\text{pH} > \text{p}K_a$) carboxyl groups of pectin are ionized. Therefore, biopolymer chains are highly hydrated and extended due to the electrostatic repulsions between the carboxylate anions. The number and distribution of negative charges is determined by the degree of methyl esterification and degree of blockiness (DB) with methyl groups. The ionization of carboxylic groups decreases with pH ($\text{pH} < \text{p}K_a$) and consequently promotes chain-to-chain associations.

Therefore, the absence of repulsion results in higher viscosity of pectin solutions and formation of pectin aggregates. The addition of salts of monovalent cations to pectin solutions results in viscosity reduction due to the suppression of electrostatic repulsions. In contrast, increase in viscosity values of pectin solutions is observed with addition of co-solutes, such as sucrose, dextrose and maltose. The co-solutes compete for water with polysaccharides. Therefore, interactions between polysaccharide molecules become greater than polysaccharide-solvent interactions leading to the increase in solution viscosity. The pH at which 50% of galacturonic acid is dissociated (pK_a) varies depending on the DM and typically is in the range of 3.55 – 4.10 for 0% DM and 65% DM, respectively (Sriamornsak, 2003). Pectic polysaccharides typically have high molecular weights ($50 - 700 \times 10^3 \text{ g mol}^{-1}$) something that hinders the dissolution rate of pectin. It has been reported that pectin molecules associate in solution and form stiff or segmented rods through non-covalent interactions (Thakur, Singh, Handa & Rao, 1997). Moreover, pectin molecules have a tendency to form supramolecular aggregates when dispersed in water and the probability of aggregation depends on pH and ionic strength of solution. The presence of pectin aggregates results in molecular weight overestimation particularly when measured with light scattering techniques. The dissociation of aggregated network is typically performed by addition of hydrogen bond breakers. It has been also shown that the strength of pectin aggregates depends on the amount of methyl-esterified groups and stronger aggregates are formed in the case of LM-pectins. Stronger aggregation of LM-pectins was attributed to the higher amount of deesterified carboxyl groups than in HM-pectin that creates more hydrogen bonds and therefore stronger aggregates. A typical pectin dissolution scenario includes the following steps: 1) solvent wets the pectin, 2) solvent diffuses into the polymer, 3) polymer

swells, 4) polymer diffuses out of the swollen mass into the solvent (Sperling, 2006). Slow solubility kinetics of pectins is explained by the fact that the disentanglement, swelling and subsequent diffusion of pectin to the bulk solution takes longer time compared to that of polymers with smaller molecular weights.

1.6.2 Molecular weight distributions and averages

Molecular weight (Mw) and molecular weight distributions (MwD) are fundamental characteristics of polysaccharides and in combination with chain conformations can be utilized for the modelling of mechanical and rheological properties of pectins. Molecular weight distributions vary depending on the botanical source of pectin and extraction condition (temperature, time, extraction medium and pH). Pectic polysaccharides are polydisperse, indicating that each polymer population composed of chains of different monosaccharide composition or length giving a distribution of molecular weights as discussed in section 1.3.4. Molecular weight of pectic polysaccharides is typically described by molecular averages, such as number average molecular weight (M_n), weight average molecular weight (M_w), z-average molecular weight (M_z), and viscosity average molecular weight (M_v) that are given by:

$$M_n = \frac{\sum_{i=1}^{\infty} M_i n_i}{\sum_{i=1}^{\infty} n_i} = \frac{\sum_{i=1}^{\infty} c_i}{\sum_{i=1}^{\infty} c_i / M_i} \quad (3)$$

$$M_w = \frac{\sum_{i=1}^{\infty} M_i^2 n_i}{\sum_{i=1}^{\infty} M_i n_i} = \frac{\sum_{i=1}^{\infty} M_i c_i}{\sum_{i=1}^{\infty} c_i} \quad (4)$$

$$M_z = \frac{\sum_{i=1}^{\infty} M_i^3 n_i}{\sum_{i=1}^{\infty} M_i^2 n_i} = \frac{\sum_{i=1}^{\infty} M_i^2 c_i}{\sum_{i=1}^{\infty} M_i c_i} \quad (5)$$

$$M_v = \left(\frac{\sum_{i=1}^{\infty} M_i^{1+\alpha} n_i}{\sum_{i=1}^{\infty} M_i n_i} \right)^{1/\alpha} = \left(\frac{\sum_{i=1}^{\infty} M_i^{\alpha} c_i}{\sum_{i=1}^{\infty} c_i} \right)^{1/\alpha} \quad (6)$$

, where n_i is number of molecules, c_i concentration and M_i molecular weight.

The choice of the molecular weight averages depends on the characteristics of polymer that are of primary interest. For instance, number average molecular weight (M_n) typically represents the chain length of biopolymer and highly sensitive to small molecules present in polymer mixture (Cui, 2005). Moreover, M_n is frequently used in the examination of thermodynamic properties of polymer material. The weight average molecular weight (M_w) describes the size of the polymer chain and is more sensitive to large polymer molecules. The M_z is typically utilized for the evaluation of elasticity of polymer melts. The viscosity average molecular weight (M_v) is based on the measurements of intrinsic viscosity calculated using Mark-Houwink relationship, which is discussed in the next section. The estimation of polysaccharide molecular weight includes not only molecular weight averages, but also distribution of molecular weights that are described by the mode of distribution and polydispersity. The ratio M_w/M_n is called polydispersity index (PDI) and varies in the range of 1.5 – 2.0 for natural polysaccharides (Sperling, 2006). Various techniques for molecular weight determination are available and vary in terms of information that is required for the statistical modelling in order to calculate molecular weight and information that can be obtained with the method. The most common techniques for Mw determination include static light scattering (LS), size exclusion chromatography (SEC), viscometry, sedimentation and membrane osmometry (Cui, 2005). Separation using size exclusion chromatography occurs on the basis of hydrodynamic volumes

and macromolecular characteristics such as M_w , M_n , R_g and polydispersity index can be determined.

1.6.3 Viscosity and flow properties of pectin solutions

The viscosity (η , Pas) of a fluid is a measure of its resistance to flow. It is defined as the ratio of applied shear stress (τ) to rate of shear strain ($d\gamma/dt$):

$$\eta = \frac{\tau}{d\gamma/dt} = \frac{\tau}{\dot{\gamma}} \quad (7)$$

A fluid that obeys Eq.7 is called a Newtonian fluid in which the viscosity is independent of the shear rate and all energy is dissipated as molecules slide past each other. A fluid that does not obey Eq.7 is called non-Newtonian fluid. The behaviour of a polymer solution is defined as shear thinning flow when its viscosity decreases with increasing shear rate. The opposite flow behaviour is called shear thickening. Dilute pectin solutions exhibit Newtonian flow. However, as the concentration increases to a critical point, shear thinning becomes dominant. The polysaccharide flow behaviour is explained in terms of pectin chain entanglements. As the pectin concentration is increased, the freedom of movement of the individual chains becomes restricted due to the increased number of entanglements. Therefore, longer time is required to form new entanglements to replace those disrupted by the externally imposed deformation (Hwang & Kokini, 1992). Moreover, increase in degree of branching of pectin results in higher shear rate dependency of viscosity (Hwang & Kokini, 1992). It is apparent that concentration influences polymer properties in solution and therefore, solutions are classified as dilute, semidilute and concentrated based on the polymer concentration. In the dilute concentration regime, each polymer behaves as an isolated chain and occupies a discontinuous hydrodynamic domain in the solution. Therefore, bulk properties of the polymer

solutions are determined by the macromolecular characteristics of individual polymer chains. As a result, the evaluation of fundamental molecular properties of polysaccharides such as chain conformation, molecular weight and intermolecular interactions are typically performed in dilute solutions ($c < c^*$). The increase of concentration to a critical point causes polymer chain crossover and entanglement. This concentration is called overlap or critical concentration (c^*) and the region above critical concentration is called semi-dilute ($c > c^*$). The critical concentration (c^*) depends on the volume occupied by each molecule and the differences in c^* between various pectin samples are attributed to the fluctuations in molecular weights and/or stiffness of polymer chains. In the semi-dilute regime polymer molecules cannot distribute themselves randomly over the solution volume and adjacent chains start to interpenetrate. Further increase of polymer concentration leads to a concentrated regime (c^{**}).

The ratio of the viscosity of the solution to that of the solvent is called relative viscosity (η_{rel}) (Eq. 8). Another associated term is specific viscosity (η_{sp}) and it expresses the incremental viscosity in the presence of the polysaccharide in solution (Eq. 9). Dividing η_{sp} by concentration c gives η_{sp}/c that corresponds to reduced viscosity (η_{red}) (Eq. 10) and expresses the capacity of a polymer to cause the solution viscosity to increase. A remaining term is inherent viscosity (η_{inh}), which is defined in Eq. 11. Similarly to η_{red} , η_{inh} is zero for pure solvent and increases with increasing concentration and therefore, η_{inh} also expresses the incremental viscosity due to the presence of the polymer in the solution. Extrapolation of both η_{red} and η_{inh} to zero concentration yields the intrinsic viscosity $[\eta]$. The $[\eta]$ is a measure of hydrodynamic volume occupied by the isolated polymer chains for a given polymer-solvent pair. Huggins and Kraemer equations (Eq. 12, 13) describe the dependence of η_{red} , η_{inh} and

$[\eta]$ with concentration in dilute solutions. K_H and K_K are the Huggins and Kraemer constants. Equations 12 and 13 form the theoretical basis for the determination of $[\eta]$ and typical Huggins-Kraemer plots used for determination of $[\eta]$ of biopolymer solution are shown in Figure 1.6.

$$\eta_{rel} = \frac{\eta}{\eta_s} \quad (8)$$

$$\eta_{sp} = \frac{\eta - \eta_s}{\eta_s} = \eta_{rel} - 1 \quad (9)$$

$$\eta_{red} = \frac{1}{c} \frac{\eta - \eta_s}{\eta_s} = \frac{1}{c} \eta_{sp} \quad (10)$$

$$\eta_{inh} = \frac{\ln \eta_{rel}}{c} \quad (11)$$

$$\eta_{red} = [\eta] (1 + K_H [\eta] c) \quad (12)$$

$$(\ln \eta_{rel}) / c = [\eta] (1 - K_K [\eta] c) \quad (13)$$

As it shown in Figure 1.6, both lines should extrapolate to the same point at zero concentration and have identical intercept values that correspond to $[\eta]$ of a pectin solution in a given solvent. The $[\eta]$ is controlled by molecular characteristics of a polymer (linearity, degree of branching, flexibility, rigidity, polyelectrolyte nature, presence of functional groups), molecular weight and solvent quality.

The most frequently used tool for intrinsic viscosity determination of polymer dilute solutions is the Ubbelohde type viscometer (Figure 1.7). The method is based on the measurement of the resistance to flow of solvent and biopolymer solution through a calibrated capillary.

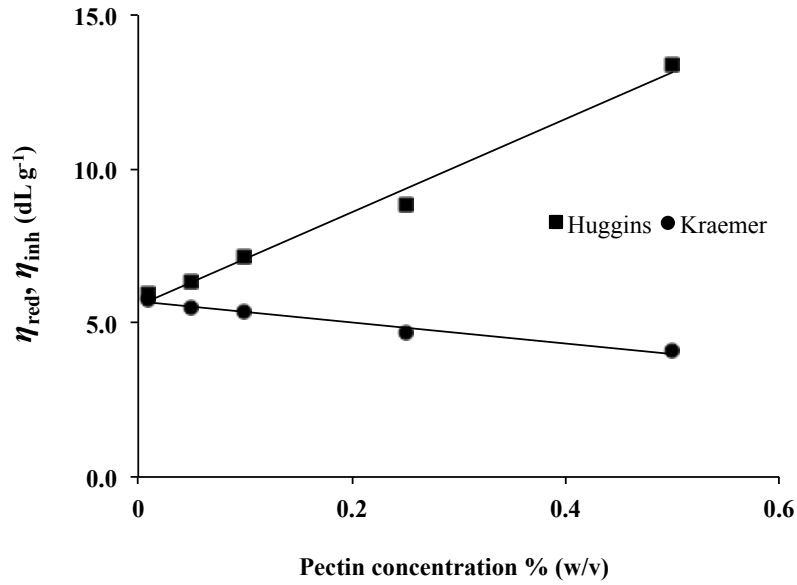


Figure 1.6. Huggins-Kraemer plots for okra pectin (OP6) in phosphate buffer and 0.1 M NaCl at 25°C.

According to Poiseuille law (resistance to flow), η_{rel} can be expressed as shown in Eq. 14, where t , t_0 and ρ , ρ_0 are the flow times and corresponding densities of solvent and biopolymer solution at a concentration c under certain experimental conditions (laminar constant flow, $T = \text{const}$) (Harding, 1997). The η_{rel} can be expressed without the density correction and in that case it will be called as a kinematic relative viscosity (η'_{rel}) (Eq. 15).

$$\eta_{rel} = \left(t\rho / t_0\rho_0 \right) \quad (14)$$

$$\eta'_{rel} = \left(t / t_0 \right) = \eta_{rel} \quad (15)$$

However, in polymer science a reasonable approximation of $\eta_{rel} = \eta'_{rel}$ has been introduced for biopolymer (polysaccharides, glycoproteins) solutions at concentration $<1 \text{ g L}^{-1}$. As it has been discussed, $[\eta]$ is a measure of hydrodynamic volume occupied by individual molecules in a very dilute biopolymer solution. Since hydrodynamic volume of polymer chains depends on macromolecular characteristics including

molecular weight (coil expansion increases with molecular weight), it has been proposed that those two parameters are interrelated. Mark, Houwink and Sakurada arrived at an empirical relationship between $[\eta]$ measured in a specific solvent and the viscosity average molecular weight (M_v):

$$[\eta] = KM_v^a \quad (16)$$

where K and a (also called coiled expansion constant) are empirical constants that depend on polymer conformation, solvent and temperature at which the $[\eta]$ was measured. Therefore, constants can be used for evaluation of biopolymer conformation. Polysaccharides with expanded random coil conformation result in high values of K whereas those with compact conformation give low K (Harding, 1997). The exponent a of polysaccharides adapting a random coil conformation is typically in the range of 0.5 - 0.8 and strongly depends on the quality of a solvent. For stiff coils the value a is about 1.0 and for rods in the range of 1.8 – 2.0 (Harding, 1997; Tanford, 1961). In a Flory θ -solvent, polysaccharide chains have more compact conformation and therefore, lower $[\eta]$. The value of a equals 0.5 under these conditions. In a good solvent, the expansion of polysaccharide chains results in high $[\eta]$ and a value is close or higher than 0.8. It has been reported that a value for pectin varies in the range of 0.62 – 0.94 corresponding to a slightly stiff conformation whereas xanthan value is about 1.23 depending on the applied solvent (Morris, Adams & Harding, 2014). Mark-Houwink constants can be obtained from literature or experimentally from a plot of $\log [\eta]$ over $\log M_v$, where the slope of regression line represents a and intercept equals to $\log K$.

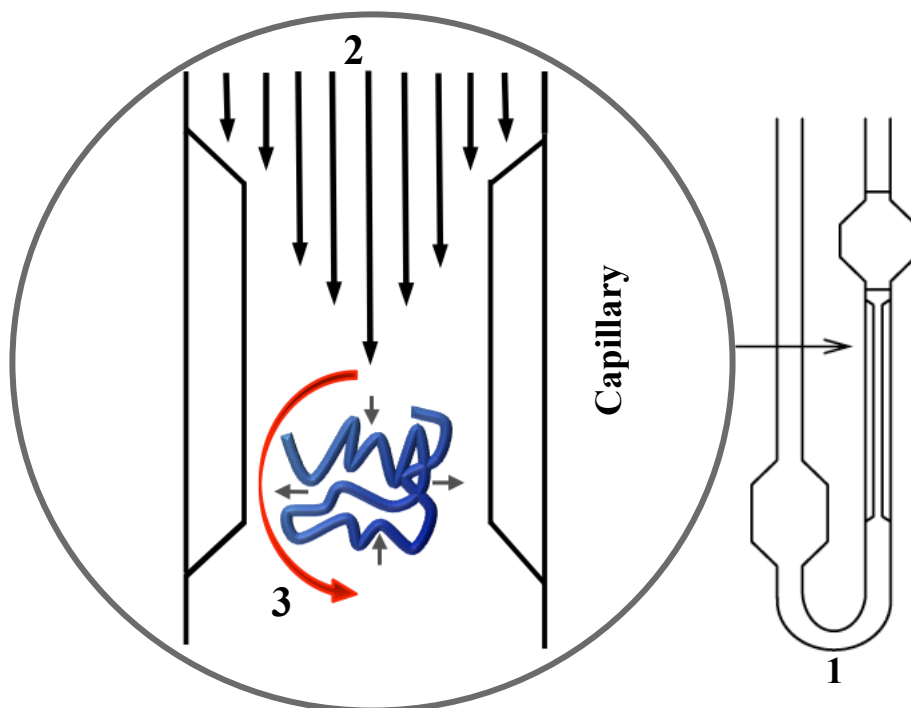


Figure 1.7. Schematic representation of the effect of shear rates on polymer chain rotation. Hydrodynamic work is converted into heat, resulting in an increased solution viscosity. 1 - Ubbelohde type viscometer, 2 – relative velocity of solvent in capillary, 3 – rotational motion of polymer molecule.

As it has been discussed earlier, the bulk properties of polysaccharide solutions are also concentration-dependent (c , c^* , c^{**}) and the critical concentration (c^*) that is used to define dilute and non-dilute concentration regimes typically depends on molecular weight and conformational characteristics (e.g., stiffness) of polysaccharide chains. However, Eq. 17 and double logarithmic plots of $(\eta_{sp})_0$ versus dimensionless coil overlap parameter, $c[\eta]$, that measures the total volume occupied by all polysaccharide coils in solution are typically used to determine the transition from the dilute to concentrated regime regardless of polysaccharide primary structure and molecular weight. The effects of concentration on η are studied using zero shear specific viscosity ($(\eta_{sp})_0$). The $c[\eta]$ can be estimated from master curves of $\log(\eta_{sp})_0$ versus $\log c[\eta]$ and typically is in the range of 2.5 – 4.0 for random coil polysaccharides, such as carboxymethylamylose and λ -carrageenan (Morris, Cutler,

Ross-Murphy, Rees & Price, 1981). However, some of polysaccharides including amylose, guar gum and locust bean gum demonstrate much lower values about 1.0 – 1.3 (Doublier & Launay, 1981; Ellis & Ring, 1985). It has been also observed that double logarithmic plots for polysaccharides of different primary structure, but with similar conformational characteristics result in the range of slope values 1.2 – 1.4 for $c < c^*$ and 3.3 – 4.4 for $c > c^*$.

$$\left(\eta_{sp}\right)_o = \left(c[\eta]\right)^n \quad (17)$$

1.7 OKRA PLANT

Okra (*Abelmoschus esculentus* L.) is an annual, flowering plant that belongs to the *Malvaceae* family and it has many local names in various parts of the world, for instance, lady's fingers in England, gumbo in the USA or bhindi in India. It is primarily cultivated in tropical and subtropical areas including India, Middle East, Southern USA and West Africa. According to (FAOSTAT, 2013) the most important okra-producing country is India with more than 70% of world okra production (5 million tonnes) followed by Nigeria (1 million tonnes) and Sudan (0.3 million tonnes) with the total trade exceeding \$4 billion. Okra is cultivated for its fibrous fruits or pods that contain white, round seeds and eaten as a vegetable. About 50 species are identified and those that are cultivated include *A. moschatus*, *A. manihot* and *A. esculentus*. Okra pods are normally harvested in an immature state when they are high in mucilage. Okra plays important role in the human diet, as it is high in vitamin C, minerals (e.g., Ca, Mg and K) as well as fibers. The high fiber content and polysaccharides present in okra have been the subject of significant research of their applications in food and pharmaceutical industries. Recently, the nutritional and functional properties of okra pods have re-awakened interest to research its potential

uses. Studies on okra flour have revealed that it possesses antioxidant activity, which increases with roasting (Adelakun, Oyelade, Ade-Omowaye, Adeyemi & Van de Venter, 2009) suggesting their application in food industry as inhibitors of lipid oxidation and microbial activity in meat products during storage (Arapitsas, 2008). Okra seeds are considered as a coffee substitute and also as a high-protein oilseed crop that can be used to complement other protein sources (Martin, 1982). Physiological studies have revealed hypoglycemic properties of okra polysaccharides (Lengsfeld, Titgemeyer, Faller & Hensel, 2004) suggesting their potential use as functional food ingredients similar to soluble fibers from cereals (β -glucan) or psyllium. In the food industry, the thick and slimy texture of okra aqueous extracts is of primary technological interest as they can be used as thickening agents or as stabilizers in food emulsions (Sengkhamparn, Sagis, de Vries, Schols, Sajjaanantakul & Voragen, 2010).

Currently, it is suggested that water extracted okra polysaccharides can be used as a diverse food ingredient (BeMiller, Whistler & Barbalowm, 1993; Costantino & Romanchik-Cerpoviez, 2004; Romanchik-Cerpovicz, Costantino & Gunn, 2006; Romanchik-Cerpovicz, Tilmon & Baldree, 2002; Woolfe, Chaplin & Otchere, 1977). Okra pectins are found to be acidic, random coil polysaccharides composed of galactose, rhamnose and galacturonic acid. The repeating unit was reported to be α -(1-2)-rhamnose and α -(1-4)-galacturonic acid residues including disaccharide side chains (Tomada, Shimada, Saito & Sugi, 1980) and they form viscous solutions that exhibit pseudoplastic behavior (Georgiadis, Ritzoulis, Sioura, Kornezou, Vasiliadou & Tsiopstias, 2011; Kontogiorgos, Margelou, Georgiadis & Ritzoulis, 2012; Sengkhamparn, Sagis, de Vries, Schols, Sajjaanantakul & Voragen, 2010). Furthermore, they differ greatly from those extracted from apple, citrus and beet in

terms of protein and acetyl contents, indicating their greater hydrophobicity and therefore substantial surface activity at the o/w interface suggesting that pectin derived from okra can be used as an effective emulsifying agent (Kravtchenko, Voragen & Pilnik, 1992; Levigne, Ralet & Thibault, 2002; Sengkhampan, Verhoef, Schols, Sajjaanantakul & Voragen, 2009; Thibault, 1988).

1.8 PECTIN AS A FUNCTIONAL FOOD INGREDIENT

1.8.1 High moisture regime - Gelation

A number of polysaccharides in a hydrated state can form gels under certain conditions. Gelation of polysaccharides occurs due to the cross-linking of polymer chains *via* covalent (in the presence of cross-linking agent) or non-covalent bond (e.g., van der Waals interactions, hydrophobic interactions, hydrogen bonding or ionic bonds for charged polymers) so as to convert polysaccharide solution into the three-dimensional metastable, viscoelastic network that fills the volume of the liquid medium (Walstra, 2003). When polysaccharides are dispersed in aqueous medium, inter- and intra-chain interactions occur alongside with chain-solvent interactions. Inter-chain interactions typically result in formation of a gelled network whereas intra-chain interactions result in aggregation of polysaccharide followed by precipitation. In order to decrease the intra-chain interactions and increase inter-chain interactions, polysaccharide solutions are subjected to various temperature profiles (e.g., cooling, heating ramps), pH variation, addition of cations and co-solutes (e.g., sucrose, glucose).

Chemical structure and molecular conformation of polysaccharides are primary determinants of gelling mechanisms and gel properties. Therefore, gels are classified based on their interactions in covalent polymeric networks, entanglement or physical networks (Flory, 1974). Gels comprised of physical networks are the most

common in food systems. In order to gel, polysaccharide chains or chain segments have to adopt short-range ordered structures (Cui, 2005). Cross-linking of ordered structures of two or more polysaccharide chains results in formation of junction zones (Sperling, 2006). A certain number of cross-links has to be formed in order to overcome the entropy barrier and form a stable network. Several idealized models of junction zones of polysaccharide gels have been reported and include the egg-box junction (e.g., low-methoxyl pectin, alginate), the aggregated double helical junction (carrageenan), cation (e.g., Ca^{2+} , Mg^{2+} , Na^+ , K^+) promoted association of double helices (e.g., low acyl gellans) and association of extended ribbon-like structure (e.g., segments of amidated pectin and of mannan segments of galactomannan) (Grant, Morris, Rees, Smith & Thom, 1973; Piculell, 1998; Racape, Thibault, Reitsma & Pilnik, 1989).

It is worth to mention that polysaccharide solutions are viscoelastic in nature and have both solid-like and liquid-like characteristics. The sol-gel transition is typically accompanied by considerable changes in flow behaviour and increase in viscoelastic properties. The dynamic mechanical experiments of gelling systems are often used to show the evolution of the storage (G') and loss (G'') moduli during the formation of gelled network. Figure 1.8 shows an example of gelation kinetics of acid-induced gelation of LM-citrus pectin where the crossover point of G' and G'' is taken as the gelation point. The gelation mechanisms can be entirely different between pectins that have variations in fine structure (e.g., DE, DA, degree of branching of RG-I). For instance, high-methoxyl (HM) and low-methoxyl (LM) pectins have different gelation mechanisms and therefore gel properties. In contrast, pectins with high degree of acetylation and branched RG-I typically do not gel.

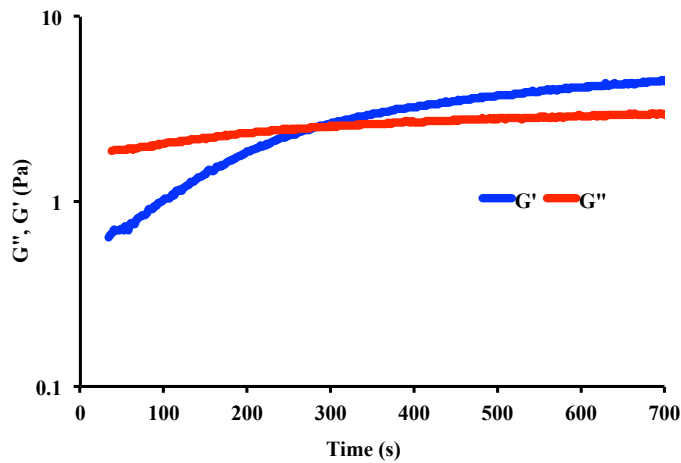


Figure 1.8. Acid-induced gelation of citrus LM-pectin ($\omega=6.283$ rad/s, 1% strain, $T=20^{\circ}\text{C}$).

The gelation of LM-pectins is induced by incorporation of divalent cations, such as Ca^{2+} over a wide range of pH values. However, binding efficiency of calcium ions to pectin chains is controlled by the pH. It has been shown that at neutral pH values pectin chains are highly extended and stiffened due to the intra-chain electrostatic repulsions and chain geometry is close to the two-fold helix structure (Gilsenan, Richardson & Morris, 2000). In contrast, more compact three-fold helix structures are formed under acidic pH due to the suppression of electrostatic repulsions and increase of hydrophobic interactions and hydrogen bonds (carboxyl groups act as a hydrogen-bond donors) (Gilsenan, Richardson & Morris, 2000). Those interactions could strengthen the gel formation of LM-pectins and, therefore, the gelation of LM-pectins could be favoured by decreased pH. Moreover, LM-pectin gels fabricated at low pH are thermally reversible and those at neutral pH are irreversible. Amidation increases the gelling ability of LM-pectins and typically less calcium is required for formation of gelled network. Reactivity to calcium depends on the number and distribution of carboxyl groups and degree of methyl-esterification. The gelation mechanism of LM-pectins is based on the egg-box junction model similarly to calcium alginate gels. The model involves long arrays of site-bound Ca^{2+}

fixed between (1→4) linked GalA chains in a highly buckled two-fold conformation as shown in Figure 1.9 (Jarvis & Apperley, 1995). The oxygen atoms of hydroxyl groups and pyranose ring, and the bridging oxygen atoms of the component sugar units are involved in covalent bonding.

In contrast, gelation of HM-pectins occurs in the presence of high concentrations of co-solute, such as sucrose at around 60 – 65% under acidic conditions. Low pH values ($< \sim 3.6$) are required for protonation of pectin carboxyl groups and elimination of electrostatic repulsions between pectin chains whereas sucrose competes with pectin for available water. These conditions (co-solute and low pH) limit the hydration of pectin chains and promote gel formation. The amount of required co-solute typically increases with increasing degree of methyl-esterification of pectin. It has been shown that hydrogen bonding and hydrophobic interactions are the major driving forces in gelation of HM-pectins (da Silva, Gonzalves & Rao, 1995). HM-pectin gels are thermally irreversible and depending on the degree of methyl-esterification are classified as rapid-set ($>79\%$ DM) or slow-set ($\sim 58 - 65\%$ DM) pectins.

1.8.2 Low moisture regime – High solid biopolymer systems

High solid systems or systems with low moisture content are widely utilized in food and pharmaceutical industry. Dehydrated, partially frozen foods, tablet coatings and encapsulated bioactive ingredients are the common examples of low moisture biopolymer systems. The typical solids level in a gelled biopolymer system is in the range of 0.5 – 2.0% whereas high solids systems usually contain $> 65\%$ of solids. Amorphous or crystalline solid states of polysaccharides can be distinguished based on the ability of polysaccharide segments to adopt disordered or long-range ordered structures (Kontogiorgos, 2014).

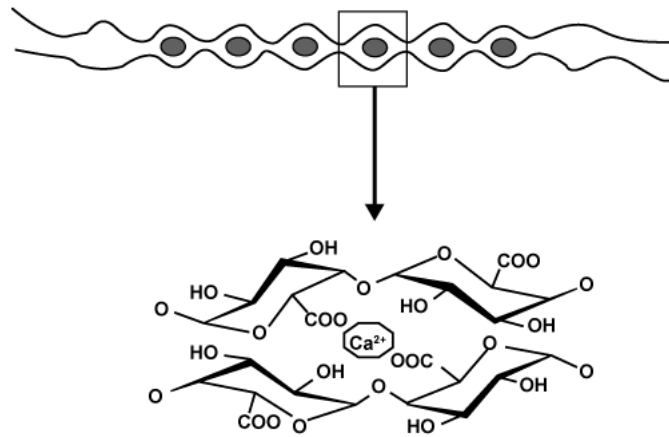


Figure 1.9. The gelation mechanism of LM-pectins is based on the egg-box model (Axelos & Thibault, 1991).

An amorphous biopolymer does not demonstrate regular periodicity in atom or molecule density and therefore does not form crystals (Walstra, 2003). Instead, amorphous systems are subjected to glass transition where disordered supercooled liquids undergo a transition from liquid to solid states. The transition occurs over a temperature range or more often referred to a definite temperature called glass transition temperature (T_g) (usually onset or midpoint of transition). The formation of glasses typically occurs when a polymer solution or rubbery system is cooled fast (or by removal of water) below its melting temperature and therefore, molecules have limited time to rearrange themselves and pack into the crystalline domain (Hutchinson, 1995). Further reduction of temperature and inhibited crystallization contribute to the considerable increase in viscosity values and the system eventually enters the glassy state.

The solutions of food biopolymers typically do not crystallize on cooling however, glass transition and glassy state are important determinants of physical stability and textural properties of food matrices (Kasapis, Mitchell, Abeysekera & MacNaughtan, 2004; Kontogiorgos, 2014). Several polysaccharides have a semi-crystalline character including starch, cellulose and chitin (Belitz, Grosch &

Schieberle, 2009). The presence of double helices of amylopectin in starch and hydroxyl groups in cellulose that are involved in intra- and intermolecular hydrogen bonding result in various ordered crystalline arrangements (microcrystalline regions) below a melting temperature. Further cooling of such systems does not result in formation of greater proportion of crystalline domains due to the restrictions in conformational and rotational freedom of polymer chains imposed by the reduction of free volume. As a result, part of the material in such systems will be crystalline and part in a glassy state. Glassy state in food systems can be achieved by removal of water (e.g., freeze drying, extrusion) and/or by cooling high solids biopolymer systems below a defined temperature range. Some properties of high solids systems could be also modified on introduction of a softening agent (plasticizer) (Kasapis, 2008). In relation to biopolymer systems, water acts as a plasticizer. The hydration of amorphous polysaccharides chain considerably affects vitrification by reducing the glass transition temperature.

Various concepts are utilized to rationalize molecular processes of a material in the glass transition. The existing theories mainly focus on the thermodynamic, kinetics, or the free volume concepts and utilize a single property or parameter to characterize the glass. Differential scanning calorimetry (DSC) is a widely used method to analyse glass transitions based on the changes in heat capacity of the material during the transition period. However, calorimetrically determined glass transition temperatures are affected by the heating rate and also do not stand the comparison with mechanically determined T_g . The mechanistic evaluation of rubber-to-glass transition and associated molecular processes is based on the concept of macromolecular free volume (Kasapis, 2005). Free volume (v_f) has been defined (Ferry, 1980) as a vacant space between the packing irregularities of long chain

segments or as the space required for large-scale rotational and vibrational motions of the molecules. In contrast, the definition of occupied volume (v_0) describes the space taken by the van der Waals radii of polymeric contours and vibrational motion of atoms. Therefore, according to the free volume concept, T_g is defined as temperature at which free volume of a system is nearly zero and molecular motions are arrested. The only molecular motions that occur below T_g are those allowed by the occupied volume and typically include local, restricted to atom or bond vibrations and/or reorientation of small groups (Champion, Le Meste & Simatos, 2000). It has been shown for polymer melts that the free volume accounts around 30% of the total volume above T_g and it reduces to 3% once the system enters glassy state (Cangialosi, Schut, Van Veen & Picken, 2003).

The molecular origin of viscoelastic behaviour of biopolymers is controlled by temperature, time, pressure, molecular weight and concentration (Angell, 2002). Small deformation oscillation on shear is used to evaluate the viscoelastic properties of biopolymer materials and glass transition region, as a function of frequency and time within the linear viscoelastic range. Typical viscoelastic spectrum of a polysaccharide system is shown in Figure 1.10. The master curves are composed of four distinct (frequency or temperature) parts based in the intersection of storage (G') and viscous (G'') modulus traces. Molecular flow ($G'' > G'$) is typically observed in biopolymer solutions (e.g., protein, polysaccharides) and concentrated glucose syrup at high temperatures (region I, Fig., 1.10). Cooling of the biopolymer system results in domination of G' over the G'' due to the formation of elastic elements forming physical associations with transient stability, but able to support the applied stress (e.g., entanglements).

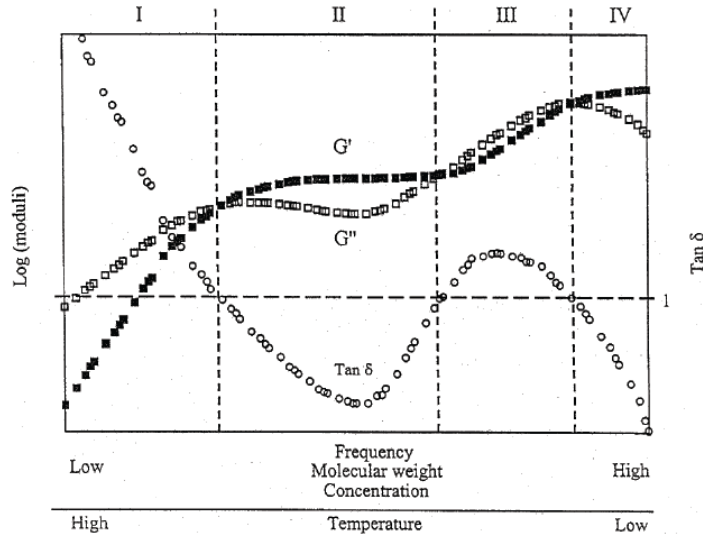


Figure 1.10. Variation of G' , G'' and $\tan \delta$ as a function of temperature, frequency, molecular weight and concentration for amorphous polymers (adopted from (Kasapis, Mitchell, Abeysekera & MacNaughtan, 2004).

The crossover point between G' and G'' demarcates the onset of the rubbery region (region II, Fig., 1.10). On further cooling, the rubbery biopolymer (in the absence of crystallization) enters the glass transition region (region III, Fig., 1.10) where viscous response becomes again dominant. At the lowest temperature the storage modulus dominates viscous and the system enters the glassy state where chemical, enzymatic and microbial activity is typically ceased. The time-temperature superposition (TTS) relation is based on the following: velocity or times of shearing and temperature have a comparable effect on sample rheological behaviour in the absence of conformational transitions or formation of supermolecular structures. The approach of master curve construction is focused on the application of William, Landel and Ferry equation (Eq., 18) (Williams, Landel & Ferry, 1955).

$$\log a_T = -\frac{C_1^o (T - T_o)}{C_2^o + (T - T_o)} \quad (18)$$

where C_1^o ($B/2.303f_o$) and C_2^o (f_o/α_f) are the WLF constants at the reference temperature T_o and related to the free volume theory (discussed below). The WLF

method is a concept of thermo-rheological simplicity (TS) indicating that all relaxation processes have the same temperature dependence and changes in temperature shifts the time and/or frequency scale of relaxations by the same amount (Kasapis, 2005; Mezger, 2011). It has been shown that TS is applicable for high molecular weight materials as opposed to the low molecular weight products where thermo-rheological complexity (TC) dominates. The WLF equation provides a good fit of the empirically derived shift factors only in the rubbery and/or glass transition state of a biopolymer system. The restrictions on applicability WLF/free volume theory are imposed by the considerable reduction of free volume (~3%) when system enters a glassy state. At this point, the thermal expansion coefficient of free volume (α_f) undergoes a discontinuity and total volume of a system does not change linearly as a function of temperature (Kasapis, 2008). Therefore, the concept of free volume reduction as a function of temperature is applicable only until the glassy state. Instead, the progress in mechanical properties at the region of the lowest temperatures and shift factors in a glassy state are typically described by the modified Arrhenius equation (Eq. 19) (Peleg, 1992). The change in relaxation processes also indicates the passage of the system controlled from free volume derived phenomena to those of energy barrier processes for the molecular rotation in the glassy state (Kasapis, 2008). Therefore, a temperature at which these modifications occur can be defined as the mechanical glass transition temperature.

$$\log a_T = \frac{E_a}{2.303R} \left(\frac{1}{T} - \frac{1}{T_0} \right) \quad (19)$$

1.8.3 Colloidal systems

Emulsions are a class of disperse systems consisting of two immiscible liquids (e.g., oil, water) (Tadros, 2005). The droplets of one phase (dispersed phase) are

dispersed in the second phase (the continuous phase). The term “oil” includes any hydrophobic liquid such as *n*-alkanes, triglycerides or mineral oils. Several classes of emulsions can be distinguished based on the distribution of the oil and aqueous phases, e.g., oil-in-water (o/w), water-in-oil (w/o) and oil-in-oil (o/o). Most of the emulsions used in the food industry have the droplet average diameters at around 0.1 - 100 μm and defined as macro-emulsions (McClements, 1999). Those emulsions that are of primary interest for pharmaceutical applications typically have smaller droplet sizes and can be divided into micro- (0.01 - 0.1 μm) and nano-emulsions (0.05 - 1 μm) (Mahdi, He & Bhandari, 2006). Emulsions are thermodynamically unstable systems and therefore kinetic stability (metastability) for a certain period of time is achieved by introducing additional components such as emulsifiers and thickening agents. Therefore, emulsion classification can be also based on the nature of emulsifier or the structure of the system (e.g., polyelectrolytes-bilayer droplets, ionic surfactants-micellar emulsions, solid particles-Pickering emulsions etc.) (Tadros, 2005). The concentration of droplets in the emulsion is described by the term dispersed-phase volume fraction (ϕ), which is the ratio of the total volume of emulsion droplets (V_D) and total volume of the emulsion (V_E) (Eq. 20).

$$\phi = \frac{V_D}{V_E} \quad (20)$$

1.8.3.1 Thermodynamics of mixing

The miscibility of two substances can be described by statistical thermodynamics. Molecule ensembles undergo self-organisation and arrange in a way that minimizes the free energy of the system (Ritzoulis, 2013). Therefore, the free energy of a system is determined by the combination of an enthalpic factor (the enthalpy of mixing of two components, ΔH_m) and an entropic factor (the entropy of

mixing ΔS_m at temperature T). The enthalpy is determined by the molecular interaction energies (e.g., bond energies, electrostatic interaction and van der Waals interactions) whereas entropy is generally governed by the propensity of a system to adopt a disordered conformation (McClements, 1999). The Gibbs free energy for a given system is given by the Eq., 21. The concept of free energy change on mixing of binary liquid systems helps to evaluate whether the resulting system will consist of two immiscible liquids or form a regular solution depending on the strength of the interactions between the liquids and entropy of mixing. The negative sign of ΔG_m indicates that mixing of two liquid systems is favourable whereas positive ΔG_m is a sign of unfavourable mixing and molecules exist as two separate (immiscible) phases.

$$\Delta G_m = \Delta H_m - T\Delta S_m \quad (21)$$

1.8.3.2 Interaction forces between emulsion droplets

In the previous section a thermodynamic approach was used to characterize the stability of a colloidal system. Since the inter- and intra-molecular forces control the kinetic development of a colloidal system, it is also important to describe the system in terms of acting forces rather than only of energy. Generally, there are three main interaction energies (forces) between emulsion droplets: the van der Waals attractive interactions, electrostatic repulsive forces and steric repulsion. Furthermore, there are three types of van der Waals attraction between atoms and molecules: dipole-dipole (Keesom), dipole-induced dipole (Debye) and dispersion (London) interactions (Tadros, 2005). The London forces typically arise from charge fluctuations and are exceptionally short-ranged, and occur at very short separations between the droplets. Hamaker (Bergström, 1997) described the relationship between the separation distance (h) and van der Waals attraction (G_A) for two droplets with equal radii (R) by the following equation

$$G_A = \frac{AR}{12h} \quad (22)$$

where A is an effective Hamaker constant that is specific for each material and depends on the number of atoms or molecules per unit volume q and the London dispersion constant β (Eq., 23). Eq. 22 also shows that G_A increases considerably with decreasing h and increasing the droplet size. The Hamaker function has electrostatic nature and depends on the interactions that involve permanent dipoles. Therefore, the strength of interactions decreases when droplets are immersed in electrolyte solution due to the electrostatic screening (McClements, 1999). In case of colloidal systems containing emulsifier the strength of the interaction will depend on the composition and thickness of interfacial layer.

$$A = \pi q^2 \beta \quad (23)$$

The sole predominance of van der Waals attraction at the molecular level will result in destabilization of colloidal system. However, colloidal systems typically are stable for a certain period of time indicating the presence of forces that counterbalance van der Waals attraction. Two main mechanisms of repulsion can be distinguished based on the nature of used emulsifier. These include electrostatic repulsion that forms due to the formation of double electric layers (e.g., ionic surfactant) and steric repulsion that occurs due to the adsorption and layer formation of emulsifier at the interface (Walstra, 2003).

The occurrence of electrostatic repulsion in emulsions is attributed to the occurrence of electrically charged surfaces. Surfaces in colloidal systems become charged due to the adsorption of ionic emulsifiers (e.g., surfactants) and/or ionization of functional groups of emulsifiers. The latter scenario is typically observed for polysaccharides and proteins where ionization of carboxyl (-COOH) and amino (-

NH₂) groups results in formation of carboxylate anion (-COO⁻) and ammonium cation (-NH₃⁺). The magnitude and the sign of the electrical charge of emulsion droplet depends not only on the type of emulsifier used, but also on environmental conditions such as pH, temperature and ionic strength. Therefore, electrostatic interaction can be either attractive or repulsive depending on the sign of the charges on the droplets. In the aqueous systems, a cloud of counter-ions surrounds a charged surface according to a charge preservation concept (Ritzoulis, 2013). According to this concept, the system must be electrically neutral and therefore the charge on the surface must be completely balanced by the excess charge of counter-ions (Figure 1.11). The concentration of counter-ions close to the immobile surface charge layer leads to the formation of electrical double layer (Tadros, 2005) (Figure 1.11). The density (σ) and potential (Ψ_0) of counter-ions fluctuates with distance (d) from the surface whereas the distribution of counter-ions in the main bulk of the liquid medium will remain constant (Ritzoulis, 2013). This first layer of solvated ions is called Stern layer. Ions are strongly bound in Stern layer as opposed to the diffuse layer, where they are less firmly associated. Within the diffuse layer there is a notional boundary inside which the ions and particles form a stable entity. The potential at this boundary is called ζ -potential and its magnitude typically indicates the potential stability of colloidal system. When two droplets approach to a distance (d) that is smaller than the double layer thickness, this leads to overlap of double layers and subsequent repulsion. The combination of van der Waals attraction and double layer repulsion results in the theory for colloidal stability described by the Deryagin, Landau, Verwey and Overbeek (DLVO theory).

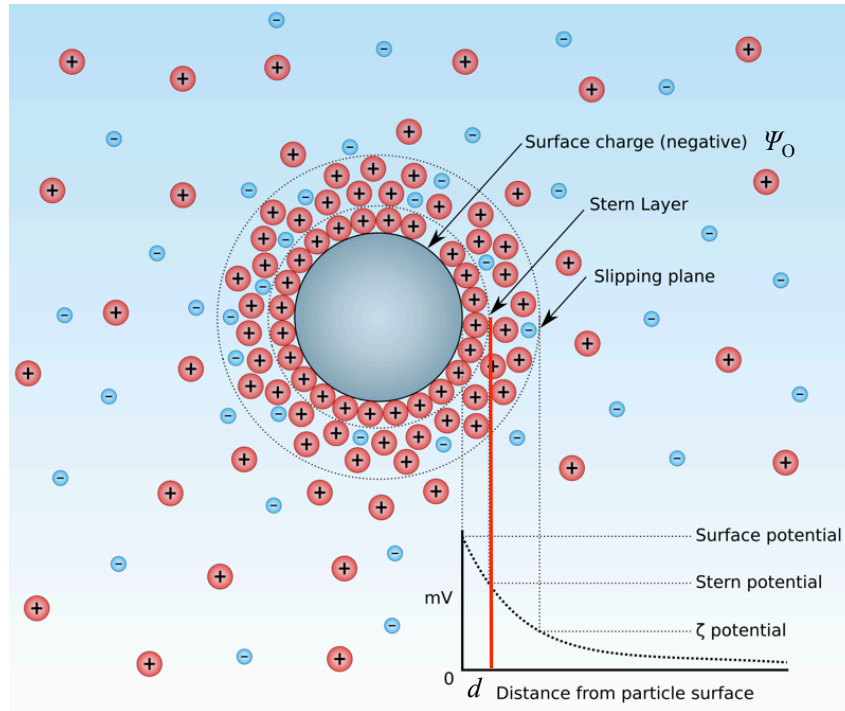


Figure 1.11. Schematic representation of the distribution of ions on the surface of a droplet (Wikipedia, 2015).

According to this theory, two droplets at a distance h have a total interactive potential ($u(h)$) that equals to the sum of attractive ($u_A(h)$) and repulsive inter-droplet interactions ($u_R(h)$) (Eq. 24, Figure 1.12). The van der Waals, steric, electrostatic, depletion and hydrophobic interactions are the most important interactions that contribute to the overall inter-droplet potential. These individual interactions vary in their sign (e.g., attractive, repulsive), magnitude (e.g., weak to strong) and range (e.g., short to long) (Piorkowski & McClements, 2013).

$$u(h) = u_A(h) + u_R(h) \quad (24)$$

The aforementioned repulsion forces occur only when a layer of charged emulsifier surrounds droplets. However, it is well known that colloidal systems are prone to mechanisms of destabilisation caused by the attractive forces even in the presence of neutral emulsifier.

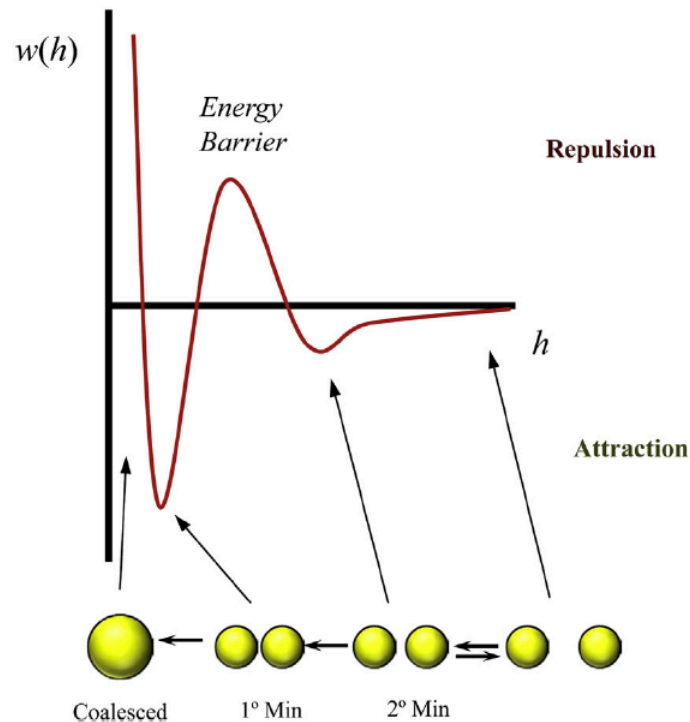


Figure 1.12. Schematic representation of the interaction potential between two emulsion droplets. Adapted from (Piorkowski & McClements, 2013).

This indicates the presence of other than electrostatic mechanisms of repulsion. The most important of these is steric stabilisation that occurs due to the presence of uncharged polymeric emulsifiers at the interface. There is a strong relationship between the conformation of emulsifier (e.g., proteins, polysaccharides) and its ability to stabilize emulsions. Typically emulsifiers tend to adopt at the interface, the conformation which minimizes the free energy of a system. The conformational arrangement at the interface is controlled by various factors including the flexibility of polymer, type and sequence of monomers along its backbone and also distribution of polar and non-polar groups. As a result, a polymer adopts the conformation that minimizes the number of unfavourable interactions with the liquid medium (Figure 1.13).

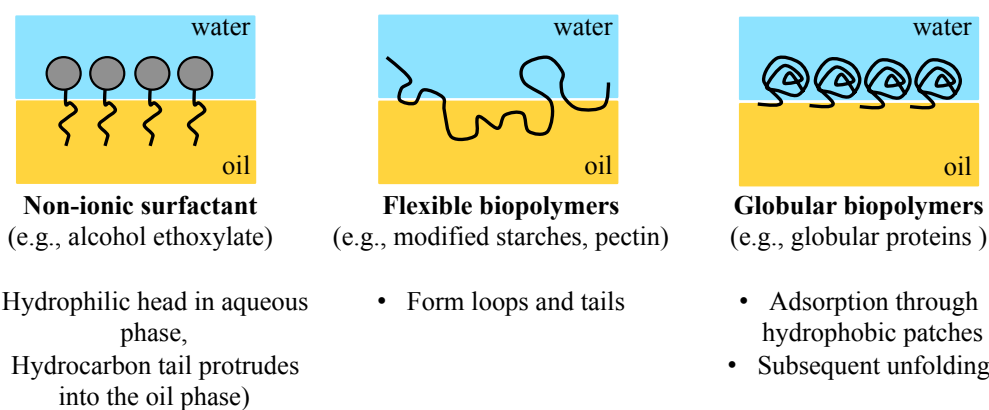


Figure 1.13. Interfacial orientation of polymeric emulsifiers.

1.8.3.3 Mechanisms of emulsification

It has been shown in the previous section that emulsion components (oil and water) are immiscible and therefore emulsions are thermodynamically unstable systems as indicated by the positive sign of their free energy of formation ($\Delta G_f > 0$). This instability is attributed to the energy associated with the large interfacial area (γ) of the droplets in emulsion (Tadros, 2005; Taylor, 1998). Therefore, a large quantity of energy is trapped as additional free energy at the interface. A positive value for γ means that energy required for expanding the interface is also positive whereas the entropy due to formation of droplets ($T\Delta S_f$) is small. As a result, the total free energy of emulsion formation is positive and a thermodynamically unstable system is formed. Therefore, a significant amount of external energy has to be applied to a system in order to compensate the interfacial free energy and initiate droplet disruption. Moreover, thermodynamic instability of emulsions can be delayed by stabilizing the system kinetically. The production of large droplets (e.g., macro-emulsions) requires lower energy inputs and is typically performed using high shear devices (e.g., colloid mills, high pressure homogenizers etc.). High-energy input methods (e.g., ultrasonication) are generally used for fabrication of submicron droplets in nano-emulsions. These examples indicate a relationship between the

droplet size and the amount of energy delivered to a system, and is related to the Laplace pressure (Δp). When colloidal particles are dispersed in a medium they adopt a shape that corresponds to a minimum surface area. A sphere is the only geometrical shape that represents the smallest surface area per unit volume and therefore droplets in an emulsion exist in a spherical shape (Ritzoulis, 2013). External energy (forces) that causes the deformation of droplets is opposed to the Laplace pressure and is defined as the work that is required to produce a curved surface (Eq. 25):

$$\Delta p = \gamma \left(\frac{1}{R_1} + \frac{1}{R_2} \right) \quad (25)$$

where γ is interfacial tension, R_1 and R_2 are the radii of curvature of droplet distorted into the ellipsoidal shape. For a spherical drop $R_1 = R_2 = R$. Consequently, a strong deformation has to be applied to a droplet in order to disrupt it into smaller ones and therefore more energy is needed to fabricate smaller droplets. The addition of surfactants to a colloidal system decreases the amount of energy needed to disrupt the droplets by lowering the interfacial tension. Emulsification is a dynamic process where droplet disruption, adsorption of surfactant and droplet collision (e.g., re-coalescence) happens simultaneously, with characteristic time scale for each event that is usually short. Therefore, droplets have to be effectively covered with emulsifier in order to provide steric and/or electrostatic repulsions and eliminate re-coalescence.

1.8.3.4 Emulsion kinetic stability

The mechanisms that result in kinetic instability of colloidal systems include gravitational separation, flocculation, coalescence, Ostwald ripening and phase inversion. Gravitational separation (creaming and sedimentation) typically occurs due to the interplay between gravitational movement and Brownian diffusion. Brownian

diffusion is a typical event for small droplets ($\sim 0.1\mu\text{m}$) whereas the gravitational forces mainly affect larger droplets. Monodisperse emulsions ($\sim >1\ \mu\text{m}$) after separating typically form two distinct layers in the form of cream/sediment and clear liquid (serum). Polydisperse emulsions typically cream or sediment at various rates. Stoke's law describes the velocity (v) of a spherical particle of radius (r) in a gravitational field (Eq. 26)

$$v = \frac{2r^2(\rho_0 - \rho)g}{9\eta_0} \quad (26)$$

where g is the acceleration due to the gravity, η_0 is the viscosity of continuous phase, ρ and ρ_0 are the densities of continuous and dispersed phases. From equation 26 it can be clearly seen that the velocity of droplets is proportional to the acceleration caused by gravity and the radius of the droplet. Therefore, higher kinetic stability can be achieved by decreasing the droplet size of the emulsion. This principle is widely utilized in the fabrication of nano-emulsions where Brownian diffusion exceeds the gravitational forces and emulsions show negligible tendency for gravitational separation (Tadros, 2005). Other prevention methods that are based on the utilization of Stoke law are focused around the application of thickeners (e.g., xanthan gum, carrageenans, hydroxymethyl cellulose etc.) that increase the viscosity of continuous phase and therefore decrease the velocity of droplets.

Flocculation is a result of the van der Waals attraction that is universal for all colloidal systems. As flocculation proceeds there is a decrease in the total number of particles in the colloidal system and the rate of flocculation can be described by the following equation

$$\frac{dn_T}{dt} = -\frac{1}{2}FE \quad (27)$$

where dn_T/dt is a flocculation rate, n_T is the total number of particles per unit volume, t is the time, F is the collision frequency and E is the collision efficiency. Therefore, the flocculation rate is proportional to the frequency of collision between the droplets and the amount of successful collisions that result in droplet aggregation. Droplet collisions occur due to their continuous movement due to thermal motion in the colloidal system and can be induced by the Brownian motion, gravitational separation and applied mechanical forces. Collision frequency can be decreased or eliminated by the increase of viscosity of the continuous phase. The colloidal attractive interactions can influence the structure that flocs will adapt. For instance, flocs are immobilized in opened structures when the attractive interactions between the droplets are greater than the thermal energy. In contrast, weak droplet attractions promote formation of floc entities with close packing due to the ability of each individual floc to undergo structural rearrangements (McClements, 1999). The effective way to control or manipulate the rate of flocculation in the colloidal system is to restrain the colloidal interactions between the droplets. Inhibition of van der Waals attractive interactions can be performed by promoting electrostatic (effective energy barrier) and steric interactions. Gravitational separation and aggregation in the form of flocculation are the processes that are not involved in the increase of droplet sizes, however, they can be precursors to coalescence.

Coalescence between two droplets refers to the merging of droplets followed by interfacial film rupture and consequently formation of a larger droplet. Generally, colloidal systems that undergo coalescence move towards the most thermodynamically stable state by decreasing the area of contact between the oil and aqueous phases. Since coalescence typically occurs during the close contact between the droplets it indicates that the process mainly depends on the short-range forces.

The rate of coalescence and physical mechanism that control the destabilisation is highly dependent on the nature of a given emulsifier. Several mechanisms of coalescence have been identified including coalescence induced by collisions, prolonged contact or "hole" formation (McClements, 1999). Coalescence induced by collisions is a common form of coalescence in colloidal systems where droplets move freely (Brownian motion, gravity or applied mechanical forces) and collide with each other. In contrast to flocculation, only those collisions are successful that contribute to the interfacial film rupture. Coalescence that occurs due to the prolonged contact between the droplets is typically spontaneous and occurs at high droplet concentrations (e.g., creamed, sedimented or flocculated droplets). It has been previously shown that coalescence frequently occurs in colloidal systems that are sterically stabilized through the formation of a "hole" in the interfacial membranes surrounding the droplets. Hole formation depends on various factors including the type of emulsifier and environmental conditions and, therefore, the rate of coalescence depends on the probability that these holes will be formed in droplet membranes. Holes are formed spontaneously and can be a result of thermal fluctuations of shape of surfactant layers, chemical breakdown of the emulsifier over time or emulsifier displacement from the droplet interface by more surface active components.

The destabilisation mechanism that is accompanied by the change in oil and water distribution in the colloidal system is called phase inversion. Phase inversion is typically triggered by some compositional or environmental conditions such as dispersed phase volume fraction, emulsifier type, concentration or mechanical agitation. Typical mechanisms of phase inversion are non-anionic surfactant and fat

crystallization induced phase inversion (e.g., butter and margarine melts). Emulsions that undergo the phase inversion are capable to retaining their kinetic stability.

As it has been previously mentioned, coalescence is a destabilisation mechanism that occurs between droplets in close proximity. In contrast, Ostwald ripening does not depend on the distance between the droplets because the process occurs due to the transport of dissolved matter through the dispersion medium. As a result, Ostwald ripening leads to the increase in average droplet radius of the emulsion with time as the small droplets dissolve and re-deposit their matter onto the large. The process of ripening can be also defined in terms of thermodynamics where the free energy of a system decreases considerably due to the decrease in interfacial area. The driving force for Ostwald ripening is the difference in solubility between small and large droplets (the small droplets have higher Laplace pressure and higher solubility than the large ones). The solubility and therefore chemical potential of the dispersed phase in the bulk phase depends on the radius of curvature of the droplet, with solubility (c) increasing with decreasing radius (r). This relationship is described by the Kelvin equation:

$$S(r) = S_{\infty} \exp\left[\frac{2\gamma M}{RrT}\right] \quad (28)$$

where M is the molar mass, $S(\infty)$ is the solubility of the solute in the continuous phase for a droplet with infinite curvature (a planar interface), γ is the interfacial tension, $S(r)$ is the solubility of the solute when contained in a spherical droplet of radius r . This is illustrated in Figure 1.13, where R_1 decreases and R_2 increases because of diffusion of molecules from the small to the large droplets and therefore Ostwald ripening is also referred to as a process of molecular diffusion (Figure 1.14). The mathematics behind the Kelvin equation in relation to Ostwald ripening rate is

complex and several treatments using model simplification were developed in order to describe the rate of Ostwald ripening. The most complete theory was proposed by Lifshitz-Slyozov-Wagner and typically referred as LSW theory. The theory assumes that the process of ripening is entirely diffusion-controlled and there is no barrier to the passage of droplet material through the interface and therefore ignoring the effect of interfacial layer formed by adsorbed surfactant (other considerations related to LSW model are also discussed in Chapter 4, section 4.3).

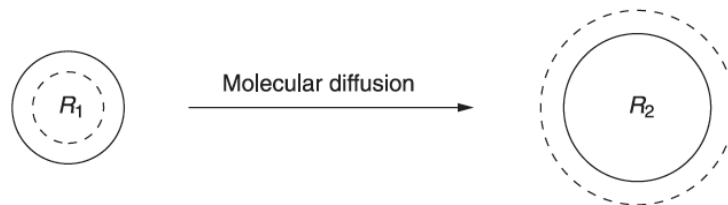


Figure 1.14. Schematic representation of Ostwald ripening-driven droplet growth.

1.9 HYPOTHESIS, AIMS AND OBJECTIVES

1.9.1 Hypothesis

Okra plant is a novel source of pectin with distinct physicochemical and bio-functional properties.

1.9.2 Aims

Develop cost-effective functional systems (e.g., gels, emulsions) from sustainable natural resources.

1.9.3 Objectives

- Design an isolation protocol for polysaccharides from okra pods
- Examine the influence of extraction conditions on molecular characteristics of pectins
- Characterize physiochemical and macromolecular properties of isolated polysaccharides
- Establish structure-function relationships of okra pectin
- Evaluate the gelation capacity of okra pectin
- Evaluate the emulsification capacity of okra pectin
- Optimize the emulsification with okra pectin
- Examine emulsification capacity of okra pectin under acidic conditions
- Analyze the interfacial composition of oil droplets
- Evaluate mechanisms of instability in okra pectin-stabilized emulsions during storage

CHAPTER 2

ISOLATION AND CHARACTERIZATION OF OKRA PECTIN

Parts of this chapter were published as:

Alba, K., Laws, A. P., & Kontogiorgos, V. (2015). Isolation and characterization of acetylated LM-pectins extracted from okra pods. *Food Hydrocolloids*, 43, 726-735.

2.1 INTRODUCTION

Okra pectins obtained by sequential extraction are described as acidic random coil heteropolysaccharides containing α -(1 \rightarrow 2)-rhamnose and α -(1 \rightarrow 4)-galacturonic acid residues with disaccharide side chains composed of galactose attached to *O*-4 of half of the rhamnose residues (Tomada, Shimada, Saito & Sugi, 1980). It has been also reported that okra extracts contain high amounts of RG-I segments and acetylation on rhamnose residues something that is uncommon for pectin from other sources (Sengkhampan, Bakx, Verhoef, Schols, Sajjaanantakul & Voragen, 2009). Isolation of polysaccharides can be performed on a laboratory scale by extractions of the cell-wall material, which involve the use of calcium-chelating agents, dilute alkali or dilute acid (Levigne, Ralet & Thibault, 2002). Alternatively, degrading enzymes can be employed in order to release polysaccharide fragments. One of the drawbacks of the extraction with chelating agents is that it is laborious to remove the residual chelates. Alkaline extraction contributes to the reduction of length and degree of acetylation and methylation by β -elimination (Rombouts & Thibault, 1986). It has been reported that the highest yields of pectic substances are generally obtained by hot acid extractions which is also the most convenient approach for industrial extraction of pectin (May, 1990; Pagan, Ibarz, Llorca & Coll, 1999). Previous studies reported that the temperature, pH and time could modify the quantity as well as the quality of the extracted pectins (Levigne, Ralet & Thibault, 2002; Pagan, Ibarz, Llorca & Coll, 1999). Furthermore, it was shown that the variations in the number of methyl-esterified groups and composition of neutral sugars of the isolated fractions are primarily governed by the extraction protocol (Kjønksen, Hiorth & Nyström, 2005; Turquois, Rinaudo, Taravel & Heyraud, 1999). The extracted materials typically are polydisperse heteropolymers having diverse chemical structures and

molecular sizes (MacDougall & Ring, 2004).

Okra polysaccharides are potentially a new source of natural polysaccharides, which can be used as functional ingredients (thickeners, viscosity enhancers, gelling agents and texture modifiers) (Georgiadis, Ritzoulis, Sioura, Kornezou, Vasiliadou & Tsiptsias, 2011). Recent studies have mainly focused on characterization of okra polysaccharides obtained with sequential extractions, starting with hot acidic buffers followed by chelating agents and dilute alkali buffers. Nevertheless, the effect of extraction pH on the physicochemical characteristics and therefore functional properties of okra isolates has not been extensively studied (Georgiadis, Ritzoulis, Sioura, Kornezou, Vasiliadou & Tsiptsias, 2011; Kontogiorgos, Margelou, Georgiadis & Ritzoulis, 2012; Ndjouenkeu, Akingbala & Oguntimein, 1997; Sengkhampan, Verhoef, Schols, Sajjaanantakul & Voragen, 2009). The aims of the present work were to extract okra pectins at different pH values and examine the effect of the extraction conditions on their molecular and compositional characteristics.

2.2 MATERIALS AND METHODS

2.2.1 Materials

Okra pods of *Abelmoschus esculentus L.* were purchased from the local market. Pods were frozen and kept at $-20\text{ }^{\circ}\text{C}$ until use. Sodium azide, all buffer salts, acetic acid, phenol, 3-phenylphenol, sodium tetraborate, sulfamic acid, 1.25 M hydrogen chloride-methanol solution, anhydrous pyridine, acetic anhydride, anhydrous ethyl acetate, ethanol (96% w/w) (all analytical grade reagents) and petroleum ether (bp $40\text{-}60^{\circ}\text{C}$) were obtained from Sigma-Aldrich (Poole, UK). De-ionized water was used throughout the extraction experiments. Dextrans (M_p 270, 410

$\times 10^3 \text{ g mol}^{-1}$), D-galacturonic acid monohydrate, D-galactose, L-rhamnose, L-arabinose, D-glucose, D-xylose, pectins from citrus fruit (esterified 55-70% and 20-34% potassium salts) and dialysis membranes (molecular weight cut-off 12000) were purchased from Sigma–Aldrich (Poole Dorset, UK).

2.2.2 Isolation of okra pectins

The isolation of pectins from okra pods was carried out according to the experimental design shown in Figure 1. The extraction protocol resulted in the isolation of two pectin samples namely OP2 and OP6 for isolates extracted at pH 2.0 and pH 6.0, respectively.

2.2.3 Chemical characterization

Total carbohydrates were determined by the phenol-sulphuric method (Dubois, Gilles, Hamilton, Rebers & Smith, 1956). Protein content was established using Bradford assay (Bradford, 1976). The galacturonic acid (anhydrous) content of pectins was estimated colorimetrically by the *m*-hydroxydiphenyl method (Filisetti-Cozzi & Carpita, 1991). The determination of ferulic acids in isolated okra pectin samples was performed using UV/VIS spectroscopy (Williams, Sayers, Viebke & Senan, 2005). The UV absorption spectrum of 0.167 % w/v pectin and 0.01 % w/v ferulic acid (trans-4-hydroxy-3-methoxycinnamic acid) standard solutions were determined from 200 to 400 nm using a Cary 60 UV-Vis (Agilent Technologies, USA). Pectin solutions were centrifuged at 14100×g for 25 min (MiniSpin Plus, Eppendorf, Hamburg, Germany) prior to ferulic acid determination. The pH of ferulic acid and pectin solutions was 4.0. Quartz cells were used for the UV/VIS measurements.

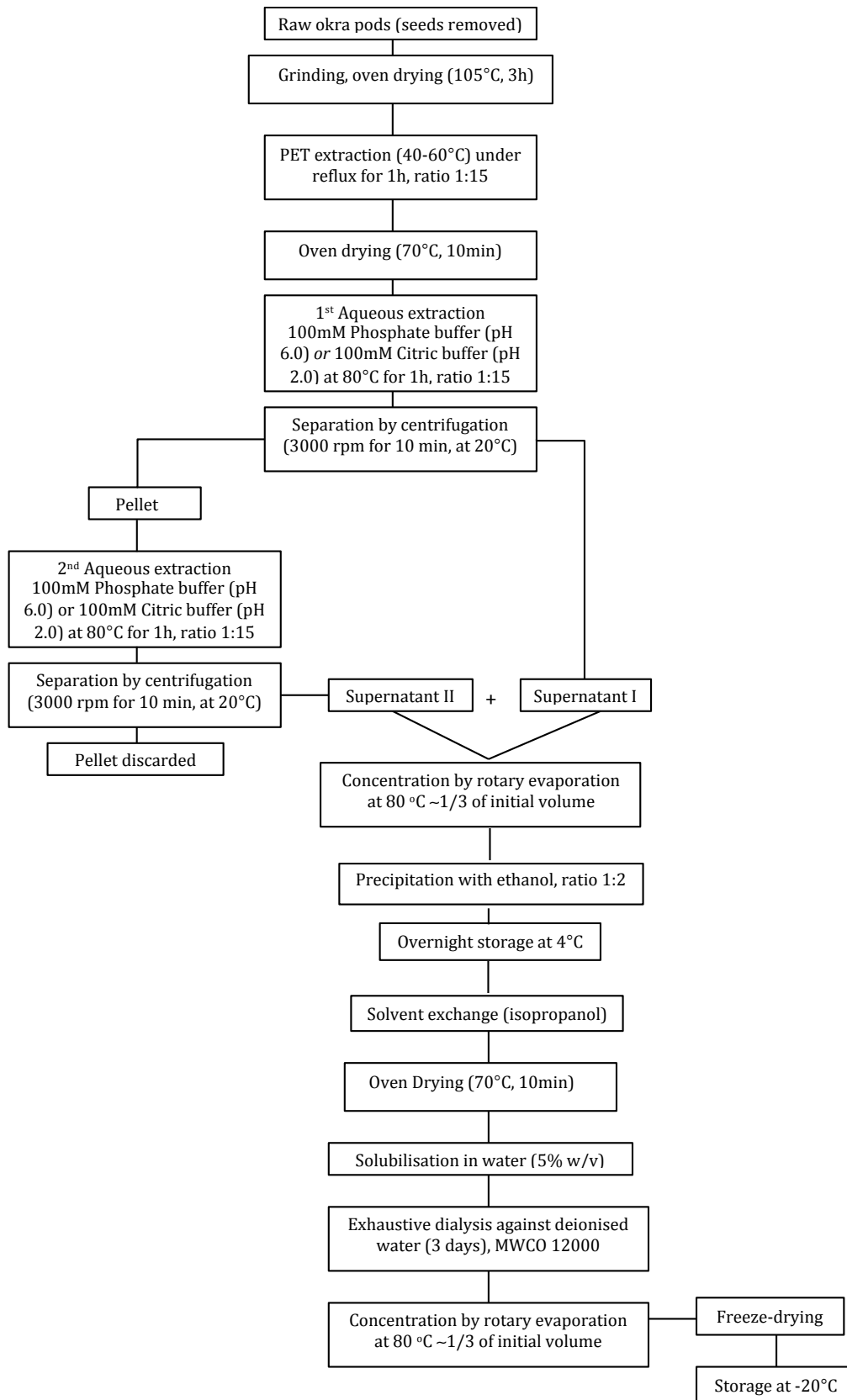


Figure 2.1. Isolation protocol for pectins isolated from okra pods.

The methoxyl (-OCH₃) content of pectins was determined by titration (Schultz, 1965). The method is based on a titration of free carboxyl groups present followed by de-esterification and titration of the carboxyl groups that have been made available. A correction was made for the acetic acid liberated due to the cleavage of the *O*-acetyl groups. The degree of methyl esterification (DM) was calculated from the galacturonic acid and methoxyl content values determined above according to the following equation (Schultz, 1965):

$$\text{DM (\%)} = \frac{176 \times \text{methoxyl content (\% (w/w))}}{31 \times \text{GA content (\% (w/w))}} \times 100 \quad (29)$$

where 176 and 31 are the molecular weights of anhydrous galacturonic acid (GA) and methoxyl, respectively. The acetyl content was determined with the hydroxamic acid method (McComb & McCready, 1957). The degree of acetylation (DA) was calculated from the galacturonic acid and acetyl content values determined above according to the following equation:

$$\text{DA (\%)} = \frac{176 \times \text{acetyl content (\% (w/w))}}{43 \times \text{GA content (\% (w/w))}} \times 100 \quad (30)$$

where 176 and 43 are the molecular weights of anhydrous galacturonic acid (GA) and acetyl, respectively. Neutral sugars were determined using methanolysis conducted with 1 M methanolic HCl solution at 85 °C for 24 h, as described previously (Bleton, Mejanelle, Sansoulet, Goursaud & Tchaplal, 1996). Sugar derivatives were analysed using an Agilent 7890A GC system (Santa Clara, CA, USA) coupled to an Agilent 5675C quadrupole MS. The samples were eluted from a HP-5 column (30 m x 0.25 mm, 0.25 µm film) using helium as carrier at a flow rate of 1 mL min⁻¹ by applying the following temperature settings: start temperature 140 °C, hold time 1 min and final column temperature 220 °C with 2.5 °C min⁻¹ gradient.

Calculations on sugar composition were performed using molar ratios formulated specifically for pectic substances (Houben, Jolie, Fraeye, Van Loey & Hendrickx, 2011). The molar percentage of homogalacturonan (HG) and rhamnogalacturonan-I (RG-I) were also calculated according to the following equations (M'sakni, Majdoub, Roudesli, Picton, Le Cerf, Rihouey & Morvan, 2006):

$$\text{HG (mol\%)} = \text{GalA (mol\%)} - \text{Rha (mol\%)} \quad (31)$$

$$\text{RG-I (mol\%)} = 2\text{Rha (mol\%)} + \text{Ara (mol\%)} + \text{Gal (mol\%)} \quad (32)$$

2.2.4 FT-IR spectroscopy

Spectra were obtained between 400-4000 cm^{-1} in Attenuated Total Reflection (ATR) mode at a resolution of 4 cm^{-1} using 128 scans (Nicolet 380, Thermo Scientific, UK). Spectral smoothing was applied using instrument software (OMNIC 3.1).

2.2.5 $^1\text{H-NMR}$ and $^{13}\text{C-NMR}$ spectroscopy

NMR spectroscopy was performed with a Bruker AV 500 spectrometer (Bruker Co., Switzerland) at 500 MHz ^1H and 125.76 MHz ^{13}C using a 5 mm probe. In order to record $^{13}\text{C-NMR}$ spectra samples were dispersed (5% w/v) in D_2O (99.9%, Goss Scientific Instruments Ltd., Essex) by continuous stirring overnight. Proton-decoupled spectra were recorded at 70°C with 19000 scans by applying 12800 pulses with a delay time of 2 s and 30 degrees pulse angle.

$^1\text{H-NMR}$ spectra were recorded for 640 scans at the same temperature. Prior to scanning, samples were sonicated (QSonica 1375, QSonica LL, Newtown) for 9 min in order to assist in aggregate dissociation. Sets of $^1\text{H-NMR}$ spectra were recorded at various okra pectin concentrations (1%, 2%, 4% and 5% w/v) with and without sonication in order to investigate how sonication affects the primary structure of the

polymers. Preliminary data (not shown) demonstrated that sonication for 9 min does not contribute to the structural modifications as evidenced by inspection of ^1H -NMR spectra of sonicated and non-sonicated samples at various concentrations. Chemical shifts were expressed in δ (ppm) relative to the resonance of internal standard: spectra were referenced to internal or external acetone (^{13}C $\delta = 31.55$ ppm and ^1H $\delta = 2.225$ ppm).

2.2.6 Molecular weight determination

To evaluate the average molar masses (M_w , weight average molar mass; M_n , number-average molar mass) samples were analyzed by size exclusion chromatography (SEC). Pectins were solubilized in 50 mM NaNO_3 solution (3 mg mL^{-1}) at room temperature under magnetic stirring overnight. Samples were injected onto an analytical SEC system comprising of three columns Aquagel-OH 40, 50 and 60 (15 μm particle size, 25cm \times 4mm, Agilent, Oxford, UK) connected in series. Pectins were eluted with 50 mM NaNO_3 (containing 0.02% NaN_3 as a preservative) at a flow rate of 1 mL min^{-1} and detected with an RI detector (differential index of refraction (dn/dc) equal to 0.1470 ml g^{-1}). Molecular parameters (M_w , M_n , R_g , M_w/M_n) were measured with a multiangle laser light scattering (MALLS) detector (mini-DAWN, Wyatt, Santa Barbara, CA, USA). Dextrans of known molecular weights (270 $\times 10^3$ and 410 $\times 10^3$ g mol^{-1}) were used as M_w standards.

2.2.7 Dilute solution rheology

Okra pectin was dispersed at 0.01 – 5.0 % g dL^{-1} at pH 7.0 in Sorensen's phosphate buffer or pH 3.0 citric buffers in the presence of 0.1 M NaCl with 0.02 g dL^{-1} NaN_3 as a preservative. Pectins were placed in sealed glass-vials and left overnight under continuous stirring to ensure complete solubilisation. Intrinsic

viscosity $[\eta]$ of okra pectins was determined at 20 °C with an Ubbelohde capillary viscometer (PSL, UK). Calculations were obtained by extrapolation of viscometric data to zero concentration according to the Huggins equation: $\eta_{sp}/c = [\eta] + k_H[\eta]^2c$ where $\eta_{sp}=(\eta_{\text{solution}}/\eta_{\text{buffer}}) - 1$ and k_H is the Huggins constant. Zero shear viscosity measurements were carried out at 20 °C using a Bohlin Gemini 200HR Nano rotational rheometer (Malvern Instruments, Malvern, UK) equipped with cone-and-plate geometry (55 mm diameter, cone angle 2°) and a Peltier temperature controller. All measurements were performed in a steady shear mode in the range 1–1000 s⁻¹.

2.3 RESULTS AND DISCUSSION

2.3.1 Isolation and compositional analysis

An isolation protocol was designed to study the influence of pH on extraction yield and the molecular characteristics of pectic substances from fresh okra pods. Extraction with petroleum ether (bp 40-65 °C) was performed as a first step in order to obtain a lipid-free material, which was subsequently used in aqueous extractions at pH 2.0 and 6.0 with 100 mM citric and phosphate buffer, respectively. The highest yields of pectic substances are usually obtained at high temperatures and low pH values in order to facilitate the cleavage of strong bonds between protopectin and other cell wall materials (Voragen, Rolin & Marr, 2003). It has been also reported that temperature has significant impact on the extraction yield of okra polysaccharides (Samavati, 2013). The isolation of the present okra polysaccharides was performed at 80 °C in order to facilitate the solubilisation of insoluble pectic substances (protopectin). Polysaccharides with different compositional characteristics can be isolated depending on the pH, time and temperature of extraction. It has been reported that pectic substances extracted at pH 3.0 have similar compositional characteristics

to water-soluble pectin but result in low yield values. Extraction at pH values below 3.0 leads to higher yields with pectins rich in rhamnogalacturonans (Levigne, Ralet & Thibault, 2002). Therefore, the extractions of pectic substances from okra were performed at two different pH values in order to obtain polysaccharides with distinct molecular characteristics. Pectic substances from okra pods could not be quantitatively recovered in a single extraction step and a second extraction was required (Figure 2.1). Similar findings have been reported for the extraction of pectins from other raw materials (Samavati, 2013; Sudhakar & Maini, 2000). The final stage, which can significantly affect the yield and chemical characteristics of pectins, is precipitation with ethanol. In the present work, precipitation was performed with ethanol at a 1:2 (v/v) supernatant to ethanol ratio and resulted in higher yields of pectic substances in comparison to preliminary 1:1 (v/v) ratio. It has been also reported that there is a pronounced effect of ethanol volume used in precipitation step on DM of isolated pectic substances (Faravash & Ashtiani, 2007). This occurs as the interaction between water, the carboxylic groups of pectin and the hydroxyl groups of ethanol facilitates cleavage of methyl ester linkages. Following alcohol precipitation, the pectin was washed with isopropanol and extensively dialysed against distilled water. Extraction with citric buffer adjusted to pH 2.0 resulted in slightly lower yield compared to extraction at pH 6.0. Furthermore, these extraction protocols result in pectin isolates of high purity as evidenced by low protein content (Table 2.1).

The highest yields of pectin are typically obtained by hot acid extraction in the pH range 1.5 to 3.0. Studies on pectin from other sources such as sugar beet pulp and banana peels also showed that the pectin yield increases significantly with a decrease in the pH of the extraction and the highest yields were obtained at pH around 1.5

(Happi Emaga, Ronkart, Robert, Wathelet & Paquot, 2008; Levigne, Ralet & Thibault, 2002; Yapo, Robert, Etienne, Wathelet & Paquot, 2007).

Table 2.1. Chemical composition of okra pectins extracted at pH 2.0 or 6.0.

	OP2	OP6
Yield (g pectin/100 g okra pods)	13.3 ± 0.3	15.7 ± 0.2
Total sugars ^a	70.0 ± 3.7	81.8 ± 6.4
D-GalA ^a	46.8 ± 2.1 (55.0) ^b	56.9 ± 6.9 (51.6) ^b
Methoxyl (-OCH ₃) ^a	3.3 ± 0.1	2.5 ± 0.1
Degree of methylation (DM%)	40.0 ± 1.6	24.6 ± 1.0
Acetyl (-COCH ₃) ^a	6.0 ± 0.6	5.2 ± 0.4
Degree of acetylation (DA%)	52.2 ± 5.5	37.6 ± 3.0
D-Gal ^a	17.0 ± 3.3 (21.7) ^b	26.1 ± 1.5 (25.7) ^b
L-Rha ^a	7.1 ± 2.0 (10.1) ^b	12.1 ± 0.9 (13.2) ^b
L-Ara ^a	4.5 ± 3.1 (7.1) ^b	6.0 ± 3.3 (7.3) ^b
D-Glc ^a	2.4 ± 0.5 (3.1) ^b	2.2 ± 0.1 (2.2) ^b
D-Xyl ^a	2.0 ± 0.7 (3.0) ^b	n/a
Protein ^a	4.3 ± 0.0	6.3 ± 0.1

^aAll values are expressed as % on wet basis of pectin powder.

^bValues in brackets are mol%.

These discrepancies with present data could be attributed to the origin of the initial material and the extraction conditions applied. The lower pectin yield at pH 2.0 could be attributed to partial acid hydrolysis that occurs at elevated temperatures as will be discussed later.

The chemical composition of okra pectins is shown in Table 2.1. The GalA content of the okra isolates varied from 46.8 to 56.9 % (Table 2.1). The GalA content was found to be significantly higher than has been previously reported for okra hot buffer soluble solids (HBSS, 35%) (Sengkhampan, Verhoef, Schols, Sajjaanantakul & Voragen, 2009) and was close to that of sugar beet pectins (29.5-52.8 %) (Levigne, Ralet & Thibault, 2002). Furthermore, the highest GalA content and pectin yield were obtained when okra pectins were extracted at pH 6.0. The results strongly indicate,

that the pectin extraction yield is related to the content of GalA reinforcing that partial degradation of pectic substances can take place under extraction conditions at pH 2.0. Both okra pectins were found to be low methoxyl (LM) pectins with DM of 40.0% and 24.6% for OP2 and OP6, considering that DM represents methoxyl content per galacturonic acid unit. The differences in DM of pectin samples could be attributed to the de-esterification process caused by β -eliminative degradation of the esterified homogalacturonan backbone that leads to the removal of methyl esters resulting in pectin with lower degree of methylation and consequently lower molecular weight (Kurita, Fujiwara & Yamazaki, 2008). Previous studies on okra extracts obtained by sequential extraction also revealed the presence of low methoxyl pectins (Sengkhampan, Verhoef, Schols, Sajjaanantakul & Voragen, 2009). Okra extracts also exhibited high acetyl content with marginal differences for 6.0 (OP2) and 5.2 % (OP6) (Table 2.1). Highly acetylated pectins have been previously isolated from sugar beet where acetyl content varied in the range of 2.2–9.0% (Dea & Madden, 1986; Endreß & Rentschler, 1999). Previous studies on okra polysaccharides obtained by sequential extraction reported DA in the range of 18–58% and also revealed uncommon acetylation patterns. It has been previously reported that not only galacturonosyl residues, but also rhamnosyl residues were acetylated in the RG-I segments (Sengkhampan, Bakx, Verhoef, Schols, Sajjaanantakul & Voragen, 2009). It should be stressed, that in the present study, DA is expressed to a first approximation as acetyl content per galacturonic acid (GalA) unit assuming acetylation only on galacturonosyl residues.

It has been widely shown that pectic polysaccharides are ester-linked to ferulic acids in some plant cell walls including spinach, sugar beet, glasswort and quinoa (Fry, 1982; Renard, Champenois & Thibault, 1993; Renard, Wende & Booth, 1999).

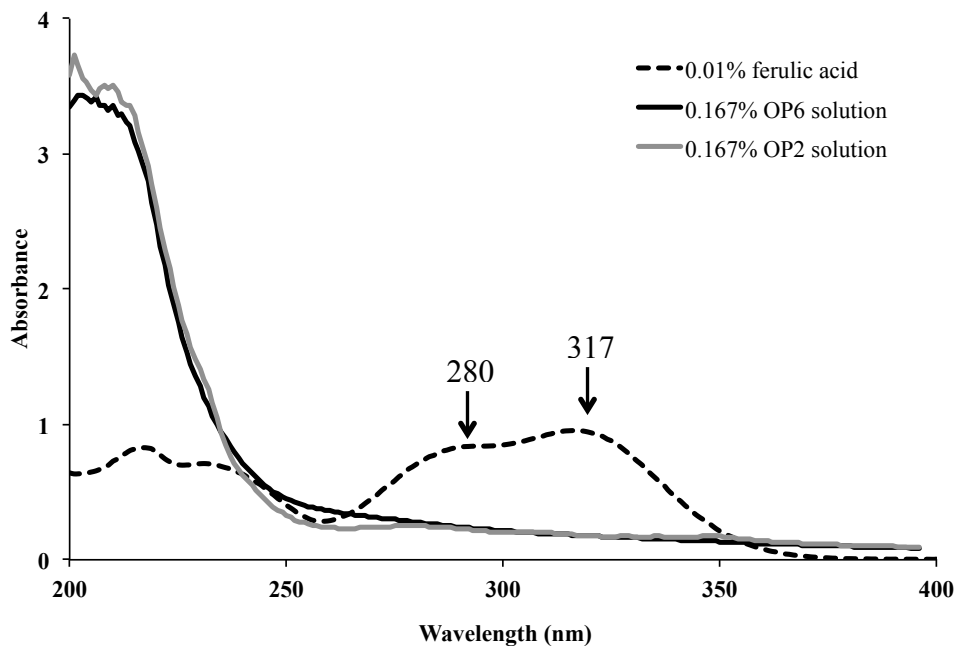


Figure 2.2. UV absorption spectra for 0.167 % w/v OP2, OP6 solutions and 0.01 % w/v of ferulic acid solution (pH 4.0).

Ferulic acid is a hydroxycinnamic acid (trans-4-hydroxy-3-methoxycinnamic acid), a type of phenolic compounds. The studies on ferulic acids from sugar beet have demonstrated that 50% of feruloyl in the beet pectins are linked to arabinose residues and 50% to galactose residues (discussed in detail in chapter 1) (Saulnier & Thibault, 1999). The presence of feruloyl groups may impact physical and chemical properties of pectic polysaccharides. For instance, sugar beet pectin has poor gelling properties, however, in the presence of oxidizing agent (e.g., H_2O_2 and peroxidase) a good quality sugar beet pectin-based gel could be formed (Thibault, Guillon & Rombouts, 1991). The network formation occurs due to the oxidative coupling of two ferulic acids and results in formation of ferulic acid dimers. The chemical structure of ferulic acids, particularly aromatic ring, produces strong absorbance in the ultraviolet region (UV) associated with electronic transitions of the molecule. The UV absorption

spectra of okra pectin solutions (OP2 and OP6) and standard of ferulic acid are shown in Figure 2.2. Ferulic acid exhibits a maximum absorbance at 317 nm and a shoulder at 280 nm that indicate the esters of cinnamic acid. The UV absorption spectra of OP2 and OP6 samples indicated the absence of any ferulic acids in okra pectin as evidenced by the absence of absorption peaks in the range of 250-350 nm.

The main neutral sugars present in OP2 and OP6 were galactose (17.0 – 26.1%), rhamnose (7.1 – 12.1%) and arabinose (4.5 – 6.0%). The retention times of sugar standards are shown in Table 2.2 and elution profiles of OP2, OP6 in Figure 2.3. The presence of 4 – 6% of the proteinaceous components may indicate that galactose and arabinose could also originate from arabinogalactans forming arabinogalactan-protein complexes (Immerzeel, Eppink, de Vries, Schols & Voragen, 2006). Very low levels of glucose (2.2 – 2.4%) and xylose (2.0% in OP2) were also detected in the okra pectins extracted at pH 2.0 suggesting the presence of rhamnogalacturonan II (RG-II) or xylogalacturonan regions. The total neutral sugar content was expressed as the sum of the individual neutral sugars and revealed that the highest neutral sugars yield was obtained with extraction at pH 6.0 (46.4%) that corresponds to milder extraction conditions which avoids degradation of pectin side chains. In addition, the content of GalA in OP2 was lower than in OP6. It seems that extraction at pH 2.0 also induces a breakdown in the smooth region composed primarily of homogalacturonan. Degradation of glycosidic linkages is usually observed at low pH values and elevated temperatures with different degree of stability (GalA – GalA > GalA – Rha > neutral sugar – neutral sugar) (Thibault, Renard, Axelos, Roger & Crépeau, 1993).

Table 2.2. Retention times of methanolysis products of standard sugars. Inositol was used as an internal standard.

Monosaccharide	Retention time (min)		
	Peak1	Peak 2	Peak 3
D-GalA	6.531	7.311	7.406
D-Gal	7.849	8.057	n/a
L-Rha	3.325	3.537	n/a
L-Ara	3.495	3.544	n/a
D-Glc	8.331	n/a	n/a
D-Xyl	3.441	3.558	
Inositol	12.498	n/a	

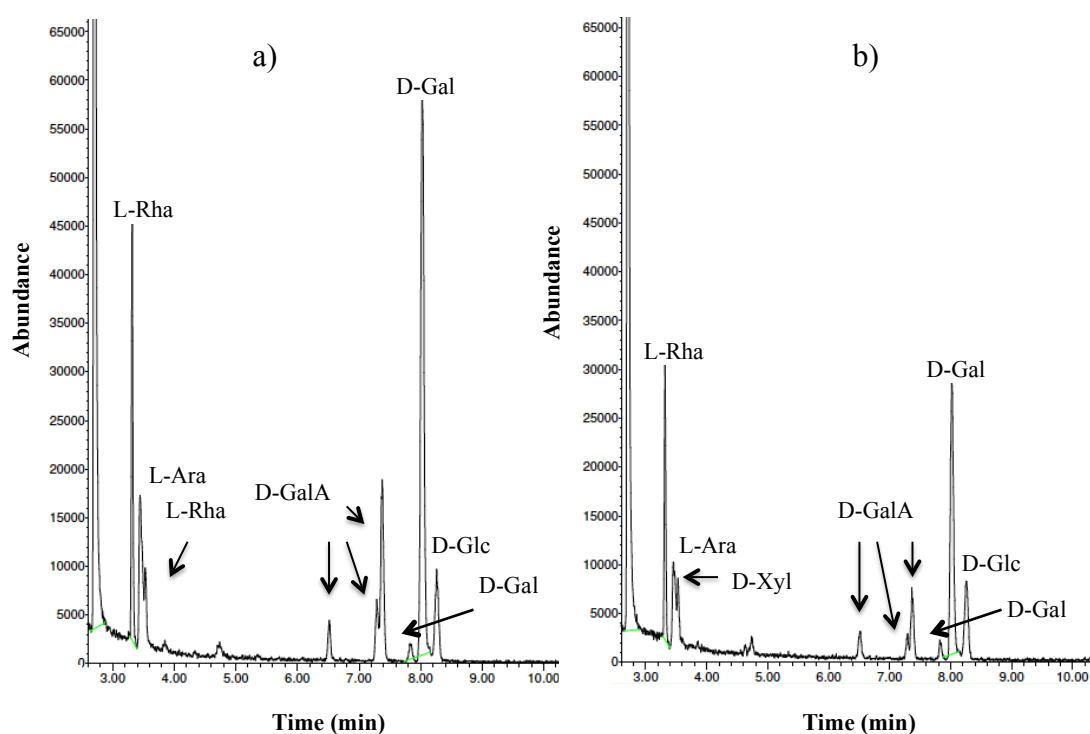


Figure 2.3. GC-chromatograms of a) OP6 and b) OP2.

The ratios of constituent sugars were used in order to investigate the structure of the extracted pectins at the molecular level. According to the sugar composition

data expressed as sugar molar ratios (Table 2.3) some interesting characteristics of the extracted polysaccharides were observed. The molar ratio of rhamnose to galacturonic acid is indicative of the presence of RG-I segments within the pectin population. The RG-I backbone is typically composed of alternating units of rhamnose and galacturonic acid and therefore the molar ratio of Rha/GalA is virtually 1:1 (Yapo, 2011).

Table 2.3. Sugar molar (%) ratios for OP2 and OP6.

Sample	GalA/ (Rha+Ara+Gal+Xyl)	Rha/GalA	(Ara+Gal)/ Rha	HG	RG-I	HG/RG
OP2	1.3	0.18	2.9	44.9	49	0.9
OP6	1.1	0.25	2.5	38.9	59.4	0.7

The contribution of RG-I to the pectin population was 0.18 and 0.25 for OP2 and OP6, respectively (Table 2.3). Furthermore, the analysis of molar percentages of HG and RG-I in both okra pectins revealed the prevalence of RG-I pectins in OP6 whereas OP2 was composed of almost equal amounts of HG and RG-I pectins (Table 2.3). These data suggest structural dissimilarities of our samples compared to common pectins isolated from apple or sugar beet, where RG-I segments constituted ~16.2 or ~31.9% of the pectin populations (Leroux, Langendorff, Schick, Vaishnav & Mazoyer, 2003). However, more than 50% of RG-I has been previously reported for hot water-extracted pectins from soybean and green tea leaves and almost as the only pectic component in okra polysaccharides obtained by hot buffer sequential extraction and linseeds mucilages (Ele-Ekouna, Pau-Roblot, Courtois & Courtois, 2011; Muralikrishna, Salimath & Tharanathan, 1987; Nakamura, Furuta, Maeda, Nagamatsu & Yoshimoto, 2001; Sengkhamparn, Verhoef, Schols, Sajjaanantakul & Voragen,

2009). The molar ratio of (Ara+Gal)/Rha is indicative for the degree of branching of RG-I segments. The molar ratio for OP2 was 2.9 and 2.5 for the OP6 suggesting slightly shorter side chains of RG-I regions in OP6 than in OP2. Generally, OP2 and OP6 demonstrated remarkably higher degree of branching of side chains than was previously reported for okra polysaccharides obtained by sequential extractions (1.3–1.4) (Sengkhampan, Verhoef, Schols, Sajjaanantakul & Voragen, 2009). In addition, the (Ara+Gal)/Rha ratio indicates the presence of galactan and arabinan side chains in the RG-I segments (Table 2.3).

2.3.2 FT-IR spectroscopy

Polysaccharides extracted at pH 2.0 or pH 6.0 were analysed using FT-IR spectroscopy in the wavenumber region 900 – 4000 cm^{-1} and their spectra were compared to low- and high-methoxyl citrus pectin (Figure 2.4). The region between 3500 and 1800 cm^{-1} shows two major identical peaks for both samples corresponding to O-H stretching absorption due to inter- and intramolecular hydrogen bonding of the GalA backbone (3000 – 3500 cm^{-1}) and C-H absorption (2940 cm^{-1}), which typically includes CH, CH₂ and CH₃ stretching vibrations (Chatjigakis, Pappas, Proxenia, Kalantzi, Rodis & Polissiou, 1998; Gnanasambandam & Proctor, 2000). A second region of the FT-IR spectra below 1800 cm^{-1} indicates the ‘fingerprint’ region for carbohydrates and corresponds to the skeletal C-O and C-C vibration bands (ca. 900 – 1200 cm^{-1}) of glycosidic bonds and pyranose rings (Kamnev, Colina, Rodriguez, Ptitchkina & Ignatov, 1998). The spectral regions with three bands at around 1044, 1072 and 1147 cm^{-1} were assigned to pyranose ring vibrations and may indicate certain similarities in the monosaccharide composition of OP2 and OP6 (Figure 2.4). Also this region of FT-IR spectra demonstrates considerable differences in neutral sugars composition between commercial citrus and extracted okra pectin. While citrus

pectin has typical bands at around 1004, 1022, 1047, 1072 cm^{-1} , the okra pectin has only at 1044, 1072 and 1147 cm^{-1} with relatively higher abundance of each band. This difference was expected as citrus pectin typically contains low amounts of galactose (2.4%) and arabinose (1.1%) as opposed to the OP2 and OP6 (Table 2.1) (Kravtchenko, Voragen & Pilnik, 1992).

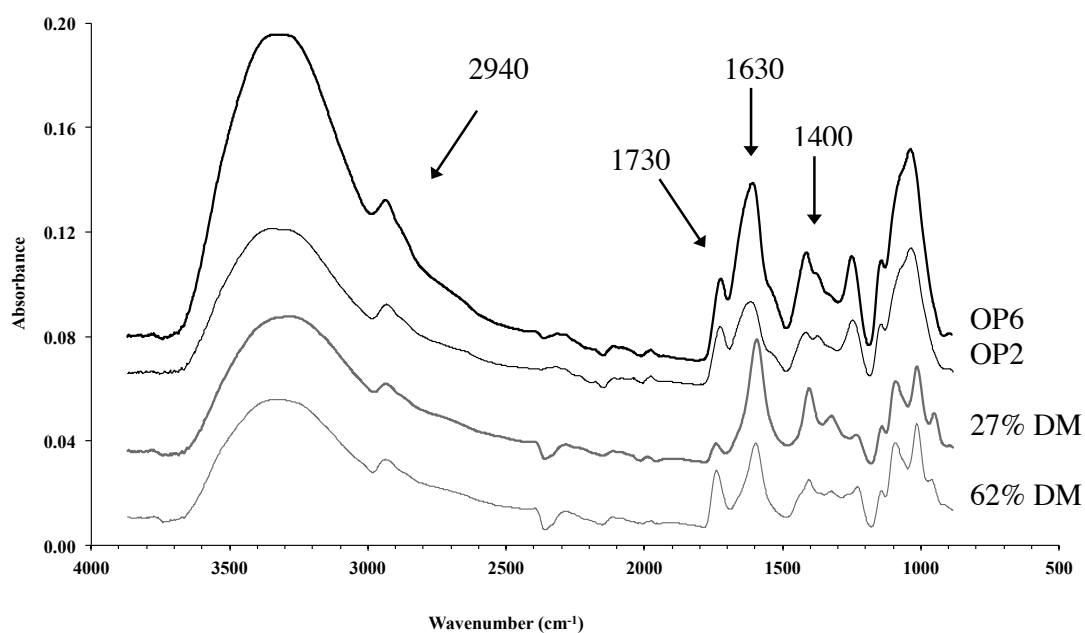


Figure 2.4. Fourier transform–infrared spectra (FT-IR) of commercial pectin standards with different DM and OP2, OP6.

The chemical analysis of OP2 and OP6 also indicated the presence of proteins (Table 2.1), which were detected also by FT-IR with absorption bands appearing at around ca. 1500–1600 cm^{-1} . Analysis of OP2 and OP6 FT-IR spectra revealed similarities with low-methoxyl citrus pectin in absorption bands corresponding to stretching vibration of free (ca. 1610 – 1630 cm^{-1}) and methyl-esterified (ca. 1730 cm^{-1}) carboxyl groups. In addition, FT-IR spectra for OP6 have demonstrated higher intensity of free carboxyl stretching band in comparison to OP2, which indicates lower degree of esterification for OP6 sample. These data further support chemical

analysis, which revealed DM of 40.0 and 24.6% for OP2 and OP6, respectively.

2.3.3 ^1H and ^{13}C -NMR spectra

NMR spectroscopy was employed in order to obtain structural information about the isolated okra polymers. ^1H -NMR spectra (Figure 2.5a, 2.5b) of both samples revealed similar resonance patterns suggesting similarities in compositional characteristics of OP2 and OP6. A large signal was detected at 3.84 ppm, which was attributed to methyl groups bonded to carboxyl groups of galacturonic acid (GalA) (Cheng & Neiss, 2012). Signals at around 2.10 ppm were assigned to acetyl groups. Previous work on okra extracts reported the acetylation of both galacturonosyl and rhamnosyl residues in the RG-I fractions. Signals at 1.27 and 1.36 ppm are from methyl groups of unbranched α -(1 \rightarrow 2)-linked and branched α -(1 \rightarrow 2) and α -(1 \rightarrow 4)-linked rhamnose. Due to the complexity of ^1H -NMR spectra in the low-field region, proton signals found at around 3.70–5.20 ppm were investigated with the aid of a COSY spectrum (data not shown), which provided the evidence of the presence of six major protons, which were assigned to D-galacturonic acid.

^{13}C -NMR spectra OP2 and OP6 are presented in Figure 2.6 (a, b). The signals at around 172.00 ppm in the carbonyl region of the spectrum were attributed to the carbonyl group (C=O) of galacturonic acid whereas the next signal at around 175 ppm corresponds to the C-6 of esterified carboxyl groups of galacturonic acid (Tamaki, Konishi, Fukuta & Tako, 2008). In the ^{13}C -NMR spectra of both pectins, two signals at around 21.87 ppm can be readily assigned to the methyl of acetyl groups. The presence of methyl groups bonded to carboxyl groups of galacturonic acid is also confirmed by a resonance at 54.18–54.21 ppm in OP2 and OP6 spectra (Figure 2.6a, 2.6b). The third signal attributed to methyl groups at 18.5 and 17.58 ppm corresponded to methyl groups of rhamnose.

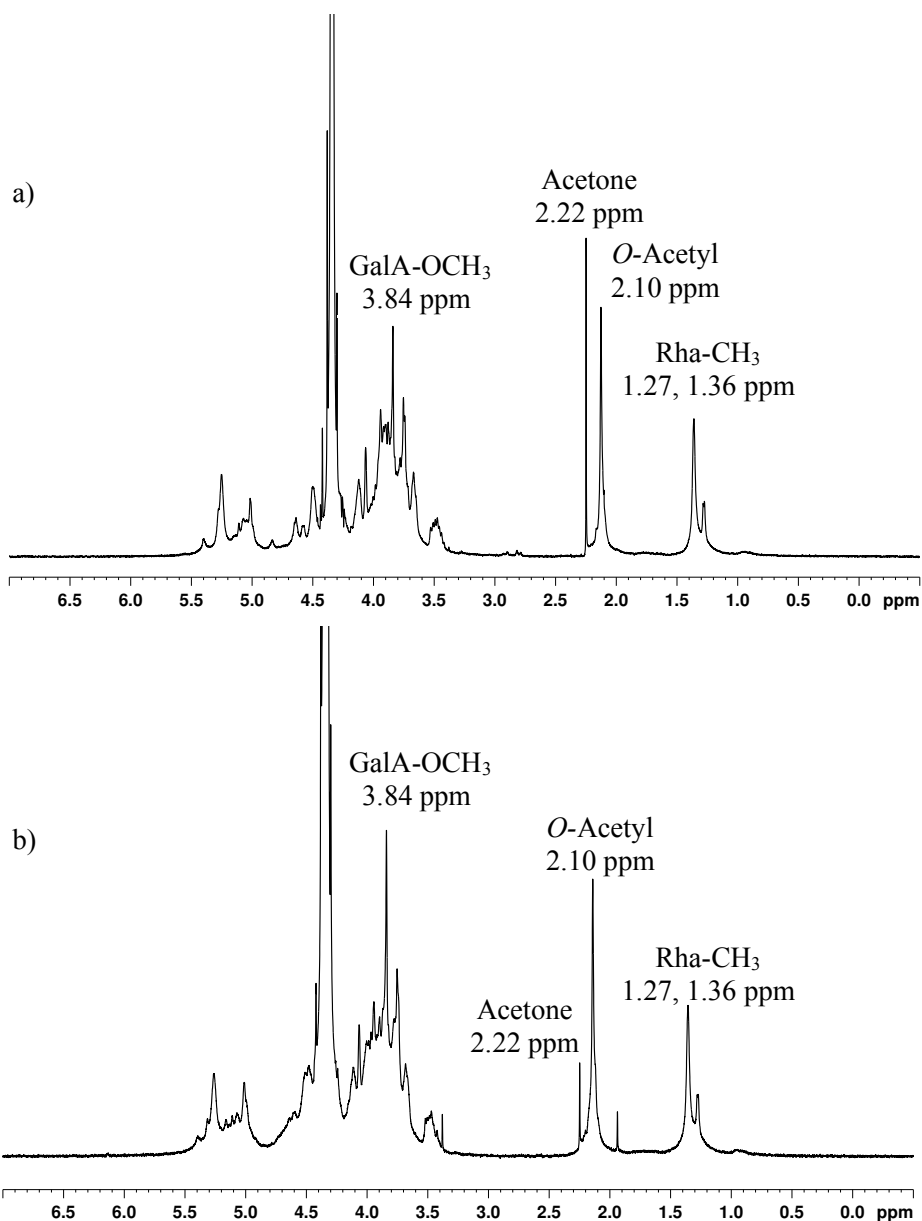


Figure 2.5. ^1H -NMR spectra of OP2 (a) and OP6 (b) samples in D_2O at $70\text{ }^\circ\text{C}$. Acetone reference at 2.22 ppm.

^1H and ^{13}C -NMR spectra of both okra polysaccharides demonstrated good match with the spectrum of okra polysaccharides isolated using sequential extractions and those isolated from pumpkin, apple, flax stems and citrus plant (Bédouet, Courtois & Courtois, 2003; Cozzolino, Malvagna, Spina, Giori, Fuzzati, Anelli, Garozzo & Impallomeni, 2006; Grasdalen, Bakøy & Larsen, 1988; Košťálová,

Hromádková & Ebringerová, 2013; Rosenbohm, Lundt, Christensen & Young, 2003; Sengkhampan, Verhoef, Schols, Sajjaanantakul & Voragen, 2009; Tamaki, Konishi, Fukuta & Tako, 2008).

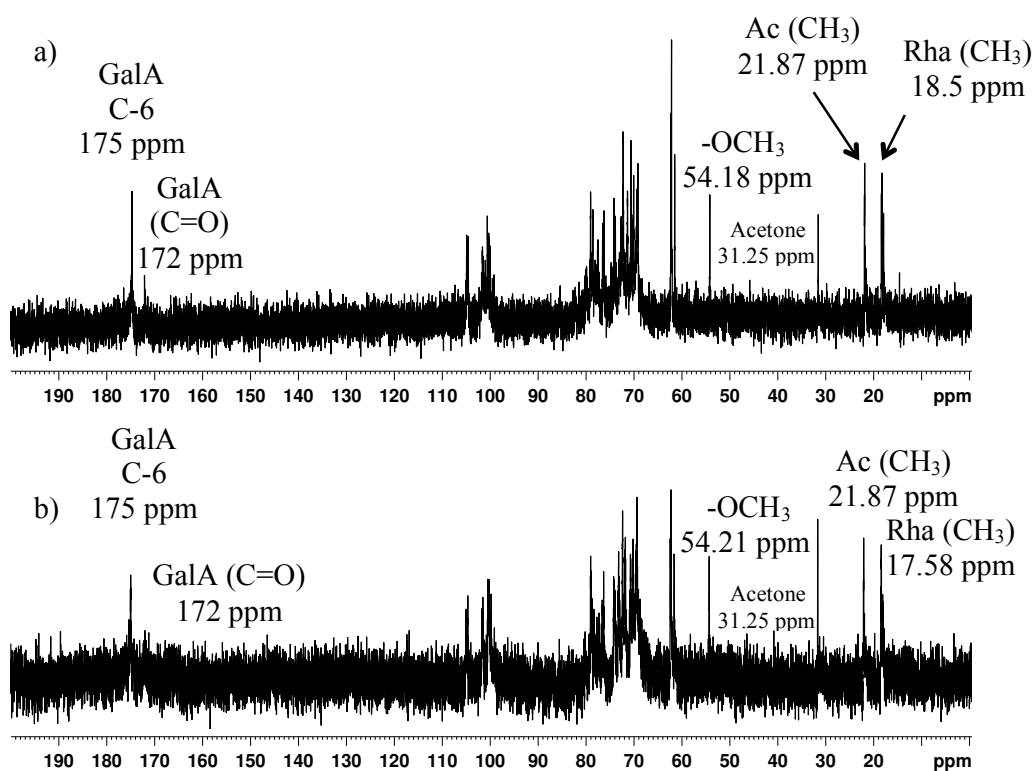


Figure 2.6. ^{13}C -NMR spectra of OP2 (a) and OP6 (b) samples in D_2O at $70\text{ }^\circ\text{C}$. Acetone reference at 31.25 ppm.

2.3.4 Macromolecular characteristics of pectin

To obtain information with regards to molecular dimensions of the pectins weight average (M_w) and number average (M_n) molecular weights, radius of gyration (R_g), and polydispersity index (M_w/M_n) were determined by size exclusion chromatography (SEC) coupled to multiangle laser light scattering. The elution RI traces of OP2 and OP6 are shown in Figure 2.7, whereas estimates of their molecular characteristics are represented in Table 2.4. The elution profiles of both samples indicated broad M_w distributions and were comprised of polymer populations of high

and low hydrodynamic volumes as indicated by the presence of three RI peaks (Figure 2.7).

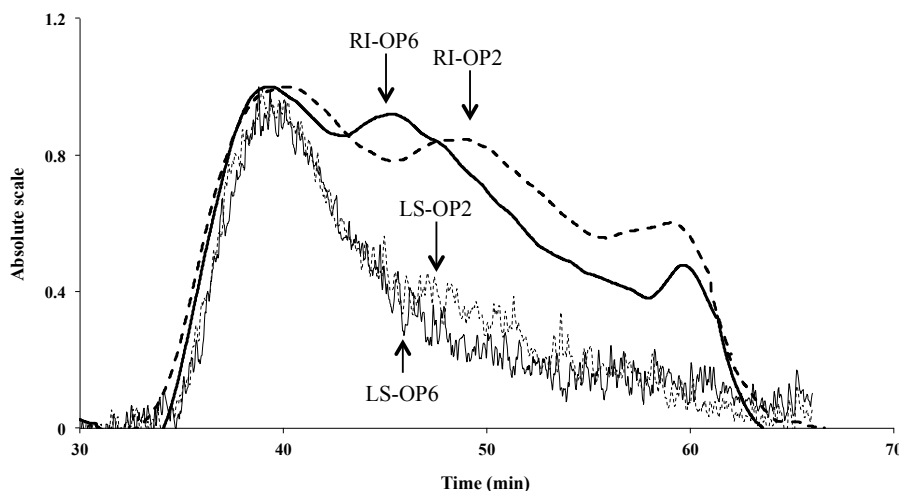


Figure 2.7. Refractive index (RI) and MALLS traces (LS) of size exclusion chromatograms of OP2 and OP6.

Moreover, it can be clearly seen that only the third peak to elute was similar for both OP2 and OP6 samples. On the contrary, a shift towards a population of polymers of lower hydrodynamic volumes was observed for the first and second peak in OP2 elution profile indicating the conformational differences between pectin samples (Figure 2.7). This variation in elution patterns should be attributed to the differences in the pH of the extraction that results in partial hydrolysis of OP2. The polydispersity index of OP2 and OP6 was relatively low in comparison to values reported for other polysaccharides (1.5 – 2.0) (Table 2.4) (Cui, 2005). The separation of polysaccharide fractions in an SEC column is based on the differences in hydrodynamic volume of polymer chains. Polysaccharide hydrodynamic volume can significantly vary with the number, positions and length of the branches in polymer chains (Gaborieau & Castignolles, 2011). Therefore, polymer chains with comparable molecular weight, but different degree of branching will elute at different times. Analysis of RI and

MALLS traces indicates that both OP6 and OP2 are composed of three distinct polymer populations of relatively comparable molecular weights, but different hydrodynamic volumes. However, similar in that aspect (three polymer populations), pectin samples differentiated significantly in terms of weight-average molar mass as shown in Table 2.4. The weight-average molar mass values were much higher than those obtained for okra polysaccharides obtained by sequential extraction ($10 - 100 \times 10^3 \text{ g mol}^{-1}$), sugar beet ($70 - 355 \times 10^3 \text{ g mol}^{-1}$) and citrus pectins ($162 \times 10^3 \text{ g mol}^{-1}$) (Leroux, Langendorff, Schick, Vaishnav & Mazoyer, 2003; Levigne, Ralet & Thibault, 2002; Sengkhampan, Verhoef, Schols, Sajjaanantakul & Voragen, 2009) indicating that the present protocol results in especially high molecular weight pectins.

Table 2.4. Molecular characteristics of OP2 and OP6. Slopes, intrinsic viscosity ($[\eta]$), critical concentration (c^*) and coil overlap parameter ($c^*[\eta]$) of OP2 or OP6 at two different buffer pH values.

Parameter	OP2		OP6	
Mw x 10^3 (g/mol)	641		767	
Mn x 10^3 (g/mol)	628		715	
Rg (nm)	108		121	
Mw/Mn	1.02		1.07	
	pH 7	pH 3	pH 7	pH 3
Slope 1	0.71	0.44	0.31	0.20
Slope 2	1.97	2.13	1.75	2.04
$[\eta]$ (dL g $^{-1}$)	4.1	3.3	4.4	2.8
c^* (g dL $^{-1}$)	0.37	0.45	0.15	0.44
$c^*[\eta]$	1.51	1.49	0.66	1.24

2.3.5 Dilute solution viscometry

Intrinsic viscosity, a measure of the hydrodynamic volume occupied by a molecule, is a measure of the capacity of a polymer molecule to enhance the viscosity of solutions. Pectins isolated from okra pods contain substantial amounts of galacturonate residues. In aqueous solutions (pH 7.0), the expansion of individual coils by intramolecular electrostatic repulsion increases intrinsic viscosity. Therefore, to avoid complications stemming from changes in coil dimensions with polymer concentrations and to obtain intrinsic viscosity values in the absence of electrostatic interactions, all measurements were performed under the electrostatic screening provided by 0.1M NaCl (Kontogiorgos, Margelou, Georgiadis & Ritzoulis, 2012; Ndjouenkeu, Akingbala & Oguntimein, 1997). Dilute solution viscometry was also performed at two different buffer pH values (7.0 and 3.0) in order to investigate the changes in coil conformations with modulation of intramolecular forces. The intrinsic viscosity values of okra pectins dispersed in phosphate buffer adjusted to pH 7.0 were 4.1 and 4.4 dL g⁻¹ for OP2 and OP6, respectively (Table 2.4). A modest difference in $[\eta]$ values for OP2 and OP6 could be attributed to the higher Mw of OP6 and higher degree of branching of RG-I segments in OP2 indicating higher flexibility of RG-I regions and formation of compact macrostructures with a shorter hydrodynamic size (Yapo, 2011). Okra pectin $[\eta]$ values were found to be higher in comparison to those previously reported for okra extracts obtained by sequential extractions ($\sim 0.9 - 2.7$ dL g⁻¹) and comparable to pectins isolated from sugar beet ($\sim 2.1 - 4.1$ dL g⁻¹) or pumpkin ($\sim 3.3 - 3.4$ dL g⁻¹) (Kontogiorgos, Margelou, Georgiadis & Ritzoulis, 2012; Levigne, Ralet & Thibault, 2002; Morris, Castile, Smith, Adams & Harding, 2010; Morris, Ralet, Bonnin, Thibault & Harding, 2010; Ndjouenkeu, Akingbala & Oguntimein, 1997; Ptitchkina, Danilova, Doxastakis, Kasapis & Morris, 1994). The

contribution of acetyl and methyl groups and degree of branching of side chains can also play a significant role to the coil dimensions of extracted pectin (Anger & Berth, 1986; Sengkhampan, Sagis, de Vries, Schols, Sajjaanantakul & Voragen, 2010). Lower amounts of RG-I regions (49.0 – 59.4%) and much higher of HG segments (44.9 – 38.9%) could account for the higher $[\eta]$ values of OP2 and OP6. It is well documented that charge density, chain length (molecular weight) and stiffness of polymer control the magnitude of $[\eta]$ (Morris, Cutler, Ross-Murphy & Rees, 1981). The polyelectrolyte nature of pectin also controls the conformation of the chains. Increase of pH results in dissociation of GalA and both samples (OP2, OP6) are negatively charged resulting in electrostatic repulsion, extended conformations and consequently high $[\eta]$ values. Intrinsic viscosity data obtained with citric buffer adjusted to pH 3.0 (Table 2.4) show that $[\eta]$ of OP2 and OP6 were 3.3 dL g⁻¹ and 2.8 dL g⁻¹, respectively. Decrease of pH leads to protonation of GalA contributing to the decrease in net charge and strength of electrostatic repulsions resulting in more compact conformations. It has been previously shown (Table 2.1) that OP6 has higher GalA content than OP2 counterpart. Therefore, changes of intramolecular forces contributed to slightly lower $[\eta]$ of OP6 indicating a decrease of the hydrodynamic volume of the macromolecular chain consequently leading to the predominance of a more compact structure in comparison to OP2 sample where expansion of individual coils takes place.

The dilute solutions of most random coil polysaccharides (with the exception of xanthan and some β -glucans) show Newtonian flow behaviour. Figure 2.8 (a, b) demonstrates a typical plot for shear rate dependence on viscosity for OP6 at pH 3.0 and 7.0. As expected for dilute OP6 solutions dispersed in citric (pH 3.0) or phosphate buffer (7.0), the measured viscosities remained independent of shear rate indicating

Newtonian flow behaviour. As the polymer concentration increased, there was a progressive development of shear thinning flow behaviour where reduction in viscosity values occurred with increasing shear rate (Figure 2.8 a, b). Moreover, Figure 2.8 (a, b) shows that OP6 dispersed in phosphate buffer (pH 7.0) exhibits a transition from Newtonian to shear thinning flow behaviour at lower polymer concentration ($\sim 0.25\%$ w/v) than in citric buffer (pH 3.0) ($\sim 0.5\%$ w/v). This indicates an increase in the number of pectin inter-chain interactions and formation of polymer chain entanglements. In order to further investigate this the solution behaviour of okra pectins was studied by measuring the zero shear specific viscosity $(\eta_{sp})_0$ at different concentrations of the polysaccharide and plotting them *versus* the dimensionless coil overlap parameter, $c[\eta]$. Double-logarithmic plots of $(\eta_{sp})_0$ vs. $c[\eta]$ were constructed to determine specific critical concentration (c^*) at which the transition from the dilute to concentrated regime appears and which is accompanied by significant changes in solution rheological properties (Figure 2.9, Table 2.5) (Morris, Cutler, Ross-Murphy & Rees, 1981). Critical concentration values (c^* , g dL⁻¹) for OP2 and OP6 dispersed in phosphate buffer (pH 7.0) were between 0.15 – 0.37 g dL⁻¹ whereas solutions prepared with citric buffer (pH 3.0) demonstrated higher values in the range 0.44 – 0.45 g dL⁻¹. In general, polymers that have high $[\eta]$ will also exhibit a transition from the dilute to concentrated region at lower polymer concentration due to the increased number of intermolecular interactions. For okra pectin solutions, c^* values were lower than those reported for okra gum (1.5 g dL⁻¹), okra polysaccharides obtained by hot buffer sequential extraction (0.83 – 1.23 g dL⁻¹), apple pectins (1.27 – 1.39 g dL⁻¹) and other random coil polysaccharides (Hwang & Kokini, 1992; Kontogiorgos, Margelou, Georgiadis & Ritzoulis, 2012; Morris, Cutler, Ross-Murphy & Rees, 1981; Ndjouenkeu, Akingbala & Oguntimein, 1997;

Sengkhampan, Sagis, de Vries, Schols, Sajjaanantakul & Voragen, 2010). The $c^*[\eta]$, a measurement of the total volume occupied by all coils within the polymer solution regardless of their molecular weight at the critical concentration, was also calculated.

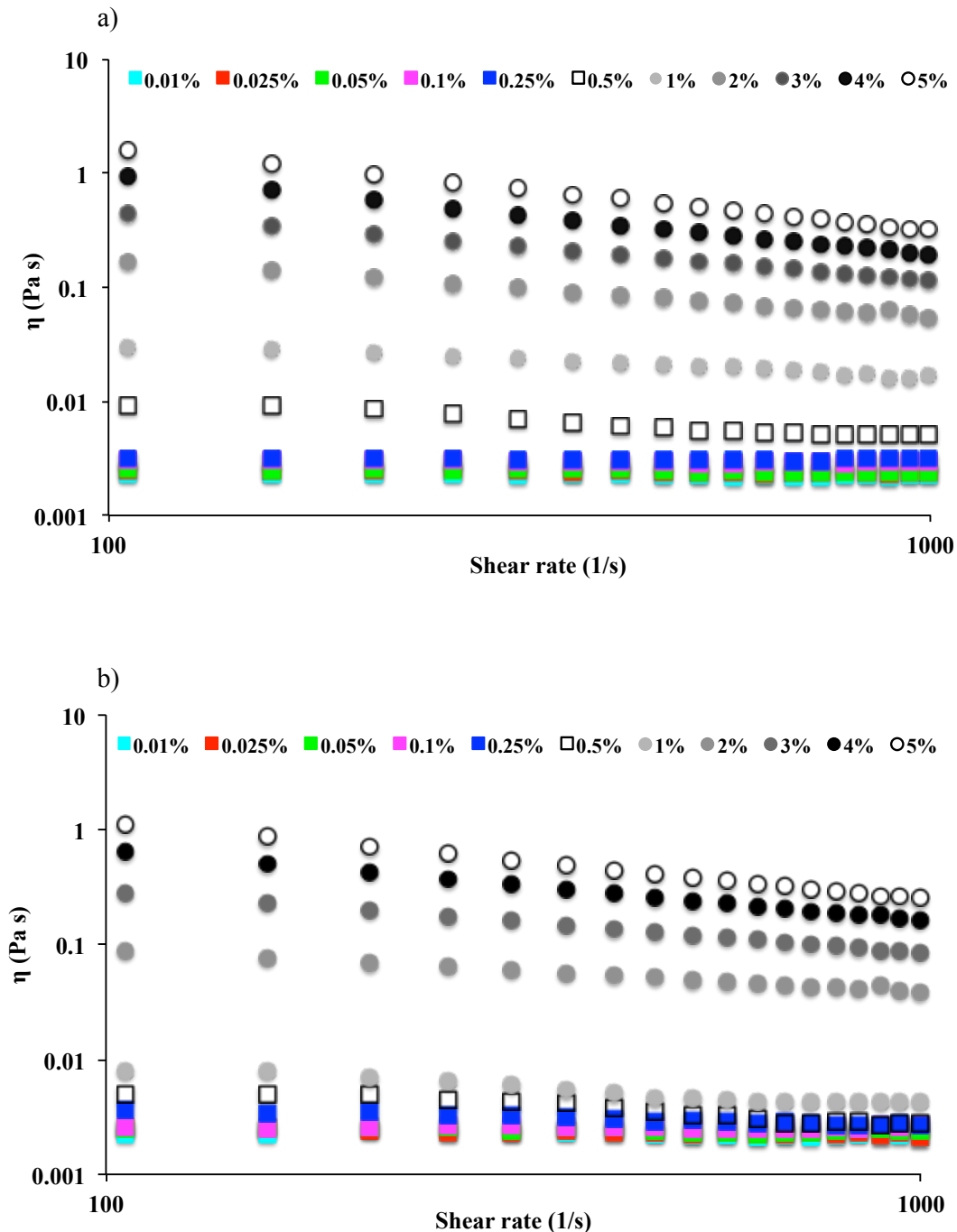


Figure 2.8. Viscosity (η) as a function of shear rate for OP6 at different concentrations (0.01 – 5% w/v) and two buffer pH values a) pH 3.0 and b) pH 7.0.

The results presented in Table 2.4 show the $c^*[\eta]$ for OP2 and OP6 in different buffer solutions. It has been reported that for most disordered linear polysaccharides double-logarithmic plots of $(\eta_{sp})_o$ vs. $c[\eta]$ superimpose closely regardless of the primary structure and molecular weight, and also fall into two linear regions with a sharp change of slopes (Morris, Cutler, Ross-Murphy & Rees, 1981; Ndjouenkeu, Akingbala & Oguntimein, 1997).

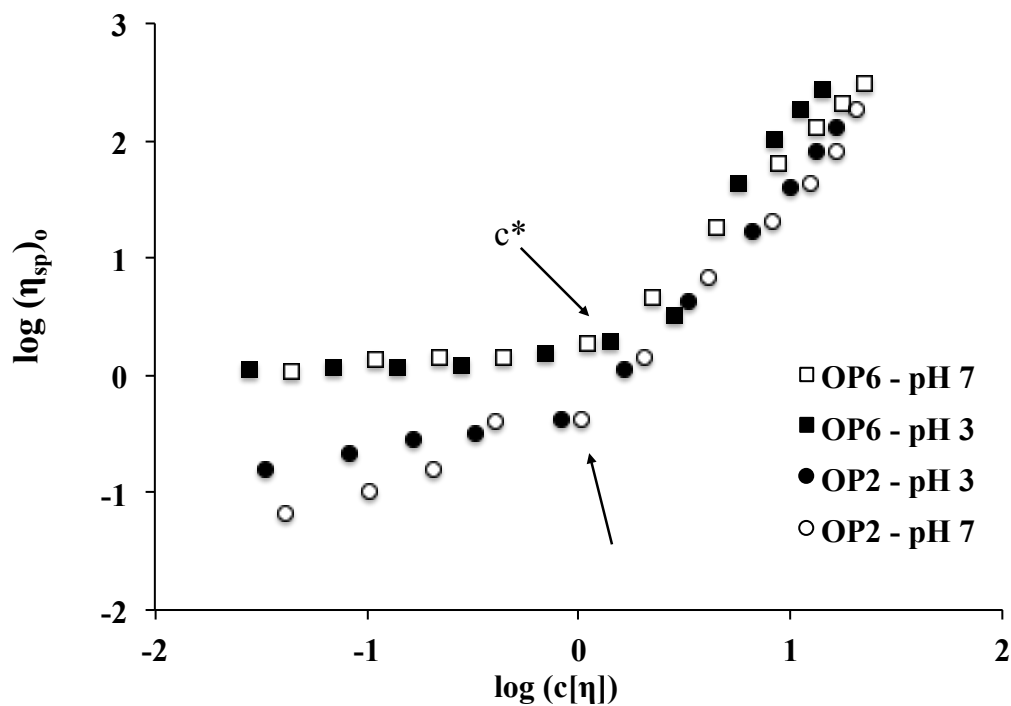


Figure 2.9. Double logarithmic plots of zero shear specific viscosity $(\eta_{sp})_o$ vs. reduced concentration $c[\eta]$ of OP2 and OP6 at pH 3 and pH 7.

However, as shown in Figure 2.9, the results obtained for present okra pectins do not comply well with this generalisation, particularly for dilute region ($c < c^*$) and demonstrate a significant deviation in slopes values regardless of solution pH. Moreover, slopes 1 of OP2 and OP6 were found to be significantly lower in comparison to those reported for polymers of different primary structure but with similar conformational characteristics (1.1 – 1.6) (Lapasin & Pricl, 1999). Therefore,

our results indicate that the polyelectrolyte nature and differences in molecular structure of extracted pectins significantly affect conformational characteristics of polymer chains within the dilute region. However, values of slopes 2 are in a good agreement with the slopes values typical for disordered polysaccharides ($\sim 1.9 - 5.6$) indicating that in dilute solutions the net charge of pectin chains plays predominant role for chain conformations (Table 2.4) (Lapasin & Prici, 1999). The above findings suggest that buffer composition and extraction strategy are principal determinants of the structural characteristics of the isolated pectins and the properties of resulting solutions.

2.4 CONCLUSIONS

In the present chapter, the molecular features of okra pectins as affected by extraction conditions were studied. Extraction conditions influenced the fine structure of pectins resulting in isolates with distinct molecular characteristics. The present isolation protocols resulted in high molecular weight pectins with low degree of methylation (DM) and high degree of acetylation (DA). Galacturonic acid (GalA) amount varied by altering the pH of the extraction with higher pH values (pH6.0) resulting in greater GalA content. Both isolates contained high amounts of branched RG-I segments as indicated by the ratio of rhamnose to galacturonic acid and the high content of galactose to rhamnose. Dilute solution viscometry revealed changes in the coil dimensions for both of the isolated biopolymers with changes in pH as evidenced by intrinsic viscosity measurements. The high molecular weight and degree of acetylation as well as the influence of pH on the conformation of the chains introduces a new source of pectins with potentially high emulsifying and emulsion-stabilizing capacity that will be dealt in detail in chapter 4.

CHAPTER 3

APPLICATIONS OF OKRA PECTIN IN HIGH AND LOW MOISTURE CONTENT SYSTEMS

Parts of this chapter were published as:

Alba, K., Kasapis, S., & Kontogiorgos, V. (2015). Influence of pH on mechanical relaxations in high solids LM-pectin preparations. *Carbohydrate Polymers*, 127, 182-188.

3.1 INTRODUCTION

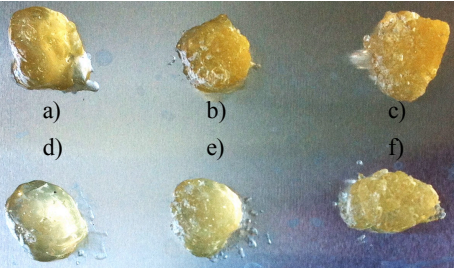
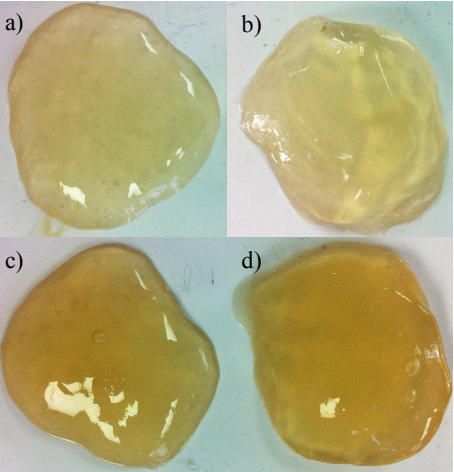

The major commercial applications of pectin in the food industry include gelling and thickening of jams, jellies, bakery fillings, confectionery and stabilization of milk and fruit beverages. The mechanisms of cross-linking of pectin molecules into the three-dimensional network are typically impacted by the degree of methyl esterification, distribution of ester groups along the chain and molecular weight distributions (discussed in detail in Chapter 1). Gelation (high moisture regime) in low methoxylated pectin is mediated by electrostatic bridging of adjacent carboxyl groups of D-GalA residues typically with calcium cations or in some instances with monovalent ions (Strom, Schuster & Goh, 2014). Sol-gel transition, however, is frequently interrupted by the presence of side-chains or acetyl groups that moderate the ability of the polymer to gel. Okra pectin is distinct because it primarily consists of RG-I units and has a high acetyl content virtually halting the gelation process. Preliminary work on okra pectin in the absence of glucose syrup confirmed that it remained in the sol-state under an extensive set of experimental conditions (e.g., calcium and pectin concentration, pH, temperature) and the results are shown in Table 3.1.

Pectic polysaccharides traditionally play a central role as major components in the development of high-solid (low moisture regime) confectionery products (Al-Ruqaie, Kasapis, Richardson & Mitchell, 1997; Almrhag, George, Bannikova, Katopo, Chaudhary & Kasapis, 2012; Kasapis, Al-Alawi, Guizani, Khan & Mitchell, 2000). Recently, their ability to create systems for controlled delivery of bioactives was also explored (Panyoyai, Bannikova, Small & Kasapis, 2015). In previous investigations, high methoxylated (HM) pectin from citrus sources was utilized to explore the relaxation properties of the pectin-co-solute systems. The structural

simplicity and usually low molecular weight of HM-pectin allows gelation under high solid (> ~50%) and low pH conditions (Evageliou, Richardson & Morris, 2000b). Depending on the chemical nature of the sugar employed (monosaccharide *vs.* disaccharide *vs.* polydisperse glucose syrups) the morphology of networks and their viscoelasticity may change dramatically (Kasapis, Al-Marhoobi, Deszczynski, Mitchell & Abeysekera, 2003). To build on previous findings, we increased the structural complexity of the polysaccharide as the fine structure of pectin influences to a great extent its physical behavior (Kim, Williams, Galant, Luzio, Savary, Vasu & Cameron, 2013) and we introduced pectin extracted as described in the previous chapter.

Relaxation studies are frequently employed in biopolymer systems as a probe to shed light on macromolecular rearrangements. These motions in turn are pertinent to vitrification that is responsible for the mechanical performance and stability of biopolymer glasses. In the low moisture (or high solids) regime, including those found in dehydrated or frozen foods and low moisture pharmaceutical formulations (e.g., tablets, powders), biopolymers are of particular importance in both academic and industrial fields. To that end, mechanical and thermal relaxations are commonly employed in the study of viscoelasticity for natural polymers and are now well understood so as to draw structure-function relationships (Kasapis, 2012). We have previously demonstrated that glassy pectin-matrix tablets slow the kinetics of drug release and furthermore create stable emulsions indicating that they could be exploited in drug or nutrient encapsulation and delivery (Alba, Ritzoulis, Georgiadis & Kontogiorgos, 2013; Ghori, Alba, Smith, Conway & Kontogiorgos, 2014).

Table 3.1. Experimental conditions used to form gelled network in okra pectin solutions.

Result	Gelator	Experimental conditions
 <p>a, b, c – 3% w/v pectin / 4, 6 and 10 mM of CaCO₃, d, e, f – 2% w/v pectin / 4, 6 and 10 mM of CaCO₃.</p>	Ca ²⁺	Calcium-mediated gelation of okra pectin solution was attempted according to experimental conditions described elsewhere ^a . Mixtures pH was set at 3.0.
 <p>a - 2.0% w/v pectin / 25mM CaCO₃/ 50 mM GDL, b - 2.0% w/v pectin / 40 mM CaCO₃/ 80 mM GDL, c - 3.0% w/v pectin / 25mM CaCO₃/ 50 mM GDL, d - 3.0% w/v pectin / 40 mM CaCO₃/ 80 mM GDL.</p>	Ca ²⁺ /GDL	Gelling of okra pectin solutions by CaCO ₃ and GDL (D-Gluconic acid δ-lactone) was attempted according to procedures described elsewhere in detail ^b . Briefly, CaCO ₃ was dispersed in the okra pectin solutions and a freshly made aqueous GDL solution was added. All gels were prepared using stoichiometric amount of GDL and CaCO ₃ in order to keep a constant pH. Mixtures pH was set at 3.0.
 <p>(2.0% w/v pectin / 65% w/v sucrose).</p>	Sucrose	Sample preparation procedure was attempted according to the following experimental conditions ^c . Mixtures pH was set at 3.0.

^a (Cardoso, Coimbra & Lopes da Silva, 2003).

^b (Draget, Østgaard & Smidsrød, 1989).

^c (Evageliou, Richardson & Morris, 2000a).

In the present chapter, we aim to gather further evidence on the influence of macromolecular conformations on the mechanical properties of pectin, as impacted by the degree of ionisation in the presence of small molecular weight co-solutes in low moisture systems.

3.2 MATERIALS AND METHODS

3.2.1 Pectin extraction

Okra pectin was isolated as described in Chapter 2.

3.2.2 Glucose syrup

Glucose syrup Sipa-Wheat 69 (Sipal Partners, Herve, Belgium) with 80% total solids and dextrose equivalent of 69 was used for sample preparation. The total carbohydrates on dry matter were 97.5% w/w and carbohydrates with degree of polymerization greater than 2 constituted 13.5% w/w of the syrup. Glucose and maltose were 35 and 49% w/w, respectively.

3.2.3 Sample preparation

Pectin dispersions were prepared by dissolving the isolated polysaccharide (OP6 sample) at 1% (w/w) in either citric (pH 3.0) or phosphate (pH 7.0) buffers (100mM) at room temperature under continuous stirring. Following dispersion of the polysaccharide, the temperature was raised to 70 °C and the appropriate amount of glucose syrup was added. The mixture was maintained at 70 °C until the required total solids content was obtained (80% w/w) by slowly evaporating water.

3.2.4 Rheological measurements

These were performed using a Bohlin Gemini 200HR-nano rotational rheometer (Malvern Instruments, Malvern, UK) equipped with plate-plate geometry

(20 mm diameter and 1 mm gap). Temperature was controlled with a Peltier supported by a low temperature ethylene glycol bath (Julabo, F12, Germany) able to reach -30 °C. Experimental protocol of the present investigation included the following steps: Cooling scans were performed between 20 and -30 °C at a cooling rate of 2 °C/min, 0.01% strain and angular frequency of 1 rad/sec. To investigate the viscoelastic behavior of the systems and create master curves of viscoelasticity, frequency sweeps were performed within the range of 0.628-62.8 rad/sec at a strain of 0.01% with 4.4 °C temperature intervals. Modeling of rheological data was performed on Prism v.6 (Graphpad Software, San Diego, USA).

3.2.5 Differential scanning calorimetry

Thermal analysis was performed using a Star System DSC1 (Mettler Toledo, Switzerland) with a Huber TC100 cooling system (Huber, Germany) to achieve temperatures down to -90 °C and a nitrogen DSC-cell purge at a flow rate of 50 ml/min. Samples with total solids of 80% (w/w) were weighed (about 15 mg) and hermetically sealed in aluminum pans, which were cooled from 10 to -90 °C at 2 °C/min. Glucose syrup was used as a reference. First derivative curve of heat flow and estimation of glass transition temperatures were determined with STARE Evaluations software supporting the instrument (v. 12.1, Mettler Toledo, Switzerland).

3.2.6 ζ -potential titration

These measurements were performed using a ZetaSizer Nano Series ZEN2600 (Malvern Instruments, Malvern, UK) at 25 °C. Pectin solutions were dispersed at 0.625% w/v in citric buffer (100 mM) at pH 3.0 and titration was performed with 0.75 M sodium hydroxide to pH 7.0 or 0.75 M hydrochloric acid to pH 1.0. All measurements were performed in duplicate. We are aware of the calculation of ζ -potential from particle electrophoretic mobility (U_E) that depends on the particle size

and shape (Tadros, 2005). Those calculations are typically performed using Henry's equation that is only applicable for spherical or nearly spherical particles (Tadros, 2005). Pectin is a random coil polyelectrolyte and therefore does not comply well with Henry's criteria. However, the measurements of ζ -potential of pectin solutions in this study (including Chapter 4) serve the purpose of demonstrating the effect of pH on the electrical and, consequently conformational, characteristics of the anionic polymer.

3.2.5 Numerical computation

This was performed in MATLAB (v7.0 R14 Service Pack 2, The Mathworks Inc., MA). The first step involves discretization of the viscoelastic functions of G' or G'' to create matrix A and was performed with the *discrG.m* script published elsewhere (Kontogiorgos, 2010). Following that step, algorithms *csvd.m* for calculation of the singular value decomposition of the matrix A and *l_curve.m* for computation of the optimum regularization parameter were used from Hansen's regularization tools package (Hansen, 1994). Finally, the algorithm *NLCSmoothReg.m* was used for the calculation of the relaxation spectra (Wendlandt, 2005).

3.3. RESULTS AND DISCUSSION

3.3.1 Viscoelasticity of pectin-co-solute mixtures

Intrinsic viscosities were determined at two different pH values (7.0 and 3.0) matching those in sample preparation. These measurements were performed under the electrostatic screening of 0.1 M NaCl. This approach masks non-specific electrostatic interactions so that changes in coil dimensions are attributed to changes in the degree of ionization with variation of buffer pH (citric and phosphate). It is evident that pH plays a decisive role in coil dimensions resulting in an expanded conformation due to

dissociation of D-GalA at high pH values (Table 2.4). It is expected that the high co-solute concentration (glucose syrup) in the samples will have an influence on the conformational properties of pectin as solvent quality changes. It has been reported for β -glucan (Grimm, Kruger & Burchard, 1995), guar and locust bean gum (Richardson, Willmer & Foster, 1998) and seed gums (Behrouzian, Razavi & Karazhiyan, 2014; Mohammad Amini & Razavi, 2012) that intrinsic viscosity reaches a minimum before starting increasing again depending on the sugar type and concentration.

This has been attributed to changes in the solvent quality as sugar concentration varies up to 40% w/w solids, and to the degree or extent of inter- and intra-chain interactions (Richardson, Willmer & Foster, 1998). Clearly, intrinsic viscosity measurements are difficult to perform at higher levels of solids, but we are aware that at the level of solids in this investigation (80% w/w) competition for water changes the phase morphology of our preparation paving the way for molecular phenomena of glassy consistency with decreasing temperature. Quoted values of intrinsic viscosity in Table 2.4 serve the purpose of demonstrating the effect of pH (from 7.0 to 3.0) on the conformational characteristics of the polymer. Thus, hydrodynamic volume can be modulated by changes in the degree of ionization, and this modification of macromolecular interactions controls the viscoelasticity of the samples, which is the subject of focus in this chapter.

Determination of functional groups content revealed that the polyelectrolyte is a low methoxylated pectin (LM) with a high degree of acetylation (DA) and an intermediate D-GalA content (Table 2.1). Branching analysis of the sample showed high contribution of RG-I units (~60%) to the pectin backbone whereas the remaining units were HG segments indicating a highly branched biopolymer (Chapter 2). At this

juncture, it should be mentioned that preparation of polysaccharide solutions at alkaline or acidic pH might affect their structural characteristics. In general, polysaccharides may undergo degradation reactions in relation to the pH of the system. For instance, β -elimination and peeling degradation reactions occur at elevated pH values whereas acid hydrolysis upon prolonged exposure to low pH values. However, reduced water content and mobility due to the presence of high levels of glucose syrup (79% w/w) dramatically decelerate hydrolysis in our materials, since water is largely unavailable to participate in chemical reactions. Furthermore, the resistance of D-GalA glycosidic bond to both acidic and alkaline hydrolysis (due to inductive effects of the carboxyl group at C-5) and the limited time that the sample remains at elevated temperatures during sample preparation (~15 min) minimize potential hydrolytic reactions. Therefore, prominent molecular characteristics from the original material remain and allow meaningful comparisons in this investigation regarding the effect of degree of ionization (pH variation from 3.0 to 7.0) on vitrification phenomena.

The following discussion deals with molecular relaxations of LM pectin–co-solute mixtures at total solids of 80% (w/w) and acidic or neutral pH (3.0 or 7.0) in the absence of network formation. Calorimetric measurements provide a first insight into the macromolecular relaxations. Usually, polydisperse polymers vitrify over a broad range of temperatures as the intermolecular energy barriers to segmental and group motions exhibit a broad distribution (Bohmer, Ngai, Angell & Plazek, 1993; Roland, 2010). Figure 3.1 shows calorimetric traces of glucose syrup and high-solid mixtures at two different pH values. The onset of glass transition temperature was estimated by the crossover of the tangents of first derivative curve of heat flow at the onset of the transition (Figure 3.1, bottom right inset). The midpoint of glass

transition temperature was estimated at the midpoint between the tangents of the heat flow curve before and after the transition (Figure 3.1). The onset and mid-point glass transition temperatures for glucose syrup were estimated to be at -35 and -53 °C, respectively. The pectin–glucose syrup mixtures at pH 3.0 revealed only marginal differences from its counterpart in the absence of pectin, with the onset and midpoints being -31 and -48 °C, respectively.

However, switching pH to 7.0 accelerates vitrification events for pectin–glucose syrup samples to about eight degrees (-27 °C (onset) and -45 °C (midpoint)). The first derivative of a glass transition gives a peak whose area is proportional to the value of Δc_p (Figure 3.1, bottom right inset). Peak temperatures of the first derivative can be used as a measure of changes in T_g or for the comparison of the effects of different treatments (Haines, Reading & Wilburn, 2003). Analysis of calorimetric traces in Figure 3.1 with this approach showed peak maxima at -55, -56 and -49 °C for glucose and high solids pectin samples at pH 3 and 7, respectively. Treatment of calorimetric data revealed the pH-induced influence of the polyelectrolyte conformation on calorimetric relaxation of the samples. Such a behavior calls for further exploration on the effect of pH on macromolecular conformation of our samples.

Top left inset in Figure 3.1 shows results on the ζ -potential titration of the pectin in the absence of sugar. It is evident that from pH 6.0 upwards, D-GalA residues on the polymeric backbone are fully dissociated. This yields an extended conformation in the macromolecule, an outcome that is also reflected in the intrinsic viscosity values of the sample discussed in Table 3.1. On the other hand, the compact molecular arrangement at pH 3.0 creates strong intra-chain associations as the charge is neutralized at around pH 1.0. A compact polymeric structure increases the overall

free volume of the pectin-glucose syrup mixture as the hydration and interaction of the polyelectrolyte with water and co-solute is restricted. This enhances the dominance of the co-solute in mixture with pectin at pH 3.0 leading to a vitrification pattern that is similar to the single glucose-syrup preparation in the DSC thermograms (Figure 3.1).

The influence of pH on pectin conformation should also play a central role in the mechanical properties of the high-solid samples. It is possible to monitor mechanical developments on cooling of our samples by employing well-established approaches from synthetic polymer science.

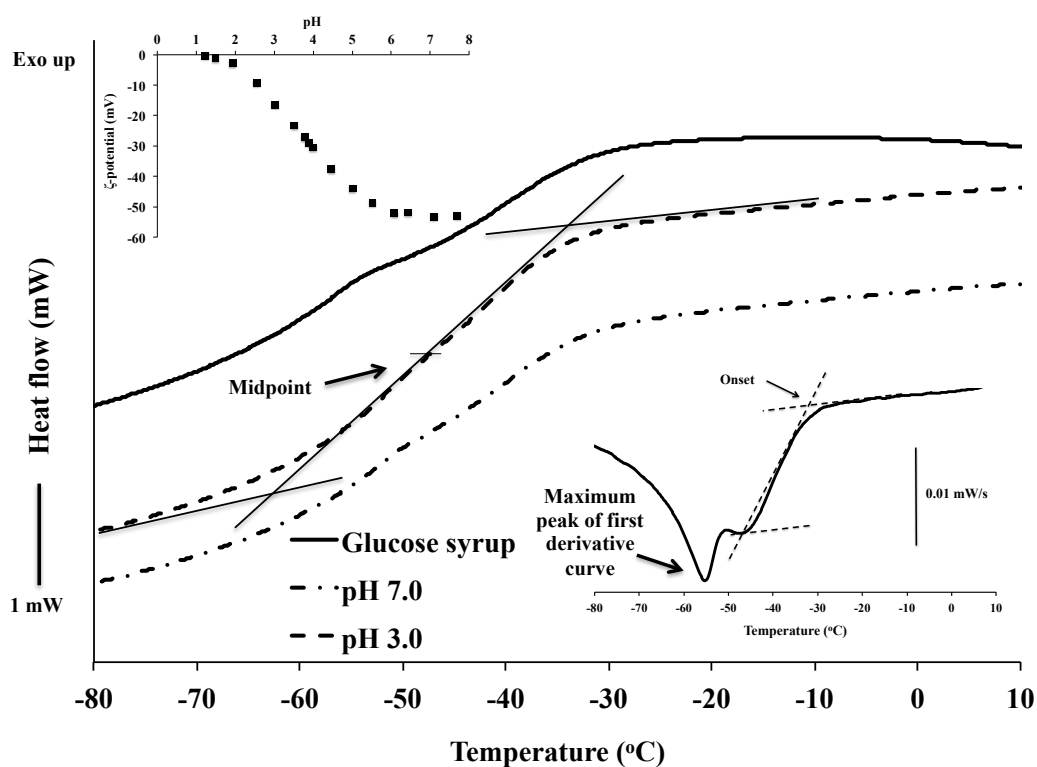


Figure 3.1. DSC thermograms of 80% glucose syrup and 1% LM-pectin plus 79% glucose syrup at pH 3.0 and 7.0. Top left inset shows ζ -potential titration of the pectin solution. Bottom right inset shows a typical first derivative curve of heat flow of the samples and calculations used to derive the onset of the glass transition.

The dependence of storage and loss modulus on temperature at pH 3.0 and 7.0 close to the onset of the calorimetric glass transition regime is recorded down to -28 °C in Figure 3.2. In both cases, G'' is higher than G' throughout the experimental temperature range, a behaviour that is typical of viscous materials. Clearly, viscoelastic functions at pH 7.0 are two orders of magnitude greater than the low pH counterparts. This is a direct evidence of the role of intermolecular interactions in the mechanical properties, with the extended pectin conformation at pH 7.0 increasing the elastic character of the mixture.

An approach to extend monitoring the viscoelastic parameters beyond the experimentally accessible range is to utilize the time-temperature superposition principle.

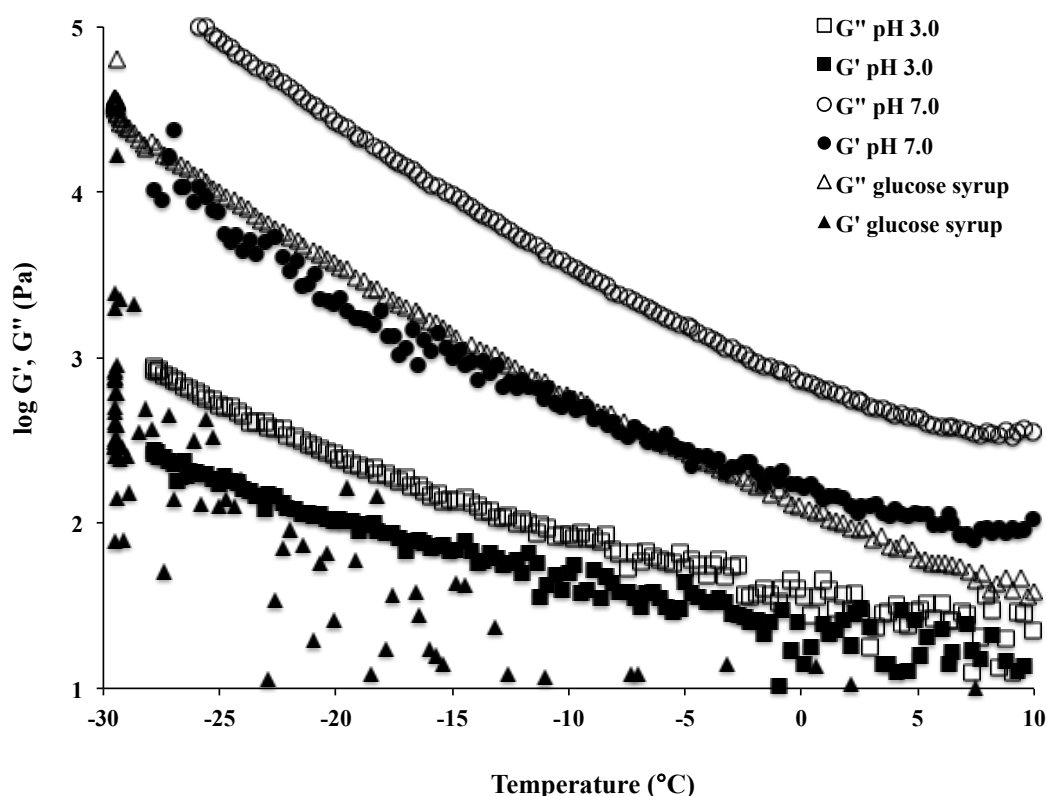


Figure 3.2. Temperature dependence of the storage and loss modulus for glucose syrup and systems containing 1% LM-pectin and 79% glucose syrup at pH 3.0 and 7.0 (scan rate: 2 °C/min; frequency: 1 rad/s; strain: 0.01%).

When materials do not exhibit structural transitions (e.g., gelation, melting or denaturation) during the course of measurement, the viscoelastic modulus measured at a set of frequencies and temperatures (ω , T) is equivalent to measurements taken at frequency ω multiplied with a shift factor (a_T) (Mezger, 2011). The master curve at a convenient reference temperature T_o can then be obtained by plotting the viscoelastic functions *versus* ωa_T . In doing so, frequency sweeps were carried out at temperature intervals of 4.4 °C from 20 to -28 °C in Figure 3.3. Enhanced intermolecular associations are evident with lowering temperature as the storage and loss modulus values are becoming progressively higher. Plateauing of the values, however, is not observed, which is typical of polymers well within the glassy state. In order to calculate the horizontal shift factors, we used the method of reduced variables ($a_T = \omega_r/\omega$) at the reference temperature of $T_o = -19$ °C. The reference temperature is usually chosen to be near to the operating temperature of the biopolymer. In our case, we have chosen a temperature that is well within the glass transition range of our biopolymer in order to appreciate the influence of pH in macromolecular dynamics.

Figure 3.4 illustrates the results of the aforementioned treatment for the mechanical spectra in Figure 3.3. The master curves of viscoelasticity extend over four orders of magnitude in frequency revealing relaxation patterns that correspond to the glass transition region of the sample at pH 7.0. To further explore the effect of temperature, horizontal shift factors, a_T , were plotted against $T-T_o$ in Figure 3.5. This approach provides information about the temperature dependence of molecular mobility upon which the various relaxation mechanisms depend (Williams, Landel & Ferry, 1955). It appears that below about 0 °C (or $T-T_o = 20$ °C) shift factors exhibit a strong temperature dependence indicating a transition to distinct relaxation kinetics with reduced temperature. This commonly occurs as the sample enters the glass

transition region in high-solid biopolymer systems (Al-Ruqaie, Kasapis, Richardson & Mitchell, 1997; Jiang, Kasapis & Kontogiorgos, 2011; Kasapis, Al-Marhoobi & Khan, 2000). Free volume theory and the empirical WLF equation are then employed to follow the process of vitrification:

$$\log a_T = \frac{C_1^o(T - T_o)}{C_2^o + T - T_o} \quad (33)$$

C_1^o and C_2^o are the WLF constants at the reference temperature T_o and are related to the free volume theory as follows:

$$C_1^o = \frac{B}{2.303f_o}, C_2^o = \frac{f_o}{\alpha_f} \quad (34)$$

where, f_o is the fractional free volume at T_o , α_f is the thermal expansion coefficient and B is a constant that equals unity.

Utilization of this approach allows association of the concept of glass transition with fundamental quantities such as the evolution of free volume during vitrification. Our experimental setup captures a significant part of this event to return estimates of C_1^o , C_2^o , f_o and α_f at T_o in Table 3.2. Values of f_o for the sample at pH 7 is in good agreement with previously studied high-solid biopolymer mixtures (Al-Ruqaie, Kasapis, Richardson & Mitchell, 1997) and amorphous synthetic polymers (Ferry, 1980) to demarcate the mechanical rubber-to-glass transition. In contrast, adjusting pH to 3 brings about a mechanical behavior with values of f_o being an order of magnitude higher than for the neutral pH counterpart. This behavior indicates that for these samples the glass transition region occurs at lower temperatures and could not be accessed in the temperature range we employed in the present work.

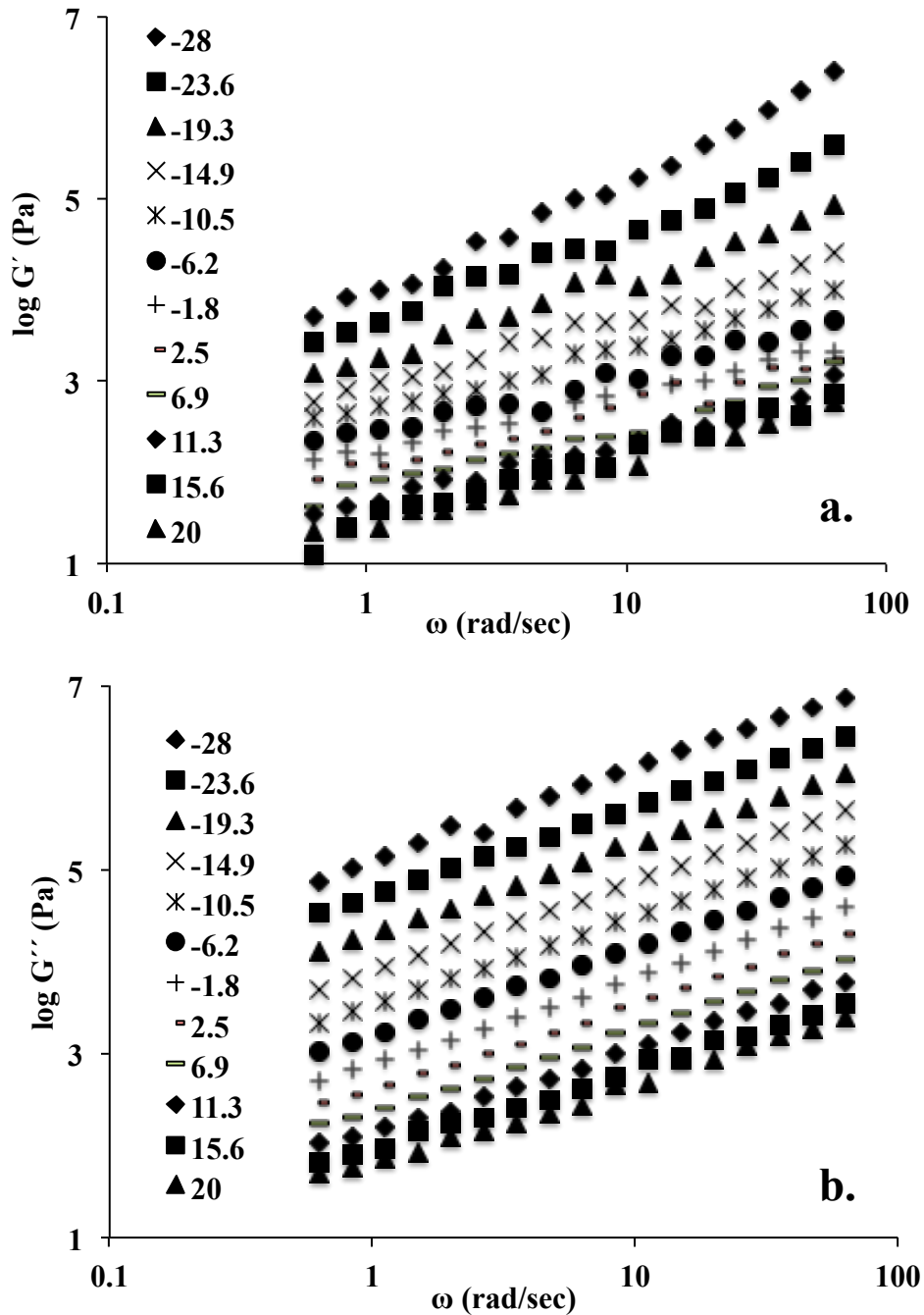


Figure 3.3. Double logarithmic plots of (a) storage and (b) loss modulus against frequency of oscillation for a sample containing 1% LM-pectin and 79% glucose syrup at pH 7.0 (temperature interval: 4.4 °C; strain: 0.01%).

The above predictions are congruent with the cooling scans in Figure 3.2 and the calorimetric data in Figure 3.1 arguing that the high pH samples move towards the glassy state at a rapid rate. Electrokinetic potential measurements also in Figure 3.1

indicate that D-GalA residues are fully dissociated at pH 7 resulting in electrostatic repulsion and an extended chain conformation. The macromolecular outcome is an efficient polymer hydration and interaction with glucose syrup that reduces the overall free volume in the mixture. Conversely, the compact pectin conformation at pH 3, due to the protonation of the D-GalA residues, results in a co-solute dominated matrix of increased diffusional mobility and free volume that delays vitrification.

Previous work on other gelling polysaccharide systems showed that the rheologically determined T_g is affected by the structural morphology, network strength and molecular weight of the biopolymer (Kasapis, 2008). Generally, the ability of the polysaccharide to form a network in the presence of high levels of co-solute accelerates vitrification events due to restricted diffusional mobility of the chains as, for example, it has been shown for κ -carrageenan with added potassium counterions (Evageliou, Kasapis & Hember, 1998), high methoxy pectin (Almrhag, George, Bannikova, Katopo, Chaudhary & Kasapis, 2012), deacylated gellan with added sodium counterions (Al-Ruqaie, Kasapis, Richardson & Mitchell, 1997) or gelatin of various molecular weights (Kasapis, Al-Marhoobi & Mitchell, 2003). Present work highlights the importance of biopolymer conformation on the vitrification of high-solid polysaccharide systems. For instance, in gelling systems including κ -carrageenan and deacylated gellan, network formation is a kinetic process being influenced by the degree of ionization. This ultimately affects gel microstructure and how rapidly the system arrives at the onset of glass transition. Careful tuning of pH seems to be a prerequisite for this, but it somehow has escaped attention thus far. Conversely, the addition of small amounts of non-gelling polysaccharides such as guar or locust bean gum has little effect on the mechanical manifestation of vitrification (Kasapis, Al-Marhoobi & Khan, 2000). The inability to

form a network results in molecular mobility in the sugar matrix thus requiring lower temperatures to achieve the glassy state. Those systems show comparable glass transition regimes and fractional free volume values with pectin samples at pH 7.0 (Kasapis, Al-Marhoobi & Khan, 2000) and are also on a par with mechanical results obtained for low methoxylated pectin in deionized water although in these studies pH was not controlled (Kasapis, Al-Alawi, Guizani, Khan & Mitchell, 2000).

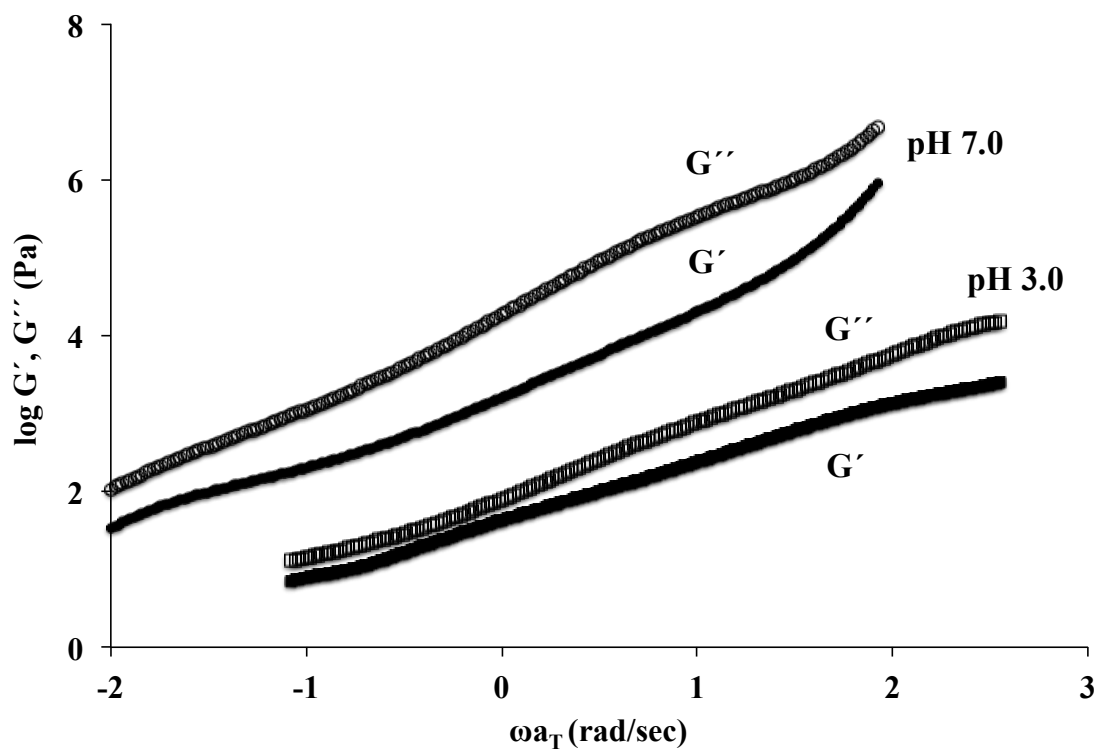


Figure 3.4. Master curves of viscoelasticity as a function of reduced frequency of oscillation (ωa_T) for systems containing 1% LM-pectin and 79% glucose syrup at pH 3.0 and 7.0 at the reference temperature of $-19\text{ }^\circ\text{C}$.

It should be noted that in neutral polysaccharides, pH effects on chain conformation are reduced, as solvent ionization does not exert the same influence as in polyelectrolytes. On the contrary, we demonstrated that in polyelectrolytes by drastically shifting the pH towards the isoelectric point changes in coil conformation result in remarkable modification in the mechanical properties of the system.

Table 3.2. Values of WLF Parameters for 1% LM-pectin and 79% glucose syrup at pH 3.0 and 7.0

Sample	C_1^o	C_2^o (°C)	f_o	α_f ($\times 10^{-4} \text{ } ^\circ\text{C}^{-1}$)
pH 3	2.07	24.12	0.209	86
pH 7	13.27	149	0.032	2.1

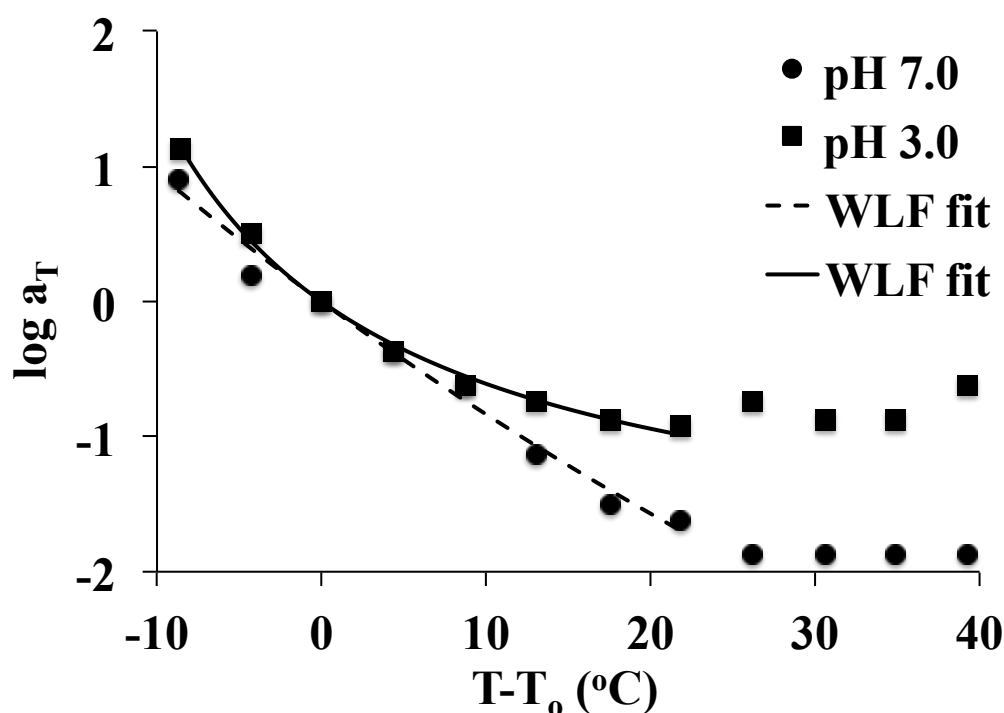


Figure 3.5. Logarithmic shift factor, a_T , for systems containing 1% LM-pectin and 79% glucose syrup at pH 3.0 and 7.0 plotted against temperature from the data of the master curves presented in Figure 3.4 (WLF fits are also shown for both samples).

Findings of the present work extend to other low-moisture glassy systems incorporating non-gelling polysaccharides for various industrial applications. For instance, encapsulation methods (spray drying and electrospraying) or edible film formation utilizes a wide range of carbohydrate polymers and co-solutes to formulate matrices of glassy consistency (Espitia, Du, Avena-Bustillos, Soares & McHugh, 2014; Fathi, Martín & McClements, 2014). Understanding the underlying molecular mechanism of polyelectrolyte vitrification and the structural relaxations occurring in

glass transitions assists in controlling optimum fabrication in industrially relevant preparations.

3.3.2 Calculation of relaxation spectra

It is possible to determine the time needed for the completion of macromolecular motion with the help of a relaxation spectrum. Appropriate conversion of mechanical spectra from master curves can be used to calculate the relaxation spectra of biopolymers. The relationship between the storage modulus, loss modulus and angular frequency (ω) in shear is given by the following integrals (Tschoegl, 1989):

$$G'(\omega) = G_o + \int_0^{\infty} H(\tau) \frac{\omega^2 \tau^2}{1 + \omega^2 \tau^2} \frac{d\tau}{\tau} \quad (35)$$

$$G''(\omega) = \int_0^{\infty} H(\tau) \frac{\omega \tau}{1 + \omega^2 \tau^2} \frac{d\tau}{\tau} \quad (36)$$

where, $H(\tau)$ is the distribution function of the structural elements with relaxation time τ , and G_o is the equilibrium modulus with a zero value for viscoelastic liquids. Equations 3 and 4 can be generalized with a Fredholm integral equation of the first-kind, which takes the form:

$$g(s) = \int_a^b K(s,t) f(t) dt, \quad \alpha \leq s \leq \beta \quad (37)$$

where, $K(s,t)$ is the kernel that describes the system being $(\omega^2 \tau^2 / (1 + \omega^2 \tau^2))$ and $\omega \tau / (1 + \omega^2 \tau^2)$ for equations 3 and 4, respectively, $g(s)$ is the measured signal ($G'(\omega)$ or $G''(\omega)$) and $f(t)$ is the relaxation spectrum $H(\tau)$. Numerical integration determines the spectral function $f(t)$ that represents the relaxation pattern of the material. Spectra calculation proceeds with discretization of the kernels of functions (3) or (4) using an algorithm that is published elsewhere (Kontogiorgos, 2010). The master curves in

Figure 3.4 were then analyzed with the L-curve criterion followed by the Tikhonov regularization.

Discretization of equations 3 and 4 was performed between $10^{-4} - 10^2$ s using a heuristic approach. Calculation of the optimum regularization parameter, λ , is a necessary step as it controls the interplay between the regularization error and the loss of resolution (Hansen, 1994). The optimum regularization parameter is located at the corner of the L-curves in Figure 3.6 (top right inset). The x -axis of the curve (residual norm) corresponds to solutions where the calculation error controls the solution, with the y -axis (solution norm) reflecting solutions that are sensitive to experimental noise. We show semi-logarithmic plots of relaxation spectra produced using both kernels of equations (35) and (36).

The two viscoelastic functions returned qualitatively similar monomodal spectra centered around 0.015 s for the sample at pH 7.0. Differences in the intensity of the spectra follow the magnitude of the modulus values in the master curve. This is in very good agreement with relaxation times of various polysaccharides that have been previously reported in the literature (Rincon, Munoz, Ramirez, Galan & Alfaro, 2014; Rodriguez-Rivero, Hilliou, Martin del Valle & Galan, 2014). Although pH does not seem to affect the overall relaxation behavior, acidic samples tend to resolve more relaxation elements in Figure 3.6 (bottom right inset).

According to the coupling model (Ngai, 2000), the extent of interactions between neighboring segments relates to the distribution of relaxation times, with strongly interacting macromolecules exhibiting a broad distribution in contrast to those with rather weak molecular interactions. Modeling indicates distinct molecular interactions due to conformational differences, with more resolved relaxation elements occurring as the isoelectric point is approached. It should be stressed,

however, although qualitatively different, the spectra reveal that that all relaxation processes are essentially complete within $< \sim 0.1$ s regardless of pH. This is an important observation that adds to the earlier discussion from the thermomechanical analysis for the identification of the molecular origin of interactions in the high-solid pectin system as a function of pH.

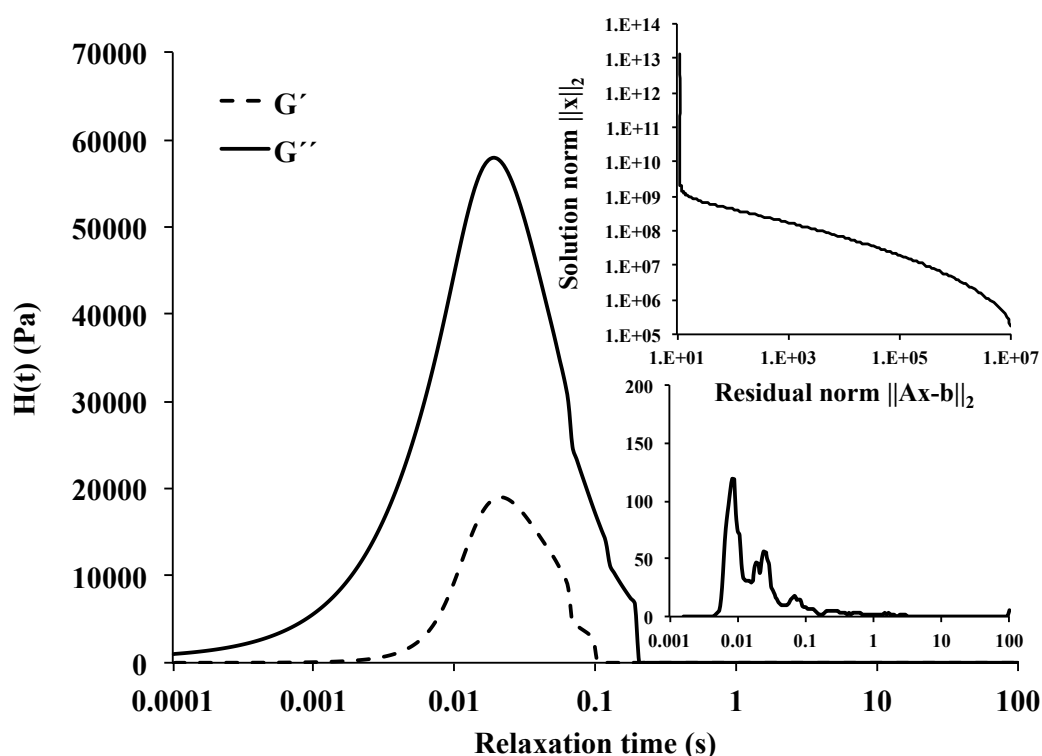


Figure 3.6. Semi logarithmic plots of relaxation spectrum of 1% LM-pectin and 79% glucose syrup at pH 7.0 obtained using data from master curves in Figure 3.4; Solid or dashed lines were obtained after discretization of the loss or storage modulus, respectively; Top right inset shows a typical shape of L-curves that were used to calculate the optimum regularization parameter, and bottom right inset shows the relaxation spectrum of 1% LM-pectin and 79% glucose syrup at pH 3.

This outcome indicates that discrepancies between the mechanical properties of the samples in the glass transition region stem from topological or steric restrictions in chain mobility in addition to the conformational changes that were induced with variations in the degree of ionization.

3.4 CONCLUSIONS

The influence of pH on the structural properties of non-gelling LM-pectin in the presence of co-solute has been investigated by means of thermomechanical analysis and theoretical modeling of results. Tuning pH at acidic or neutral conditions affects the conformation of the polysaccharide, hence impacting its micro- and macromolecular behaviour within the experimentally accessible temperature range. Dissociation of galacturonic acid residues at the high pH values results in extended chain conformation and early vitrification events. Conversely, as the polyelectrolyte approaches its isoelectric point at low pH, recorded viscoelastic functions decrease and vitrification is delayed. Time-temperature superposition extended the experimental timeframe of observations yielding master curves of viscoelasticity and enabling calculation of the corresponding shift factors. These were utilised in WLF modeling to confirm the early vitrification of the pectin molecule in mixture with glucose syrup at neutral pH. Spectral analysis of the viscoelastic master curves revealed the exact positioning of the relaxation events characterized by one dominant regime where the relaxation of the macromolecules concludes.

In the present chapter, it has been shown that pectin isolated from okra pods is non-gelling pectin due to the high degree of acetylation and branching of the side-chains. However, pectin with aforementioned properties could be utilized as an emulsifier in fabrication of emulsions. Therefore, emulsion-stabilizing properties of OP2 and OP6 will be investigated in the next chapter.

CHAPTER 4

EMULSIFYING PROPERTIES OF OKRA PECTIN

Parts of this chapter were published as:

- 1) Alba, K., Ritzoulis, C., Georgiadis, N., & Kontogiorgos, V. (2013). Okra extracts as emulsifiers for acidic emulsions. *Food Research International*, 54(2), 1730-1737.
- 2) Ghori, M. U., Alba, K., Smith, A. M., Conway, B. R., & Kontogiorgos, V. (2014). Okra extracts in pharmaceutical and food applications. *Food Hydrocolloids*, 42, 342-347.

4.1 CRUDE OKRA EXTRACTS AS EMULSIFIERS FOR ACIDIC EMULSIONS

4.1.1 Introduction

High emulsification capacity is usually attributed to proteins whereas polysaccharides typically demonstrate negligible surface activity at the o/w interface due to their hydrophilic character and are, therefore, not so useful as emulsifying agents. Similarly to most polysaccharides, pectins are not normally considered as emulsifying agents except the acetylated pectin from sugar beet (Siew & Williams, 2008b). It has been shown that it possesses greater surface activity than commercially produced low- or high-methoxyl pectins and is capable of producing and stabilizing fine o/w emulsions (Williams, Sayers, Viebke & Senan, 2005). The emulsifying properties of sugar beet pectins were attributed to the presence of acetyl groups (4–5%), co-extracted protein fraction and ferulic acid moieties covalently attached to the pectin molecule (Dea & Madden, 1986; Endreß & Rentschler, 1999; Leroux, Langendorff, Schick, Vaishnav & Mazoyer, 2003). Citrus pectins with low molecular weight of about 60-70 g mol⁻¹ and high degree of methoxylation were found also to be good emulsifying agents (Akhtar, Dickinson, Mazoyer & Langendorff, 2002). The emulsifying capacity of pectin under acidic conditions is another property that can be utilized in the food industry particularly in acidified dairy and/or fruit drink products where direct acidification with fruit juices and/or acids is typically performed. The pH of these products ranges from 3.4 to 3.6 and protein (caseins) instability at this pH range usually occurs (Nakamura, Yoshida, Maeda & Corredig, 2006). Therefore, alternative stabilizer needs to be added in order to prevent protein aggregation and eliminate changes in the colloidal system. In addition, the resistance of pectin to

acidic environments can be effectively exploited in pharmaceutical industry in the form of drug delivery agents.

The aim of present chapter was to determine the emulsifying capacity of okra crude extracts in model o/w emulsions under acidic conditions.

4.1.2 Materials and Methods

4.1.2.1 Isolation and partial characterization of okra extracts

Okra extracts for this part of the project have been kindly donated by Associate Professor Christos Ritzoulis (Department of Food Technology, ATEI of Thessaloniki, Thessaloniki, Greece) and isolation and characterization procedures are described elsewhere in detail (Alba, Ritzoulis, Georgiadis & Kontogiorgos, 2013; Vierhuis, Schols, Beldman & Voragen, 2000). Briefly, seeds and calyces were removed and the remaining okra pods were freeze-dried. These were then defatted and alcohol insoluble solids (AIS) were recovered. AIS were then used to extract okra polysaccharides at pH 6.0 or pH 4.0 and these samples were labeled as “OE6” and “OE4”, respectively. Insoluble particles were removed by centrifugation and the resulting fractions were freeze-dried. The molecular weights of extracted polysaccharides were evaluated using high-pressure size exclusion chromatography (HPSEC).

4.1.2.4 Preparation of okra extract solutions and emulsions

Preliminary experiments on the optimum concentration of okra extracts towards emulsion stability showed that okra extracts at concentration 1.5% w/v with dispersed phase volume fraction $\varphi = 0.2$ (*n*-hexadecane) and under acidic conditions (pH 3.0) produce fine emulsions. The aqueous phases of the emulsions were prepared by means of dissolving okra extract powders at 1.875% w/v concentration in citric

buffer (0.01 M, pH 3.0) at room temperature. Okra extract solutions were characterized at 1.875% w/v concentration. For 1.5% w/v emulsion preparation, the above aqueous phases were magnetically stirred with hexadecane for 3 min in order to produce emulsion pre-mixes with oil volume fraction $\varphi = 0.2$ and 1.5% w/v final extract concentration in the entire emulsion. This pre-mix was immediately homogenized (IKA T18 basic, Ultra-Turrax, Germany) for 1 min. For the determination of the long-term stability all emulsions were stored in an incubation chamber at 25°C.

4.1.2.5 Determination of particle droplet distribution

Droplet size distribution was measured immediately after the emulsion preparation and after 5, 10, 20 and 30 days of storage using a Malvern Mastersizer 2000 (Malvern Instruments Ltd, Worcestershire, UK) laser diffraction particle size analyzer using the small volume sample dispersion unit Hydro 2000SM (Malvern Ltd, UK). Refractive index of hexadecane and dispersion medium (citric buffer, 10 mM, pH 3.0) was set to 1.434 and 1.333, respectively. Consequently, droplet size was described using the surface-weighted mean diameter ($d_{3,2}$) and volume-weighted mean diameter ($d_{4,3}$). The measurements were performed in duplicate in three different emulsion preparations yielding in total six replicates for each sample.

4.1.2.6 Rheological measurements of okra extracts and emulsions

Rheological properties of samples were measured using a Bohlin Gemini 200HR Nano rotational rheometer (Malvern Instruments, Malvern, UK) equipped with cone-and-plate geometry (40 mm diameter, cone angle 4°) and Peltier temperature controller. All measurements were performed in a steady shear mode in the range 0.01–1000 s⁻¹ at 25 °C. Viscosity measurements were conducted

immediately after preparation of okra extract solutions and emulsions and after 5, 10, 20 and 30 days of storage. All measurements were performed in duplicate.

4.1.2.7 Determination of interfacial protein concentration

Okra extract stabilized o/w emulsions were centrifuged at 2727×g for 5 min (Centrifuge 5702, Eppendorf, Hamburg, Germany) in order to separate the dispersed phase (oil droplets) from the continuous phase and serum was then carefully collected using a syringe. Interfacial protein concentration (Γ , mg m⁻²) was calculated as the protein concentration difference in the extract and serum solutions divided by the specific surface area of the oil droplets:

$$\Gamma = \frac{\text{mg of adsorbed protein}}{\text{SSA} \times \text{mL of oil in emulsion}} \quad (37)$$

where specific surface area (SSA), m²/mL was obtained by the result analysis report of the instrument. Protein was measured in both solutions and serum of centrifuged emulsions according to the Bradford method (Bradford, 1976) using Quick Start™ Bradford Protein Assay kit. Calibration curve was constructed using bovine serum albumin (BSA) and absorption was measured at 595 nm. All measurements were performed at least six times.

4.1.2.8 Determination of ζ -potential

All ζ -potential measurements were performed using a ZetaSizer Nano Series ZEN2600 (Malvern Instruments, Malvern, UK) at 25 °C. Emulsions were diluted 1000 times in citric buffer (0.01 M, pH 3.0) in order to avoid multiple scattering effects. All measurements were performed in duplicate immediately after emulsion preparation and after 5, 10, 20 and 30 days of storage.

4.1.2.9 Emulsion morphology

Fluorescence microscopy was performed using an Olympus BX41TF microscope (Olympus Optical Co. Ltd, Japan) and an Olympus U-RFL-T-200 burner (Olympus Optical Co. Ltd, Japan). The fluorescent dye (Rhodamine B, 0.02%) was added into the extract solutions prior to emulsification. Emulsions were placed on a glass slide and were consequently covered with a coverslip prior to imaging. Filter cubes with wide band UV excitation/emission filter 555/595nm were used to observe the protein phase.

4.1.3 Results and discussion

4.1.3.1 Emulsification capacity – emulsion stability

OE4 and OE6 were constituted of three polymer populations that corresponded to peak molecular weights of 1400×10^3 , $50\text{-}80 \times 10^3$ and about 1×10^3 g/mol. Overall, OE6 was composed of higher Mw polysaccharides than OE4 counterparts (Alba, Ritzoulis, Georgiadis & Kontogiorgos, 2013). The capacity of the extracts to act as emulsifiers was tested by means of emulsifying *n*-hexadecane into an aqueous medium buffered at pH 3.0 containing 1.875% w/v of extract so as to yield emulsions of $\varphi = 0.2$ of a nominal extract concentration in the entire emulsion volume of 1.5% w/v. In order to quantify the capacity of these emulsifiers towards long-term emulsion stability, the droplet size distribution and the average droplet sizes were measured at set time intervals. Both extracts showed good emulsification ability, considering that the homogenizer was a colloidal mill and not a high-power ultrasonic or high-pressure homogenizer, producing emulsions with d_{32} of about 12 μm in the case of OE4 and d_{32} of about 11 μm in the case of OE6 both of monomodal droplet size distribution (Figures 4.1.1a, b, Table 4.1.1).

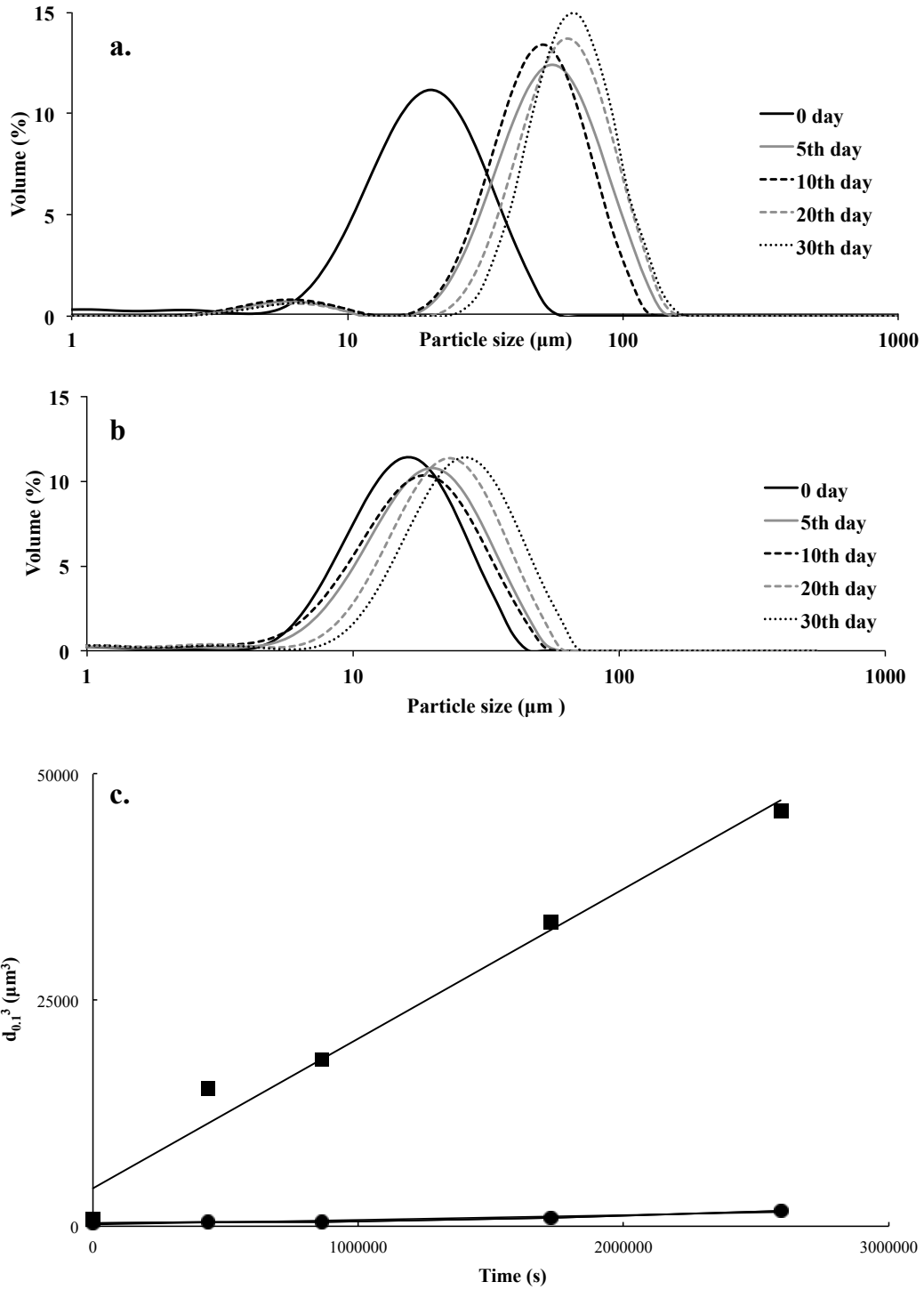


Figure 4.1.1. Particle size distributions of emulsions prepared using a) 1.5% OE4 and b) 1.5% OE6. The time development of the distributions is also shown. c) Variations in the cube of $d_{0.1}$ with time for emulsions stabilized by extract OE4 (square) or OE6 (circle).

Although similar in that aspect (stabilization against re-coalescence immediately after emulsification), the two emulsifiers differentiated vividly in terms of their efficiency towards long-term emulsion stability (protection against droplet size increase over time). Emulsions prepared using OE4 presented a marked increase in average droplet size, i.e, $d_{3,2}$ rising from 12.5 μm to 33.4 μm after 5 days of storage and then 41.5 μm after 30 days of storage (Table 4.1.1).

Fluorescence micrographs (Figures 4.1.2a-c) suggest that this measured increase in average particle diameter is related to the increase of the average droplet size rather than the formation of strong, compact flocs. Moreover, white arrows depict droplets, which have shrunk at the expense of the larger ones that is a typical result of Ostwald ripening. In the case of OE6, the droplet size distributions (Figure 4.1.1b) and the average droplet diameters (Table 4.1.1) remain stable for the duration of the 30 days of the experiment, although a gradual shifting of the monomodal particle size distribution towards larger sizes (from 11.2 μm to 14.5 μm) was observed (Figure 4.1.1b). These are in agreement with the fluorescent micrographs (Figures 4.1.2b, d), where droplet size was at around 10 μm and do not appear to be strongly flocculated.

The above suggest that OE6 has good potential to act as an effective emulsifier in acidic emulsions such as the ones modeled here. As mentioned in the previous paragraphs, a similar shift of the droplet populations towards larger average droplet sizes was also observed for OE4. In this case, however, the increase was more dramatic where d_{32} changes from about 12.5 to 33.4 μm . The pattern of change in the droplet distributions (Figure 4.1.1a) was a shift of a single monomodal peak towards larger sizes, rather than the appearance of a coalescence-generated second peak corresponding to a population of larger droplets.

Table 4.1.1. Influence of okra extract type and storage time (days) on the average droplet diameters ($d_{3,2}$ and $d_{4,3}$) and ζ -potential in emulsions formed with 1.5% (w/v) OE4 and OE6.^a

Sample	Time (days)	$d_{3,2}$ (μm)	$d_{4,3}$ (μm)	ζ -potential (mV)
OE4	0	12.5 \pm 0.3	19.5 \pm 0.5	-10.6 \pm 0.2
	5	33.4 \pm 1.3	51.5 \pm 0.9	-10.1 \pm 0.2
	10	23.5 \pm 1.6	44.1 \pm 4.4	-9.3 \pm 0.4
	20	39.0 \pm 0.7	57.6 \pm 1.7	-8.2 \pm 0.4
	30	41.5 \pm 0.1	61.8 \pm 0.1	-9.0 \pm 0.5
OE6	0	11.2 \pm 0.6	15.0 \pm 0.8	-8.4 \pm 0.2
	5	12.4 \pm 0.4	20.8 \pm 2.9	-8.6 \pm 0.2
	10	10.8 \pm 0.8	20.6 \pm 4.4	-8.6 \pm 0.2
	20	16.4 \pm 4.3	22.6 \pm 1.5	-8.5 \pm 0.2
	30	14.5 \pm 0.8	25.1 \pm 0.3	-6.9 \pm 0.4

^aData are means \pm SD. Sample OE4 indicates 1.5% w/v emulsion stabilized with OE4; sample OE6 indicates 1.5% w/v emulsion stabilized with OE6. Both emulsions have $\varphi = 0.2$, citric buffer pH 3.0.

This gradual shifting of a monomodal size distribution towards higher droplet sizes is generally related to emulsion destabilization by an Ostwald ripening mechanism (Dickinson, Galazka & Anderson, 1991; McClements, 2005), as opposed to the development of a bimodal droplet distribution over time, which is more representative of droplet coalescence (Dickinson, Golding & Povey, 1997). In a typical Ostwald ripening scenario, according to the LSW (Lifshitz–Slyozov–Wagner) theory (Lifshitz & Slyozov, 1961), the average change in number droplet diameter cubed ($d_{0,1}^3$) is linear to the time of observation. Figure 4.1.1c presents such a plot for both samples, in which $d_{0,1}^3$ vs. *time* was linear with the slope for OE4 being steeper than OE6. This was a strong indication that Ostwald ripening, rather than coalescence, should be considered as the principal coarsening mechanism in the case of these emulsions. These observations are in agreement with micrographs of OE4 (Figure

4.1.2c), where the diameter of large droplets was several microns, while the smaller droplets shrunk significantly (white arrows). The Ostwald ripening as major destabilisation mechanism has been previously observed on caseinate-stabilized *n*-hexadecane-in-water or surfactant stabilised *n*-hexadecane- or triglyceride-in-water emulsions (Nazarzadeh, Anthonypillai & Sajjadi, 2013; Wooster, Golding & Sanguansri, 2008).

4.1.3.2 Surface coverage

The question arising from the emulsification tests is related to the difference observed between the efficiency of the two extracts and in their mode of action towards stabilization. It is commonly argued that the main contribution of such extracts towards emulsion stability is related to the presence of co-extracted proteins that adsorb at the o/w interface of the droplets. However, since the o/w interface is composed of a complex mixture of proteins and polysaccharides, contribution from functional groups of the pectin structure such as acetyl and methyl or of smaller molecules (ferulic acid moieties) can result to a greater hydrophobicity of okra extracts, increasing their surface activity (Leroux et al., 2003). As a first step in addressing the above, the amount of protein adsorbed at the hexadecane-water interface was determined both in terms of absolute value and also as a percentage of the total protein present in each extract (Table 4.1.2).

In the case of OE4, protein surface coverage of the emulsions was 0.6 mg m^{-2} accounting for 33% of the total protein present. In the case of OE6, surface coverage was almost twice that value (1.0 mg m^{-2}) close to other surface-active protein material, while a far larger proportion (57%) of the total protein was transferred from the bulk to the interface.

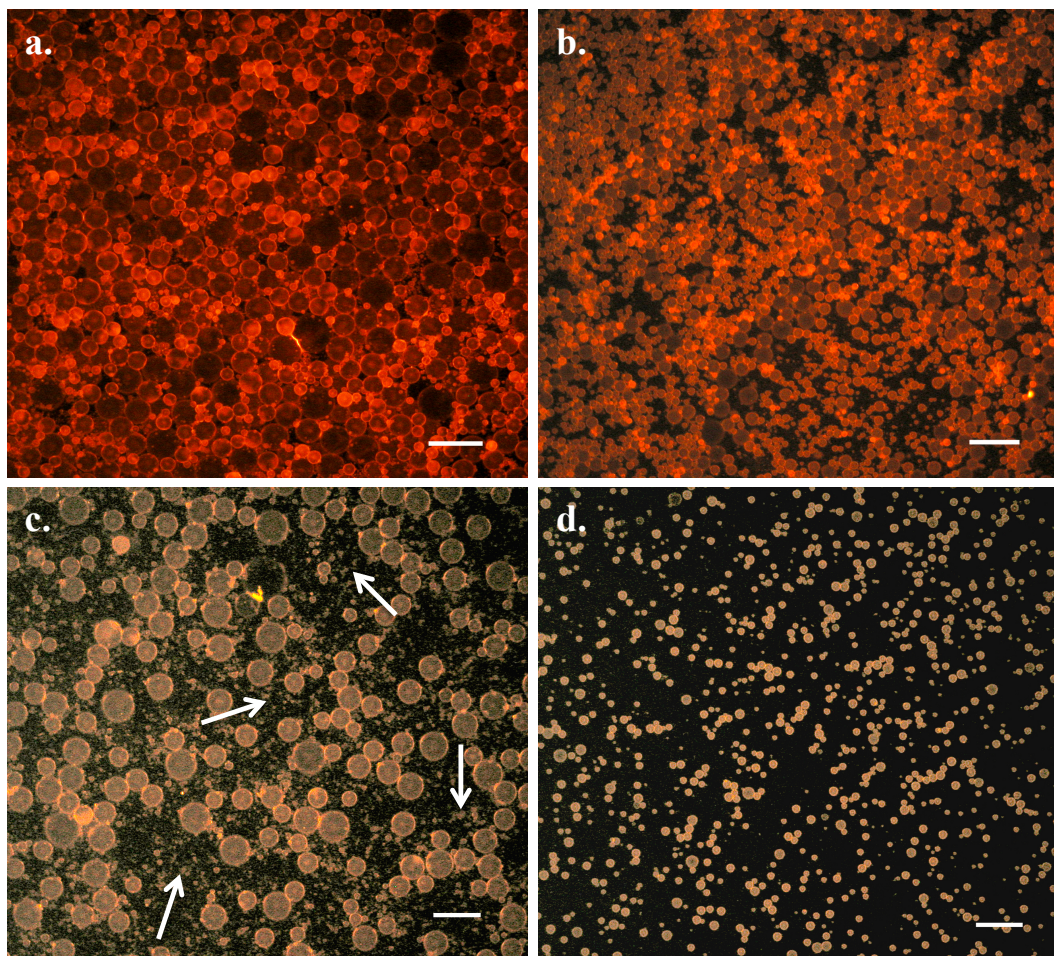


Figure 4.1.2. Fluorescent micrographs of emulsions containing 1.5% w/v (a) OE4 and (b) OE6 after 6 hours of preparation ($\phi = 0.2$, 25 °C, citric buffer pH 3.0). The bottom micrographs (c) and (d) depict the same emulsions after dilution in buffer (1:1000). Scale bars represent 100 μm .

Table 4.1.2. Interfacial protein concentration Γ (mg m^{-2}), percentage of protein adsorbed at the oil-water interface of fresh emulsions and protein content of okra extracts.

Sample	Γ (mg m^{-2})	Adsorbed protein (%)	Protein (% w/v)
OE4	0.6 ± 0.1	33.3 ± 6.4	2.0 ± 0.3
OE6	1.0 ± 0.2	57.0 ± 11.9	3.0 ± 0.1

Although the protein content of extracts was marginally different (Table 4.1.2), since the pH of extraction was different (4.0 or 6.0) we expect variations in the structure as well as the amino acid composition of the extracted proteins. This influences the capacity of the proteins to unfold and arrange at the interface as was evidenced from the interfacial protein load measurements that they showed variable ability of the proteins to adsorb at the interface. The higher protein coverage can account for the differences observed in the emulsification capacity of the two extracts. The difference in protein surface coverage (Table 4.1.2) and molecular weight distribution of biopolymers can provide some useful insights on the higher Ostwald ripening rate observed for OE4 as compared to OE6. It is well-documented that a mechanically strong and elastic interfacial layer can provide stability against Ostwald ripening. This was also the case for emulsions prepared with OE6 where the interface has greater Γ values (Table 4.1.2) and composed of higher Mw of polysaccharides than the OE4 counterparts. The above can contribute to a far more rigid interfacial network for OE6 that are expected to reduce the rate of Ostwald ripening to a higher extent as compared to OE4, allowing for extended stability against this destabilization mechanism.

4.1.3.3 ζ -Potential measurements

ζ -Potential was measured for fresh okra extract solutions and fresh emulsions after 5, 10, 20 and 30 days of storage. ζ -Potential of fresh 1.875% w/v okra extract solutions at pH 3.0 (hence continuous phase) was investigated first (data not shown). The ζ -potential of solutions containing OE4 or OE6 was found to be -9.6 mV and -8.2 mV, respectively. The negative value of ζ -potential was attributed to the presence of anionic polysaccharides in both okra extracts and was higher in comparison to other recently investigated okra extracts that were below -14 mV (Georgiadis, Ritzoulis,

Sioura, Kornezou, Vasiliadou & Tsiptsias, 2011). Both fresh emulsions (pH 3.0) have manifested negative ζ -potential value with -10.6 mV for OE4 stabilized emulsion and -8.4 mV for emulsion composed of OE6 (Table 4.1.1). These values do not differ significantly from those of the aqueous solutions used to prepare the emulsion indicating first that the interfacial layer has similar composition to that of the continuous phase and second that the biopolymers in the extracts do not adsorb preferentially at the interface (e.g., proteins over polysaccharides). Generally, it can be seen that ζ -potential values for both emulsions was not sufficient to produce a strong electrostatic repulsion between the droplets thereby causing an increase in the d_{43} value (Gharsallaoui, Yamauchi, Chambin, Cases & Saurel, 2010). This also indicates the contribution of steric repulsion into the emulsion stability. In Table 4.1.1, ζ -potential values for both emulsions show a marginal tendency to decrease over the duration of the experiment that can be attributed to the decrease of droplet mobility due to their increase in size (Table 4.1.1) rather than to any actual changes in the interfacial charge density. In order to further explore the microstructural changes of emulsions flow behaviour measurements were performed.

4.1.3.4 Rheology of emulsions

Figure 4.1.3 shows viscosity curves for fresh okra extract solutions (continuous phase viscosity) and emulsions containing OE4 or OE6. At low shear rates the viscosity of 1.875% w/v OE6 solutions was about two times greater as compared to those OE4 (Figure 4.1.3). Viscosity of polysaccharide solutions is governed by various factors, such as molecular mass, stiffness, charge and charge density of the chains (Williams & Phillips, 2000). The macromolecular analysis of extracts shows that although polymer components of OE6 and OE4 have similar molecular weight distributions, OE6 was richer in high-molecular weight

components. The differences in viscosity of its solutions should be attributed to the effect of the impact of the higher molecular weight of the OE6 components, but also to conformational differences of their composing macromolecules, as has been previously reported (Kontogiorgos, Margelou, Georgiadis & Ritzoulis, 2012).

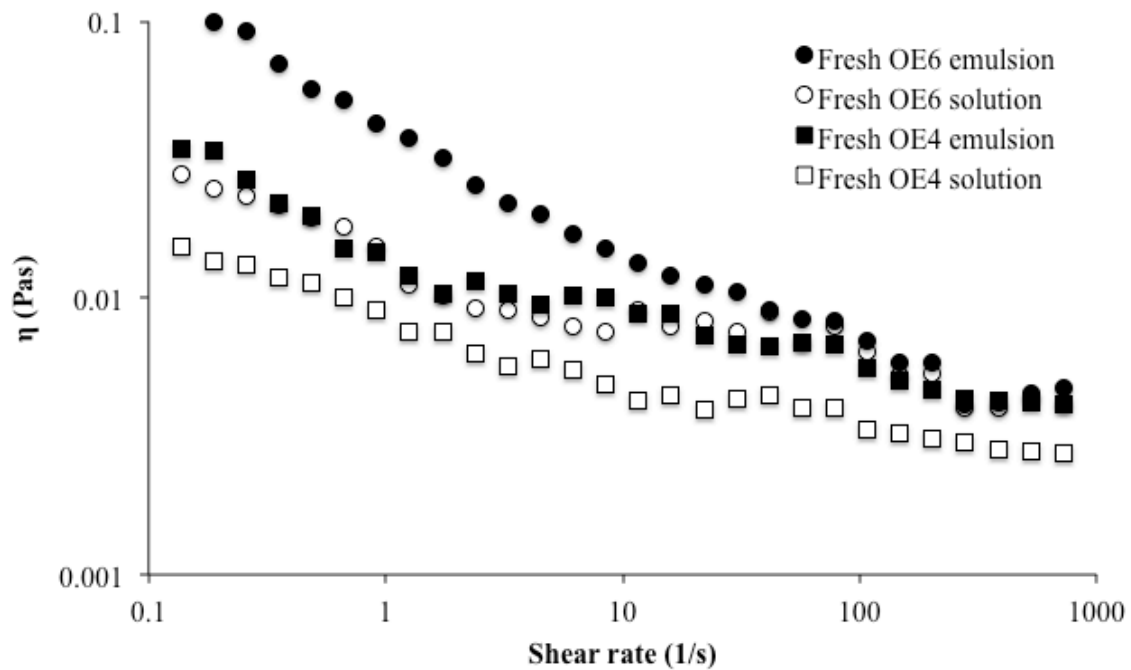


Figure 4.1.3. Rheological behavior of 1.5% w/v emulsions containing OE4, OE6 and rheological behavior of fresh 1.875% w/v okra extract solutions pH 4.0 or 6.0 (25 °C).

The difference in viscosities of the present okra solutions at low shear rates could be also attributed to the molecular structure of pectins as it has been reported that the hydrophobic acetylated rhamnogalacturonan I (RG-I) moieties increase the viscosity to a much higher level than acetylated galacturonic acid (GalA) residues (Sengkhampan, Sagis, de Vries, Schols, Sajjaanantakul & Voragen, 2010). In addition, similar remarks can be made due to the differences in degree of methylation (DM) of investigated samples. As has been previously reported (Pagan, Ibarz, Llorca & Coll, 1999) pectins extracted at higher pH (OE6 in the present investigation) may

have greater DM and therefore contribute to stronger intermolecular interactions under acidic conditions. Finally, the viscosity curves (Figure 4.1.3) of OE4 and OE6 solutions demonstrate a shear-thinning behaviour that can be attributed to the tendency for self-association that is increasing with concentration (Kontogiorgos, Margelou, Georgiadis & Ritzoulis, 2012).

Figure 4.1.4a depicts the rheological behavior of emulsions containing OE4 at different storage times. The viscosity of fresh emulsions was found to be significantly greater than that of OE4 solutions throughout the shear rate range. This was expected, as the presence of oil droplets raises the overall viscosity of a system. Fresh OE6 emulsions demonstrated higher low-shear viscosity than those containing OE4 (Figure 4.1.4b) that was consistent with the viscosity data of OE4 and OE6 solutions, (Figure 4.1.3). In addition, the OE4 and OE6 emulsions have comparable high shear rate viscosity, but at low shear rates, the viscosity of OE6 is two orders of magnitude higher than that of OE4 (Figures 4.1.4a, b). This should be attributed to the higher component of high molecular weight polysaccharides in OE6 as compared to OE4. The above suggest that at least OE6 was involved to some sort of reversible flocculation process as can be seen in Figure 4.1.2b, before the droplets become isolated after dilution. This weak flocculation could originate either from weak depletion due to unadsorbed macromolecules from the extract or from bridging of droplets due to interactions of the interfacial macromolecules. The tendency for self-association noticed in the solutions could well also apply to the hydrocolloids adsorbed at adjacent droplets, leading to a weakly flocculated droplet network. By comparing viscosities of fresh, 5 and 30 days old emulsions, it can be noticed that the latter demonstrate a significant increase in viscosity in the low shear rate regime ($<1 \text{ s}^{-1}$). The effect was far more pronounced in the case of OE4-stabilized emulsions.

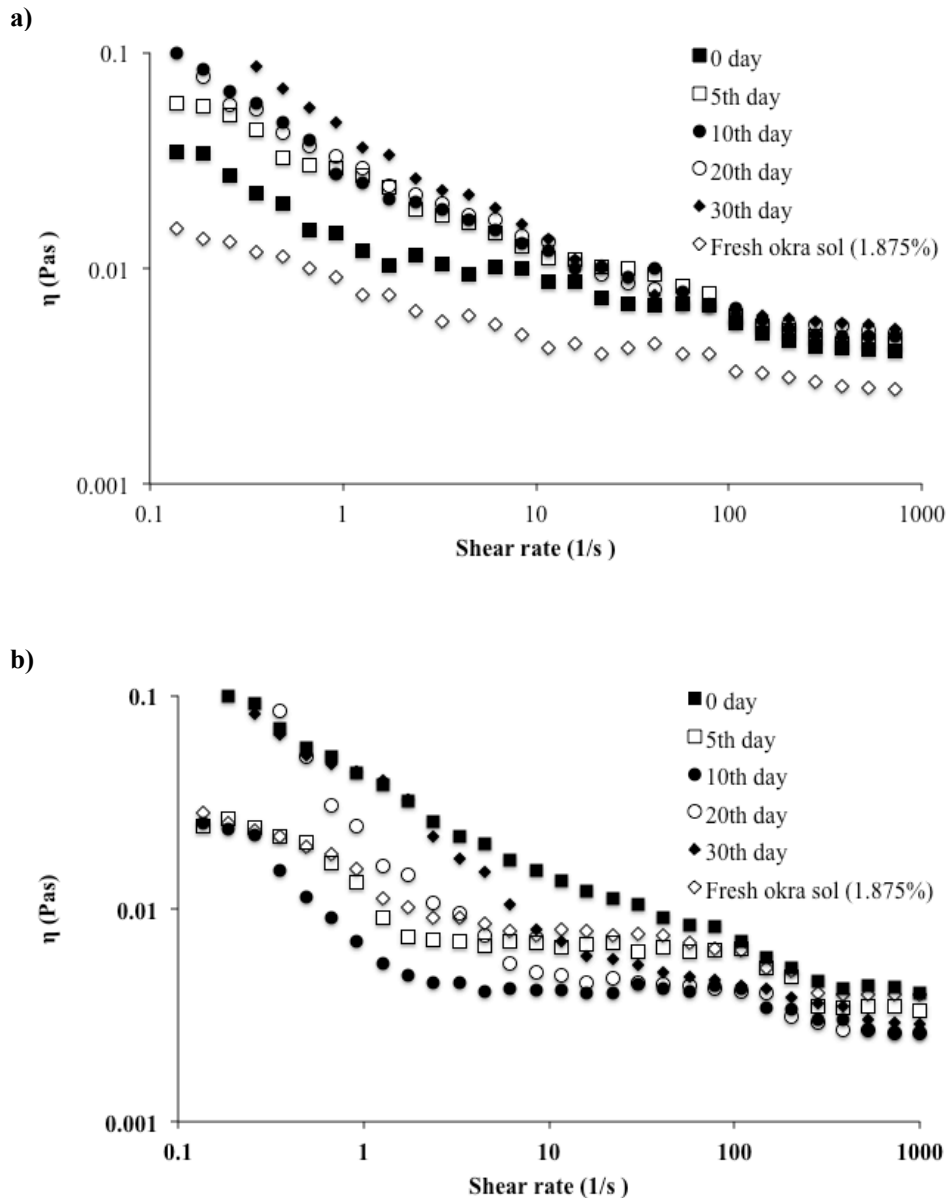


Figure 4.1.4. (a): Influence of ageing (0-30 days) on the rheological behavior of 1.5% w/v emulsion containing OE4 and rheological behavior of fresh 1.875% w/v okra extract solution pH 4.0 (25 °C), (b): Influence of ageing (0-30 days) on the rheological behavior of 1.5% w/v emulsion containing OE6 and rheological behavior of fresh 1.875% w/v okra extract solution pH 6.0 (25 °C).

It was also observed that high-shear rate viscosity of emulsions during aging was comparable for both extracts (5–6 mPas), suggesting that the floc structures are almost disrupted at high shear rates and viscosity in such stresses depends on the rheology of the continuous phase. This increase in viscosity should not be related to

existing flocculated structures, as such would tend to rearrange to produce more compact flocs, bringing about an overall reduction in viscosity. In the present case, the most plausible explanation is desorption of adsorbed polysaccharide and protein from the interface due to the reduction in free surface area, as the average droplet increases (Table 4.1.1). Such fresh bulk macromolecules would both increase the bulk phase viscosity itself and also enhance the depletion potential, strengthening any depletion flocculation. Therefore, the rheological data are in complete agreement with the results of the other measurements, such as alterations in the volume-weighted average diameters ($d_{4,3}$) and particle size distributions between day 5 and 30, especially in OE4.

4.1.4 Conclusions

Extraction protocols have considerably affected the physiochemical properties of okra extracts and had an effect on physical stability resulting emulsions. Both okra extracts showed good emulsification capacity, producing fine emulsions but the two emulsifiers differentiated significantly in terms of their efficiency towards long-term stabilization against coarsening. Emulsions containing OE6 were found to be stable as evidenced by particle size distribution measurements during the 30 days storage trial. Those composed of OE4 were more susceptible to coarsening mechanisms resulting in droplets of greater average size. Ostwald ripening was identified to be one of the major destabilization mechanisms particularly for emulsions prepared with OE4. Overall, OE6 demonstrated higher surface activity at the o/w interface and its viscosity was found to be two times greater in comparison to OE4. Consequently, emulsions containing OE6 manifested greater stability than the OE4 counterparts.

4.2 EFFECT OF ISOLATION CONDITIONS ON INTERFACIAL ACTIVITY OF OKRA BIOPOLYMERS.

4.2.1 Introduction

Like many other biopolymers, the physicochemical properties of okra polysaccharides are amenable to interdisciplinary applications between the food and pharmaceutical industry in both dry and hydrated systems. In the previous section, good emulsion stabilising properties of okra extracts in acidic environments have been demonstrated. The emulsifying capacity of okra polysaccharides can be utilized in the food industry particularly in fruit drinks or acidified dairy products. The interfacial activity of okra polysaccharides may also find applications in emulsion-based flavour or drug delivery systems. However, such functional properties are controlled by the extraction protocol that influences the backbone composition of the isolated biopolymer (Chapter 2). Therefore, the aim of this part of investigation was to fabricate *n*-hexadecane-in-water emulsions stabilized with OP6 that was isolated using the extraction protocol presented in Chapter 2 and evaluate its emulsifying capacity.

4.2.2 Materials and methods

4.2.2.1 Isolation of okra pectin

Isolation of okra pectin was performed at pH 6.0 and detailed description of procedure was presented in Chapter 2. Okra pectin sample was labeled as OP6.

4.2.2.3 Preparation of emulsions

O/W emulsions with OP6 at concentration 0.625% w/v with dispersed-phase (*n*-hexadecane) volume fraction $\varphi = 0.2$ and under acidic conditions (pH 3.0) were prepared in accordance to emulsification procedure previously applied for OE4/OE6

stabilized emulsions and described in detail in subchapter 4.1, section 4.1.2.4. For the determination of the long-term stability, all emulsions were stored in an incubation chamber at 25°C.

4.2.2.4 Determination of particle droplet size distribution

Droplet size distribution was measured immediately after the emulsion preparation and after 5, and 30 days of storage using the same protocol described in section 4.1.2.5.

4.2.2.5 Determination of ζ -potential

All ζ -potential measurements were performed according to protocol described in section 4.1.2.8. All measurements were performed in duplicate immediately after emulsion preparation and after 5, 15, and 30 days of storage.

4.2.2.6 Rheological measurements of okra extracts and emulsions

Rheological properties of samples were measured using experimental conditions described in section 4.1.2.6. Viscosity measurements were conducted immediately after preparation of okra extract solutions and emulsions and after 5 and 30 days of storage. All measurements were performed in duplicate.

4.2.3 Results and discussion

4.2.3.1 Emulsification capacity of OP6

The emulsification capacity of OP6 was examined at pH 3.0 in order to investigate the emulsification properties of okra extracts in acidic food matrices and their possible stability in the acidic environment of the stomach. *n*-Hexadecane ($\varphi = 0.2$) was dispersed in okra aqueous solution (0.625% w/v) to obtain emulsions of a nominal extract concentration in the entire emulsion volume of 0.5% w/v.

Quantification of emulsification capacity in relation to long-term emulsion stability proceeds with measurement of the droplet size distribution and the average droplet sizes. Fresh *n*-hexadecane-in-water emulsions stabilized with OP6 demonstrated droplet mean diameter ($d_{3,2}$) about 6 μm (Figure 4.2.1, Table 4.2.1) indicating that finer emulsions were fabricated with OP6 than those that have been previously prepared with OE6 ($\sim 11 \mu\text{m}$, described in section 4.1). This can be attributed to either changes in the fine structure of pectins due to different extraction procedures (e.g., degree of methylation, presence of acetyl groups, MW) or to higher protein content in the extracts (Chapter 2, Table 2.1).

Table 4.2.1. Influence of ageing on the surface weighted average droplet size ($d_{3,2}$), ($d_{4,3}$) and ζ -potential in emulsions formed with 0.5% OP6.

Time (days)	$d_{3,2}$ (μm)	$d_{4,3}$ (μm)	ζ -potential (mV)
0	5.9 \pm 1.4	11.2 \pm 2.5	-19.3 \pm 0.8
5	23.5 \pm 0.9	89.8 \pm 16.0	-21.7 \pm 0.1
15	24.2 \pm 1.6	91.5 \pm 5.2	-21.4 \pm 0.5
30	25.9 \pm 3.8	100.0 \pm 17.1	-24.0 \pm 0.4

The average droplet size of the emulsions increased during ageing with $d_{3,2}$ rising from $\sim 6 \mu\text{m}$ to $\sim 23 \mu\text{m}$ after 5 days and staying relatively constant after 30 days of storage ($\sim 25 \mu\text{m}$). The horizontal shift of the major peak to larger droplet sizes (Figure 4.2.1) instead of the emergence of a coalescence-generated second peak is usually attributed to an Ostwald ripening coarsening mechanism (Dickinson, Galazka & Anderson, 1991; McClements, 2005). Droplets coalescence generally contributes to the development of a bimodal curve or broadening of monomodal curve on ageing, but Ostwald ripening leads to a sharpening of particle size distribution curves, something that can be also observed in Figure 4.2.1 (Dickinson, Golding &

Povey, 1997). Ostwald ripening is significant in polydisperse emulsions containing oils with some solubility in the continuous phase and the rate-limiting step of the growth rate is the diffusion of the dissolved droplets through the bulk (Taylor, 1995). Hydrocarbons such as *n*-hexadecane are poorly soluble in water, something that may hinder development of Ostwald ripening. However, transport of oil through the aqueous phase assisted by the presence of surface-active impurities in the extract (Kabalnov, 1994; McClements, Dungan, German & Kinsella, 1992) or enhancement of depletion effects due to the presence of unadsorbed biopolymers (Djerdjev & Beattie, 2008) are possible pathways to Ostwald ripening. Gradual reduction of the small peak on ageing in the fresh emulsions (Figure 4.2.1) where the small droplets are incorporated into the major peak may also indicate the possibility of the occurrence of depletion flocculation. It has been also reported that in the systems where two distinct instability processes may be distinguished, coalescence occurs when droplets are not completely covered with surface-active biopolymer whereas Ostwald ripening becomes dominant only at high biopolymer concentrations (Nazarzadeh, Anthonypillai, & Sajjadi, 2013).

ζ -Potential was measured for fresh okra extract solutions and emulsions after 0 (fresh), 5, 15 and 30 days of storage (Table 4.2.1). The ζ -potential of OP6 solutions was -26.3 mV showing that continuous phase carried negative charge at pH 3.0. Most proteins associated with food components usually have pI in the range of ~ 4.0 . Below pI proteins are positively charged but the fact that solutions carry negative charge indicates that the electrical properties are dominated by the presence of pectins rather than proteins that may be present as contaminants during the extraction.

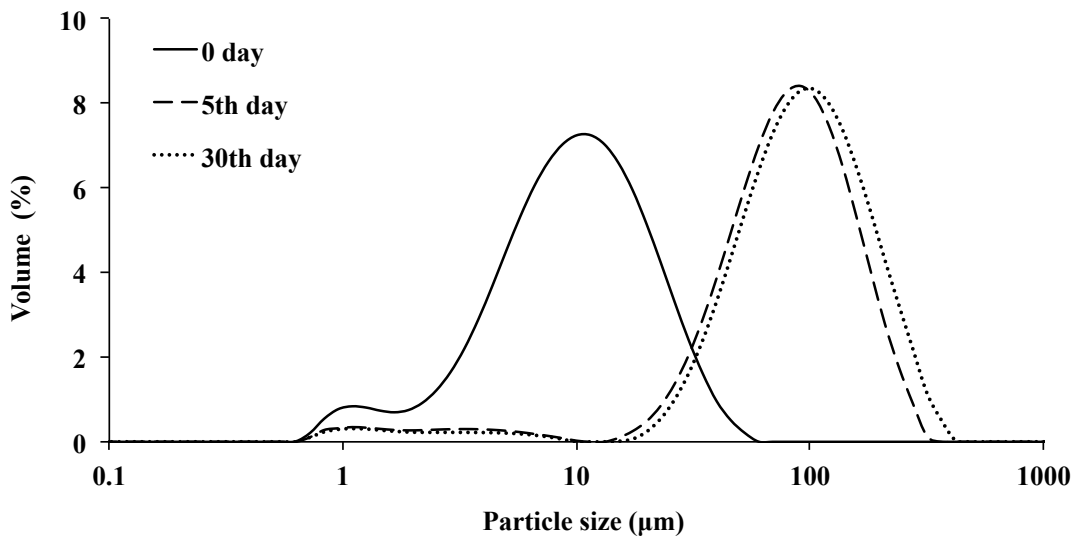


Figure 4.2.1. Particle size distributions of 0.5% w/v emulsions stabilized with OP6. The time development of the distributions is also shown.

Similar behavior has been observed with mixed pectin solutions in the presence of β -lactoglobulin where pectins controlled the charge of the solutions (Cho, Decker & McClements, 2010). This value was lower in comparison to those obtained for okra extract investigated in subchapter 4.1 indicating the influence of extraction procedures on the molecular characteristics of pectins. ζ -Potential values of fresh emulsions (-19.3 mV) did not depart significantly from that of the continuous phase indicating that the droplet interface has similar electrical properties with the bulk. These observations suggest the presence of pectin at the interface. With ageing surface charge does not change appreciably and after thirty days of storage increases to -24.0 mV.

4.2.3.2 Flow behaviour of okra pectin solutions and emulsions

Figure 4.2.2 shows viscosity curves for continuous phase and emulsions containing OP6. Continuous phase shows weak pseudoplastic behaviour with the onset becoming apparent only at high shear rates ($>100 \text{ s}^{-1}$). The viscosity of freshly prepared emulsions was greater than that of the continuous phase throughout the shear

range (Figure 4.2.2). This was anticipated, as the presence of oil droplets increases the viscosity of dispersions (McClements, 1999). Emulsions did not show appreciable changes in the viscosity curves with storage time (30 days) and they generally followed the flow behavior of the continuous phase. The absence of a significant shear-thinning pattern in the presence of droplets indicates that emulsions do not flocculate during ageing. At pH 3 droplets have negative ζ -potential (-19.3 mV) mostly due to the dissociation of carboxyl groups of galacturonic acid. This renders negative charge to pectins that also results in extended conformation at the hydrocarbon-water interface. This weakly negative surface potential along with possible steric hindrance increases the repulsion between the droplets thus impeding substantial droplet flocculation. Similar behaviour has been observed with okra extract-stabilized emulsions prepared at pH 3.0 in subchapter 4.1 where samples also showed weak flocculation with ageing. Therefore, it can be assumed that depletion flocculation is improbable pathway to Ostwald ripening in the investigated system as opposed to the surfactant-stabilized octane- and decane-in-water emulsions (Djerdjev & Beattie, 2008). Moreover, in the absence of flocculation coalescence in emulsions leads to a reduction of their viscosity. Since the changes in viscosities at low shear rates of fresh, 5 and 30 days old emulsions were found negligible, the occurrence of coalescence cannot be considered as a major destabilization mechanism.

Particle size distribution and rheological data suggest that Ostwald ripening is a probable mechanism of coarsening in the investigated systems. Ostwald ripening was previously observed for biopolymer-stabilised alkane-in-water emulsions as demonstrated in subchapter 4.1 or surfactant-stabilised *n*-hexadecane- or triglyceride-in-water emulsions (Nazarzadeh, Anthonypillai & Sajjadi, 2013; Wooster, Golding & Sanguansri, 2008).

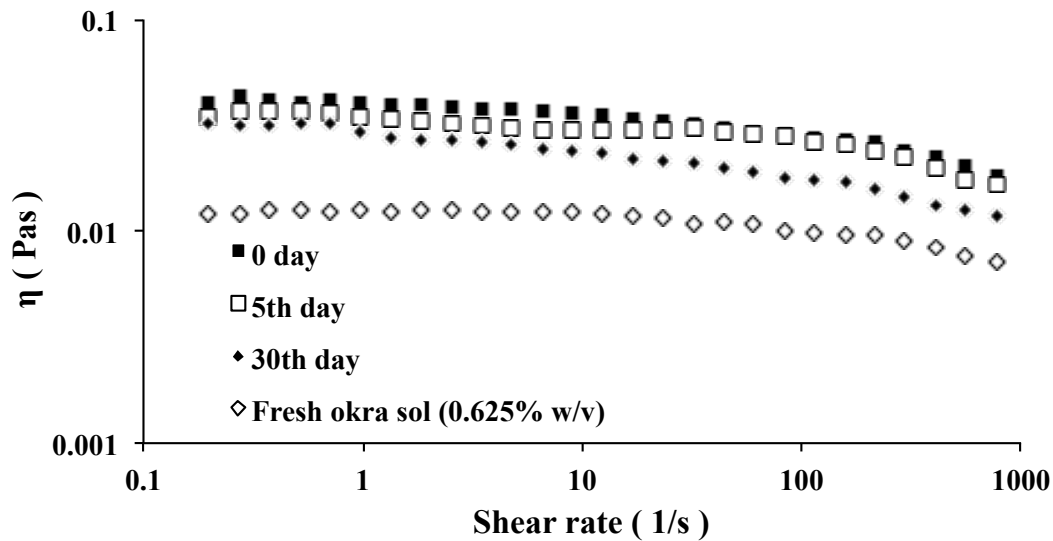


Figure 4.2.2. Influence of aging (0–30 days) on the rheological behaviour of 0.5% w/v emulsion containing OP6 and rheological behaviour of fresh 0.625% w/v OP6 solution (25 °C).

This behaviour shows the great potential of okra extracts to act as emulsifiers in acidic environments and at the same time providing emulsions with relatively low viscosity (<0.1 Pas).

4.2.4 Conclusions

Okra biopolymers isolated using hot aqueous extraction at pH 6.0 also showed potential as emulsifiers in acidic environments producing fine emulsions with good stability against coarsening. Flow behaviour and particle size distributions of OP6 stabilized emulsions demonstrated that modification of extraction protocol results in biopolymers with distinct physicochemical structures and tuning of these characteristics allows the design of emulsion formulations for specific applications. Such a property could be exploited in delivering emulsified hydrophobic drugs or nutrients through the acidic environment of stomach. Overall, the physicochemical attributes of pectins extracted from okra seem to be promising for uses in drug or nutrient encapsulation and delivery.

4.3 SURFACE ENGINEERING OF O/W INTERFACES WITH OKRA PECTIN

4.3.1 Introduction

Industrial convergence between food and pharma has gathered pace in the last five years with the demand for controlled and targeted delivery systems for nutrients, supplements and drugs of particular focus for disease prevention and treatment. Food-grade emulsions are increasingly being utilized for encapsulating and delivering functional food ingredients and nutraceuticals (Abbas, Hayat, Karangwa, Bashari & Zhang, 2013). A wide variety of lipophilic food bioactives, including flavors, vitamins (D, E), carotenoids, flavonoids, phytosterols and polyunsaturated lipids have been encapsulated in colloidal systems (Guttoff, Saberi & McClements, 2015; Mayer, Weiss & McClements, 2013; McClements, 2012; McClements, Decker, Park & Weiss, 2009; McClements & Rao, 2011). High hydrophobicity and low solubility in water of these bioactive compounds limit their utilization in aqueous-based foods and beverages. Emulsion technology is particularly suited for the design and fabrication of delivery systems in order to resolve this issue. Emulsions as delivery vehicles allow sustained release and protection from degradation during the storage of lipophilic bioactive components incorporated into the hydrophobic core of the lipid droplets. Furthermore, protection of the bioactive when loaded in the emulsion internal phase from environmental conditions (*e.g.*, gastric fluids) is another advantage that may result in more efficient delivery of bioactive.

Emulsions are most typically fabricated with proteins, low molecular weight surfactants and surface-active carbohydrate polymers. Most protein is easily digested within the gastrointestinal tract and is often highly sensitive to the alterations in pH, ionic strength, and temperature resulting in changes of surface composition of oil

droplets and modification of the physical properties of the colloidal system (Joye & McClements, 2014). This causes the droplets that arrive in the small intestines to be different from those that were ingested. Polysaccharides such as hydroxypropylmethylcellulose, guar gum and xanthan gum have been effectively utilized as delivery vehicles due to their biocompatibility, biodegradability, and high potential to be modified to achieve the required properties (Fathi, Martín & McClements, 2014). Pectin is a linear anionic polysaccharide at high pH that is resistant to enzymatic digestion in the mouth and stomach and therefore makes it suitable for delivery of acid sensitive bioactives (Sinha & Kumria, 2001). A number of studies have also shown that pectin can be used to form nano-scale particles suitable for delivery of bioactive ingredients (Yu, Cao, Zhang, Zhou, Cheng & Zhang, 2009).

In the previous sections 4.1 and 4.2, the effect of extraction protocol on physicochemical properties of isolated biopolymers (crude okra extract and okra pectin) has been established and the emulsifying capacity of these carbohydrate polymers has been demonstrated in model *n*-hexadecane-in-water emulsions at pH 3.0. That part of the investigation mainly focused on fabrication of okra pectin stabilized emulsions with colloidal mill and resulted in particle mean diameters ($d_{3,2}$) in the range of 5 – 11 μm . Changes in particle mean diameters lead to the variations in functional performance of emulsion-based delivery systems. The smaller particle sizes are typically associated with higher solubility of emulsion and kinetic stability to mechanisms of coarsening determined by gravity and/or droplet dimensions. Moreover, it has been reported that the bioavailability and encapsulation efficiency of bioactive compounds incorporated in the colloid system tends to increase with reduction in particle sizes (McClements & Rao, 2011).

Therefore, in this part of investigation, we aim to fabricate okra pectin stabilized emulsions of smaller droplet sizes using ultrasound-assisted emulsification at lower pH values (pH 2.0), evaluate the fundamental mechanisms that lie behind the functionality of this biopolymer and identify the suitability of emulsions to act as a delivery agents for hydrophobic compounds (e.g., drugs, flavors) in highly acidic environments.

4.3.2 Materials and Methods

4.3.2.1 Materials

Pectin powders isolated in Chapter 2 and labeled as OP2 and OP6 were used in this part of investigation. Sodium azide, citric acid monohydrate, sodium citrate dihydrate, phenol, *n*-hexane, *n*-decane, *n*-hexadecane, *n*-dodecane, formaldehyde (37-40%), 0.01M phosphate buffer saline (PBS) (all analytical grade reagents) were obtained from Sigma-Aldrich (St Louis, MO). Anti-homogalacturonan antibody LM19 and LM4 (non-pectin specific antibody) were supplied by Plant Probes, Leeds, United Kingdom. De-ionized water was used throughout the extraction experiments. The measurements were performed in duplicates in three different emulsion preparations yielding in total six replicates for each sample.

4.3.2.2 Preparation of okra emulsions

Preliminary experiments on the optimum concentration of okra pectin towards emulsion stability showed that fine emulsions are produced at pectin concentration of 1.5% w/v with dispersed phase volume fraction $\phi = 0.1$ (*n*-dodecane or *n*-hexadecane) and under acidic conditions (pH 2.0). The aqueous phases of the emulsions were prepared by means of dissolving okra pectin powders at 1.67% w/v concentration in citric buffer (0.01 M, pH 2.0) at room temperature. Emulsions were fabricated in two

stages: a) pre-emulsions were obtained with a high-speed (IKA T18 basic, Ultra-Turrax, Germany) homogenizer for 2 min and, b) the coarse emulsions were then further emulsified using an ultrasound device (Hielscher Ultrasonics, Model UP 100H) equipped with 7 mm diameter MS7 tip immersed (two-thirds) in the coarse emulsion and operating at 30 kHz. An ultrasonic treatment of emulsions was performed for 40 s with pulsed ultrasound (30% per second) at 100% amplitude (corresponding to ultrasonic wave of 125 μm). These sonication conditions were chosen in accordance to the preliminary data that showed the absence of “over processing” of pectin-stabilized emulsions. All experiments were performed in 8 mL sample tubes containing 7.5 mL of the pre-emulsion. Emulsions were placed in the temperature-cooling bath, keeping the sample temperature at 25° C.

4.3.2.3 Determination of droplet size distribution

Droplet size distribution was measured immediately after the emulsion preparation and after 1 hour followed by measurements after 1, 10 and 30 days of storage using the same protocol described in section 4.1.2.5. Refractive indexes of *n*-dodecane, *n*-hexadecane and dispersion medium citric buffer (10 mM, pH 2.0) were set to 1.421, 1.434 and 1.333, respectively. Consequently, droplet size was described using the surface-weighted mean diameter ($d_{3,2}$) and volume-weighted mean diameter ($d_{4,3}$). The development of droplet sizes was monitored at 5 min increments for 1h using $d_{0,1}$ diameters. The width of the droplet distributions was expressed using span $((d_{0,9}-d_{0,1})/d_{0,5})$ that was obtained from the result analysis report of the instrument.

4.3.2.4 Interfacial composition analysis

Interfacial composition analysis was performed by determining protein, pectin and acetyl contents at the of oil-water interface. Okra pectin (OP2 and OP6) stabilized

o/w emulsions were centrifuged at 60000×g for 1 h (Optima L-100K ultracentrifuge, rotor 50.2 Ti, Beckman Coulter, USA) until equilibrium phase separation conditions were achieved and serum was collected using a syringe. The interfacial composition was evaluated as the protein, pectin or acetyl concentration difference between the pectin solutions (*i.e.*, aqueous phase before emulsification) and serum solutions. Protein was measured with Bradford analysis using Quick Start™ Bradford Protein Assay kit (Bradford, 1976). The quantification of adsorbed pectin was expressed as determination of total carbohydrates in pectin and serum solutions using the phenol-sulphuric method (Dubois, Gilles, Hamilton, Rebers & Smith, 1956). The acetyl content was determined with the hydroxamic acid method (McComb & McCready, 1957). Interfacial protein and pectin concentrations (Γ , mg m⁻²) were calculated as protein or pectin concentration difference between the biopolymer and serum solutions divided by the specific surface area (SSA) of the oil droplets:

$$\Gamma = \frac{\text{mg of adsorbed protein or pectin}}{\text{SSA} \times \text{mL of alkane in emulsion}} \quad (38)$$

where specific surface area (SSA), m²/mL was obtained by the result analysis report of the instrument.

Surface (pectin solution/air) tensions of OP2 and OP6 solutions were measured using tensiometer (Leybold Didactic GMBH, Hürth, Germany) equipped with 60 mm diameter ring. Deionised water was used as a reference.

4.3.2.5 Rheological characterization of okra pectin solutions and emulsions

Rheological properties of samples were measured using the same protocol described in section 4.1.2.6. Viscosity measurements were conducted immediately after preparation of okra extract solutions and emulsions and after 1, 10 and 30 days of storage. All measurements were performed in duplicate.

4.3.2.6 Determination and titration of ζ -potential

All ζ -potential measurements were performed using protocol previously described in section 4.1.2.8. The ζ -potential titration of 1.67% w/v OP2 or OP6 solutions and 1.5% w/v emulsions was conducted under the same conditions described in Chapter 3, section 3.2.6.

4.3.2.7 Pectin immunolocalization at the o/w interface

Anti-homogalacturonan antibody LM19 (Plant Probes, Leeds, United Kingdom) was used to localize pectin at the alkane-water interface and LM4 (non-pectin specific antibody) was used as a negative control. A set of OP2 aqueous phases (1.67% w/v) and OP2 stabilized *n*-dodecane emulsions (1.5% w/v) were prepared in phosphate-buffered saline (0.01M PBS, pH 7.4). A drop of OP2 solution was spread out on the microscopy glass with a spatula and dried using Bunsen burner. Dried sample was fixed using 10% formalin solution buffered in 0.01M PBS. Following the washing step, samples were blocked with 5% BSA (bovine serum albumin) in 0.01M PBS. The immunolabeling of pectic epitopes started with an incubation with primary antibody (LM19 was used as 5-fold dilutions of hybridoma supernatant) overnight at 4°C followed by a washing step in PBS. LM19 was visualized using secondary labelling with anti-rat IgG coupled to fluorescein isothiocyanate (FITC) (Sigma-Aldrich, St. Louis, USA). The secondary antibody was diluted 1:5 in PBS and incubation was performed for 2 h at room temperature.

In order to use the probes for specific *in situ* immunolocalisation of pectin at the alkane-water interface, 1.5% w/v coarse OP2 stabilized emulsions were prepared using high-speed homogenizer (IKA T18 basic, Ultra-Turrax, Germany) for 2 min. Monoclonal antibody LM19 (100 μ L, diluted 1:5) was added to 0.5 mL of coarse emulsion and left overnight at 4°C. For localizing pectin at the o/w interface,

secondary antibody IgG-FITC (100 μ L, diluted 1:5) was added and emulsions were incubated for 2 h at room temperature. Emulsions were centrifuged at 14100 \times g for 25 min (MiniSpin Plus, Eppendorf, Hamburg, Germany) in order to separate creamed layer from serum. Diluted creamed layer was analysed using microscopy.

Immunostained emulsion droplets and OP2 solutions were visualized using an Olympus IX70 microscope (Olympus, Optical Co. Ltd, Tokyo, Japan) equipped with epifluorescence illumination and using 10x and 40x oil immersion objectives. FITC was excited at 490 nm and emitted signal collected between 528 and 538 nm. Image acquisition and analysis were performed with SoftWoRx software (Applied precision Inc.).

4.3.3. Results and discussion

4.3.3.1 Emulsifying capacity of okra pectin and ageing of emulsions

n-Hexadecane-in-water emulsions (1.5% w/v) were stabilized by either okra pectin isolated at pH 2.0 (OP2) or okra pectin isolated at pH 6.0 (OP6). Change in particle size distributions (PSD) and the average droplet sizes were monitored for a period of 30 days (Table 4.3.1). The temporal evolution of the particle size distributions for OP2 and OP6 stabilized emulsions containing *n*-hexadecane are presented in Figures 4.3.1a and 4.3.2a. Both samples demonstrated good emulsification capacity producing emulsions with $d_{3,2}$ in the range of 1.7 – 3.0 μ m (Table 4.3.1). Figure 4.3.3a shows that fresh emulsions stabilized with OP2 have monomodal narrow droplet size distributions with span \sim 1.8 (Table 4.3.1). On the contrary, emulsions fabricated with OP6 demonstrated bimodal and broader particle size distributions as indicated by $d_{3,2}$ (3.0 μ m), $d_{4,3}$ (7.3 μ m), and span (\sim 3.0). The presence of a second peak composed of population of larger droplets in emulsion stabilized with OP6 could be explained by the disruption of just those oil droplets that

are close to the probe due to the insufficient mixing caused by ultrasound. It has been also previously reported that high viscosity of the continuous phase restricts the induction of cavitation phenomena (Camino, Sánchez, Rodríguez Patino & Pilosof, 2011). These factors contribute to the low emulsification uniformity in case of OP6-stabilized emulsions. The behaviour of bimodal dispersed systems, when referring to the mechanisms of instability, is typically governed by the presence of higher droplet sizes, even if they are present as a small proportion of the total number of droplets in emulsion (McClements, 1999). Therefore, it is expected that population of larger droplets in OP6-stabilized emulsions may result in emergence of coalescence as the predominant destabilisation mechanism. However, Figure 4.3.1a shows that emulsions stabilized with OP6 do not exhibit any appreciable development of coalescence-induced second peak with time and any appreciable degradation over a period of 30 days. These observations may indicate the formation of mechanically rigid interfacial layer in OP6-stabilized emulsions that restricts coalescence. The width of distributions (span $\sim 3.0 - 2.4$) and droplet size ($d_{4,3} \sim 7.3 - 11.4 \mu\text{m}$) of OP6 stabilized emulsions did not show appreciable changes throughout the ageing period, but the maximum in the distribution slightly shifted with time towards larger average droplet sizes indicating that the colloidal system may evolve under the effect of Ostwald ripening (Figure 4.3.1a). Coalescence events typically increase the polydispersity and therefore accelerate the rate of coarsening (Schmitt, Cattelet & Leal-Calderon, 2004), something that can be observed in OP2-stabilized emulsions. Figure 4.3.2a shows that emulsions prepared with OP2 destabilise rapidly and demonstrate a marked increase in average droplet size, i.e., $d_{4,3}$ rising from $2.4 \mu\text{m}$ to $10.0 \mu\text{m}$ after 1 hour of storage.

Table 4.3.1. Influence of okra pectin type and storage time on the average droplet diameters ($d_{3,2}$ and $d_{4,3}$) and span in *n*-dodecane and *n*-hexadecane emulsions formed with 1.5% (w/v) OP2 and OP6.

Sample	Time	$d_{3,2}$ (μm)		$d_{4,3}$ (μm)		Span	
		C ₁₂ H ₂₆	C ₁₆ H ₃₄	C ₁₂ H ₂₆	C ₁₆ H ₃₄	C ₁₂ H ₂₆	C ₁₆ H ₃₄
OP2	fresh	1.8 ± 0.1	1.7 ± 0.1	2.6 ± 0.1	2.4 ± 0.1	2.0 ± 0.0	1.8 ± 0.0
	1 hour	5.1 ± 0.2	4.1 ± 0.1	11.9 ± 0.4	10.0 ± 0.4	2.5 ± 0.0	2.7 ± 0.0
	1 day	5.7 ± 0.1	4.6 ± 0.2	52.2 ± 1.4	34.5 ± 1.7	7.0 ± 0.2	7.5 ± 0.2
	10 days	7.0 ± 1.3	5.5 ± 1.1	122.5±38.2	107.9±21.2	11.0 ± 1.6	11.4 ± 2.6
	30 days	8.7 ± 1.3	6.0 ± 0.2	162.4±30.8	132.7±0.9	3.0 ± 0.3	3.6 ± 0.2
OP6	fresh	2.8 ± 0.0	3.0 ± 0.3	7.6 ± 2.6	7.3 ± 1.9	2.9 ± 0.5	3.0 ± 0.1
	1 hour	3.3 ± 0.1	3.1 ± 0.1	11.2 ± 2.6	7.4 ± 1.1	2.7 ± 0.1	2.5 ± 0.1
	1 day	5.0 ± 0.1	3.2 ± 0.0	11.8 ± 0.9	7.7 ± 0.4	2.2 ± 0.2	2.4 ± 0.0
	10 days	9.1 ± 0.2	4.1 ± 4.1	19.2 ± 1.3	10.5 ± 2.1	2.2 ± 0.1	2.4 ± 0.3
	30 days	8.9 ± 0.2	4.5 ± 0.4	20.7 ± 0.9	11.4 ± 1.2	2.2 ± 0.1	2.4 ± 0.1

^a Data are means ± SD. Sample OP2 indicates 1.5% w/v emulsion stabilized with OP2; sample OP6 indicates 1.5% w/v emulsion stabilized with OP6. Both emulsions have $\varphi = 0.1$, pH 2.0.

Considerable destabilisation of emulsion occurs after 1 day of storage as evidenced by the broader PSD curve (span ~ 7.5) and $d_{4,3}$ (34.5 μm) (Table 4.3.1, Figure 4.3.2a). At the later point, the distribution becomes polymodal followed by the formation of a new mode at large droplet mean diameters ($d_{4,3}$ around 132.7 μm) after 30 days of ageing. Polymodal nature of PSD curve on ageing shows that coalescence could play a major role in determining droplet instability in OP2-stabilized emulsions.

Table 4.3.1 and Figures 4.3.1b, 4.3.2b demonstrate that droplet mean diameters ($d_{3,2}$ and $d_{4,3}$), shape and width of PSD of *n*-dodecane-in-water OP2 and OP6-stabilized emulsions are comparable to those observed in the corresponding *n*-hexadecane-in-water emulsions, but the sharpening of PSD curve is more pronounced and in accordance to alkane solubility values.

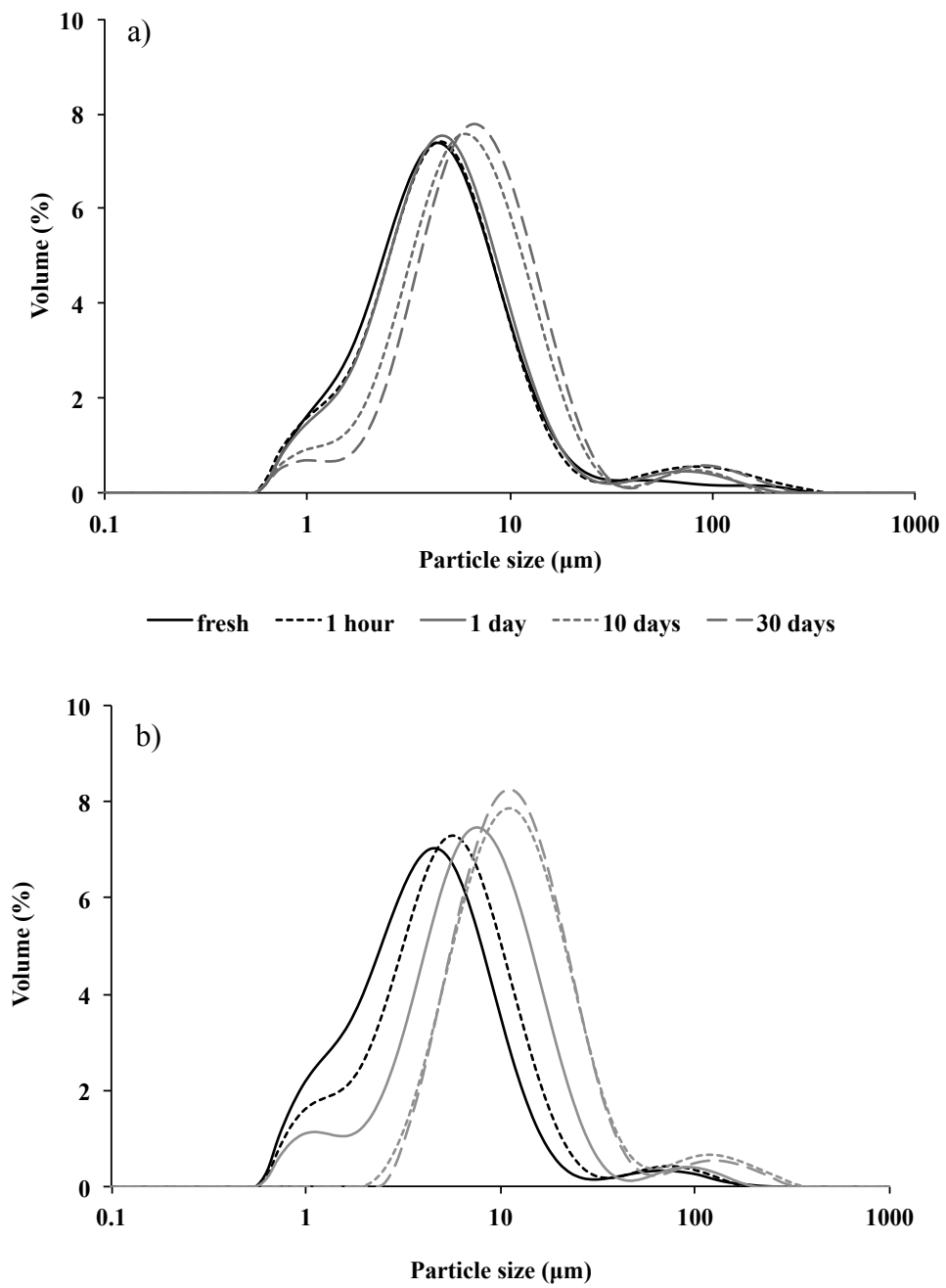


Figure 4.3.1. Particle size distributions of a) *n*-hexadecane-in-water emulsion with OP6 and b) *n*-dodecane-in-water emulsion with OP6 at 25 °C.

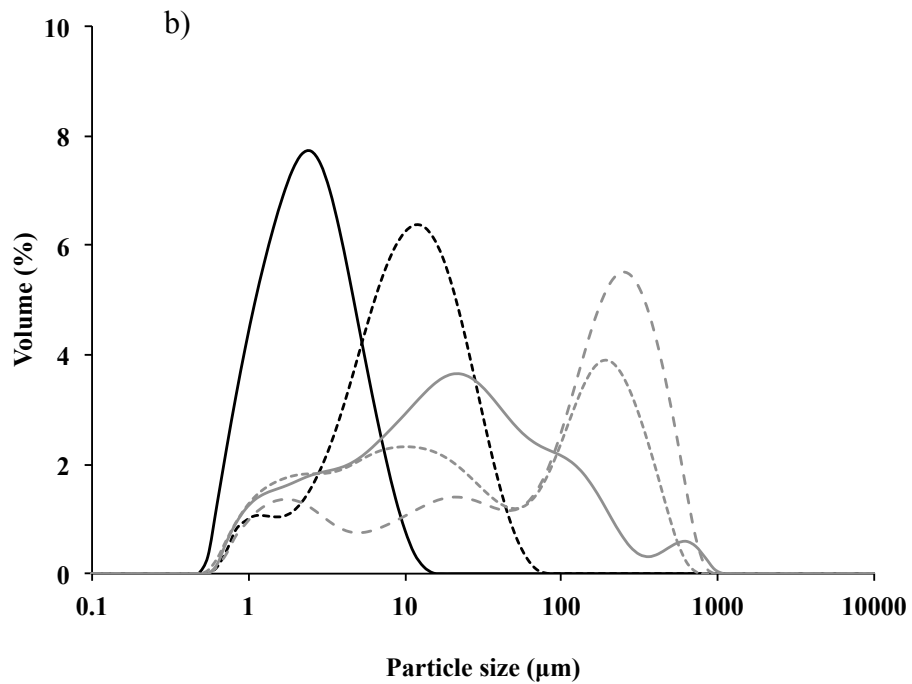
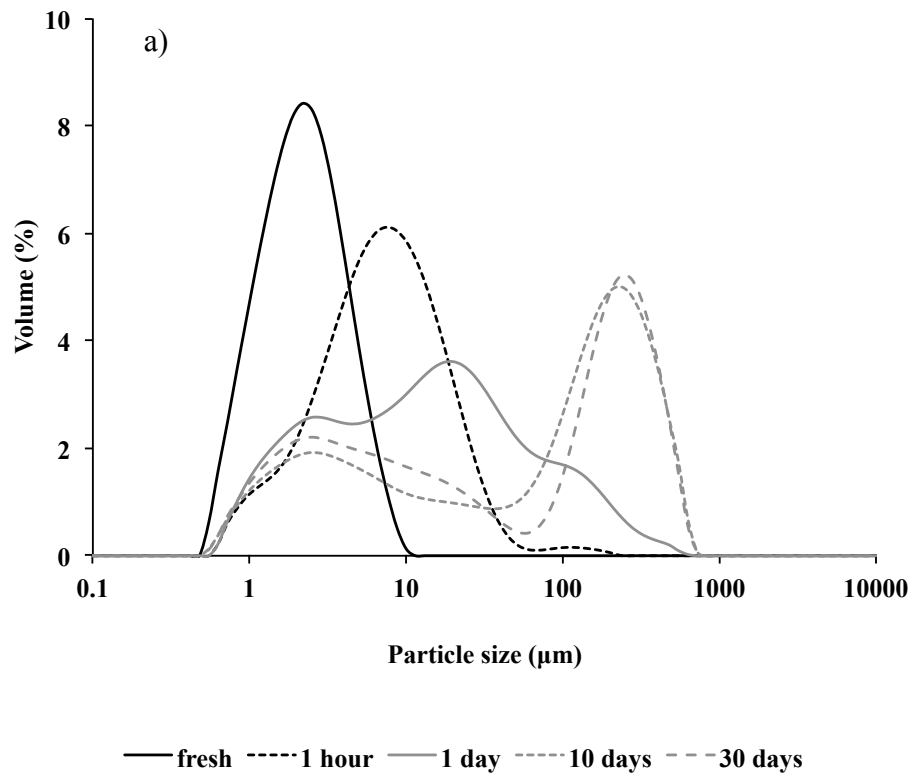


Figure 4.3.2. Particle size distributions of a) *n*-hexadecane-in-water emulsion with OP2 and b) *n*-dodecane-in-water emulsion with OP2 at 25°C.

The macroscopic examination of *n*-hexadecane-in-water emulsions on storage also denotes the variations in interfacial properties of both biopolymers. Figure 4.3.3. demonstrates that emulsions stabilized with OP2 show creaming after 1 day of storage whereas OP6 counterpart remains stable. Furthermore, Figures 4.3.3 also shows the formation of macroscopic *n*-hexadecane layer in OP2 stabilized emulsions after 30 days of storage.

It is critical to determine the mechanisms of emulsions coarsening (coalescence or Ostwald ripening) in order to construct effective strategies to improve emulsions stability on ageing. Therefore, further analysis was performed in order to assess the magnitude of coalescence and Ostwald ripening events in OP2 and OP6 stabilized emulsions that is described in the next section.

4.3.3.2 Examination of destabilisation mechanisms

The susceptibility of droplets to Ostwald ripening can be described by the LSW (Lifshitz–Slyozov–Wagner) model that is based on the assumption that diffusion of oil through the water determines the overall ripening rate (Lifshitz & Slyozov, 1961). In a typical Ostwald ripening scenario, at asymptotically long times, the change in number droplet diameter cubed ($d_{0.1}$)³ is a linear function of time. Brownian motion-induced coalescence also results in linear correlation of droplet growth rate as a function of time (Wang & Davis, 1993). Brownian motion is not expected to influence the destabilisation mechanisms of the dispersion of the present study due to the predominance of gravity as evidenced by droplet size (1.7 – 3.0 μm). The destabilisation of emulsions may occur due to the interplay between Ostwald ripening and coalescence (Schmitt, Cattelet & Leal-Calderon, 2004). The examination of coarsening mechanisms is commonly performed under conditions where one type of instability dominates the other in order to monitor its progress more accurately.

Therefore, OP2 and OP6 stabilized emulsions were fabricated at the optimum biopolymer concentrations (1.5 % w/v). The preliminary data have shown that increase of okra pectin concentration up to ~ 2.0 % w/v did not result in further reduction of droplet diameter indicating saturation of the *n*-hexadecane-in-water interface. A sufficient surface coverage of droplets with emulsifier ensures that coalescence does not dominate the destabilisation kinetics and therefore enables to monitor Ostwald ripening without coalescence interference at early stages of the coarsening process.

Plots of $(d_{0.1})^3$ vs. time were constructed (Figure 4.3.5) to evaluate whether droplet growth could be accounted for Ostwald ripening or coalescence. The change in $(d_{0.1})^3$ with time was monitored for 1 h with 5 min intervals due to the fast kinetics of destabilisation that typically occurs at the early stages of storage. The *n*-hexadecane-in-water emulsions fabricated with both OP2 and OP6 demonstrated a linear increase of $(d_{0.1})^3$ with time. OP2-stabilised *n*-hexadecane-in-water emulsions exhibited considerably steeper slope than their OP6 counterparts indicating higher rate of droplet growth. In general, droplet stability increases to Ostwald ripening with size due to the decrease in Laplace pressure and therefore solubility. Slower coarsening kinetics of OP6-stabilized emulsions (as long as Ostwald ripening is concerned) could be attributed to the larger droplet mean diameters ($d_{3,2} \sim 2.9 \mu\text{m}$) as opposed to the OP2-stabilized emulsions with $d_{3,2} \sim 1.8 \mu\text{m}$ and consequently higher solubility according to a process described by Kelvin equation.



Figure 4.3.3. Macroscopic examination of *n*-hexadecane-in-water emulsions stored at 25°C.

Moreover, the temporal evolution of droplet size distributions in Figure 4.3.4 shows that OP6-stabilized *n*-hexadecane-in-water emulsions were stable to droplet growth throughout the observation period (1 h) i.e., there was a modest change in droplet size distributions or mean droplet diameter with time. Therefore, neither Ostwald ripening nor coalescence had an appreciable influence on the stability of these emulsions during 1 hour of observation. In contrast, PSD curve of OP2-stabilized emulsions further corroborated the presence of faster coarsening kinetics as indicated by the increase in droplet mean diameters and considerable broadening of droplet distribution (Figure 4.3.4b).

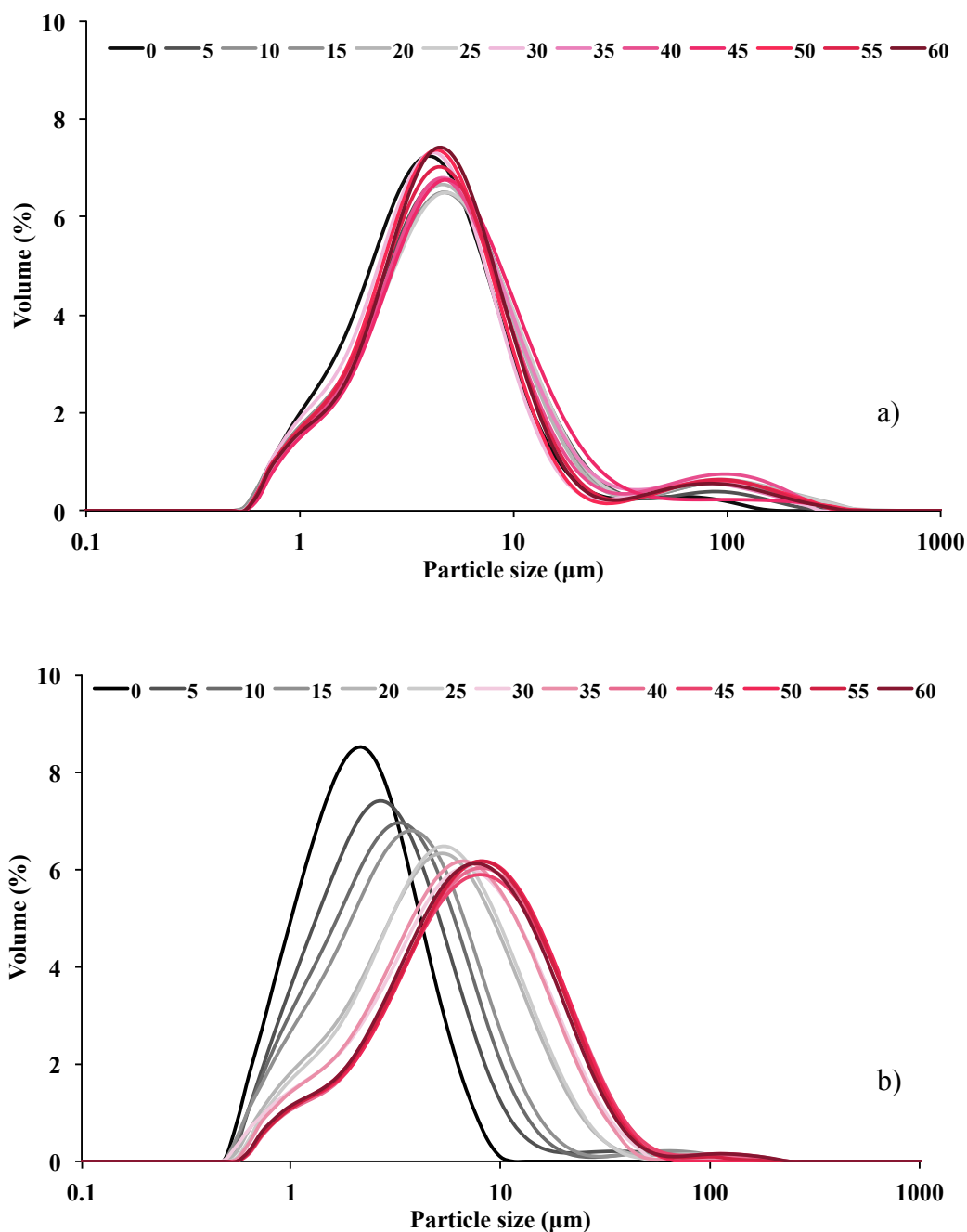


Figure 4.3.4. Time evolution of *n*-hexadecane-in-water emulsions stabilized with a) OP6 and b) OP2 at 25°C for 1 h (0-60 min) with 5 min increments.

This behaviour is typically attributed to the development of coalescence rather than Ostwald ripening that typically results in sharpening of PSD curves. Moreover, the differences in the shape of PSD curves (Figure 4.3.4) of OP2 and OP6 stabilized emulsions suggest that colloidal systems evolve under different mechanisms of

destabilisation and aforementioned difference in droplet size have negligible effect on the overall stability of colloidal system.

The linearity of $(d_{0.1})^3$ vs. time plots cannot be solely utilized in assessment of mechanisms of instability in such complex colloidal systems. The possible origins of emulsion coarsening can be further established with respect to the alkane chain length. The impact of hydrocarbon physical properties such as water solubility and polarity on Ostwald ripening rate has been extensively investigated (Chanamai, Horn & McClements, 2002; Kabalnov & Shchukin, 1992; Weiss, Herrmann & McClements, 1999).

LSW model describes the change in cubed mean droplet number diameter as a function of time is given by:

$$\overline{d_t^3} - \overline{d_{t=0}^3} = \left(\frac{64\gamma D c_{r \rightarrow \infty} V_m^2 t}{9RT} \right) = \omega t \quad (39)$$

where t is time, d is mean number droplet diameter, γ is the interfacial tension at the oil-water interface, D is the diffusion coefficient of the oil through aqueous (continuous) phase, $c_{r \rightarrow \infty}$ is the solubility of the oil in the aqueous phase, V_m is the molar volume of the oil, R is the gas constant, T is the absolute temperature and ω is the Ostwald ripening rate. Equation 39 shows that diffusion-controlled Ostwald ripening rate is proportional to the solubility of the hydrocarbon in dispersed phase. The solubilities of alkanes vary considerably with the alkane chain length, therefore, appreciable variation in Ostwald ripening rate is expected on changing the alkane chain length. In contrast, coalescence rate for this type of colloidal system depends on the initial droplet size and concentration and therefore modification in hydrocarbon chain length at the same emulsifier concentration and droplet size would not change the coalescence rate.

Equation 39 is in principle valid in the limit of highly dilute emulsions ($\phi < 0.01$) and ignores the droplet-droplet interactions as in the case of concentrated emulsions (Wooster, Golding & Sanguansri, 2008). Dispersed systems with higher oil volume fractions (ϕ), will have broader particle size distributions and faster absolute growth rates than those predicted by the LSW theory (Taylor, 1998). The theoretical rate (ω_0) of Ostwald ripening predicted by LSW equation should, therefore, be corrected by a factor $k_f = 1.75$ that reflects the dependence of the coarsening rate (ω_f) on the dispersed phase volume fraction $\phi = 0.1$ (Enomoto, Tokuyama & Kawasaki, 1986). Theoretical growth rates have been calculated with Eq.39 using the parameters shown in Table 4.3.2.

$$\omega_f = k_f \times \omega_0 \quad (40)$$

As indicated by Eq.39, the cube of the droplet mean diameter should be a linear function of time with slope equal to the experimental rate of ripening. Table 4.3.3 shows the outcome of theoretical (ω_{th}) calculations and compares them with experimental (ω_{exp}) growth rates. Generally, experimental droplet growth rates for the systems under investigation were considerably greater than the theoretical Ostwald ripening rates (Table 4.3.3). Faster experimental droplet growth kinetics has been previously reported for Tween 20, sodium dodecyl sulphate and gum Arabic stabilized emulsions, and typically attributed to the limitations of LSW model (Chanamai, Horn & McClements, 2002; Schmitt, Cattelet & Leal-Calderon, 2004; Soma & Papadopoulos, 1996). The discrepancy between experimental and theoretical Ostwald ripening rates of colloidal dispersions could be attributed to the a) variation of interfacial energy at a curved droplet surface and at a planar alkane-aqueous phase boundary, b) water solubility of long-chain hydrocarbons ($n > 12$) which is greater in real systems than expected from commonly used extrapolation technique. The

presence of bimodal PSD in OP6-stabilized emulsions could also initiate the considerable acceleration of the ripening rate (Figure 4.3.2a). Alternatively, faster experimental coarsening kinetics of studied emulsions could occur due to the development of coalescence that may progress simultaneously with Ostwald ripening or flocculation which enhances it by reducing the diffusion path length (Djerdjev & Beattie, 2008).

Emulsions fabricated with OP2 demonstrated faster coarsening kinetics on replacing the *n*-hexadecane with *n*-dodecane (Figure 4.3.5). These observations are in a good agreement with water solubility values of the hydrocarbons (Table 4.3.2) and suggest that Ostwald ripening is the predominant coarsening mechanism in OP2 emulsions within a time frame of 1 h. Emulsions fabricated with OP6 also demonstrated acceleration of coarsening rate by introducing hydrocarbons with higher water solubility (*n*-dodecane), however, at a lower extent than their OP2 counterparts.

Table 4.3.2. Physical properties required for calculations of theoretical Ostwald ripening rates in *n*-dodecane and *n*-hexadecane-in-water emulsions (25°).

Physical property	<i>n</i> -alkane type	
	C ₁₂ H ₂₆	C ₁₆ H ₃₄
$c_{r \rightarrow \infty}$ (mol m ⁻³) ^a	2.3×10^{-5}	9.3×10^{-8}
$10^{-10} \times D$ (m ² s ⁻¹) ^b	5.4	4.6
$10^{-4} \times V_m$ (m ³ mol)	2.27	2.92
$10^{-3} \times \gamma$ (N m ⁻¹) ^c	52.5	53.3
M_w (kg mol ⁻¹)	0.170	0.226

^a (Weiss, Herrmann & McClements, 1999).

^b (Wilke & Chang, 1955), (Weiss, Herrmann & McClements, 1999).

^c (Aveyard & Haydon, 1965), (Zeppieri, Rodriguez & Lopez de Ramos, 2001).

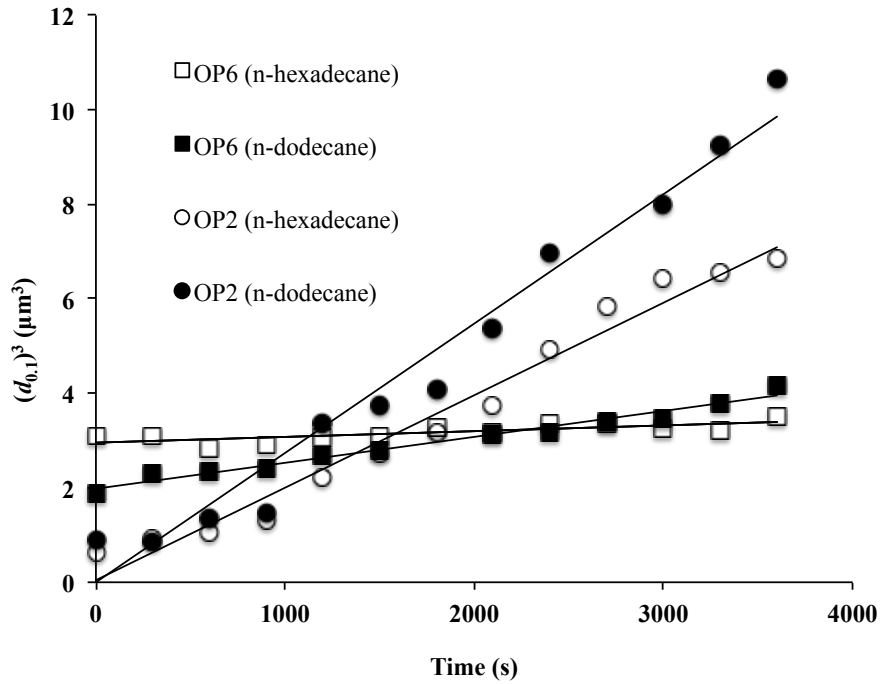


Figure 4.3.5. Dependence $((d_{0,1})^3$ versus time) of Ostwald ripening rates on *n*-hydrocarbon type in 1.5% w/v OP2 and OP6 stabilized emulsions at pH 2.0 (25 °C).

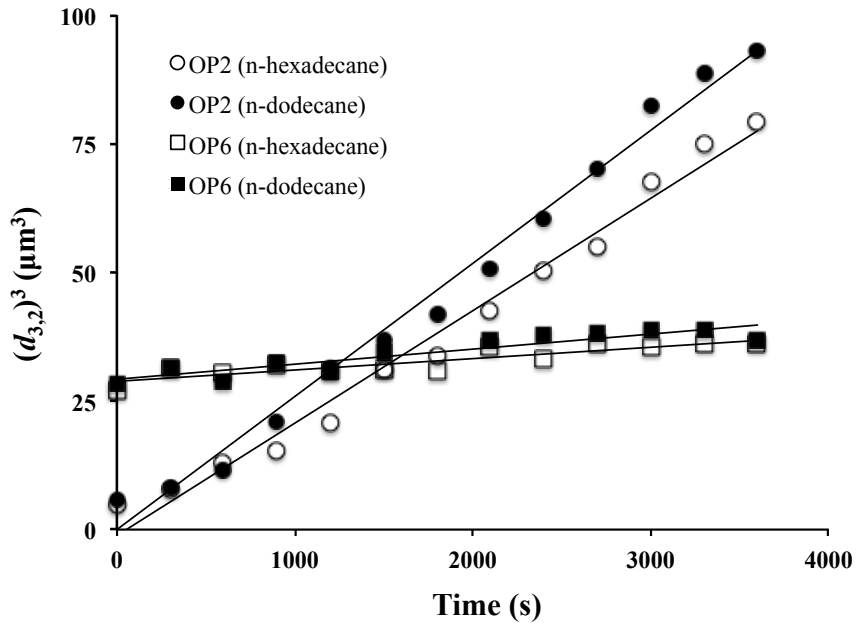


Figure 4.3.6. Dependence $((d_{3,2})^3$ vs time) of Ostwald ripening rates on *n*-hydrocarbon type in 1.5% w/v OP2 and OP6 stabilized emulsions at pH 2.0 (25 °C).

Table 4.3.3. Theoretical (ω_{th}) and experimental (ω_{exp}) rates of Ostwald ripening for various oil-in-water emulsions.

Sample <i>n</i> -alkane type	OP2		OP6	
	C ₁₂ H ₂₆	C ₁₆ H ₃₄	C ₁₂ H ₂₆	C ₁₆ H ₃₄
$\omega_{th} (m^3 s^{-1}) \times 10^{-26}$	16.6	0.1	16.6	0.1
$\omega_{exp}^a (m^3 s^{-1}) \times 10^{-22}$	$20.0 \pm 1.1 \times 10^{-3}$	$16.0 \pm 4.9 \times 10^{-4}$	$4.5 \pm 7.1 \times 10^{-5}$	$1.5 \pm 7.1 \times 10^{-5}$
$\omega_{exp}^b (m^3 s^{-1}) \times 10^{-21}$	$26.0 \pm 0.4 \times 10^{-2}$	$21.0 \pm 3.2 \times 10^{-3}$	$2.6 \pm 6.4 \times 10^{-3}$	$2.5 \pm 2.1 \times 10^{-2}$

^a experimental rate calculated based on $(d_{0,1})^3$ vs. time plot.

^b experimental rate calculated based on $(d_{3,2})^3$ vs. time plot.

Further analysis of kinetic plots for OP6 emulsions demonstrate that *n*-dodecane emulsions have steeper slopes than those containing *n*-hexadecane indicating faster coarsening rates. However, one should note that colloidal systems should have similar initial droplet size when evaluating the dependence of Ostwald ripening rates on hydrocarbons solubility, something that can be clearly observed for OP2-stabilized emulsions where $d_{0,1}$ was about 0.9 μm for *n*-dodecane and *n*-hexadecane emulsions (Figure 4.3.5). On the contrary, OP6-stabilized emulsions had initial droplet size of marginally smaller mean diameter ($d_{0,1} \sim 1.2 \mu m$) with *n*-dodecane than with *n*-hexadecane ($d_{0,1} \sim 1.4 \mu m$) (Figure 4.3.5). Small droplets diffuse faster than large and therefore, destabilisation of OP6-stabilized emulsions containing *n*-dodecane occurs at higher rate resulting in overestimation of Ostwald ripening. In order to address this $(d_{3,2})^3$ vs. time plots were constructed for the same set of emulsions (Figure 4.3.6, Table 4.3.3). These plots show that the change of hydrocarbon did not affect the coarsening rate of OP6-stabilized emulsions and emulsions were stable to droplet growth during 1 h as also was demonstrated by the PSD (Figure 4.3.4). Moreover, Figure 4.3.6 further corroborates that destabilisation kinetics of OP2-stabilized emulsions is triggered by the solubility of dispersed phase.

The analysis of temporal evolution of PSD and LWS model was applied in the assessment of mechanisms of emulsions instability. It has been shown that Ostwald ripening or coalescence do not affect OP6-stabilized emulsions during 1 hour of storage as evidenced by the evolution of the particle size distribution and diffusion-controlled model during this period of observation. However, these emulsions could undergo Ostwald ripening at later stage of coarsening process as indicated by the sharpening of PSD after 30 days of storage. Ostwald ripening as a rate-determining mechanism has been previously reported for gum Arabic stabilized decane-in-water emulsions and sodium caseinate stabilized *n*-hexadecane-in-water emulsions (Chanamai, Horn & McClements, 2002; Dickinson, Ritzoulis, Yamamoto & Logan, 1999). In contrast, the coarsening process in OP2-stabilized emulsions was more complex and could be determined by Ostwald ripening in conjunction with coalescence. It should be noted that most of high molecular weight polysaccharides including pectin, do not tend to adsorb at the oil-water interface and are typically defined as weakly adsorbing biopolymers. It can be proposed that as an OP2-stabilized emulsion ripens during the first hour of storage, OP2 pectin has a tendency to desorb from the interface leading to a poorer coverage of the newly formed larger droplets. Therefore, coalescence becomes of prime importance when droplets have insufficient surfactant coverage. The evolution of PSD, formation of macroscopic oil layer at the top of the sample tube after 30 days of storage (Figure 4.3.3) and rate of droplet growth also provide convincing evidence that coalescence takes place and influences the droplet growth after 1 day of storage in OP2 stabilized emulsions. It should be also mentioned that depletion flocculation can also contribute to emulsion ripening. As the small alkane droplets solubilize the total surface area in the colloidal system decreases during ripening, and consequently pectin is released in the aqueous

phase. A fraction of the released OP2 pectin cannot readsorb and will induce depletion flocculation. The enhancement of Ostwald ripening rate due to the depletion flocculation has been previously reported in surfactant-stabilized octane- or decane-in-water stabilized emulsions and sodium caseinate stabilized oil-in-water emulsions (Djerdjev & Beattie, 2008). Therefore, it can be proposed that the coarsening of OP2 stabilized *n*-hexadecane emulsions follows a complex mechanism, where Ostwald ripening of the emulsion initiates the gradual thinning of adsorbed layer that eventually leads to coalescence through deletion mechanism.

The variations in destabilisation kinetics of okra pectin-stabilized emulsions also suggest that OP2 and OP6 have different mechanisms of adsorption and arrangement at the *n*-alkane-water interface and therefore the interfacial composition was performed in order to further investigate the quality of alkane-water interface and the magnitude of okra biopolymers adsorption.

4.3.3.3 Interfacial composition

Table 4.3.4 shows the interfacial composition of OP2 and OP6-stabilized *n*-hexadecane-in-water emulsions. During emulsification using sonication droplet disruption and re-coalescence occur simultaneously (Kaltsa, Michon, Yanniotis & Mandala, 2013). The kinetics of each one affects the final droplet size of emulsions and depends on the interfacial properties of emulsifier. According to Table 4.3.1, emulsions fabricated with okra pectin of higher degree of methylation (OP2, DM=40.0) resulted in smaller (1.7 μm) droplet mean diameters ($d_{3,2}$) than their counterparts of lower DM (OP6, DM=24.6, $d_{3,2} \sim 3.0 \mu\text{m}$). Higher hydrophobicity of methyl ester groups in comparison to carboxyl groups can influence the surface activity of pectin molecules. It has been previously shown that an increase in emulsifying capacity of citrus pectin is correlated to the increase in number of methyl

esters within the backbone of biopolymer (Schmidt, Koch, Rentschler, Kurz, Endreß & Schuchmann, 2014).

Table 4.3.4. Weight percentage and amount of adsorbed protein, pectin and acetyl at the oil-water interface of fresh 1.5% w/v *n*-hexadecane emulsions stabilized with OP2 and OP6 at $\varphi = 0.1$, pH 2.0.

Sample	OP2	OP6
Adsorbed acetyl (%)	9.7 ± 0.4	9.1 ± 0.6
Adsorbed protein (mg/m ²)	0.3 ± 0.1	1.6 ± 0.5
Adsorbed protein (%)	17.1 ± 6.0	49.5 ± 15.6
Adsorbed pectin (mg/m ²)	3.3 ± 0.2	9.4 ± 0.2
Adsorbed pectin (%)	14.2 ± 1.1	16.3 ± 5.7

It has been proposed that higher methyl esterification of carboxyl groups leads to the formation of more compact and less extended pectin conformation, something that facilitates the mobility of molecules. Consequently, pectin adsorbs faster at the interface thus limiting the re-coalescence of newly formed droplets during emulsification. However, extensive coiling could also restrict the accessibility of hydrophobic groups and therefore decrease polymer adsorption at the interface. In contrast, other studies on citrus pectin reported that degree of methyl esterification is of minor importance for the emulsifying capacity of pectins as opposed to the molecular weight of biopolymer (Akhtar, Dickinson, Mazoyer & Langendorff, 2002; Leroux, Langendorff, Schick, Vaishnav & Mazoyer, 2003). It has been shown that $50 - 80 \times 10^3 \text{ g mol}^{-1}$ is an optimum molecular weight required for an effective emulsification and stabilizing properties of citrus pectin. Reduced molecular weight promotes faster adsorption rate of pectin at the *n*-alkane-water interface. In our case,

okra pectin samples used for fabrication of *n*-hexadecane-in-water emulsions have remarkably higher molecular weights (OP2, $641 \times 10^3 \text{ g mol}^{-1}$ and OP6, $767 \times 10^3 \text{ g mol}^{-1}$) than those previously reported for citrus pectin and some fractions of sugar beet pectin (Akhtar, Dickinson, Mazoyer & Langendorff, 2002; Leroux, Langendorff, Schick, Vaishnav & Mazoyer, 2003). However, the OP2 that has lower molecular weight exhibited similar behaviour as evidenced by the droplet mean diameters ($d_{3,2}$) of fresh emulsions (Table 4.3.1). The smaller droplet mean diameters of OP2 stabilized emulsions can be also attributed to the lower viscosity of its composing solutions (Figure 4.3.5), as it will be discussed in section 4.3.3.5 indicating that less energy input is required for effective droplet disruption.

The hydrophobic character of pectin is also frequently attributed to the presence of acetyl groups within the polymer backbone (Dea & Madden, 1986; Schmidt, Koch, Rentschler, Kurz, Endreß & Schuchmann, 2014). Table 4.3.4 shows that comparable amounts of acetyl were adsorbed at the interface in both OP2 and OP6-stabilized emulsions, suggesting a preference for acetyl groups to arrange at the interface. These results are also in a good agreement with the chemical composition data that report marginal differences in the number of acetyl groups (6.0 – 5.2 %) for OP2 and OP6 samples (Chapter 2, Table 2.1). Since both biopolymers have the similar amount of acetyl adsorbed at the o/w interface, it can be proposed that the differences in the droplet mean diameters of fresh emulsions are more likely attributed to the variations in molecular weight, protein and degree of methyl esterification of OP2 and OP6. Surface (pectin solution/air) tensions of OP2 and OP6 as a function of polymer concentration were measured (Figure 4.3.7). Both biopolymers showed lower surface tension than deionised water at concentrations higher than 0.1% w/v and decreased surface tension to a similar extent (OP6, $63.7 \times$

10^{-3} N m^{-1} , OP2, $65.0 \times 10^{-3} \text{ N m}^{-1}$) at 1.67% w/v concentration. Surface tension values of OP2 and OP6 were higher than those reported for high-methoxyl citrus pectin $\sim 50.8\text{-}62.7 \times 10^{-3} \text{ N m}^{-1}$, sugar beet pectin $\sim 54.5 \times 10^{-3} \text{ N m}^{-1}$, gum Arabic $\sim 57.1 \times 10^{-3} \text{ N m}^{-1}$ and lower than for high-methoxyl apple pectin $\sim 66.9 \times 10^{-3} \text{ N m}^{-1}$ (Schmidt, Koch, Rentschler, Kurz, Endreß & Schuchmann, 2014; Siew & Williams, 2008b). Surface tension, adsorption data and droplet mean diameter measurements show that interfacial activity of biopolymers in such complex colloidal systems depends not only on chemical composition, but also on accessibility of hydrophobic sites and conformation of pectin.

An effective emulsifier should rapidly adsorb at the freshly formed droplet interface, reduce interfacial tension in order to facilitate droplet disruption and provide a protective coating that prevents the droplets from aggregating (McClements, 2004).

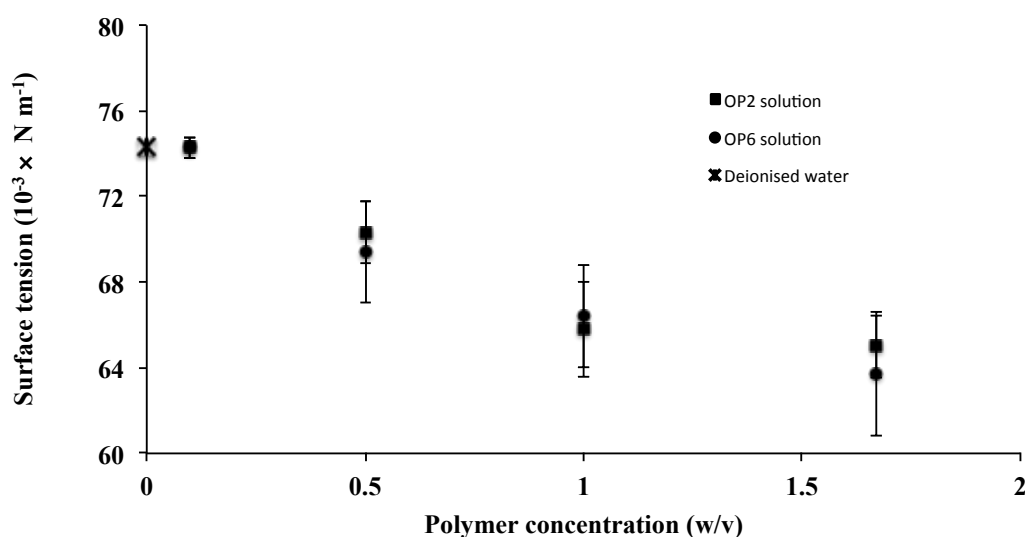


Figure 4.3.7. Surface tension of OP2 and OP6 solutions (pH 2.0) as a function of polymer concentration at 25°C.

In general, it has been shown that OP2 with relatively smaller molecular weight and higher DM adsorbs faster at the o/w interface as evidenced by $d_{3,2}$ values for fresh OP2 and OP6-stabilized emulsions (Table 4.3.1). Therefore, OP2 provides an efficient stabilization against re-coalescence of freshly formed droplets during emulsification. However, it has been demonstrated that OP6 exhibits more efficient emulsion stabilization during long-term storage as opposed to the OP2 counterpart (Figures 4.3.1, 4.3.2). The pectin and protein adsorption capacities of OP2 and OP6 were also determined in order to evaluate the strength of interactions that take place between the polymer and interface during emulsification and storage. Table 4.3.4 shows the amount of protein adsorbed at the *n*-hexadecane-water interface for OP2 or OP6 emulsions. In the case of OP2-stabilized emulsions, protein surface coverage of emulsions was 0.3 mg m^{-2} accounting for a total of 17.1 % of the protein present in pectin sample. In contrast, protein surface coverage in OP6 stabilized emulsion was almost five times higher (1.6 mg m^{-2}) representing a far larger proportion of the total protein (49.5 %) transferred from continuous phase to the interface. Similar protein surface coverage (1.0 mg m^{-2}) and amount of adsorbed protein (57.0 %) were observed for OE6 stabilized *n*-hexadecane emulsions (Chapter 4.1). The protein surface coverage in OP6 stabilized emulsion was also comparable to the 0.9 mg m^{-2} in limonene oil-in-water emulsion ($\phi=0.2$) stabilized with sugar beet pectin at 1.5 % (w/w) concentration (Siew & Williams, 2008b). Other studies on sugar beet pectin and depolymerized citrus pectin also reported that pectin fraction adsorbed at the interface was significantly enriched in protein and played a key role in emulsion stabilizing capacity (Akhtar, Dickinson, Mazoyer & Langendorff, 2002; Leroux, Langendorff, Schick, Vaishnav & Mazoyer, 2003). The protein content in okra pectin is 4.3% and 6.3% w/v for OP2 and OP6, respectively (Chapter 2, Table 2.1).

According to these values the amount of adsorbed protein at the *n*-hexadecane-in-water interface should be comparable for both emulsions, something that is not reflected by the protein adsorption data (Table 4.3.4). These observations suggest that not only protein content, but also accessibility to the interface of the protein within the biopolymer backbone and composition of amino acids (polar/non-polar sites) influence the emulsification properties of okra pectin.

Table 4.3.4 shows that the surface coverage with pectin in OP6-stabilized emulsions was about 9.4 mg m^{-2} and the amount of adsorbed pectin at the interface amounted for 16.3% of total carbohydrates present in the OP6. This value is higher than previously reported for sugar beet pectin (Akhtar, Dickinson, Mazoyer & Langendorff, 2002; Siew & Williams, 2008b) $\sim 7.5 \text{ mg m}^{-2}$ at the same polymer concentration in limonene oil-in-water emulsion and depolymerized citrus pectin (Akhtar, Dickinson, Mazoyer, & Langendorff, 2002) $\sim 9.8 \text{ mg m}^{-2}$ at 3 % polymer concentration in entire volume of rapeseed oil-in-water emulsion. However, it has to be stressed that emulsions in the previous studies were fabricated with higher oil volume fractions ($\phi=0.2$) than those investigated in this study ($\phi=0.1$). In contrast, emulsions fabricated with OP2 had considerably lower pectin interfacial load (3.3 mg m^{-2}) than its OP6 counterpart (Table 4.3.4). The comparison of the amount of adsorbed protein and pectin indicate that *n*-hexadecane-in-water interface is dominated by pectin (Table 4.3.4). Interestingly, the total amount of adsorbed pectin was accounted for 14.2 % of total carbohydrates present in the OP2 and was comparable to the values obtained for OP6 stabilized emulsions (16.3 %). The decrease in droplet sizes typically leads to the increase in specific surface area. Fresh emulsions stabilized with OP2 demonstrated smaller droplet mean diameters ($d_{3,2}$) and therefore have much larger surface area that need to be covered with monolayer

of biopolymer in order to impeded coalescence. Therefore, it can be proposed that mechanically weak and thin interfacial layer was formed in emulsions stabilized with OP2 as evidenced by adsorption capacities of protein and pectin, and biopolymer molecular weight (Table 4.3.3). On the other hand, emulsions stabilized with OP6 demonstrated higher interfacial load and consequently thicker protective layer around the droplets that made them more resistant to the mechanisms of emulsion coarsening during the storage. This is also further supported by the fact that for many dispersed systems the interfacial load is in the order of 1 mg m^{-2} , which is consistent with monolayer coverage (Siew & Williams, 2008b). Higher values shown for investigated dispersed systems indicate the presence of multilayer adsorption or adsorption of biopolymer at *n*-hexadecane-in-water interface with long tails protruding into the continuous phase. The multilayer adsorption has been previously reported for the naturally occurring polysaccharide–protein complexes, such as Arabic gum and sugar beet pectin (Evans, Ratcliffe & Williams, 2013).

These results indicate that OP2 and OP6 have distinct adsorption kinetics as evidenced by the PSD and interfacial composition data. OP2 has faster adsorption rate to the *n*-hexadecane-in-water interface, however, the formed biopolymer film has insufficient thickness to impede Ostwald ripening and coalescence. In contrast, OP6 demonstrated slower adsorption velocity and formation of thick, multi-layered droplet protective coverage that hinders droplet growth. It can be concluded that the interfacial activity of OP2 and OP6-stabilized emulsions was attributed to the proteinaceous components, the molecular mass of biopolymers and the amount, and distribution of ester groups within the biopolymer backbone.

4.3.3.4 Electric properties of alkane-in-water interface

The ζ -potential titration measurements of solutions (OP2 and OP6) and emulsions were determined in the pH range of 1.0 – 9.0 (Figure 4.3.8). The ζ -potential titration curves of OP2 and OP6 solutions demonstrated the strong influence of pH on the charge of the polyelectrolyte. At pH values above 6.0 galacturonic acid groups are fully dissociated. In contrast, the protonation of carboxyl groups of galacturonic acids results in considerable decrease in ζ -potential values at pH below 6.0. Preliminary work with OP2 and OP6-stabilized emulsions at pH 4.0 and 7.0 revealed the inability of the samples to stabilize dispersions. This indicates that the strong repulsions and extended chain conformations between the negatively charged biopolymer chains hinder its arrangement and adsorption at the *n*-alkane-water interface (Figure 4.3.8, inset). Furthermore, decrease in pH value to 4.0 resulted in formation of fine *n*-dodecane and *n*-hexadecane-water-emulsion when it was stabilized exclusively with OP2 (Figure 4.3.8, inset). This can be attributed to the relatively higher ζ -potential of OP2 (~ -30 mV) than OP6 solutions (~ -35 mV) together with the surface composition characterization that we described in the previous section. These observations suggest that OP2 and OP6 manifest an emulsifying capacity only at pH values below 4.0 where an effective steric stabilization occurs due to the biopolymer compact conformation resulting in formation of a thick protective layer around the droplets. In contrast, extended conformations of both biopolymers at pH 6.0 restrict their alignment and adsorption at the *n*-alkane-water interface.

The amount of a biopolymer adsorbed at the alkane-water interface depends on various factors including the interactions between polymer and the surface, conformation of the polymer and surface physical properties (polarity, solubility).

Figure 4.3.8 (inset) demonstrates the effect of alkane type on the emulsion stability. It has been observed that OP2 and OP6 did not exhibit any interfacial activity in emulsions, where hexane and/or decane were used as dispersed phases (Figure 4.3.8, inset). These results can be attributed to the high – water solubility of both alkanes and relatively slow adsorption kinetics of biopolymers.

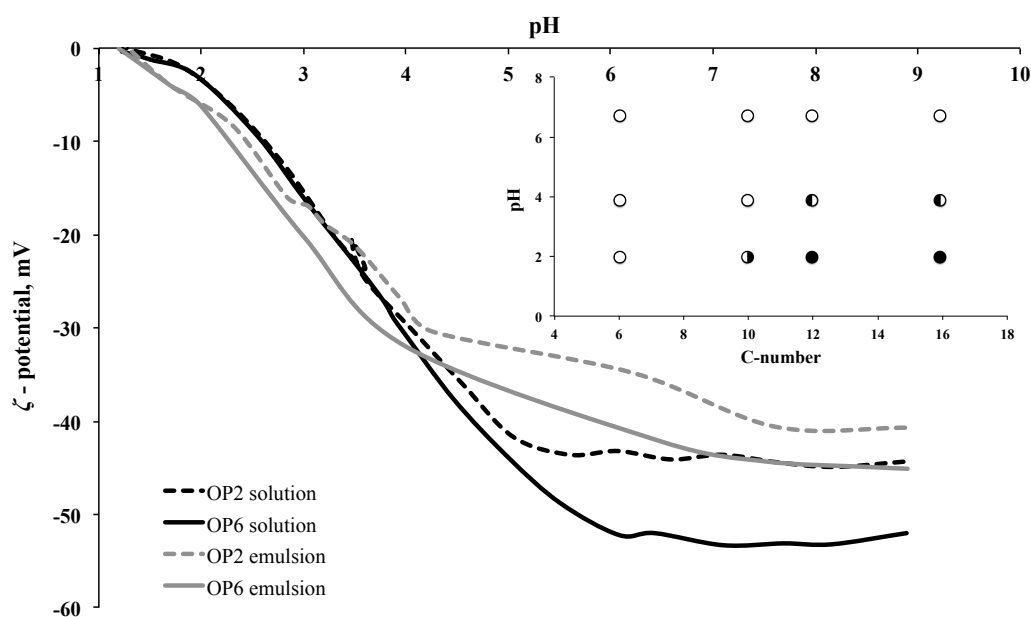


Figure 4.3.8. ζ -potential titration of 1.67% w/v pectin solutions and 1.5% w/v pectin stabilized emulsions at 1/1000 dilution. Inset shows the emulsifying capacity of okra biopolymers as affected by the pH and hydrocarbon chain length (25 °C).

Inset - ○ both biopolymers do not form emulsion, ● both biopolymers form emulsion, ◐ OP6 forms emulsion, ◑ OP2 forms emulsion.

Both fresh emulsions (pH 2.0) exhibited negative ζ -potential values of - 5.5 mV for OP2-stabilized emulsions and - 6.1 mV for OP6-stabilized emulsions and were slightly lower than those found for the aqueous phase (- 3.9 mV and -4.0 mV for OP2 and OP6 solutions, respectively). These results denote that the *n*-hexadecane-in-water interface has similar electrical properties to that of the continuous phase and is dominated by the presence of pectin rather than protein as also evidenced by the analysis of interfacial composition. The increase in ζ -potential values could be

attributed to the formation of electrostatic complexes at the interface as also evidenced by the occurrence of multilayer adsorption for both colloid systems.

The electrostatic complexes could arise due to the possible cross-linking of pectin molecules at the surface by calcium ions, ferulic acid or protein (Siew & Williams, 2008b). It has been previously reported that the removal of calcium from the sugar beet pectin has no effect on the adsorbed layer thickness and therefore calcium cross – linking is highly implausible (Siew & Williams, 2008a). In order to evaluate the effect of ferulic acids to the cross–linking of pectin chains, the UV absorption spectrum of 0.5 % w/v of OP2 and OP6 solutions was determined and revealed the absence of ferulic acids in both okra biopolymers (Chapter 2, section 2.3.1). Therefore, the formation of electrostatic polysaccharide - protein complexes at the interface can occur through the interactions of charged protein moieties with charged galacturonic acid residues. However, low ζ -potential values for fresh OP2 and OP6 stabilized emulsions indicate that electrostatic repulsion can have insignificant effect on the overall stability of emulsions (Figure 4.3.8). Therefore, these results indicate that the proteinaceous components, as an integral part of OP2 and OP6, anchor pectin at the *n*-alkane-water interface, while the covalently cross – linked carbohydrate moieties protrude out into the continuous phase and provide an effective steric barrier that prevents droplet aggregation (Leroux, Langendorff, Schick, Vaishnav & Mazoyer, 2003; Siew & Williams, 2008a; Siew & Williams, 2008b).

ζ -Potential values of fresh emulsions (OP2, -5.5 mV, OP6, -6.1 mV) did not depart significantly from those of the continuous phase indicating that droplet interface has similar composition with the bulk. With ageing surface charge does not

change appreciably and after thirty days of storage increases to 5.9 and 6.6 mV for OP2 and OP6-stabilized emulsions, respectively.

4.3.3.5 Flow behavior of emulsions and pectin solutions

The effect of continuous phase viscosity on the overall stability of *n*-hexadecane-in-water emulsions was evaluated using rheological measurements. Figure 4.3.9 shows the viscosity curves for continuous phases and fresh emulsions containing OP2 and OP6. The comparison of viscosities of sonicated and non-sonicated OP2 solutions shows the absence of sonication effect on viscosity. In contrast, sonication of OP6 solutions resulted in a moderate decrease in viscosity values indicating the disaggregation of biopolymer chains (Figure 4.3.9). The OP6 solution exhibited weak shear-thinning behaviour and its viscosity was greater compared to OP2. In contrast, OP2 solutions manifested stronger shear-thinning behaviour with the distinct onset at low shear rates ($< 0.5 \text{ s}^{-1}$). Lower viscosity values and higher shear rate dependency of OP2 solutions can be attributed to the lower molecular weight and higher degree of branching of side chains compared to OP6. The flow behaviour of both biopolymers has been examined at concentrations (1.67 g dL^{-1}) beyond c^* ($0.45 - 0.44 \text{ g dL}^{-1}$ at pH 3.0, Chapter 2). High shear rate dependency of OP2 solutions was attributed to stronger disentanglement of biopolymer coils than in OP6 samples indicating higher polymer flexibility.

Figures 4.3.10a and 4.3.10 b depict the flow behaviour of fresh emulsions fabricated with OP6 and OP2. Fresh emulsions demonstrated relatively higher low-shear rate viscosity and generally followed the flow behaviour of the continuous phase (Figure 4.3.9a and b). Figure 4.3.8a shows that emulsions stabilized with OP6 did not exhibit appreciable changes in viscosity curves with storage time (10 days) indicating that emulsions do not flocculate on storage.

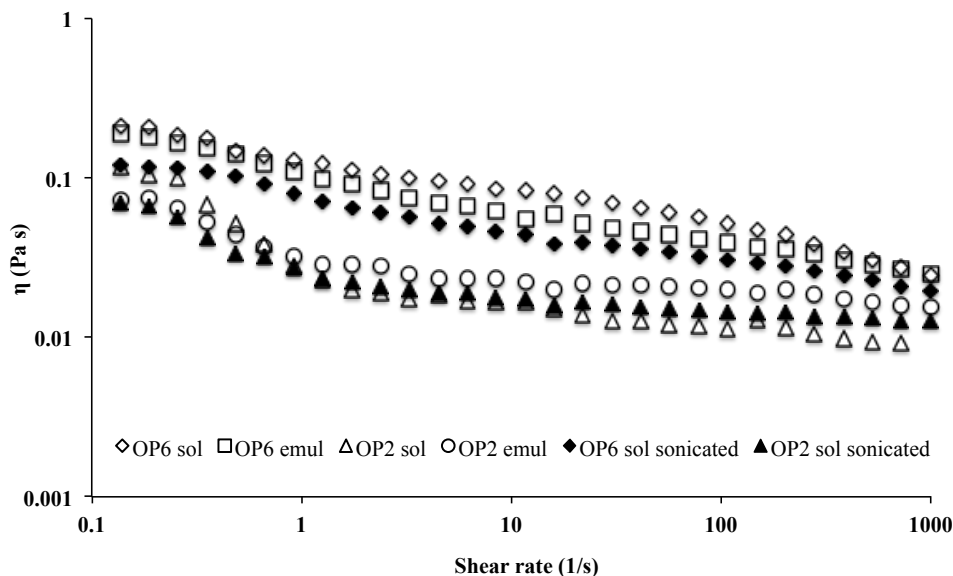


Figure 4.3.9. Flow behavior of 1.5% w/v emulsions stabilized with OP2 and OP6 and flow behavior of fresh 1.67% w/v okra pectin sonicated and non-sonicated solutions at pH 2.0 (25 °C). Okra biopolymer solutions were sonicated under the same conditions as emulsions.

Furthermore, a drop in viscosity values was observed for OP6-stabilized emulsions after 30 days of storage (Figure 4.3.10a). Coalescence in the absence of flocculation typically leads to a reduction of the emulsion viscosity. This suggests that mild Ostwald ripening-induced coalescence was activated after 10 days of storage and appreciable modifications of flow behaviour were observed after 30 days of storage with the coalescence onset. In contrast, the comparison of flow curves (Figure 4.3.10b) of OP2-stabilized emulsions revealed a considerable increase in viscosity values at day 1, 10 and 30 particularly in low-shear rate regime ($>1 \text{ s}^{-1}$). Flow curves of OP2-stabilized emulsions show that colloidal system breaks after 1 day of storage and strong shear-thinning behaviour is attributed to the aggregates from pectin that has been desorbed from the alkane-water interface during emulsion ripening.

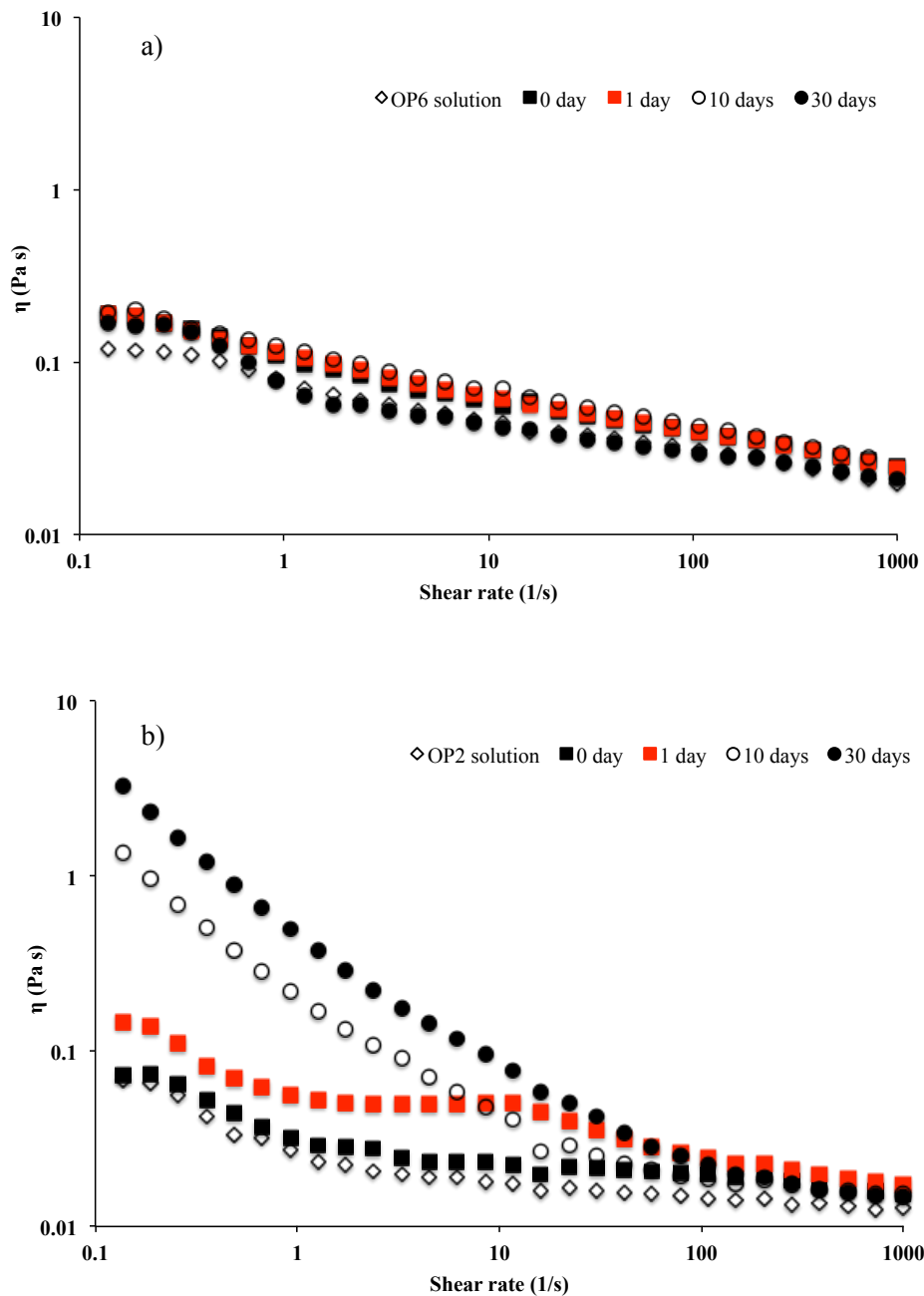


Figure 4.3.10. a) Influence of aging (0–30days) on the flow behavior of 1.5% w/v emulsion stabilized with OP6 and flow behavior of 1.67% w/v OP6 sonicated solution (25 °C), b) influence of aging (0–30 days) on the flow behavior of 1.5% w/v emulsion stabilized with OP2 and flow behavior of 1.67% w/v OP2 sonicated solution (25 °C).

4.3.3.6 Pectin immunolocalization at the alkane-water interface.

Fluorescence microscopy was used to locate okra pectin at the hydrocarbon-water interface. Because of the non-specific nature of conventional fluorescent dyes used for pectin staining, our focus moved to the implementation of monoclonal

antibodies that allow the precise localisation of distinct structural elements of the pectin molecules (Christiaens, Van Buggenhout, Ngouémazong, Vandevenne, Fraeye, Duvetter, Van Loey & Hendrickx, 2011). The LM19 monoclonal rat antibody has affinity for pectin with low degree of esterification and therefore, was chosen for the *in situ* localization of pectin at the interface (Verhertbruggen, Marcus, Haeger, Ordaz-Ortiz & Knox, 2009).

The interaction between antibody and epitope consists of hydrogen bonds, electrostatic, van der Waals, and hydrophobic interactions (Arltoft, Madsen & Ipsen, 2007). These interactions are pH-sensitive and therefore, pH of investigated emulsions and solutions was adjusted to pH 7.4 in order to achieve a high binding capacity. A model coarse emulsion was fabricated with OP2 due to the modest emulsifying capacity of OP6 at pH above 4.0 as was demonstrated in the previous sections. Figure 4.3.11 shows maximum intensity z-projected images of the morphology of OP2 solutions and coarse emulsions. Figures 4.3.11a (1-3) correspond to the micrographs of controls that included OP2 solution, OP2 solution with anti-rat IgG coupled with FITC and OP2 solution with a negative control. A weak signal was spread evenly over the polymer sample and can be attributed to the intrinsic fluorescence emission of pectin. It has been previously reported that pectin demonstrates auto-fluorescence at around 530-550 nm (Liu, Jin, Liu, Hicks, Mohanty, Bhardwaj & Misra, 2008). Figure 4.3.11 a(4) shows that LM19 binds to the HG domains of OP2 as evidenced by the presence of small entities (arrow) in the vicinity of the polymer network that was also observed in controls (Figures 4.3.11a, 1-3).

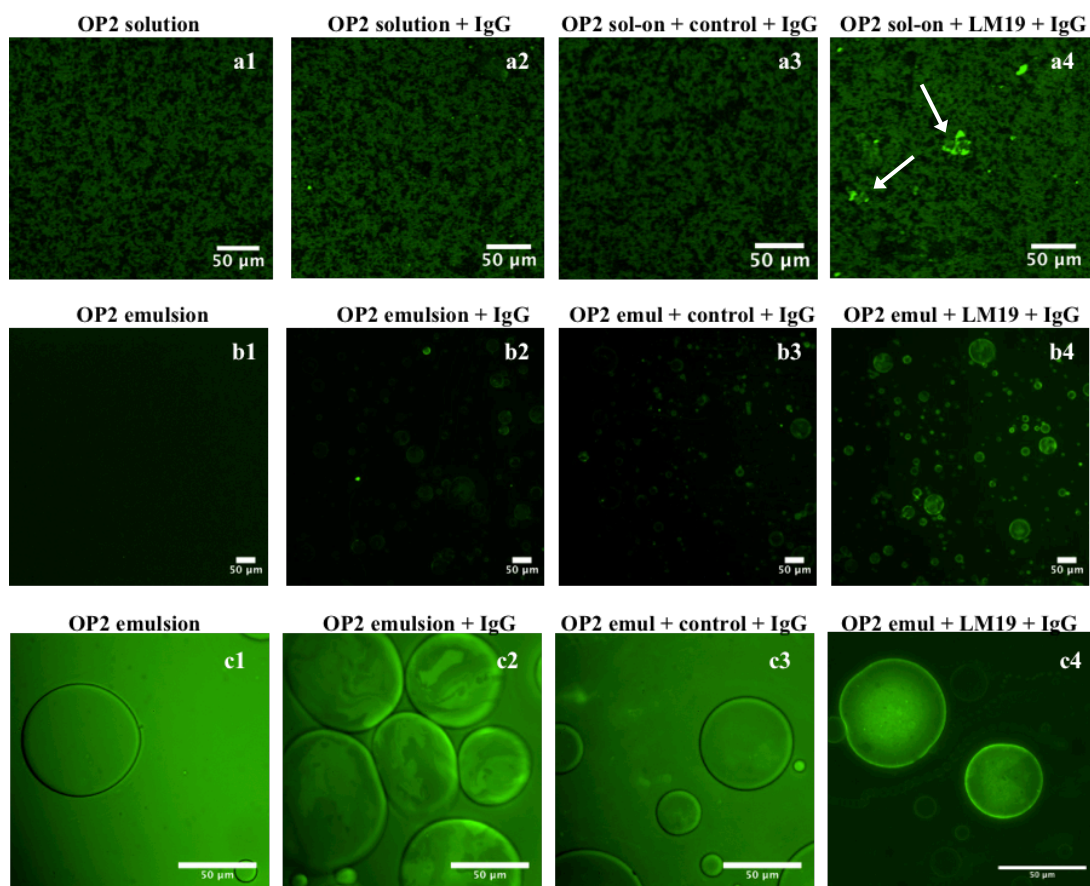


Figure 4.3.11. Fluorescent images a1-4) 1.67% fixed OP2 solutions at pH 7.4, b1-4) 1.5% w/v emulsions stabilized with OP2 at pH 7.4, c1-4) 1.5% w/v *n*-dodecane-in-water emulsions stabilized with OP2 at pH 7.4 (images are in hydrated state).

The binding specificity of LM19 probes in polymer solutions was established with indirect immunostaining method, the methodology that is not achievable with dispersed systems. Therefore, the direct immunostaining technique was used to specifically localize pectin at the *n*-dodecane-in-water interface in the hydrated state (Figures 4.3.12b, c1-4). OP2-stabilized emulsions show the absence of signal and those emulsions containing fluorescent dye exhibit weak signal due to the possible aggregation of IgG-FITC (Figures 4.3.12b, 1-3).

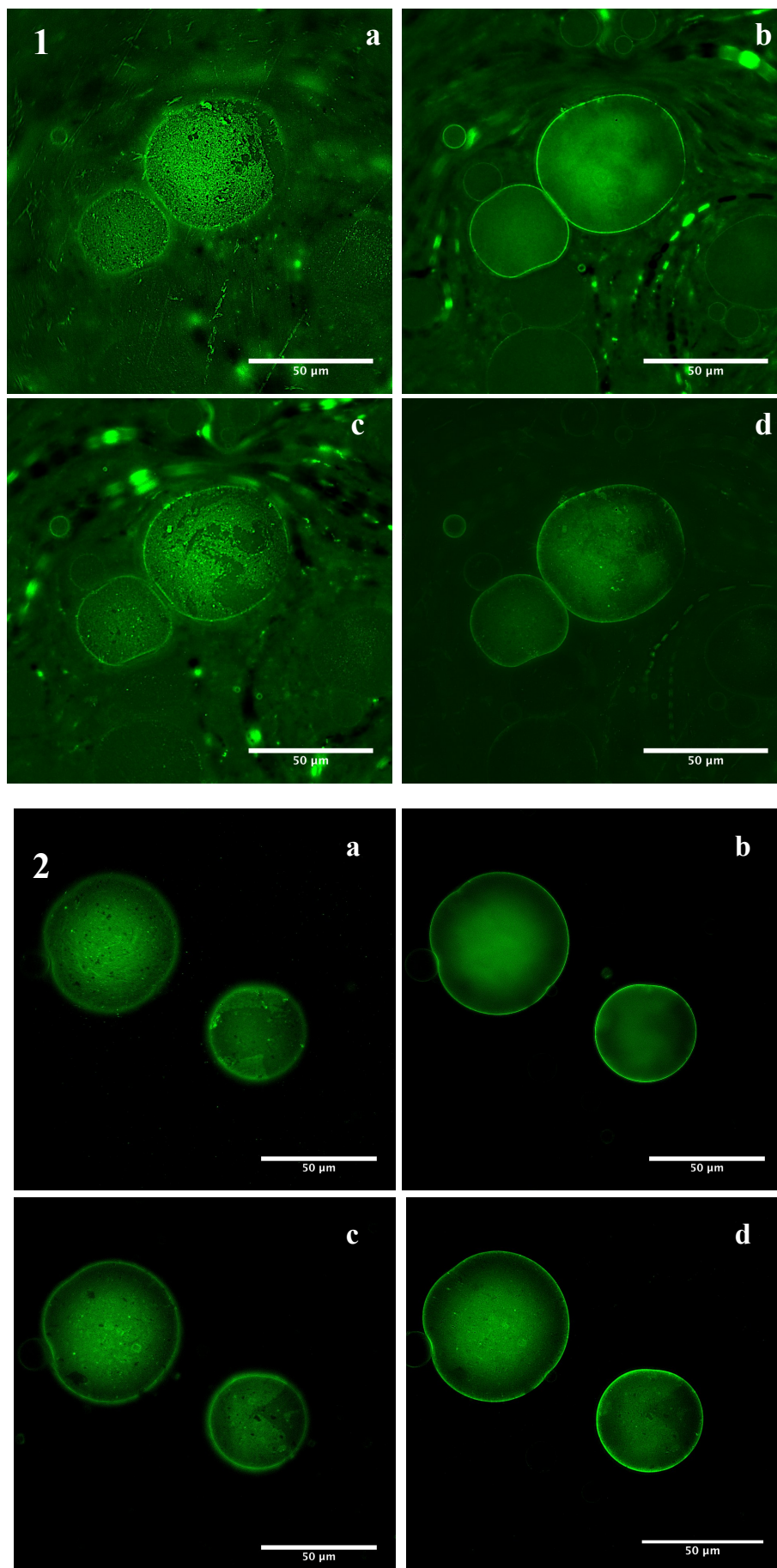


Figure 4.3.12. Fluorescent images (1, 2) of 1.5% w/v *n*-dodecane-in-water OP2-stabilized emulsions at pH 7.4, a- bottom, b- middle, c- top planes and d- z-projected image.

Figure 4.3.11 b(4) provides the evidence that OP2 did adsorb at the *n*-dodecane-in-water interface and *in situ* localisation of OP2 was effectively performed as indicated by the presence of much brighter green emulsion droplets in comparison to control images. It should be stressed that images were z-projected and therefore, they demonstrate the network (in case of solutions) and droplet (in emulsion) in three dimensions from top to bottom of the image plane (Figure 4.3.11).

Micrographs (Figure 4.3.11, c4) of OP2 stabilized emulsion at higher magnification enable to distinguish green fluorescent spots at the droplet surface and also fluorescence bands around the droplets both indicating the presence of interfacial layer composed of pectin. It should be noted that the model emulsions that were used for the microscopic examination were fabricated at pH that hinders the effective biopolymer adsorption at the alkane-water interface. Nevertheless, pectin was successfully visualized at the interface using direct immunostaining technique indicating its interfacial activity.

4.3.4 Conclusions

The influence of physicochemical characteristics of okra biopolymers on emulsifying capacity has been investigated by means of particle size evolution, flow behaviour and direct localisation of pectin at the alkane-water interface using immunostaining. It has been shown that both biopolymers exhibit interfacial activity, however, higher stability of emulsions was achieved only when was stabilized with OP6. Pectin adsorption at the *n*-alkane-water interface was evidenced by localisation of pectin with specific antibodies. Emulsions undergo different destabilisation kinetics and mechanisms depending on the biopolymer applied. It has been shown that OP6-stabilised emulsions are stable to coalescence or Ostwald ripening during 1

h of storage, however Ostwald ripening becomes predominant destabilisation mechanism after 1 day of storage. OP2-stabilized emulsion showed lower stability to coarsening mechanisms and considerable destabilisation of emulsions occurred after 1 h of storage. It has been shown that coarsening of OP2-stabilized emulsions is a complex mechanism that has been identified as combination of Ostwald ripening and coalescence.

CHAPTER 5

GENERAL CONCLUSIONS AND FUTURE WORK

In the present work, the molecular features of okra pectins as affected by extraction conditions were studied. Extraction conditions influenced the fine structure of pectins resulting in isolates with distinct molecular characteristics. The present extraction protocols resulted in isolation of acetylated LM-pectins with high molecular weight. Galacturonic acid (GalA) amount varied by altering the pH of the extraction with higher pH values (pH6.0) resulting in greater GalA content. Isolates contained different amounts of branched RG-I segments as indicated by the ratios of rhamnose to galacturonic acid and galactose to rhamnose. It has been shown that OP6 is mainly composed of RG-I whereas OP2 contained almost equal amounts of HG and RG-I. Dilute solution viscometry revealed changes in the coil dimensions for both of the isolated biopolymers with changes in pH as evidenced by intrinsic viscosity measurements.

It has been shown that okra pectins are non-gelling pectins due to the high degree of acetylation and branching of side-chains. Furthermore, the influence of pH on the structural properties of non-gelling LM-pectin in the presence of co-solute has been investigated by means of thermomechanical analysis and theoretical modeling of results. Dissociation of galacturonic acid residues at the high pH values results in extended chain conformation and early vitrification events. Conversely, as the polyelectrolyte approaches its isoelectric point at low pH, recorded viscoelastic functions decrease and vitrification is delayed. Spectral analysis of the viscoelastic master curves revealed the exact positioning of the relaxation events characterized by one dominant regime where the relaxation of the macromolecules concludes.

Okra extracts and pectins demonstrate a good emulsifying capacity in model oil-in-water emulsions. Extraction protocols have considerably affected the physiochemical properties of okra extracts and pectins, and had an effect on physical

stability of resulting emulsions. Overall, okra extracts (OE4 and OE6) differentiated significantly in terms of their efficiency towards long-term stabilization of emulsions against coarsening. Emulsions containing OE6 demonstrated higher surface activity at the o/w interface and stability during the 30 days storage than its OE4 counterparts. In contrast, emulsions composed of OE4 were more susceptible to coarsening mechanisms resulting in droplets of greater average size. It has been identified that Ostwald ripening is the major destabilization mechanisms particularly for emulsions prepared with OE4.

Okra pectins (OP2 and OP6) isolated using hot aqueous extractions demonstrated higher interfacial activity than okra extracts. It has been shown that OP2 and OP6-stabilized emulsions undergo different destabilisation kinetics and mechanisms depending on the biopolymer applied. OP2-stabilized emulsion showed low stability to coarsening mechanisms and considerable destabilisation of emulsions occurred after 1 h of storage. It has been shown that coarsening of OP2-stabilized emulsions was a complex mechanism that has been identified as combination of Ostwald ripening and coalescence. In contrast, OP6-stabilised emulsions were relatively stable for a period of 30 days indicating the potential of OP6 to act as emulsifier in acidic emulsions.

The rapid growth of functional food, medical nutrition and nutritional supplement markets results in a demand for development of delivery systems that can control the digestion, release and absorption of hydrophobic compounds such as drugs, bioactive nutrients. Emulsions are systems that are particularly suited for the fabrication of such type delivery systems. Therefore, based on the results of current work, further investigation of functionality of okra pectin in emulsion-based delivery systems has to be performed in the future. An advantage of an emulsion system based

on OP6 would be the resistance to proteolytic enzymes and the acidic pH of stomach (1.5-3.5). Furthermore, as emulsions are not stable at neutral pH, the emulsified bioactive would be released in the small intestine where pH is slightly alkaline making OP6 an effective delivery vehicle with a distinct functional attributes. Further investigation is also required in the application of okra pectin in the fabrication of edible films. Films produced from natural products are of increasing interest due to their biodegradability and that they can be utilized for human consumption and pharmaceutical applications. Edible films from pectin have been previously used as barriers to gas and solutes resulting in prolonged food quality and shelf life. Moreover, film-forming properties of okra pectin could be used for pharmaceutical applications such as in fabrication of drug coatings.

CHAPTER 6

REFERENCES

- Abbas, S., Hayat, K., Karangwa, E., Bashari, M., & Zhang, X. (2013). An Overview of Ultrasound-Assisted Food-Grade Nanoemulsions. *Food Engineering Reviews*, 5(3), 139-157.
- Adelakun, O. E., Oyelade, O. J., Ade-Omowaye, B. I. O., Adeyemi, I. A., & Van de Venter, M. (2009). Chemical composition and the antioxidative properties of Nigerian Okra Seed (*Abelmoschus esculentus* Moench) Flour. *Food and Chemical Toxicology*, 47(6), 1123-1126.
- Akhtar, M., Dickinson, E., Mazoyer, J., & Langendorff, V. (2002). Emulsion stabilizing properties of depolymerized pectin. *Food Hydrocolloids*, 16(16), 249-256.
- Al-Ruqaie, I. M., Kasapis, S., Richardson, R. K., & Mitchell, G. (1997). The glass transition zone in high solids pectin and gellan preparations. *Polymer*, 38(22), 5685-5694.
- Alba, K., Ritzoulis, C., Georgiadis, N., & Kontogiorgos, V. (2013). Okra extracts as emulsifiers for acidic emulsions. *Food Research International*, 54(2), 1730-1737.
- Almrhag, O., George, P., Bannikova, A., Katopo, L., Chaudhary, D., & Kasapis, S. (2012). Analysis on the effectiveness of co-solute on the network integrity of high methoxy pectin. *Food Chemistry*, 135(3), 1455-1462.
- Angell, C. A. (2002). Liquid fragility and the glass transition in water and aqueous solutions. *Chemical Reviews*, 102(8), 2627-2650.
- Anger, H., & Berth, G. (1986). Gel permeation chromatography and the Mark-Houwink relation for pectins with different degrees of esterification. *Carbohydrate Polymers*, 6, 193-202.
- Arapitsas, P. (2008). Identification and quantification of polyphenolic compounds from okra seeds and skins. *Food Chemistry*, 110, 1041-1045.
- Arltoft, D., Madsen, F., & Ipsen, R. (2007). Screening of probes for specific localisation of polysaccharides. *Food Hydrocolloids*, 21(7), 1062-1071.
- Aveyard, R., & Haydon, D. A. (1965). Thermodynamic properties of aliphatic hydrocarbon/water interfaces. *Transactions of the Faraday Society*, 61, 2255.
- Axelos, M. A. V., & Thibault, J. F. (1991). The chemistry of low-methoxyl pectin gelation. In R. H. Walter (Ed.). *The chemistry and technology of pectin*. New York: Academic Press.
- Bagherian, H., Zokaee Ashtiani, F., Fouladitajar, A., & Mohtashamy, M. (2011). Comparisons between conventional, microwave- and ultrasound-assisted methods for extraction of pectin from grapefruit. *Chemical Engineering and Processing: Process Intensification*, 50(11-12), 1237-1243.
- Bédouet, L., Courtois, B., & Courtois, J. (2003). Rapid quantification of O-acetyl and O-methyl residues in pectin extracts. *Carbohydrate Research*, 338(338), 379-383.

- Behrouzian, F., Razavi, S. M. A., & Karazhiyan, H. (2014). Intrinsic viscosity of cress (*Lepidium sativum*) seed gum: Effect of salts and sugars. *Food Hydrocolloids*(35), 100-105.
- Belitz, H. D., Grosch, W., & Schieberle, P. (2009). *Food chemistry*. Berlin; London: Springer.
- BeMiller, J. N., Whistler, R. L., & Barbalowm, D. G. (1993). *Industrial gums, polysaccharides and their derivatives*. San Diego, CA: Academic Press.
- Bergström, L. (1997). Hamaker constants of inorganic materials. *Advances in Colloid and Interface Science*, 70(1-3), 125-169.
- Bleton, J., Mejanelle, P., Sansoulet, S., Goursaud, A., & Tchaplal, A. (1996). Characterization of neutral sugars and uronic acids after methanolysis and trimethylsilylation for recognition of plant gums. *Journal of Chromatography A*, 720, 27-49.
- Bohmer, R., Ngai, K. L., Angell, C. A., & Plazek, D. J. (1993). Nonexponential relaxations in strong and fragile glass formers. *The Journal of Chemical Physics*, 99(5), 4201-4209.
- Bradford, M. M. (1976). A rapid and sensitive method for the quantitation of microgram quantities of protein utilizing the principle of protein-dye binding. *Analytical Biochemistry*, 72(72), 248–254.
- Caffall, K. H., & Mohnen, D. (2009). The structure, function, and biosynthesis of plant cell wall pectic polysaccharides. *Carbohydrate Research*, 344(14), 1879-1900.
- Camino, N. A., Sánchez, C. C., Rodríguez Patino, J. M., & Pilosof, A. M. R. (2011). Hydroxypropylmethylcellulose at the oil–water interface. Part I. Bulk behaviour and dynamic adsorption as affected by pH. *Food Hydrocolloids*, 25(1), 1-11.
- Cangialosi, D., Schut, H., Van Veen, A., & Picken, S. J. (2003). Positron annihilation lifetime spectroscopy for measuring free volume during physical aging of polycarbonate. *Macromolecules*, 36(1), 142-147.
- Cardoso, S. M., Coimbra, M. A., & Lopes da Silva, J. A. (2003). Calcium-mediated gelation of an olive pomace pectic extract. *Carbohydrate Polymers*, 52, 125-133.
- Champion, D., Le Meste, M., & Simatos, D. (2000). Towards an improved understanding of glass transition and relaxations in foods: Molecular mobility in the glass transition range. *Trends in Food Science and Technology*, 11(2), 41-55.
- Chanamai, R., Horn, G., & McClements, D. J. (2002). Influence of Oil Polarity on Droplet Growth in Oil-in-Water Emulsions Stabilized by a Weakly Adsorbing Biopolymer or a Nonionic Surfactant. *Journal of Colloid and Interface Science*, 247(1), 167-176.
- Chatjigakis, A. K., Pappas, C., Proxenia, N., Kalantzi, O., Rodis, P., & Polissiou, M. (1998). FT-IR spectroscopic determination of the degree of esterification of cell wall

- pectins from stored peaches and correlation to textural changes. *Carbohydrate Polymers*, 37, 395-408.
- Cheng, H. N., & Neiss, T. G. (2012). Solution NMR Spectroscopy of Food Polysaccharides. *Polymer Reviews*, 52(2), 81-114.
- Cho, Y.-H., Decker, E. A., & McClements, D. J. (2010). Formation of Protein-Rich Coatings around Lipid Droplets Using the Electrostatic Deposition Method. *Langmuir*, 26(11), 7937-7945.
- Christiaens, S., Van Buggenhout, S., Ngouémazong, E. D., Vandevenne, E., Fraeye, I., Duvetter, T., Van Loey, A. M., & Hendrickx, M. E. (2011). Anti-homogalacturonan antibodies: A way to explore the effect of processing on pectin in fruits and vegetables? *Food Research International*, 44, 225-234.
- Costantino, A. J., & Romanchick-Cerpoviez, J. E. (2004). Physical and sensory measures indicate moderate fat replacement in frozen dairy dessert is feasible using okra gum as a milk-fat ingredient substitute. *Journal of American Diet Association*, 104(104), 44.
- Cozzolino, R., Malvagna, P., Spina, E., Giori, A., Fuzzati, N., Anelli, A., Garozzo, D., & Impallomeni, G. (2006). Structural analysis of the polysaccharides from *Echinacea angustifolia* radix. *Carbohydrate Polymers*, 65(3), 263-272.
- Cui, S. W. (2005). *Food carbohydrates: chemistry, physical properties, and applications*. Boca Raton; London: Taylor & Francis.
- da Silva, J. A. L., Gonzalves, M. P., & Rao, M. A. (1995). Kinetics and thermal behaviour of the structure formation process in HMP/sucrose gelation. *International Journal of Biological Macromolecules*, 17(1), 25-32.
- Dea, I. C. M., & Madden, J. K. (1986). Acetylated pectic polysaccharides of sugar beet. *Food Hydrocolloids*, 1(1), 71-88.
- Dickinson, E., Galazka, V. B., & Anderson, D. M. W. (1991). Emulsifying behaviour of gum arabic. Part 1: Effect of the nature of the oil phase on the emulsion droplet-size distribution. *Carbohydrate Polymers*, 14(4), 373-383.
- Dickinson, E., Golding, M., & Povey, M. J. W. (1997). Creaming and flocculation of oil-in-water emulsions containing sodium caseinate. *Journal of Colloid and Interface Science*, 185(2), 515-529.
- Dickinson, E., Ritzoulis, C., Yamamoto, Y., & Logan, H. (1999). Ostwald ripening of protein-stabilized emulsions: effect of transglutaminase crosslinking. *Colloids and Surfaces B: Biointerfaces*(12), 139-146.
- Djerdjev, A. M., & Beattie, J. K. (2008). Enhancement of ostwald ripening by depletion flocculation. *Langmuir*, 24, 7711-7717.
- Doublier, J. L., & Launay, B. (1981). Rheology of galactomannan solutions: Comparative study of guar gum and locust bean gum. *Journal of Texture Studies*, 12, 151-172.

- Draget, K. I., Østgaard, K., & Smidsrød, O. (1989). Alginate-based solid media for plant tissue culture. *Applied Microbiology and Biotechnology*, 31(1), 79-83.
- Duan, J., Wang, X., Dong, Q., Fang, J. N., & Li, X. (2003). Structural features of a pectic arabinogalactan with immunological activity from the leaves of *Diospyros kaki*. *Carbohydrate Research*, 338(12), 1291-1297.
- Dubois, M., Gilles, K. A., Hamilton, J. K., Rebers, P. A., & Smith, F. (1956). Colorimetric method for determination of sugars and related substances. *Analytical Chemistry*, 28, 350-356.
- Ele-Ekouna, J.-P., Pau-Roblot, C., Courtois, C., & Courtois, J. (2011). Chemical characterization of pectin from green tea (*Camellia sinensis*). *Carbohydrate Polymers*, 83, 1232-1239.
- Ellis, H. S., & Ring, S. G. (1985). A study of some factors influencing amylose gelation. *Carbohydrate Polymers*(5), 201-214.
- Endreß, H. U., & Rentschler, C. (1999). Chances and limit for the use of pectin as emulsifier—Part 1. *The European Food and Drink Review, Summer*(Summer), 49-53.
- Enomoto, Y., Tokuyama, M., & Kawasaki, K. (1986). Finite volume fraction effects on Ostwald ripening. *Acta Metallurgica*, 34(11), 2119-2128.
- Espitia, P. J. P., Du, W.-X., Avena-Bustillos, R. d. J., Soares, N. d. F. F., & McHugh, T. H. (2014). Edible films from pectin: Physical-mechanical and antimicrobial properties - A review. *Food Hydrocolloids*, 35(0), 287-296.
- Evageliou, V., Kasapis, S., & Hember, M. W. N. (1998). Vitrification of κ -carrageenan in the presence of high levels of glucose syrup. *Polymer*, 39(17), 3909-3917.
- Evageliou, V., Richardson, R. K., & Morris, E. R. (2000a). Effect of pH, sugar type and thermal annealing on high-methoxy pectin gels. *Carbohydrate Polymers*, 42, 245-259.
- Evageliou, V., Richardson, R. K., & Morris, E. R. (2000b). Effect of pH, sugar type and thermal annealing on high-methoxy pectin gels. *Carbohydrate Polymers*, 42(3), 245-259.
- Evans, M., Ratcliffe, I., & Williams, P. A. (2013). Emulsion stabilisation using polysaccharide-protein complexes. *Current Opinion in Colloid and Interface Science*, 18(4), 272-282.
- FAOSTAT. (2013). <http://faostat3.fao.org/faostat-gateway/go/to/home/E>.
- Fathi, M., Martín, Á., & McClements, D. J. (2014). Nanoencapsulation of food ingredients using carbohydrate based delivery systems. *Trends in Food Science & Technology*, 39(1), 18-39.
- Ferry, J. D. (1980). Dependence of viscoelastic behavior on temperature and pressure. *Viscoelastic Properties of Polymers* (pp. 264-320). New York: John Wiley.

- Filisetti-Cozzi, T. M. C. C., & Carpita, N. C. (1991). Measurement of uronic acids without interference from neutral sugars. *Analytical Biochemistry*, *197*, 157-162.
- Fissore, E. N., Rojas, A. M., Gerschenson, L. N., & Williams, P. A. (2013). Butternut and beetroot pectins: Characterization and functional properties. *Food Hydrocolloids*, *31*(2), 172-182.
- Flory, P. J. (1974). *Faraday Discussions*, *57*, 8.
- Fry, S. C. (1982). Phenolic components of the primary cell wall. Feruloylated disaccharides of D-galactose and L-arabinose from spinach polysaccharide. *Biochemical Journal*, *203*(2), 493-504.
- Gaborieau, M., & Castignolles, P. (2011). Size-exclusion chromatography (SEC) of branched polymers and polysaccharides. *Analytical and Bioanalytical Chemistry*, *399*, 1413–1423.
- Georgiadis, N., Ritzoulis, C., Sioura, G., Kornezou, P., Vasiliadou, C., & Tsiptsias, C. (2011). Contribution of okra extracts to the stability and rheology of oil-in-water emulsions. *Food Hydrocolloids*, *25*(5), 991-999.
- Gharsallaoui, A., Yamauchi, K., Chambin, O., Cases, E., & Saurel, R. (2010). Effect of high methoxyl pectin on pea protein in aqueous solution and at oil/water interface. *Carbohydrate Polymers*, *80*(3), 817-827.
- Ghori, M. U., Alba, K., Smith, A. M., Conway, B. R., & Kontogiorgos, V. (2014). Okra extracts in pharmaceutical and food applications. *Food Hydrocolloids*, *42*, 342-347.
- Gilsenan, P. M., Richardson, R. K., & Morris, E. R. (2000). Thermally reversible acid-induced gelation of low-methoxy pectin. *Carbohydrate Polymers*, *41*(4), 339-349.
- Gnanasambandam, R., & Proctor, A. (2000). Determination of pectin degree of esterification by diffuse reflectance Fourier transform infrared spectroscopy. *Food Chemistry*, *68*, 327–332.
- Grant, G. T., Morris, E. R., Rees, D. A., Smith, P. J. C., & Thom, D. (1973). Biological interactions between polysaccharides and divalent cations: The egg-box model. *Febs Letters*, *32*, 195-198.
- Grasdalen, H., Bakøy, O. E., & Larsen, B. (1988). Determination of the degree of esterification and the distribution of methylated and free carboxyl groups in pectins by ¹H NMR spectroscopy. *Carbohydrate Research*, *184*, 183–191.
- Grimm, A., Kruger, E., & Burchard, W. (1995). Solution properties of β-D-(1, 3)(1, 4)-glucan isolated from beer. *Carbohydrate Polymers*, *27*(3), 205-214.
- Guttoff, M., Saberi, A. H., & McClements, D. J. (2015). Formation of vitamin D nanoemulsion-based delivery systems by spontaneous emulsification: Factors affecting particle size and stability. *Food Chemistry*, *171*, 117-122.

- Haines, P. J., Reading, M., & Wilburn, F. W. (2003). Differential thermal analysis and differential scanning calorimetry. In E. M. Brown (Ed.). *Handbook of thermal analysis and calorimetry* (Vol. 1). Amsterdam: Elsevier.
- Hansen, P.-C. (1994). Regularization tools: A MATLAB package for analysis and solution of discrete ill-posed problems. *Numerical Algorithms*, 6, 1-35.
- Happi Emaga, T., Ronkart, S. N., Robert, C., Wathelet, B., & Paquot, M. (2008). Characterisation of pectins extracted from banana peels (*Musa AAA*) under different conditions using an experimental design. *Food Chemistry*, 108(2), 463-471.
- Harding, S. E. (1997). The intrinsic viscosity of biological macromolecules. Progress in measurement, interpretation and application to structure in dilute solution. *Progress in Biophysics and Molecular Biology*, 68(2-3), 207-262.
- Houben, K., Jolie, R. P., Fraeye, I., Van Loey, A. M., & Hendrickx, M. E. (2011). Comparative study of the cell wall composition of broccoli, carrot, and tomato: Structural characterization of the extractable pectins and hemicelluloses. *Carbohydrate Research*, 346(9), 1105-1111.
- Huisman, M. M. H., Brüll, L. P., Thomas-Oates, J. E., Haverkamp, J., Schols, H. A., & Voragen, A. G. J. (2001). The occurrence of internal (1,5)-linked arabinofuranose and arabinopyranose residues in arabinogalactan side chains from soybean pectic substances. *Carbohydrate Research*, 330(1), 103-114.
- Hutchinson, J. M. (1995). Physical aging of polymers. *Progress in Polymer Science*(20), 703-760.
- Hwang, J., & Kokini, J. L. (1992). Contribution of side branches to rheological properties of pectins. *Carbohydrate Polymers*, 19, 41-50.
- Immerzeel, P., Eppink, M. M., de Vries, S. C., Schols, H. A., & Voragen, A. G. J. (2006). Carrot arabinogalactan proteins are interlinked with pectins. *Physiologia Plantarum*, 128(1), 18-28.
- Jarvis, M. C., & Apperley, D. C. (1995). Chain conformation in concentrated pectic gels: evidence from ¹³C NMR. *Carbohydrate Research*, 275(1), 131-145.
- Jiang, B., Kasapis, S., & Kontogiorgos, V. (2011). Combined use of the free volume and coupling theories in the glass transition of polysaccharide/co-solute systems. *Carbohydrate Polymers*, 83, 926-933.
- Joye, I. J., & McClements, D. J. (2014). Biopolymer-based nanoparticles and microparticles: Fabrication, characterization, and application. *Current Opinion in Colloid & Interface Science*, 19(5), 417-427.
- Kabalnov, A. S. (1994). Can micelles mediate a mass transfer between oil droplets? *Langmuir*, 10(3), 680-684.
- Kabalnov, A. S., & Shchukin, E. D. (1992). Ostwald ripening theory: applications to fluorocarbon emulsion stability. *Advances in Colloid and Interface Science*, 38(C), 69-97.

- Kaltsa, O., Michon, C., Yanniotis, S., & Mandala, I. (2013). Ultrasonic energy input influence on the production of sub-micron o/w emulsions containing whey protein and common stabilizers. *Ultrasonics Sonochemistry*, 20(3), 881-891.
- Kamnev, A. A., Colina, M., Rodriguez, J., Ptitchkina, N. M., & Ignatov, V. V. (1998). Comparative spectroscopic characterization of different pectins and their sources. *Food Hydrocolloids*, 12, 263-271.
- Kasapis, S. (2005). Glass transition phenomena in dehydrated model systems and foods: A review. *Drying Technology*, 23(4), 731-757.
- Kasapis, S. (2008). Recent advances and future challenges in the explanation and exploitation of the network glass transition of high sugar/biopolymer mixtures. *Critical Reviews in Food Science and Nutrition*, 48(2), 185-203.
- Kasapis, S. (2012). Relation between the structure of matrices and their mechanical relaxation mechanisms during the glass transition of biomaterials: A review. *Food Hydrocolloids*, 26(2), 464-472.
- Kasapis, S., Al-Alawi, A., Guizani, N., Khan, A. J., & Mitchell, J. R. (2000). Viscoelastic properties of pectin-co-solute mixtures at iso-free-volume states. *Carbohydrate Research*, 329(2), 399-407.
- Kasapis, S., Al-Marhoobi, I. M., Deszczynski, M., Mitchell, J. R., & Abeysekera, R. (2003). Gelatin vs Polysaccharide in Mixture with Sugar. *Biomacromolecules*, 4(5), 1142-1149.
- Kasapis, S., Al-Marhoobi, I. M., & Mitchell, J. R. (2003). Molecular weight effects on the glass transition of gelatin/cosolute mixtures. *Biopolymers*, 70(2), 169-185.
- Kasapis, S., Al-Marhoobi, I. M. A., & Khan, A. J. (2000). Viscous solutions, networks and the glass transition in high sugar galactomannan and κ -carrageenan mixtures. *International Journal of Biological Macromolecules*, 27(1), 13-20.
- Kasapis, S., Mitchell, J., Abeysekera, R., & MacNaughtan, W. (2004). Rubber-to-glass transitions in high sugar/biopolymer mixtures. *Trends in Food Science and Technology*, 15(6), 298-304.
- Kashyap, D. R., Vohra, P. K., Chopra, S., & Tewari, R. (2001a). Applications of pectinases in commercial sector: a review. *Bioresource Technology*, 77(77), 215-227.
- Kashyap, D. R., Vohra, P. K., Chopra, S., & Tewari, R. (2001b). Applications of pectinases in the commercial sector: a review. *Bioresource Technology*, 77, 215-227.
- Kim, Y., Williams, M. A. K., Galant, A. L., Luzio, G. A., Savary, B. J., Vasu, P., & Cameron, R. G. (2013). Nanostructural modification of a model homogalacturonan with a novel pectin methylesterase: Effects of pH on nanostructure, enzyme-mode of action and substrate functionality. *Food Hydrocolloids*, 33(1), 132-141.
- Kjøniksen, A.-L., Hiorth, M., & Nyström, B. (2005). Association under shear flow in aqueous solutions of pectin. *European Polymer Journal*, 41(4), 761-770.

- Kliemann, E., de Simas, K. N., Amante, E. R., Prudêncio, E. S., Teófilo, R. F., Ferreira, M. M. C., & Amboni, R. D. M. C. (2009). Optimisation of pectin acid extraction from passion fruit peel (*Passiflora edulisflavicarpa*) using response surface methodology. *International Journal of Food Science & Technology*, *44*(3), 476-483.
- Kontogiorgos, V. (2010). Calculation of relaxation spectra from mechanical spectra in MATLAB. *Polymer Testing*, *29*, 1021-1025.
- Kontogiorgos, V. (2014). Polysaccharide Nanostructures. In A. Marangoni & D. Pink (Eds.). *Edible Nanostructures: A Bottom-up Approach*. London: Royal Society of Chemistry.
- Kontogiorgos, V., Margelou, I., Georgiadis, N., & Ritzoulis, C. (2012). Rheological characterization of okra pectins. *Food Hydrocolloids*, *29*(2), 356-362.
- Koštalová, Z., Hromádková, Z., & Ebringerová, A. (2013). Structural diversity of pectins isolated from the Styrian oil-pumpkin (*Cucurbita pepo* var. *styriaca*) fruit. *Carbohydrate Polymers*, *93*(1), 163-171.
- Kravtchenko, T. P., Voragen, A. G. J., & Pilnik, W. (1992). Analytical comparison of three industrial pectin preparations. *Carbohydrate Polymers*, *18*(1), 17-25.
- Kumar, A., & Chauhan, G. S. (2010). Extraction and characterization of pectin from apple pomace and its evaluation as lipase (steapsin) inhibitor. *Carbohydrate Polymers*, *82*(2), 454-459.
- Kurita, O., Fujiwara, T., & Yamazaki, E. (2008). Characterization of the pectin extracted from citrus peel in the presence of citric acid. *Carbohydrate Polymers*, *74*(3), 725-730.
- Lapasin, R., & Prici, S. (1999). *Rheology of industrial polysaccharides: Theory and applications*. Gaithersburg, MD: Aspen Publishers.
- Lengsfeld, C., Titgemeyer, F., Faller, G., & Hensel, A. J. (2004). Glycosylated compounds from okra inhibit adhesion of *Helicobacter pylori* to human gastric mucosa. *Journal of Agricultural and Food Chemistry*, *52*, 1495-1503.
- Leroux, J., Langendorff, V., Schick, G., Vaishnav, V., & Mazoyer, J. (2003). Emulsion stabilizing properties of pectin. *Food Hydrocolloids*, *17*(4), 455-462.
- Levigne, S., Ralet, M.-C., & Thibault, J.-F. (2002). Characterization of pectins extracted from fresh sugar beet under different conditions using an experimental design. *Carbohydrate Polymers*, *49*(2), 145-153.
- Lifshitz, I. M., & Slyozov, V. V. (1961). The kinetics of precipitation from supersaturated solid solutions. *Journal of Physics and Chemistry of Solids*, *19*(1-2), 35-50.
- Liu, L. S., Jin, T., Liu, C. K., Hicks, K., Mohanty, A., Bhardwaj, R., & Misra, M. (2008). A preliminary study on antimicrobial edible films from pectin and other food hydrocolloids by extrusion method. *Journal of Natural Fibers*, *5*(4), 366-382.

- M'sakni, N. H., Majdoub, H., Roudesli, S., Picton, L., Le Cerf, D., Rihouey, C., & Morvan, C. (2006). Composition, structure and solution properties of polysaccharides extracted from leaves of *Mesembryanthemum crystallinum*. *European Polymer Journal*, 42(4), 786-795.
- MacDougall, A. J., & Ring, S. G. (2004). Pectic polysaccharides. . In P. Tomasik (Ed.). *Chemical and functional properties of food saccharides*. USA: CRC Press LLC.
- Mahdi, J. S., He, Y., & Bhandari, B. (2006). Nano-Emulsion Production by Sonication and Microfluidization—A Comparison. *International Journal of Food Properties*, 9(3), 475-485.
- Martin, F. (1982). Okra, potential multiple-purpose crop for the temperate zones and tropics. *Economic Botany*, 36(3), 340-345.
- Matsunaga, T., Ishii, T., Matsunamoto, S., Higuchi, M., Darvill, A., Albersheim, P., & O'Neill, M. (2004). Occurrence of the primary cell wall polysaccharide rhamnogalacturonan-II in peridophytes, lycophytes, and bryophytes. Implications for the evolution of vascular plants. *Plant Physiology*(134), 339-351.
- May, C. D. (1990). Industrial pectins: sources, production and applications. *Carbohydrate Polymers*, 12(12), 79–99.
- Mayer, S., Weiss, J., & McClements, D. J. (2013). Vitamin E-enriched nanoemulsions formed by emulsion phase inversion: Factors influencing droplet size and stability. *Journal of Colloid and Interface Science*, 402, 122-130.
- McCann, M. C., & Roberts, K. (1991). Architecture of the primary cell wall. In C. W. Lloyd (Ed.). *The Cytoskeletal Basis of Plant Growth and Form* (pp. 109–129). London: Academic Press.
- McClements, D. J. (1999). *Food Emulsions-principles, practice and techniques*. New York: CRC Press LLC.
- McClements, D. J. (2004). Protein-stabilized emulsions. *Current Opinion in Colloid & Interface Science*, 9(5), 305-313.
- McClements, D. J. (2005). *Food emulsions - principles, practice and techniques*. CRC Press.
- McClements, D. J. (2012). Nanoemulsions versus microemulsions: terminology, differences, and similarities. *Soft Matter*, 8(6), 1719-1729.
- McClements, D. J., Decker, E. A., Park, Y., & Weiss, J. (2009). Structural Design Principles for Delivery of Bioactive Components in Nutraceuticals and Functional Foods. *Critical Reviews in Food Science and Nutrition*, 49(6), 577-606.
- McClements, D. J., Dungan, S. R., German, J. B., & Kinsella, J. E. (1992). Oil exchange between oil-in-water emulsion droplets stabilised with a non-ionic surfactant. *Food Hydrocolloids*, 6(5), 415-422.

- McClements, D. J., & Rao, J. (2011). Food-Grade Nanoemulsions: Formulation, Fabrication, Properties, Performance, Biological Fate, and Potential Toxicity. *Critical Reviews in Food Science and Nutrition*, 51(4), 285-330.
- McComb, E. A., & McCready, R. M. (1957). Determination of acetyl in pectin and in acetylated carbohydrate polymers. *Analytical Chemistry*, 29(5), 819–921.
- McMurry, J. (2008). *Organic Chemistry*. Thomson Brooks/Cole.
- Mezger, T. G. (2011). *The rheology handbook: for users of rotational and oscillatory rheometers*. Hannover: Vincentz Network.
- Mohammad Amini, A., & Razavi, S. M. A. (2012). Dilute solution properties of Balangu (*Lallemantia royleana*) seed gum: Effect of temperature, salt, and sugar. *International Journal of Biological Macromolecules*, 51(3), 235-243.
- Mohnen, D. (2008). Pectin structure and biosynthesis. *Current Opinion in Plant Biology*, 11(3), 266-277.
- Morris, E. R., Cutler, A. N., Ross-Murphy, S. B., & Rees, D. A. (1981). Concentration and shear rate dependence of viscosity in random coil polysaccharide solutions. *Carbohydrate Polymers*, 1, 5–21.
- Morris, E. R., Cutler, A. N., Ross-Murphy, S. B., Rees, D. A., & Price, J. (1981). Concentration and shear rate dependence of viscosity in random coil polysaccharide solutions. *Carbohydrate Polymers*, 1(1), 5-21.
- Morris, E. R., Rees, D. A., Thom, D., & Welsh, E. J. (1977). Conformation and intermolecular interactions of carbohydrate chains. *Journal of Supramolecular and Cellular Biochemistry*, 6(2), 259-274.
- Morris, G. A., Adams, G. G., & Harding, S. E. (2014). On hydrodynamic methods for the analysis of the sizes and shapes of polysaccharides in dilute solution: A short review. *Food Hydrocolloids*, 42(P3), 318-334.
- Morris, G. A., Castile, J., Smith, A., Adams, G. G., & Harding, S. E. (2010). The effect of different storage temperatures on the physical properties of pectin solutions and gels. *Polymer Degradation and Stability*, 95(12), 2670-2673.
- Morris, G. A., Ralet, M.-C., Bonnin, E., Thibault, J.-F., & Harding, S. E. (2010). Physical characterisation of the rhamnogalacturonan and homogalacturonan fractions of sugar beet (*Beta vulgaris*) pectin. *Carbohydrate Polymers*, 82(4), 1161-1167.
- Muralikrishna, G., Salimath, P. V., & Tharanathan, R. N. (1987). Structural features of an arabinoxylan and a rhamnogalacturonan derived from linseed mucilage. *Carbohydrate Research*, 161, 265–271.
- Nakamura, A., Furuta, H., Maeda, H., Nagamatsu, Y., & Yoshimoto, A. (2001). Analysis of structural components and molecular construction of soybean soluble polysaccharides by stepwise enzymatic degradation. *Bioscience Biotechnology Biochemistry*, 65, 2249–2258.

- Nakamura, A., Yoshida, R., Maeda, H., & Corredig, M. (2006). The stabilizing behaviour of soybean soluble polysaccharide and pectin in acidified milk beverages. *International Dairy Journal*, 16(4), 361-369.
- Nazarzadeh, E., Anthonypillai, T., & Sajjadi, S. (2013). On the growth mechanisms of nanoemulsions. *Journal of Colloid and Interface Science*, 397, 154-162.
- Ndjouenkeu, R., Akingbala, J. O., & Oguntimein, G. B. (1997). Emulsifying properties of three African food hydrocolloids: okra (*Hibiscus esculentus*), dika nut (*Irvingia gabonensis*) and khan (*Belschmiedia* sp.). *Plant Foods for Human Nutrition*, 51(51), 245-255.
- Ngai, K. L. (2000). Short-time and long-time relaxation dynamics of glass-forming substances: a coupling model perspective. *Journal of Physics: Condensed Matter*, 12(29), 6437.
- O'Neill, M. A., Ishii, T., Albersheim, P., & Darvill, A. G. (2004). Rhamnogalacturonan II: Structure and function of a borate cross-linked cell wall pectic polysaccharide. *Annual Review of Plant Biology* (Vol. 55, pp. 109-139).
- O'Neill, M. A., Warrenfeltz, D., Kates, K., Pellerin, P., Doco, T., Darvill, A. G., & Albersheim, P. (1996). Rhamnogalacturonan-II, a pectic polysaccharide in the walls of growing plant cell, forms a dimer that is covalently cross-linked by a borate ester. In vitro conditions for the formation and hydrolysis of the dimer. *Journal of Biological Chemistry*, 271(37), 22923-22930.
- Obro, J., Harholt, J., Scheller, H. V., & Orfila, C. (2004). Rhamnogalacturonan I in *Solanum tuberosum* tubers contains complex arabinogalactan structures. *Phytochemistry*, 65(10), 1429-1438.
- Pagan, J., Ibarz, A., Llorca, M., & Coll, L. (1999). Quality of industrial pectin extracted from peach pomace at different pH and temperatures. *Journal of the Science of Food and Agriculture*, 79, 1038-1042.
- Panyoyai, N., Bannikova, A., Small, D. M., & Kasapis, S. Diffusion kinetics of ascorbic acid in a glassy matrix of high-methoxy pectin with polydextrose. *Food Hydrocolloids*, *In press*.
- Panyoyai, N., Bannikova, A., Small, D. M., & Kasapis, S. (2015). Controlled release of thiamin in a glassy κ -carrageenan/glucose syrup matrix. *Carbohydrate Polymers*, 115(0), 723-731.
- Peleg, M. (1992). On the use of WLF model in polymers and foods. *Critical Reviews in Food Science and Nutrition*(32), 59-66.
- Perez, S., Mazeau, K., & Herve du Penhoat, C. (2000). The three-dimensional structures of the pectic polysaccharides. *Plant Physiology and Biochemistry*, 38(1-2), 37-55.
- Piculell, L. (1998). Gelling polysaccharides. *Current Opinion in Colloid and Interface Science*, 3(6), 643-650.

- Piorkowski, D. T., & McClements, D. J. (2013). Beverage emulsions: Recent developments in formulation, production, and applications. *Food Hydrocolloids*.
- Ptitchkina, N. M., Danilova, I. A., Doxastakis, G., Kasapis, S., & Morris, E. R. (1994). Pumpkin pectin: gel formation at unusually low concentration. *Carbohydrate Polymers*, 23, 265–273.
- Racape, E., Thibault, J. F., Reitsma, J. C. E., & Pilnik, W. (1989). Properties of amidated pectins. II. Polyelectrolyte behavior and calcium binding of amidated pectins and amidated pectic acids. *Biopolymers*, 28, 1435-1439.
- Renard, C. M. G. C., Champenois, Y., & Thibault, J. F. (1993). Characterisation of the extractable pectins and hemicelluloses of the cell wall of glasswort, *Salicornia ramosissima*. *Carbohydrate Polymers*, 22(4), 239-245.
- Renard, C. M. G. C., Wende, G., & Booth, E. J. (1999). Cell wall phenolics and polysaccharides in different tissues of quinoa (*Chenopodium quinoa* Willd). *Journal of the Science of Food and Agriculture*, 79(14), 2029-2034.
- Richardson, P. H., Willmer, J., & Foster, T. J. (1998). Dilute solution properties of guar and locust bean gum in sucrose solutions. *Food Hydrocolloids*, 12(3), 339-348.
- Ridley, B. L., O'Neill, M. A., & Mohnen, D. (2001). Pectins: Structure, biosynthesis, and oligogalacturonide-related signaling. *Phytochemistry*, 57(6), 929-967.
- Rihouey, C., Morvan, C., Borissova, I., Jauneau, A., Demarty, M., & Jarvis, M. (1995). Structural features of CDTA-soluble pectins from flax hypocotyls. *Carbohydrate Polymers*, 28(2), 159-166.
- Rincon, F., Munoz, J., Ramirez, P., Galan, H., & Alfaro, M. C. (2014). Physicochemical and rheological characterization of *Prosopis juliflora* seed gum aqueous dispersions. *Food Hydrocolloids*, 35(0), 348-357.
- Ritzoulis, C. (2013). *Introduction to the Physical Chemistry of Foods*. GB: CRC Press Inc.
- Rodriguez-Rivero, C., Hilliou, L., Martin del Valle, E. M., & Galan, M. A. (2014). Rheological characterization of commercial highly viscous alginate solutions in shear and extensional flows. *Rheologica Acta*, 53(7), 559-570.
- Roland, C. M. (2010). Relaxation phenomena in vitrifying polymers and molecular liquids. *Macromolecules*, 43(19), 7875-7890.
- Romanchik-Cerpovicz, J. E., Costantino, A. C., & Gunn, L. H. (2006). Sensory evaluation ratings and melting characteristics show that okra gum is an acceptable milk-fat ingredient substitute in chocolate frozen dairy dessert. *Journal of the American Dietetic Association*, 106(4), 594-597.
- Romanchik-Cerpovicz, J. E., Tilmon, R. W., & Baldree, K. A. (2002). Moisture retention and consumer acceptability of chocolate bar cookies pre-pared with okra gum as a fat ingredient substitute. *Journal of American Diet Association*, 102(102), 1301–1303.

- Rombouts, F. M., & Thibault, J.-F. (1986). Feruloylated pectic substances from sugar beet pulp. *Carbohydrate Research*, *154*, 177-188.
- Rosenbohm, C., Lundt, I., Christensen, T. I. E., & Young, N. G. (2003). Chemically methylated and reduced pectins: preparation, characterisation by ¹H NMR spectroscopy, enzymatic degradation, and gelling properties. *Carbohydrate Research*, *338*(7), 637-649.
- Rubinstein, M., & Colby, R. H. (2003). *Polymer physics*. Oxford: Oxford University Press Oxford.
- Sakamoto, T., & Sakai, T. (1995). Analysis of structure of sugar-beet pectin by enzymatic methods. *Phytochemistry*, *39*(4), 821-823.
- Samavati, V. (2013). Polysaccharide extraction from *Abelmoschus esculentus*: Optimization by response surface methodology. *Carbohydrate Polymers*, *95*(1), 588-597.
- Saulnier, L., & Thibault, J. F. (1999). Ferulic acid and diferulic acids as components of sugar-beet pectins and maize bran heteroxylans. *Journal of the Science of Food and Agriculture*, *79*(3), 396-402.
- Schmidt, U. S., Koch, L., Rentschler, C., Kurz, T., Endreß, H. U., & Schuchmann, H. P. (2014). Effect of Molecular Weight Reduction, Acetylation and Esterification on the Emulsification Properties of Citrus Pectin. *Food Biophysics*.
- Schmitt, V., Cattelet, C., & Leal-Calderon, F. (2004). Coarsening of Alkane-in-Water Emulsions Stabilized by Nonionic Poly(oxyethylene) Surfactants: The Role of Molecular Permeation and Coalescence. *Langmuir*(20), 46-52.
- Schols, H. A., & Voragen, A. G. J. (1996). Complex Pectins: Structure elucidation using enzymes. *Progress in Biotechnology* (Vol. 14, pp. 3-19).
- Schultz, T. (1965). Determination of the degree of esterification of pectin. *Methods in Carbohydrate Chemistry*, *5*, 189-194.
- Sengkhampan, N., Bakx, E. J., Verhoef, R., Schols, H. A., Sajjaanantakul, T., & Voragen, A. G. J. (2009). Okra pectin contains an unusual substitution of its rhamnosyl residues with acetyl and alpha-linked galactosyl groups. *Carbohydrate Research*, *344*(14), 1842-1851.
- Sengkhampan, N., Sagis, L. M. C., de Vries, R., Schols, H. A., Sajjaanantakul, T., & Voragen, A. G. J. (2010). Physicochemical properties of pectins from okra (*Abelmoschus esculentus* (L.) Moench). *Food Hydrocolloids*, *24*(1), 35-41.
- Sengkhampan, N., Verhoef, R., Schols, H. A., Sajjaanantakul, T., & Voragen, A. G. J. (2009). Characterisation of cell wall polysaccharides from okra (*Abelmoschus esculentus* (L.) Moench). *Carbohydrate Research*, *344*(14), 1824-1832.
- Siew, C. K., & Williams, P. A. (2008a). Characterization of the surface-active components of sugar beet pectin and the hydrodynamic thickness of the adsorbed pectin layer. *Journal of Agricultural and Food Chemistry*, *56*, 8111-8120.

- Siew, C. K., & Williams, P. A. (2008b). Role of protein and ferulic acid in the emulsification properties of sugar beet pectin. *Journal of Agricultural and Food Chemistry*, 56, 4164-4171.
- Sinha, V. R., & Kumria, R. (2001). Polysaccharides in colon-specific drug delivery. *International Journal of Pharmaceutics*, 224, 19-38.
- Sinnott, M. L. (2007). *Carbohydrate Chemistry and Biochemistry: Structure and Mechanism*. Cambridge: Royal Society of Chemistry.
- Soma, J., & Papadopoulos, K. D. (1996). Ostwald Ripening in Sodium Dodecyl Sulfate-Stabilized Decane-in-Water Emulsions. *Journal of Colloid and Interface Science*, 181(1), 225-231.
- Sperling, L. H. (2006). *Introduction to Physical Polymer Science*. New Jersey: Wiley-Interscience.
- Sriamornsak, P. (2003). Chemistry of pectin and its pharmaceutical uses: A review. *Silpakorn University International Journal*, 3, 206-228.
- Stevenson, T. T., Darvill, A. G., & Albersheim, P. (1988). Structural features of the plant cell-wall polysaccharide rhamnogalacturonan II. *Carbohydrate Research*, 179, 269-288.
- Strom, A., Schuster, E., & Goh, S. M. (2014). Rheological characterization of acid pectin samples in the absence and presence of monovalent ions. *Carbohydrate Polymers*, 113(0), 336-343.
- Sudhakar, D. V., & Maini, S. B. (2000). Isolation and characterization of mango peel pectins. *Journal of Food Processing Preservation*, 24, 209-227.
- Sun, S. F. (2004). *Physical Chemistry of Macromolecules: Basic Principles and Issues*. New Jersey: John Wiley & Sons.
- Tadros, T. F. (2005). *Applied Surfactants: Principles and Applications*. Weinheim: Wiley-VCH.
- Tamaki, Y., Konishi, T., Fukuta, M., & Tako, M. (2008). Isolation and structural characterisation of pectin from endocarp of Citrus depressa. *Food Chemistry*, 107(1), 352-361.
- Tanford, C. (1961). Ionization-linked changes in protein conformation. I. Theory. *Journal of the American Chemical Society*, 83(7), 1628-1634.
- Taylor, P. (1995). Ostwald ripening in emulsions. *Colloids and Surfaces A: Physicochemical and Engineering Aspects*, 99(2-3), 175-185.
- Taylor, P. (1998). Ostwald ripening in emulsions. *Advances in Colloid and Interface Science*, 75(2), 107-163.
- Thakur, B. R., Singh, R. K., Handa, A. K., & Rao, M. A. (1997). Chemistry and uses of pectin — A review. *Critical Reviews in Food Science and Nutrition*, 37(1), 47-73.

Thibault, J.-F., Guillon, F., & Rombouts, F. M. (1991). Gelation of sugar beet pectins by oxidative coupling. In R. Walter (Ed.). *The Chemistry and Technology of Pectins* (pp. 109-118). San Diego: Academic Press.

Thibault, J.-F., Renard, C. M. G. C., Axelos, M. A. V., Roger, P., & Crépeau, M.-J. (1993). Studies of the length of homogalacturonic regions in pectin by acid hydrolysis. *Carbohydrate Research*, 238, 271-286.

Thibault, J. F. (1988). Characterization and oxidative crosslinking sugarbeet pectins extracted from cossetes and pulps under different conditions. *Carbohydrate Polymers*, 8(8), 209–223.

Tomada, M., Shimada, K., Saito, Y., & Sugi, M. (1980). Plant mucilages. XXVI. Isolation and structural features of a mucilage, “okra mucilage”, from the immature fruit of *Abelmoschus esculentus*. *Chemical and Pharmaceutical Bulletin*, 28(28), 2933–2940.

Tschoegl, W. N. (1989). *The phenomenological theory of linear viscoelastic behavior*. Berlin: Springer-Verlag.

Turquois, T., Rinaudo, M., Taravel, F. R., & Heyraud, A. (1999). Extraction of highly gelling pectic substances from sugar beet pulp and potato pulp: influence of extrinsic parameters on their gelling properties. *Food Hydrocolloids*, 13(13), 255–262.

Verherbruggen, Y., Marcus, S. E., Haeger, A., Ordaz-Ortiz, J. J., & Knox, J. P. (2009). An extended set of monoclonal antibodies to pectic homogalacturonan. *Carbohydrate Research*, 344, 1858–1862.

Vierhuis, E., Schols, H. A., Beldman, G., & Voragen, A. G. J. (2000). Isolation and characterisation of cell wall material from olive fruit (*Olea europaea cv koroneiki*) at different ripening stages. *Carbohydrate Polymers*, 43, 11-21.

Vincken, J. P. (2003). If Homogalacturonan Were a Side Chain of Rhamnogalacturonan I. Implications for Cell Wall Architecture. *Plant Physiology*, 132(4), 1781-1789.

Visser, J., & Voragen, A. G. J. (1996). Pectins and Pectinases. *Progress in Biotechnology* (Vol. 14). Amsterdam: Elsevier.

Voragen, A. C. J., Rolin, C., & Marr, B. U. (2003). Pectins. In A. C. G. Voragen, C. Rolin, B. U. Marr, I. Challen, A. Riad & R. Lebarbar (Eds.). *Polysaccharides; Ullmann's Encyclopedia of Industrial Chemistry* (Vol. 28). Weinheim: Wiley-VCH Verlag GmbH & Co.

Walstra, P. (2003). *Physical chemistry of foods*. New York: Marcel Dekker.

Wang, H., & Davis, R. H. (1993). Droplet growth due to Brownian, gravitational, or thermocapillary motion and coalescence in dilute emulsions. *Journal of Colloid and Interface Science*, 159, 108-118.

- Wang, S., Chen, F., Wu, J., Wang, Z., Liao, X., & Hu, X. (2007). Optimization of pectin extraction assisted by microwave from apple pomace using response surface methodology. *Journal of Food Engineering*, 78(2), 693-700.
- Weiss, J., Herrmann, N., & McClements, D. J. (1999). Ostwald ripening of hydrocarbon emulsion droplets in surfactant solutions. *Langmuir*, 15(20), 6652-6657.
- Wendlandt, M. (2005). NLCSmoothReg.
- Western, T. L., Young, D. S., Dean, G. H., Tan, W. L., Samuels, A. L., & Haughn, G. W. (2004). Mucilage-modified4 encodes a putative pectin biosynthetic enzyme developmentally regulated by *Apetala2*, transparent Testa *Glabra1*, and *Glabra2* in the arabidopsis seed coat. *Plant Physiology*, 134(1), 296-306.
- Wikipedia. (2015). Zeta potential.
- Wilke, C. R., & Chang, P. (1955). Correlation of diffusion coefficients in dilute solutions. *American Institute of Chemical Engineers Journal*, 1(2), 264-270.
- Williams, M. L., Landel, R. F., & Ferry, J. D. (1955). The temperature dependence of relaxation mechanisms in amorphous polymers and other glass-forming liquids. *Journal of the American Chemical Society*, 77, 3701-3707.
- Williams, P. A., & Phillips, G. O. (2000). Introduction of food hydrocolloids. In G. O. Phillips & P. A. Williams (Eds.). *Handbook of Hydrocolloids* (pp. 3-22). USA: CRC Press.
- Williams, P. A., Sayers, C., Viebke, C., & Senan, C. (2005). Elucidation of the emulsification properties of sugar beet pectin. *Journal of Agricultural and Food Chemistry*, 53(53), 3592-3597.
- Woolfe, M. L., Chaplin, M. F., & Otchere, G. (1977). Studies on the mucilages extracted from okra fruits (*Hibiscus esculentus* L.) and baobab leaves (*Adansonia digitata* L.). *Journal of the Science of Food and Agriculture*, 28(28), 519-529.
- Wooster, T. J., Golding, M., & Sanguansri, P. (2008). Impact of oil type on nanoemulsion formation and ostwald ripening stability. *Langmuir*, 24(22), 12758-12765.
- Yapo, B. M. (2011). Rhamnogalacturonan-I: A Structurally Puzzling and Functionally Versatile Polysaccharide from Plant Cell Walls and Mucilages. *Polymer Reviews*, 51(4), 391-413.
- Yapo, B. M., Robert, C., Etienne, I., Wathelet, B., & Paquot, M. (2007). Effect of extraction conditions on the yield, purity and surface properties of sugar beet pulp pectin extracts. *Food Chemistry*, 100(4), 1356-1364.
- Yu, C.-Y., Cao, H., Zhang, X.-C., Zhou, F.-Z., Cheng, S.-X., & Zhang, X.-Z., et al. . (2009). Hybrid nanospheres and vesicles based on pectin as drug carriers. *Langmuir*, 25(19), 11720-11726.

Zandleven, J., Sørensen, S., Harholt, J., Beldman, G., Schols, H. A., Scheller, H. V., & Voragen, A. J. (2007). Xylogalacturonan exists in cell walls from various tissues of *Arabidopsis thaliana*. *Phytochemistry*, *68*(8), 1219-1226.

Zeppieri, S., Rodriguez, J., & Lopez de Ramos, A. L. (2001). Interfacial tension of alkane-water systems. *Journal of Chemical and Engineering Data*, *46*, 1086-1088.